



**HAL**  
open science

# Experimental determination and thermodynamic modélisation of Mo-Ni-Re system

Khurram Yaqoob

► **To cite this version:**

Khurram Yaqoob. Experimental determination and thermodynamic modelisation of Mo-Ni-Re system. Other. Université Paris-Est, 2012. English. NNT : 2012PEST1172 . tel-00805384

**HAL Id: tel-00805384**

**<https://theses.hal.science/tel-00805384>**

Submitted on 27 Mar 2013

**HAL** is a multi-disciplinary open access archive for the deposit and dissemination of scientific research documents, whether they are published or not. The documents may come from teaching and research institutions in France or abroad, or from public or private research centers.

L'archive ouverte pluridisciplinaire **HAL**, est destinée au dépôt et à la diffusion de documents scientifiques de niveau recherche, publiés ou non, émanant des établissements d'enseignement et de recherche français ou étrangers, des laboratoires publics ou privés.



UNIVERSITÉ  
— PARIS-EST



Université Paris-Est Créteil  
École Doctorale: Sciences, Ingénierie et Environnement

### Thesis

To obtain Ph.D. degree from the Université Paris-Est Créteil, France  
Specialty: Materials Science

# Experimental determination and thermodynamic modeling of the Mo-Ni-Re ternary system

Submitted by: Khurram YAQOOB

Thesis defense: December 20, 2012

### Jury

Pr. Jacques LACAZE	ENSIACET, Toulouse, France	Reporter
Pr. Peter Franz ROGL	University of Vienna, Austria	Reporter
Dr. Radovan ČERNÝ	University of Geneva, Switzerland	Examiner
Pr. Catherine COLINET	SIMAP, Grenoble, France	Examiner
Pr. Bo SUNDMAN	KTH, Stockholm, Sweden	Examiner
Dr. Jean-Marc JOUBERT	CNRS, Thiais, France	Thesis director



## Abstract

The Mo-Ni-Re system is one of the important subsystems of the Ni based superalloys engineered for use in high temperature applications. Considering the contradictions among previously reported information, the present study was devoted to the complete experimental determination of the phase equilibria in the Mo-Ni-Re system, structural characterization of its intermetallic phases and thermodynamic modeling of the system with the help of the CALPHAD method. The experimental investigation of phase equilibria was carried out with the help of equilibrated alloys and phase diagrams of the Ni-Re and Mo-Ni-Re system (at 1200°C and 1600°C) were proposed. In comparison with previous investigations, the Ni-Re phase diagram determined during the present study showed significant differences in terms of homogeneity domains, freezing ranges and peritectic reaction temperature. The 1200°C isothermal section of the Mo-Ni-Re system proposed during the present study showed large extension of the Mo-Re  $\sigma$  phase and Mo-Ni  $\delta$  phase in the ternary region. In addition, presence of two previously unknown ternary phases was also observed. The isothermal section of the Mo-Ni-Re system at 1600°C also showed large extension of  $\sigma$  phase in the ternary region whereas extension of the Mo-Re  $\chi$  phase in both isothermal sections was restricted to narrow composition range. The presence of ternary phases observed in the 1200°C isothermal was not evidenced in 1600°C isothermal section. On the other hand, partial investigations of phase boundaries in the Mo-Ni and Mo-Re binary systems and determination of liquidus projection of the Mo-Ni-Re system was also carried out. The liquidus projection of the Mo-Ni-Re system proposed during present study also showed largely extended primary crystallization fields of the Mo-Re  $\sigma$  phase and Re solid solution in the ternary region. Since isothermal sections of the Mo-Ni-Re system showed largely extended homogeneity domain of  $\sigma$ , structural characterization of the Mo-Ni-Re  $\sigma$  with particular emphasis on determination of site occupancy trends as a function of composition was carried out by combined Rietveld refinement of the X-ray and neutron diffraction data. The experimental results gathered during the present study along with the information available in the literature were used as input for thermodynamic modeling of the Mo-Ni-Re system. The thermodynamic description of the Mo-Re system was taken from literature whereas thermodynamic modeling of the Mo-Ni, Ni-Re and Mo-Ni-Re system was carried out during the present study with the help of the CALHAD method.

Keywords: Mo-Ni; Mo-Re; Ni-Re; Mo-Ni-Re; phase diagram; isothermal section; structural characterization; thermodynamic modeling; CALPHAD method.

## Résumé

Le système Mo-Ni-Re est un sous-système majeur des superalliages à base de Ni conçus pour une utilisation dans les applications à haute température. Compte tenu des contradictions entre les informations publiées antérieurement, cette étude a été consacrée à la détermination expérimentale complète des équilibres entre phases dans le système Mo-Ni-Re, à la caractérisation structurale des phases intermétalliques et à la modélisation thermodynamique du système à l'aide de la méthode CALPHAD. L'étude expérimentale des équilibres entre phases a été effectuée en utilisant des alliages à l'équilibre, et les diagrammes de phases du système Ni-Re et Mo-Ni-Re (à 1200°C et à 1600°C) ont été proposées. En comparaison avec les études précédentes, le diagramme de phases Ni-Re déterminé au cours de ce travail a montré des différences significatives en termes de domaines d'homogénéité, des domaines de cristallisation et de température de réaction péritectique. La coupe isotherme à 1200°C du système Mo-Ni-Re proposée lors de cette étude a montré l'extension importante de la phase  $\sigma$  du système binaire Mo-Re et de la phase  $\delta$  du système Mo-Ni dans le diagramme ternaire. En outre, la présence de deux phases ternaires jusque-là inconnues a également été observée. La coupe isotherme du système Mo-Ni-Re à 1600°C a également montré une grande extension de la phase  $\sigma$  dans le diagramme ternaire tandis que l'extension de la phase  $\chi$  du système Mo-Re dans les deux coupes isothermes est limitée à un étroit domaine de composition. Les phases ternaires observées dans la coupe isotherme à 1200°C ne sont pas présentes dans la coupe isotherme à 1600°C. D'autre part, les études partielles des domaines de composition des phases dans les systèmes binaires Mo-Ni et Mo-Re ainsi que la détermination de la projection du liquidus du système Mo-Ni-Re ont également été effectuées. La projection du liquidus du système Mo-Ni-Re proposée lors de la présente étude a également montré des champs de cristallisation primaire de la phase  $\sigma$  de système Mo-Re et la solution solide de Re dans la région ternaire qui sont largement étendus. Puisque la coupe isotherme du système Mo-Ni-Re a montré un domaine d'homogénéité de la phase  $\sigma$  très étendu, la caractérisation structurale de la phase  $\sigma$  du système ternaire Mo-Ni-Re a été effectuée en mettant l'accent sur la détermination de l'occupation des sites en fonction de la composition par affinement de Rietveld combiné des données de diffraction des rayons X et des neutrons. Les résultats expérimentaux recueillis au cours de cette étude ainsi que les informations disponibles dans la littérature ont été utilisés comme données d'entrée pour la modélisation thermodynamique du système Mo-Ni-Re. La description thermodynamique du système Mo-Re a été prise de la

littérature tandis que les optimisations thermodynamiques des systèmes Mo-Ni, Ni-Re et Mo-Ni-Re ont été effectuées au cours de ce travail avec la méthode CALHAD.

Mots-clés: Mo-Ni, Mo-Re, Ni-Re, Mo-Ni-Re; diagramme de phases; coupe isotherme; caractérisation structurale; modélisation thermodynamique; méthode CALPHAD

## Acknowledgement

Before presenting results of this work, I would like to acknowledge the support of many people without whom I would not have completed the program.

First and Foremost, I would like to thank Michel Latroche (Director of the team CMTR in 2009) who placed me with complete generosity as a PhD student in his team at Institut de Chimie et des Matériaux Paris-Est (ICMPE), Thiais, France. I express my deep and sincere gratitude to Dr. Jean-Marc Joubert who provided me with the opportunity to do PhD under his supervision. His guidance, encouragement, support and availability helped me a lot in conducting thesis research work as well as in writing of research articles and thesis manuscript.

Besides my PhD supervisor, I am grateful to rest of my thesis committee: Prof. Jacques Lacaze from ENSIACET Toulouse, Prof. Peter Franz Rogl from University of Vienna Austria, Dr. Radovan Černý from University of Geneva Switzerland, Prof. Catherine Colinet from SIMAP Grenoble, and Prof. Bo Sundman from KTH Sweden for taking out the time to read and evaluate the present work.

The work carried out in this thesis has been part of a much larger project named as ARMIDE dedicated to the study of rhenium alloys. I would like to extend my sincere thanks to all the members of ARMIDE group specially to our lab colleague Jean-Claude Crivello for performing DFT calculations and to Prof. Jean-Marc Fiorani of Institut Jean Lamour Nancy and Nathalie Dupin of Calcul Thermodynamique Orcet for precious discussions and useful suggestions.

I am highly grateful to Eric Leroy for performing EPMA measurements and to Rémy Pires Brazuna and Marie-France Trichet for their assistance in the use of scanning electron microscope. I would also like to pay thanks to Florence Porcher of Laboratoire Léon Brillouin for conducting neutron diffraction measurements and to Radovan Černý and Laure Guénée from University of Geneva Switzerland for performing single crystal diffraction experiments. I am also grateful to Valérie Lalanne, Fabrice Couturas, Benjamin Villeroy, Olivier Rouleau and Léon Preira for their technical assistance in the use of different apparatus and to all those persons (Permanent and Trainees) who in the team CMTR have indirectly supported me during three years of my PhD.

I am highly thankful to my fellow PhD students Hoda Emami Meibody and Aurore Mascaro with whom I shared an office and to all other fellow PhD students in the team CMTR for creation of a pleasant and friendly atmosphere and sharing their experience and knowledge.

The scholarship offered by Higher Education Commission (HEC) Pakistan has provided me an opportunity to carry out Masters leading to PhD studies in France. My PhD thesis research work was a part of the Project ARMIDE funded by Agence Nationale de la recherche (ANR). I would like to acknowledge both organizations for their generous support.

Last but not the least; I would like to thanks my parents for their love, support and encouragement. To them, I dedicate this thesis.

# Table of Contents

<b>Abstract .....</b>	<b>1</b>
<b>Résumé .....</b>	<b>2</b>
<b>Acknowledgement .....</b>	<b>4</b>
<b>Table of contents .....</b>	<b>6</b>
<b>List of Figures .....</b>	<b>9</b>
<b>List of Tables .....</b>	<b>14</b>
<b>List of abbreviations .....</b>	<b>16</b>
<b>Introduction .....</b>	<b>17</b>
<b>1. Context of Study .....</b>	<b>19</b>
1.1. High temperature materials .....	21
1.1.1. Superalloys .....	22
1.1.2. Classes of superalloys .....	22
1.1.3. Nickel selection as principal alloying element .....	23
1.1.4. Alloying additions and microstructure of Ni based superalloys .....	24
1.1.5. Effect of refractory elements addition on the mechanical properties .....	26
1.2. General information related to the metals used .....	28
1.3. Phase diagrams .....	30
1.3.1. Equilibrated alloy method .....	30
1.3.2. Diffusion couple method .....	31
1.3.3. Comparison of the diffusion couple and equilibrated alloy method.....	33
1.4. Thermodynamic modeling of phase diagrams .....	33
1.5. Topologically closed packed phases .....	34
1.6. Bibliographic research .....	35
1.6.1. The Mo-Ni system .....	35
1.6.2. The Ni-Re system .....	40
1.6.3. The Mo-Re system .....	44

1.6.4. The Mo-Ni-Re system .....	48
1.7. Objectives of present work .....	55
<b>2. Experimental Techniques .....</b>	<b>61</b>
2.1. Alloy preparation .....	63
2.2. Homogenization heat treatment and quenching .....	65
2.2.1. Annealing at 1200°C .....	65
2.2.2. Annealing at 1600°C .....	66
2.3. Characterization of alloys .....	67
2.3.1. X-ray diffraction (XRD) .....	67
2.3.2. Neutron diffraction (ND) .....	70
2.3.3. Analysis of the diffraction data .....	72
2.3.4. Electron probe micro analysis (EPMA) .....	74
2.3.5. Differential thermal Analysis (DTA).....	78
2.4. Conclusion of the chapter .....	80
<b>3. The Calphad Method .....</b>	<b>81</b>
3.1. Principle .....	83
3.2. Selection of data .....	84
3.3. Selection of models .....	85
3.3.1. Description of pure elements .....	85
3.3.2. Description of the stoichiometric compounds .....	87
3.3.3. Description of substitutional solutions .....	88
3.3.4. Sublattice model .....	90
3.4. Principle of optimization .....	92
3.5. Calculation of phase diagrams .....	92
3.6. Combination of phase diagrams and extrapolation.....	95
3.7. Conclusion of the chapter .....	96
<b>4. The Ni-Re System .....</b>	<b>99</b>
Introduction.....	101
Article.....	103
<b>5. The Mo-Ni-Re System.....</b>	<b>109</b>
Introduction.....	111
Article.....	113

<b>6. Structural Characterization of the Mo-Ni-Re <math>\sigma'</math> Phase .....</b>	<b>141</b>
Introduction .....	143
Article.....	145
<b>7. Structural Characterization of the Mo-Ni-Re <math>\sigma</math> Phase .....</b>	<b>155</b>
Introduction .....	157
Article.....	159
<b>8. Thermodynamic Modeling of the Mo-Ni-Re System .....</b>	<b>167</b>
8.1. The Mo-Ni binary system .....	169
8.1.1. Introduction .....	169
8.1.2. Selection of data .....	171
8.1.3. Selection of model .....	172
8.1.4. Results and discussion .....	174
8.1.5. Conclusion .....	179
8.2. The Ni-Re system .....	179
8.3. The Mo-Re system .....	179
8.4. The Mo-Ni-Re system .....	181
8.4.1. Selection of data .....	181
8.4.2. Selection of model .....	181
8.4.3. Results and discussion .....	187
8.4.4. Conclusion .....	193
8.5. Conclusion of the chapter .....	194
<b>Conclusion and Perspectives .....</b>	<b>197</b>
<b>Annexes .....</b>	<b>205</b>
Annex I.....	207
Annex II.....	210
Annex III .....	211

## List of Figures

<b>Chapter 1.....</b>	<b>19</b>
Figure 1-1: Microstructure of a single crystal superalloys [3] .....	25
Figure 1-2: Variations of the diffusion couples .....	31
Figure 1-3: Mo-Ni phase diagram proposed by Casselton et al. [26] .....	36
Figure 1-4: Ni-Re phase diagram suggested by Pogodin et al. [33] .....	41
Figure 1-5: Ni-Re phase diagram suggested by Savitskii et al. [34].....	42
Figure 1-6: Ni-Re phase diagram proposed by Nash et al. and its comparison with other investigations.....	43
Figure 1-7: Mo–Re phase diagram assessed by Brewer et al. [54] .....	44
Figure 1-8: Preliminary investigation of Mo-Ni-Re system at 1200°C by Burhanov et al. [62] .....	49
Figure 1-9: Isothermal cross-section of the Mo-Ni-Re system at 1152°C proposed by Kodentsov et al. [6] .....	50
Figure 1-10: Isothermal cross-section of the Mo-Ni-Re system at 1152°C proposed by Borisov et al. and Slyusarenko et al. [7, 8] .....	51
Figure 1-11: Isothermal cross-section of the Mo-Ni-Re system at 1200°C proposed by Feng et al. [9] .....	53
<b>Chapter 2.....</b>	<b>61</b>
Figure 2-1: Schematic (left) and photograph (right) of the electric arc furnace used for the alloy preparation during the present study .....	64
Figure 2-2: Alloys encapsulated in silica tubes under argon atmosphere (left) and resistance furnace used for annealing (right) .....	66
Figure 2-3: Schematic (left) and photograph (Right) of the high frequency induction furnace used for annealing at 1600°C .....	67
Figure 2-4: Bragg’s Law .....	68
Figure 2-5: Bruker D8 advance diffractometer .....	70
Figure 2-6: Schematic of the LLB 3T2 diffractometer .....	71

Figure 2-7: Physical phenomena underlying the operation of electron probe micro analyzer.	74
Figure 2-8: Schematic diagram of electron probe microanalyzer .....	76
Figure 2-9: Sorting of EPMA data for determining phase composition .....	77
Figure 2-10: Schematic of the differential thermal analyzer.....	79
<b>Chapter 3.....</b>	<b>81</b>
Figure 3-1: Reference Gibbs energy of the hcp phase in a binary system A-B when A and B has different SER states.....	87
Figure 3-2: Plot of reference term (a), ideal term (b) and excess terms ( ${}^0L$ to ${}^3L$ )(c) and effect of different values of ${}^0L$ term on the total Gibbs energy curve (d) .....	90
Figure 3-3: Phase diagram of the binary system A-B with their corresponding Gibbs energy curves at 200°C and 480°C .....	94
Figure 3-4: Ternary extrapolation methods presented graphically .....	96
<b>Chapter 4 .....</b>	<b>99</b>
Figure 1: Recently published experimental data superimposed on the Ni-Re phase diagram assessed by Nash [1] .....	104
Figure 2: XRD plot and BSE image of Ni <sub>52</sub> Re <sub>48</sub> annealed at 1500°C for 10 hours.....	105
Figure 3: DTA scans for Ni <sub>50</sub> Re <sub>50</sub> composition at 10°C/min (left) and 5°C/min (right) .....	106
Figure 4: DTA scans for Ni <sub>90</sub> Re <sub>10</sub> composition at 10°C/min (left) and 5°C/min (right) .....	106
Figure 5: Ni-Re phase diagram according to the present study .....	106
Figure 6: Comparison of the present (solid) and previously (dashed) suggested experimental Ni-Re phase diagram [1] .....	107
Figure 7: Calculated Ni-Re phase diagram .....	108
<b>Chapter 5.....</b>	<b>109</b>
Figure 1: Previous investigations of the Mo-Ni-Re system: (a) Kodentsov et al. [2], (b) Borisov et al. [3], and (c) Feng et al. [5] .....	133
Figure 2: Isothermal section of the Mo-Ni-Re system at 1200°C proposed during the present study .....	134

Figure 3: Back scattered electron images of (a) a two phase sample annealed at 1200°C (number 14 in table 1), (b) a three phase sample annealed at 1200°C (number 18 in table 1), (c) a two phase sample showing presence of liquid at 1600°C (number 15 in table 3) (d) as-cast sample (number 24 in Figure 5).....	135
Figure 4: Isothermal section of the Mo-Ni-Re system at 1600°C proposed during the present study .....	136
Figure 5: Partial liquidus projection of the Mo-Ni-Re system.....	137
Figure 6: Variation of unit cell volume of (a) (Re) phase as a function of Ni content at 1200°C, (b) (Re) phase as a function of Ni content at 1600°C, (c) $\sigma$ phase as a function of Ni content at 1200°C (d) $\sigma$ phase as a function of Ni content at 1600°C (e) $\delta$ phase as a function of Re content at 1200°C. ....	138
Figure 7: Comparison of the 1200°C isothermal section proposed during present study with the tie lines determined by (a) Borisov et al. [3], and (b) Feng et al. [5]. ....	139
<b>Chapter 6.....</b>	<b>141</b>
Figure 1: Rietveld refinement of the XRD pattern with $\sigma$ phase. ....	150
Figure 2: Comparison between the measured XRD powder pattern and that simulated from the single crystal XRD images. ....	151
Figure 3: Reciprocal lattice of the $\sigma'$ phase from the single crystal diffraction along two planes: 0kl on (a) and h1l on (b). Additional diffraction spots indexed approximately with a modulation vector 0,0,0.2 are indicated by dashed lines. ....	152
Figure 4: Reciprocal lattice of the $\sigma'$ phase from the single crystal diffraction along the plane $hk\bar{2}$ . ....	153
<b>Chapter 7.....</b>	<b>155</b>
Figure 1: Crystal structure of the $\sigma$ phase .....	159
Figure 2: Plot of the compositions studied experimentally and by DFT calculations. The area surrounded by green dashed lines represents the indicative homogeneity domain of Mo-Ni-Re $\sigma$ phase at 1873 K. The positions of the experimentally studied compositions named as N <sub>1</sub> , N <sub>2</sub> and N <sub>3</sub> , are symbolized by blue filled circles whereas the empty blue circle represents the composition studied previously <sup>[5]</sup> . The two blue dashed lines i.e. L <sub>1</sub> and L <sub>2</sub> , correspond to sections studied by DFT calculations. The 90 unique compositions generated during DFT	

calculations by the ordered distribution of 3 elements on the 5 sites of the  $\sigma$  phase are indicated by black squares. Among the 90 unique compositions, 26 compositions are located on the ground state surface and are symbolized by red squares whereas among 26 compositions, 11 compositions present negative heats of formation and are indicated by red filled squares. .... 161

Figure 3: Combined Rietveld refinement of the X-ray (left) and neutron (right) diffraction patterns of the sample composition  $N_2$ . The experimental curves are symbolized as black dots, calculated ones as red lines, Bragg positions as vertical green marks and the difference between experimental and calculated curves as a blue line situated under the vertical green marks. .... 162

Figure 4: Calculated heats of formation  $\Delta H_{ijklm}^{for,\sigma}$  of the 32 configurations in the 3 binaries Ni-Re, Mo-Re, Mo-Ni  $\sigma$  phase with respect to SER states. The Gibbs energy lines obtained in the BW approximation are displayed at 100, 1000 and 2000K. .... 163

Figure 5: The Gibbs energy surface of the Mo-Ni-Re  $\sigma$  phase obtained in the BW approximation are displayed at 100 K. Corresponding iso-contour plots at 100 and 1000 K are also presented. .... 164

Figure 6: Comparison of experimental and calculated site occupancies of Mo-Ni-Re  $\sigma$  phase at 1873 K along the line  $L_1$  of the Fig. 2. The squares and lines correspond to the experimental ( $N_1$  and  $N_2$ ) and calculated site occupancies respectively. .... 164

Figure 7: Comparison of experimental and calculated site occupancies of Mo-Ni-Re  $\sigma$  phase at 1873 K along the line  $L_2$  of the Fig. 2. The squares correspond to the experimental ( $N_3$  and experimental data from literature [5]) and the lines to the calculated site occupancies. .... 165

**Chapter 8..... 167**

Figure 8-1: Comparison of calculated Mo-Ni phase diagram before optimization with experimental data ..... 175

Figure 8-2: Comparison of calculated Mo-Ni phase diagram after optimization with experimental data [9, 12, 13]..... 176

Figure 8-3: Mo-Ni ground state ..... 177

Figure 8-4: Comparison of calculated enthalpies of mixing of bcc referred to bcc-Ni and bcc-Mo and enthalpies of mixing of fcc referred to fcc-Ni and fcc-Mo with SQS values for bcc and fcc structure ..... 178

Figure 8-5: Comparison of calculated activity of Mo (in fcc and $\delta$ phase) with experimental data .....	178
Figure 8-6: Position of end-members of $\delta$ phase, $\sigma'$ phase, phase with structural prototype $\text{Mo}_3\text{CoSi}$ and unique configurations of $\chi$ phase .....	187
Figure 8-7: Calculated 1200°C isothermal section before optimization .....	188
Figure 8-8: Comparison of experimental (blue dashed lines) and calculated 1200°C (solid black line) isothermal section after optimization .....	190
Figure 8-9: Comparison of experimental (blue dashed lines) and calculated 1600°C (solid black line) isothermal section after optimization .....	190
Figure 8-10: Calculated Mo-Ni-Re isothermal section at 1300°C .....	192
Figure 8-11: Calculated Mo-Ni-Re isothermal section at 1400°C .....	193
Figure 8-12: Calculated Mo-Ni-Re isothermal section at 1500°C .....	193

## List of Tables

<b>Chapter 1</b> .....	<b>19</b>
Table 1-1: Compositional ranges of major alloying elements in superalloys [2] .....	25
Table 1-2: Crystal structure information of Mo, Ni and Re [14] .....	29
Table 1-3: Comparison of the previous investigations of the Mo-Ni system .....	38
Table 1-4: Crystallographic data of the $\delta$ phase [30] .....	39
Table 1-5: Crystallographic data of the $\gamma$ -phase [25] .....	40
Table 1-6: Crystallographic data of the $\beta$ -phase [32] .....	40
Table 1-7: Crystallographic data of the $\sigma$ -phase [57].....	47
Table 1-8: Crystallographic data of the $\chi$ -phase [57].....	48
Table 1-9: Comparison of different investigations of the Mo-Ni-Re system .....	54
<b>Chapter 4</b> .....	<b>99</b>
Table 1: Metallurgical characterization results of the equilibrated arc melted alloys .....	104
Table 2: Thermal analysis results of the studied compositions .....	105
Table 3: List of optimized parameters (J/mol of the formula unit) .....	107
<b>Chapter 5</b> .....	<b>109</b>
Table 1: Characterization results of the samples annealed at 1200°C. Standard deviation of the last significant digit is indicated in parentheses. ....	129
Table 2: Crystal structure information of the phases appearing in the 1200°C isothermal section of Mo-Ni-Re system .....	131
Table 3: Characterization results of the samples annealed at 1600°C. Standard deviation of the last significant digit is indicated in parentheses .....	132
<b>Chapter 6</b> .....	<b>141</b>
Table 1: Structural parameters of the average structure of $\sigma'$ phase, s.g. $P4_2nm$ , $a=9.2851(19)$ , $c=4.912(3)$ Å .....	149
<b>Chapter 7</b> .....	<b>155</b>
Table 1: Rietveld refinement details of the experimentally studied compositions .....	160

Table 2: Occupancy factors for the composition $N_1$ , $N_2$ and $N_3$ .....	162
Table 3: Energetic and crystallographic property comparison between experiments and calculations with two different functionals in the $Mo_xRe_{1-x}$ system .....	163
<b>Chapter 8</b> .....	<b>167</b>
Table <b>Error! No text of specified style in document.</b> -1: Calculated values of enthalpies of mixing (in bcc and fcc phases) and enthalpies of formation ( $\delta$ , $\gamma$ and $\beta$ phases) used for thermodynamic modeling of the Mo-Ni system [2].....	171
Table <b>Error! No text of specified style in document.</b> -2: Thermodynamic parameters of the Mo-Ni binary system .....	176
Table <b>Error! No text of specified style in document.</b> -3: Thermodynamic models for $\sigma$ and $\chi$ phases used in previous Mo-Re assessments [18-20] .....	180
Table <b>Error! No text of specified style in document.</b> -4: Thermodynamic models for $\sigma$ and $\chi$ phases used by Nathalie Dupin [1].....	180
Table <b>Error! No text of specified style in document.</b> -5: Enthalpies of formation of $\delta$ phase and phase with prototype $Mo_3CoSi$ obtained with the help of DFT calculations [21] .....	181
Table <b>Error! No text of specified style in document.</b> -6: Optimized parameters of the Mo-Ni-Re system.....	189
<b>Annexes</b> .....	<b>205</b>
Table A-I: Enthalpies of formation of the Mo-Ni-Re $\sigma$ phase obtained with the help of DFT calculations by J.-C Crivello [1] .....	207
Table A-II: Enthalpies of formation of the Mo-Ni-Re $\chi$ phase obtained with the help of DFT calculations by J.-C Crivello unpublished work [2].....	210

## List of abbreviations

The abbreviations used during the present manuscript are listed below in alphabetical order.

bcc: body centered cubic

BSE: Back Scattered Electrons

CN: Coordination Number

DFT: Density Functional Theory

DTA: Differential Thermal Analysis

EPMA: Electron Probe Micro Analysis

fcc: face centered cubic

hcp: hexagonal closed packed

ND: Neutron Diffraction

PGMs: Platinum Group Metals

SEM: Scanning Electron Microscope

SER: Stable Element Reference

SGTE: Scientific Group Thermodata Europe

SQS: Special Quasirandom Structures

TCP: Topologically closed packed

WDX: Wavelength Dispersive X-ray spectroscopy

XRD: X-Ray Diffraction

## Introduction

Nickel based superalloys are commonly employed for high temperature applications. One of their most important applications includes turbine blades used in the jet engines. The efficiency of a jet engine depends on the turbine entry temperature (TET) and can be improved if Ni based superalloys capable of bearing higher TET can be developed. To improve their high temperature properties, several alloying additions are made. Molybdenum and rhenium (despite of its small abundance in nature and very high cost), are ranked among the highly interesting elements for development of the Ni based superalloys. They increase stability, creep resistance and high temperature strength because of their high melting temperatures. However, if their concentration is too large, topologically closed-packed (TCP) phases also called as Frank-Kasper phases may precipitate. The TCP phases are brittle intermetallic phases and have detrimental effect on the mechanical properties. The precipitation of the TCP phases depletes the matrix of molybdenum and rhenium and reduces their strengthening effect which may decrease service life of the material. In addition, precipitation of the TCP phases is frequently associated with void formation which may acts as initiation sites for fracture [1]. Therefore, formation of TCP phases in general should be avoided and for that, concentrations of the TCP phase forming elements should not exceed a certain limit.

To avoid the precipitation resulting by addition of Mo and Re, phase equilibria investigation of the Mo-Ni-Re system is of primary importance. Some attempts have been previously made to investigate Mo-Ni-Re system. However, comparison of such attempts revealed contradictory results. Therefore, in order to develop a better understanding of the Mo-Ni-Re system, its complete experimental redetermination was required. In recent years, the field of computational modeling of phase diagrams has completely renewed the possibility of prediction of precipitation in multi-component systems. The Calphad method yields very good results provided that simple subsystems have been well described thermodynamically. Therefore, during the present study, complete investigation of the Mo-Ni-Re system was carried out with the following objectives:

- Experimental investigation of the phase equilibria
- Structural characterization of the intermetallic phases
- Thermodynamic modeling of the system with the help of the Calphad method

Due to contradictions in the existing literature of the related binary systems, redetermination of the Ni-Re binary system and confirmation of the phase boundaries in other related binary systems was required and was also planned to be carried out.

The first chapter of the thesis manuscript starts with an introduction to the Ni based superalloys, its microstructure, different alloying additions and effect of TCP phase precipitation on the mechanical properties. A brief introduction to the commonly used methods for experimental determination of the isothermal sections and significance of thermodynamic modeling is also provided. After introducing Ni based superalloys and methods for the study of phase equilibria, the bibliographic research carried out on the Mo-Ni-Re and its related binary systems is presented. The goals defined for the duration of this Ph.D. thesis are presented at the end of the chapter.

In order to achieve the goals defined in chapter 1, experimental as well as computational methods have been employed. The experimental techniques used during the course of present study are presented in chapter 2 whereas the Calphad method used for thermodynamic modeling of the studied system is discussed in chapter 3.

The results gathered during the present study are discussed in detail in chapter 4 to chapter 8. Since majority of our work has already been published or submitted to different journals, most of the chapters are presented in the article format with an introduction in the context of present thesis. The results of experimental investigation and thermodynamic modeling of the Ni-Re binary system are presented in chapter 4. The results of the experimental phase equilibria investigation of the Mo-Ni-Re system are presented in chapter 5. The crystal structure identification of one of the new phases found in the Mo-Ni-Re system and structural characterization of a binary phase showing large extension in the ternary system are presented in chapter 6 and chapter 7 respectively. The experimental results reported in chapter 4 to chapter 7 were used as input data and thermodynamic modeling of the Mo-Ni-Re system was carried out with the help of the Calphad method. The results of thermodynamic modeling of the Mo-Ni-Re system are provided in chapter 8. A general discussion on the obtained results and perspectives of the present study is presented at the end.

- [1] C. M. Rae, R. C. Reed, The precipitation of topologically close-packed phases in rhenium-containing superalloys, *Acta Mater.* 49 (2001) 4113-4125.

# **Chapter 1**

## **Context of Study**



# 1. Context of Study

## 1.1. High temperature materials

Material designers have long had a need for the materials possessing elevated temperature load bearing and corrosion resistance properties for applications such as jet engines. The groups of materials that displayed characteristic of maintaining their properties at elevated temperatures were designated as the high temperature materials. The desirable characteristics of high-temperature materials include:

1. Load bearing capability at an operating temperature close to its melting. For high temperature materials, the value of the homologous temperature ( $\tau$ ) defined as the ratio of operating temperature ( $T_{oper}$ ) of a material to its melting temperature ( $T_m$ ) using the Kelvin scale, should be greater than 0.6. Therefore, a nickel based superalloy functioning at 1000°C is working at a  $\tau$  of  $(1000+273)/(1455+273) \sim 0.75$  and is therefore ranked among the high temperature materials [1].
2. Another desirable characteristic of a high temperature material is the significant resistance to the mechanical degradation over large periods of time [1]. For ordinary operating temperatures, the strength of most metals are reported in terms of yield strength or ultimate strength [2]. However, promotion of thermally activated processes at higher  $\tau$  values results in a time-dependent, inelastic and irrecoverable deformation known as creep. Therefore, creep strength of a material should also be considered for high temperature applications. The creep strain,  $\epsilon$ , accumulates with the passage of time and may lead to fracture if allowed to continue for longer periods of times [2]. Thus materials with low rates of creep accumulation are desirable for most of the applications. In addition to the creep, values of other mechanical properties such as yield strength, ultimate tensile strength and fracture toughness are also critical and should be maintained over time [1].
3. A third desirable characteristic of a high temperature material is its ability to withstand in the severe operating environments. For example high sulphur content in the hot gases generated in a coal fired electricity generating turbine or presence of impurities such as potassium salts in the kerosene used as an aeroengine fuel can cause corrosion during operation. Any surface degradation as a result of oxidation and/or corrosion under severe operating conditions may result in a drastic decrease in the components

life [1]. Although ceramics such as silicon carbide and nitride show substantial resistance to oxidation and/ or corrosion but they are not considered for such applications due to their poor toughness and ductility.

### **1.1.1. Superalloys**

The performance characteristics of any material depend upon the operating conditions. The hot sections of a jet engine have been ranked among the most demanding conditions for any structural material and therefore became a primary driver for alloy and process development and/or adaptation during the 20<sup>th</sup> century. A group of alloys developed for use in the hot section of the aircraft turbine engines that required excellent mechanical strength and corrosion resistance at higher temperatures were named as "superalloy" shortly after World War II [1]. They have been, and are still the subject of substantial research and development activity in the quest for higher strengths in severe operating conditions. After decades of basic and applied research, superalloys now show excellent resistance to mechanical and chemical degradation at elevated temperatures. As a result of their extraordinary properties, their use is not only restricted to jet engines for which first superalloys grades were designed but are now employed in wide variety of high temperature applications [1] which include steam turbine power plant components, selected automotive components, metal processing, medical components, space vehicle components, heat treating equipment, nuclear power systems, chemical and petrochemical industries. Thus, superalloys are fundamental to our society and economy [2]. The preeminence of the superalloys is also reflected in the fact that their weight percentage in an aircraft gas turbine engine has increased from 10 % in 1950s to around 50 % in 1985 [2].

### **1.1.2. Classes of superalloys**

Depending on the principal alloying elements in the composition, superalloys can be divided into three main categories:

- Co based superalloys
- Fe based superalloys
- Ni based superalloys

The Co based superalloys are not considered for turbine disc applications because of their much lower strength capability. The Fe-Ni-based superalloys which are good up to about 649 °C find their application in lower temperature discs [2]. However in case of the gas

turbines used for the jet propulsion where operating temperatures are higher than 800°C and significant resistance to loading under static, fatigue and creep conditions is required, Ni based superalloys have been considered as the materials of choice [1]. The nickel based superalloys due to their extraordinary properties are probably the most successful and most widely used alloys among different categories of superalloys. They have been discussed in detail in the following sections

The justification of Ni as a principal alloying element for high temperature applications is provided in the section 1.1.3, other alloying additions and resulting microstructure are reported in section 1.1.4 whereas effect of some important alloying additions on the mechanical properties of Ni based superalloys is discussed in the section 1.1.5.

### **1.1.3. Nickel selection as principal alloying element**

Ni has been considered as the most suitable principal alloying element for the high temperature applications. In this section, factors contributing in the selection of Ni as a solvent for high temperature alloys and its preeminence over other metals employed for the same purpose have been discussed.

Firstly Ni belongs to the group of transition metals. It has the face-centered cubic structure (fcc) structure and is therefore both tough and ductile. Other metals in the transition metal series that possess the fcc crystal structure are limited in number and belong to the platinum group metals (PGMs) which are characterized by their high density and cost. Secondly, Ni remains stable in its fcc structure and undergoes no phase transformation until it melts that makes it suitable for high temperature applications. Thirdly, it has low rates of thermally activated creep due to low diffusion rates in Ni and consequently shows a considerable microstructural stability at elevated temperatures [1].

Among the elements displaying hcp crystal structure, only Co shows an acceptable density and cost. Therefore, it has also been used as principal alloying element for superalloys. In comparison with Ni, Co is relatively more expensive and also undergoes phase transformation from fcc to hcp structure at around 417°C. On the other hand, bcc metals such as Cr exhibit a ductile-brittle transformation. The toughness of these metals decreases significantly with decreasing temperature and may show a brittle fracture at low temperature regimes [1].

### 1.1.4. Alloying additions and microstructure of Ni based superalloys

In order to improve the high temperature properties of the Ni based superalloy, a wide variety of alloying elements are added in different proportions. The number of alloying elements in superalloys is usually greater than ten. Therefore, in terms of number of alloying elements, they can be considered as the most complex engineering materials. The role played by each alloying element strongly depends upon its position within the periodic table. Most of the alloying elements added in the Ni based superalloys belong to the d-block of the transition metals [1]. Depending on the role played by each alloying element, the alloying additions made in the nickel based superalloys can be divided in to three main categories.

#### 1. $\gamma$ formers

A first category of elements including cobalt, iron, chromium, ruthenium, molybdenum, rhenium and tungsten are known as austenitic  $\gamma$  phase formers. The atomic radii of these alloying elements are not very different from that of the primary matrix element i.e. Ni [1]. Addition of these alloying elements increases strength (molybdenum, tungsten, and rhenium), oxidation resistance (chromium), hot corrosion resistance (titanium), and volume fractions ( $V_f$ ) of favorable secondary precipitates (cobalt) [2].

#### 2. $\gamma'$ formers

The elements such as titanium, aluminum, tantalum and niobium constitute a second group of elements and favors the formation of ordered phases such as the compound  $\text{Ni}_3(\text{Al,Ta,Ti})$ , also known as  $\gamma'$  phase. The atomic radii of the  $\gamma'$  formers are greater than principal alloying element i.e. Ni [1].

#### 3. Grain boundary effect

A third group of the alloying elements added to the Ni based superalloys consist of boron and carbon. The atomic radii of these elements are very different from that of Ni. Due to their smaller atomic size, these elements tend to segregate to the grain boundaries of the  $\gamma$  phase and promote grain boundary effect. In addition, carbon and boron also form carbides and borides. The elements such as chromium, molybdenum, tungsten, niobium, tantalum and titanium are considered as strong carbide formers whereas chromium and molybdenum also enhance the borides formation [1].

The compositional ranges of some important alloying elements in the nickel based superalloys have been provided in Table 1-1.

Table 1-1: Compositional ranges of major alloying elements in superalloys [2]

Elements	Cr	Mo	W	Al	Ti	Co	Nb	Ta	Re
Compositional range (wt. %)	5-25	0-12	0-12	0-6	0-6	0-20	0-5	0-12	0-6

As a result of the above mentioned alloying additions, the microstructure of the Ni based superalloys consists of the following phases:

1. **Gamma ( $\gamma$ ):** All nickel-base superalloys contain a nickel-base austenitic gamma ( $\gamma$ ) phase that forms a continuous matrix phase in which other phases reside. It displays the face-centered-cubic (fcc) crystal structure and usually contains a high percentage of solid-solution elements [1, 2].
2. **Gamma Prime ( $\gamma'$ ):**  $\text{Ni}_3(\text{Al,Ti})$ , named as the gamma prime ( $\gamma'$ ) phase, is the primary strengthening phase in nickel-based superalloys. Other elements such as niobium, tantalum, and chromium also enter  $\gamma'$  phase. It also exhibits the fcc crystal structure and forms as a precipitate phase, which is usually coherent with the austenitic  $\gamma$  matrix [1, 2]. As a result of the close match in the lattice parameters of the  $\gamma$  matrix and  $\gamma'$  precipitates and chemical compatibility, it precipitates homogeneously throughout the matrix.

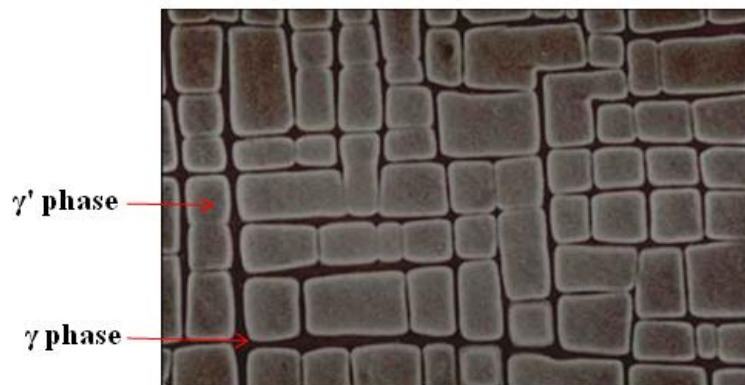


Figure 1-1: Microstructure of a single crystal superalloys [3].

3. **Carbides and Borides:** Carbon is usually added at the levels of up to 0.2 wt.% which in the presence of reactive and refractory elements such as titanium, tantalum and hafnium forms metal carbides (MC). These metal carbides (MC) may decompose during heat treatment and/or service to form lower carbides such as  $\text{M}_{23}\text{C}_6$  and  $\text{M}_6\text{C}$  that tend to reside on the  $\gamma$ -grain boundaries. In case of the superalloys with the grain

boundaries, the presence of carbides is generally considered beneficial as it can increase their rupture strength at elevated temperature. On the other hand boron in the presence of elements such as chromium or molybdenum may form borides which also prefer to reside on the  $\gamma$ -grain boundaries [1, 2]

- 4. Topologically Close-Packed Phases (TCP):** During heat treatment or service, some solid solution strengtheners i.e.  $\gamma$  formers, may result in the precipitation of topologically close-packed phases (TCP). These phases have been ranked among the undesirable phases due to their detrimental effect on the mechanical properties. The compositions of superalloys are carefully selected to avoid precipitation of TCP phases [1, 2, 4].

### **1.1.5. Effect of refractory elements addition on the mechanical properties**

The thermodynamic efficiency of a turbine engine can be improved by increasing the turbine entry temperature (TET) which depends on the high temperature strength of the Ni based superalloys employed in the hottest sections of the turbo machinery. As discussed in the section 1.1.4, several alloying additions are made to improve high temperature properties of Ni based superalloys. The addition of the refractory elements such as W, Ta, Mo, Ru in general and Re in particular to the Ni based superalloys, imparts significant resistance to creep deformation at higher temperatures and therefore they are also called as creep strengthening elements. The extent of improvement in the creep resistance by addition of the refractory elements can be shown by considering creep rupture lives of the first-, second-, and third generation single crystal superalloys. In case of operating conditions such as 850°C/500 MPa, the creep rupture lives of Ni based superalloys has improved ten-fold from 250 hours for a first generation alloy superalloy such as SRR99 to about 2500 hours for a third generation alloys such as CMSX-10/RR3000. In case of more demanding conditions, for example 1050°C/150MPa, the creep rupture life has improved from 250 hours to 1000 hours. The major differences between the composition of these first-, second-, and third-generation alloys lies in the Re concentration. Rhenium was absent in the first-generation single crystal superalloys, the second-generation alloys contained about 3 % by weight of Re, with higher concentrations of the Re (between 5 and 6 wt %) in third-generation alloys. Therefore a strong creep strengthening effect can be attributed to Re. The elements which diffuse slowly in nickel are considered to be the best strengtheners because of low rates of thermally activated creep [1].

However, concentration of the refractory elements in the Ni based superalloys should not exceed a certain amount. Higher quantities of the refractory elements such as Mo, W, Ta, Re and Ru may lead to the precipitation of topologically close-packed (TCP) phases also called as Frank-Kasper phases [5-11]. These are brittle intermetallic phases usually formed between the transition metal elements, and as the name suggest, are characterized by high compactness.

The precipitation of the TCP phases in the Ni based superalloys has a detrimental effect on their mechanical properties. Besides their ductility shortcomings, the extent of degradation in the mechanical properties due to the presence of the TCP phases depends to a large extent on the following [2]:

- Phase morphology
- Volume fraction of TCP phase
- The extent to which TCP phase may deplete the  $\gamma$  matrix of alloy elements required for  $\gamma$  or  $\gamma'$  strengthening

The TCP phases usually display plate or a needle like structure which adversely affects ductility and creep-rupture strength of the material. The extent of degradation in the mechanical properties also depends on the volume fraction of the TCP phases. In principle, the TCP phases should not be present in more than trace amounts. The volume fraction of the  $\gamma'$  phase in the Re containing superalloys can be as high as 0.70, and as a result the refractory elements may concentrate in the  $\gamma$  phase and exacerbate the TCP formation [4]. Unfortunately TCP phases are usually composed of the elements (Ni, Cr, Mo, Co, W and Re), which are considered as most effective at imparting resistance to creep deformation in the Ni based superalloys. Any precipitation of TCP phases during service may reduce the solid strengthening effect achieved by addition of refractory elements to the matrix phase [4]. In addition, TCP phase precipitation at elevated temperatures is usually accompanied by the void formation which may act as initiation sites for fracture [12]. Therefore TCP phase precipitation and resulting degradation in the mechanical properties may contribute in decreasing the service life of the Ni based superalloys.

The TCP phases may not necessarily be present as a constituent phase in a given superalloy, but may form as result of minor composition variations. For example,  $\mu$  phase was not evidenced during the study of a cast nickel-base superalloy consisting of 10 wt % W and normal carbon contents. However, when the carbon content was reduced in the alloy,

formation of the  $\mu$  phase took place. In fact, reduction of the carbon content in the alloy made more tungsten available which resulted in the formation of the  $\mu$  phase. The problem of the  $\mu$  phase precipitation was resolved by restoring the carbon content in the alloy [2].

To conclude, high temperature properties of the Ni based superalloys can be significantly improved by addition of the mentioned refractory element but their concentration should not be high enough to yield precipitation of the topologically closed packed phases. Therefore in order to avoid precipitation of the TCP phases, selection of the superalloy composition during the alloy design process is very critical. In this respect, binary and ternary phase diagrams of refractory elements with Ni can be helpful in understanding phase relationships and would therefore serve as a guideline for the selection of a suitable alloy composition. Another useful tool for development of alloys and prediction of precipitation is the thermodynamic modeling with the help of the Calphad method. This technique consists in extrapolating the description of subsystems into multi-component systems to be able to predict phase equilibrium.

Considering the solid solution strengthening effect of molybdenum and remarkable improvement in the high temperature properties (such as creep strength) by addition of the Re, the study of Mo-Ni-Re system is of primary importance for the development of Ni based superalloys. Therefore, it has been selected as the subject of present study. In this regard, some basic information about Mo, Ni and Re elements is provided in the section 1.2, experimental methods used for determination of phase diagrams are presented in the section 1.3, a very brief introduction to thermodynamic modeling of phase diagrams is given in the section 1.4, previously existing data on the Mo-Ni-Re and its related binary system are discussed in the section 1.6 and the goals set for the present study in the light of previously bibliographic research are introduced in the section 1.7.

## **1.2. General information related to the metals used**

### **Molybdenum**

The atomic number of Mo is 42 and is a second-row transition element in the group 6 of the periodic table. The atomic weight is 95.94. It has a bcc crystal structure. The melting temperature of Mo is 2623°C which is the sixth highest melting temperature of any element. The density under ambient conditions is 10.2 g/cm<sup>3</sup>. It shows a good corrosion and wear characteristics and is used in many stainless steels. However it oxidizes rapidly at 600°C [13, 14].

## Nickel

It is the fifth most common naturally occurring element on earth. The atomic number of Ni is 28, which places it in the group 10 and first row of transition d-block transition metal elements. It has an atomic weight of 58.69. The melting temperature of Ni is 1453°C. As discussed earlier, Nickel displays fcc crystal structure and undergoes no phase transformation between room temperature and melting temperature which makes it a suitable candidate for the superalloys. It has a density of 8.9 g/cm<sup>3</sup> and is rather dense in comparison with other elements used for the aerospace industry such as Ti (4.508 g/cm<sup>3</sup>) and Al (2.698 g/cm<sup>3</sup>). Ni has low rates of oxidation and is considered as corrosion resistant at room temperature. Besides its use as the principal alloying element for the superalloys, most of the Ni produced every year is alloyed with steels to form stainless alloys. Other important alloys of nickel include invar (Fe-Ni alloy), nichrome (Ni-Cr alloy), platinite (Fe-Ni alloy) etc [1, 13, 14].

## Rhenium

Rhenium is one of the rarest elements in the earth's crust and because of its low availability; it is among the most expensive of metals costing approximately US\$4,600 per Kg. The atomic number of Re is 75 and this places it in the third row of the d-block transition metals alongside tantalum and tungsten. The atomic weight of rhenium is 186.207. Rhenium displays hcp crystal structure. It has a high melting temperature of 3186°C, which is the third highest after tungsten and carbon. Rhenium has fourth highest density of all elements i.e. 21 g/cm<sup>3</sup> exceeded only by platinum, iridium and osmium. The alloys of rhenium with molybdenum and tungsten are used to form filaments for lamps and ovens. Rhenium is also employed in thermocouples for measuring temperatures higher than 2000°C and for electrical contacts which stand up well to electrical arcs [13, 14].

The crystal structure information of Mo, Ni and Re is provided in Table 1-2.

Table 1-2: Crystal structure information of Mo, Ni and Re [14]

Phases	Pearson symbol	Prototype	Space group	Lattice parameters	
				<i>a</i>	<i>c</i>
Mo	<i>cI2</i>	W	$Im\bar{3}m$	3.147	-
Ni	<i>cF4</i>	Cu	$Fm\bar{3}m$	3.524	-
Re	<i>hP2</i>	Mg	$P6_3/mmc$	2.7609	4.458

### 1.3. Phase diagrams

As discussed in the section 1.1.5, properties of any material depend to a large extent on type, number, and amount of the phases present in equilibrium. Therefore, determination of the conditions under which different phases exist and transform to other phases is of primary importance. The best method of reporting such information is in the form of the phase diagram which is a graphical representation of the phase relationships in the multi-component systems [15]. In case of a binary system, interactions of the constituent elements are shown on a temperature vs. composition plot whereas for the ternary systems, phase relationships are usually studied at constant temperature and pressure. As phase diagrams report the phase relationships under equilibrium conditions, therefore, they are also called as equilibrium diagrams [15]. They play a very vital role in providing guidelines for the production, processing, and application of materials. It is therefore not surprising that substantial efforts have been made for the accurate experimental determination of phase diagrams.

To study isothermal sections of a multi-component systems, different experimental [16] and theoretical [17, 18] methods have been developed. The experimental investigation of phase equilibria is usually carried out with the help of

- Equilibrated alloy method
- Diffusion couple method

#### 1.3.1. Equilibrated alloy method

The equilibrated alloy method is a traditional and most widely used method for determination of phase diagrams. The primary step in the equilibrium alloy method consists of alloy preparation which is usually carried out either by melting or by using powder metallurgy techniques. The alloys, once prepared, are annealed at different temperatures for suitable periods of times and subjected to different characterization techniques. The main advantage of using this method is that alloys can be characterized by a number of techniques which permit determination of phase boundaries, identification of phases present in equilibrium, their structural characterization and determination of phase transformation temperatures. The equilibrated alloys method has been discussed in detail in chapter 2.

### 1.3.2. Diffusion couple method

The diffusion couple method is another useful experimental approach for determination of phase diagram. The principle of diffusion couple and its application for the determination of the multi-component phase diagram has been discussed in detail by Kodentsov et al. [19, 20]. This method is based on the assumption of local equilibria at the phase interfaces in the diffusion zone. The presence of local equilibria implies that infinitesimally thick neighboring layers in such a diffusion zone are present in thermodynamic equilibrium at the interphase interface [19, 20]. Consequently the series of layers of phases in the reaction zone and their compositions at the interfaces could be used for determination of phase diagrams.

In principle, the preparation of the solid state diffusion couple consists of bringing different materials in such an intimate contact that one diffuse into the other. The most common procedure used for the preparation of diffusion couple includes grinding and polishing the bonding faces, and clamping them together. Different variations of the diffusion couples used for the determination of a multi-component phase diagrams are shown in the Figure 1-2.

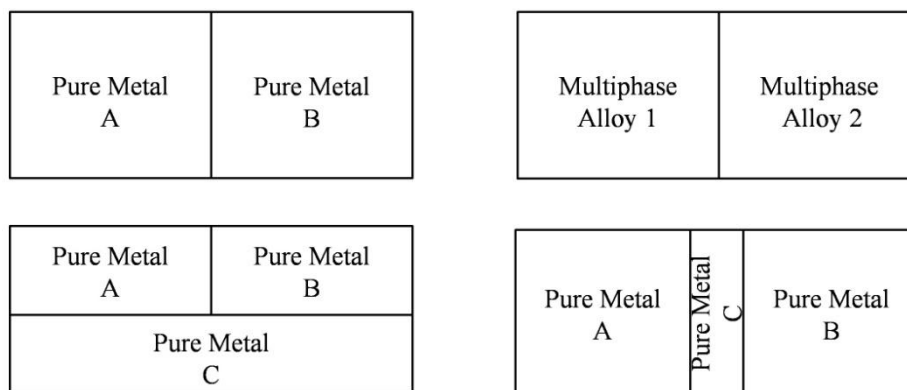


*Figure 1-2: Variations of the diffusion couples.*

The diffusion couples after preparation are annealed at the desired temperatures and chemical compositions of the diffusion layers of the reaction zone are investigated. The EPMA technique has been most commonly employed in conjunction with diffusion couple technique for chemical characterization of the diffusion zones because of its ability to investigate very small volumes. The EPMA technique performs quantitative analysis by comparing the count rates of the X-ray of a particular wavelength generated as a result of incident electron and target material interaction with the count rates obtained from pure elements used as standards. The details about the electron probe microanalysis technique are provided in chapter 2.

The main advantage of diffusion couple method is that it permits determination of the phase boundaries in a multi-component phase diagram with limited number of diffusion couples. However, identification of the phases present in equilibrium, their structural characterization, and determination of the phase transformation temperature, in general, is not possible by using diffusion couple method.

### **1.3.2.1. Error sources encountered in the diffusion couple method**

Although diffusion couple has been considered as an efficient way for the determination of phase diagrams, it also has some shortcomings. The experimental results obtained by using diffusion couple method may contain some errors resulting from the nature of the sample, experimental measurements, and development of quasi-equilibrated diffusion zones. A brief summary of error sources encountered in the diffusion couple technique is presented below

#### **Nature of sample**

The phase equilibria investigations of a system in which the terminal compositions (end-members) are solids but a liquid phase appears at the annealing temperature, the diffusion path may wander in the liquid region and give disastrous results. In addition, presence of the defects such as cracks at the interfaces may result in the poor adherence and thereby complicate the interpretation of the diffusion experiments [19, 20].

#### **Experimental measurements**

The accurate determination of the boundary concentrations in the diffusion zone is quite difficult. Besides the inherent experimental errors associated with the EPMA technique, electron scattering in the diffusion zone also complicates the accurate determination of phase relationship [19, 20]. Due to electron scattering, generation of the characteristic X-rays from a volume much smaller than 1-2  $\mu\text{m}$  in diameter is not possible and consequently its chemical composition cannot be determined explicitly. However, if the constituent phases have significant layer width, the interfacial compositions can be obtained by extrapolation of the measured concentrations profiles to the interface location. The extrapolation approach may also sometimes lead to the erroneous results when the concentration gradients near the phase boundaries in the diffusion-grown layers are steep [19, 20].

#### **Quasi-equilibrated diffusion zones**

The accurate experimental determination of the phase diagram with the help of diffusion couple requires equilibrium to be established at the interphase interface. Sometimes an

equilibrium phase may be absent in the diffusion zone due to presence of any barrier layer such as oxide film at the interface. On the other hand, it is also possible that segregation of impurities in the diffusion zone may sometimes stabilize non equilibrium phases which may be misinterpreted as equilibrium phases. For example carbides like  $\text{Mo}_5\text{Si}_3\text{C}$  and  $\text{Mo}_6\text{Ni}_6\text{C}$  [21], can be misinterpreted as pure binary  $\text{Mo}_5\text{Si}_3$  and  $\text{MoNi}$  phases respectively. The absence of equilibrium phases or presence of non equilibrium phases in the diffusion zone may lead to the erroneous/inaccurate phase diagrams [19, 20].

### **1.3.3. Comparison of the diffusion couple and equilibrated alloy method**

The equilibrated alloy method is the most powerful, reliable and commonly used method for the determination of equilibrium phase diagrams. However, it is more time consuming in comparison with the diffusion couple method as one has to investigate a large number of alloy compositions for the complete determination of phase diagram. On the other hand, diffusion couple technique has been considered as an efficient way for the understanding the phase relationship but the difficulties in concentration measurement at the interface and problems associated with the formation of quasi-equilibrated diffusion zone makes the diffusion couple results less reliable. In addition, the diffusion couple method also does not permit crystal structure identification of the phases present in equilibrium with the help of conventional X-ray diffraction measurements. Therefore, to increase the reliability of the phase boundary information gathered using diffusion couple technique, investigation of selected equilibrated alloy compositions (or powder compacts) is necessary. This is the reason why the diffusion couple method should be used not as independent but in conjunction with equilibrated alloy method. The information gathered from the multiphase diffusion couples can be employed to map a constitutional diagram and to help in selecting the compositions of the alloys to be examined whereas for accurate determination of position of the phase field boundaries, direction of tie-lines, phase identification and structural characterization, equilibrated alloy sample should be used.

## **1.4. Thermodynamic modeling of phase diagrams**

As discussed earlier, phase diagrams are the maps for materials and process development. Traditionally, they have been determined purely by experimental approach that is costly, meticulous, and time-consuming. Furthermore, in case of complex engineering materials such as Ni based superalloys that usually contain more than 10 alloying elements, the experimental

investigation of the phase equilibria is a huge engineering undertaking as there are many different sections or projections one might be interested in. In principle, they can be determined experimentally, but the time required to do so can be significantly longer. This is where the computer simulation and the Calphad (an acronym for CALculation of PHASE Diagrams) method comes in and plays an important role. The Calphad method is based on the description of the Gibbs energies of the different phases present in a system. These are evaluated in simple systems by least-square fitting of model parameters in order to describe as well as possible the available experimental data (phase diagram and thermodynamic data) on a given system. One of the merits of the technique is its ability to describe metastable equilibrium since the phases are most often described out of their temperature and composition stability ranges. In this frame, the technique has recently benefitted from the input of calculations of the enthalpies of formation of compounds and solutions obtained in the frame of the Density Functional Theory (DFT).

Simple systems are modeled independently and may be grouped in larger databases. The combination of the different systems may allow, by extrapolation, the prediction of the phase equilibrium in multi-component systems. The details about the Calphad methodology and its associated advantages are provided in the chapter 3.

## 1.5. Topologically closed packed phases

Most of the intermetallic phases found in the present work are TCP phases. These phases are also called Frank-Kasper phases, after the names of two researchers that have described and classified them. They are intermetallic compounds generally formed by the association of two transition metals. The larger element which is generally the element with lower number of valence electrons is called *A* element, while the second element with smaller atomic radius is called *B* element. The main structural characteristic of TCP phases is the only presence of tetrahedral interstices in the crystal structure. This has for consequence a limited number of possible coordination polyhedra for each atom in the structure ranging from low coordination number (CN) 12 (icosahedron) to high CN 14, 15 and 16.

Well known examples of TCP phases are the  $A_{15}A_3B$ , the  $C_{14}$ ,  $C_{15}$  and  $C_{36}AB_2$  Laves phases, and the phases present in the Mo-Ni-Re system, the  $\delta$ ,  $\sigma$  and  $\chi$  phases.

In ordered phases, *A* atom occupies the sites of higher CN, while *B* occupies the sites of lower CN (generally CN12), particularly for size reasons. One of the main features of the TCP

phases is their ability to accommodate extremely large ranges of non-stoichiometry. For example, the  $\sigma$  phase may exist in different systems for nearly any  $A/B$  concentration [22]. In this case, the non-stoichiometry is accommodated by mixing of atoms on the different sites [23]. This phenomenon has been studied in detail for the  $\sigma$  [22] and  $\chi$  [24] phases by the measurement of the site occupancies. In some systems, phases may be close to completely ordered while in other system, a strong disorder is observed. However, in the most disordered systems, a slight preference of the  $A$  atoms for the high CN is always observed.

## **1.6. Bibliographic research**

Several investigations have been carried out previously to determine phase diagrams of the Mo-Ni-Re system and its constituent binary systems. In this section, a review of the previous investigations is presented.

### **1.6.1. The Mo-Ni system**

The Mo-Ni system has been the subject of several previous investigations. The first review of the Mo-Ni system was carried out by Hansen [25] which revealed that exact compositions of the intermediate phases and homogeneity domain of the Mo solid solution were unknown [26]. In order to confirm and complete the previously reported results, Casselton et al. [26] carried out a complete experimental redetermination of the Mo-Ni. They used a combination of thermal, microscopical and X-ray methods for phase equilibria investigation and proposed a Mo-Ni phase diagram which is shown in the Figure 1-3.

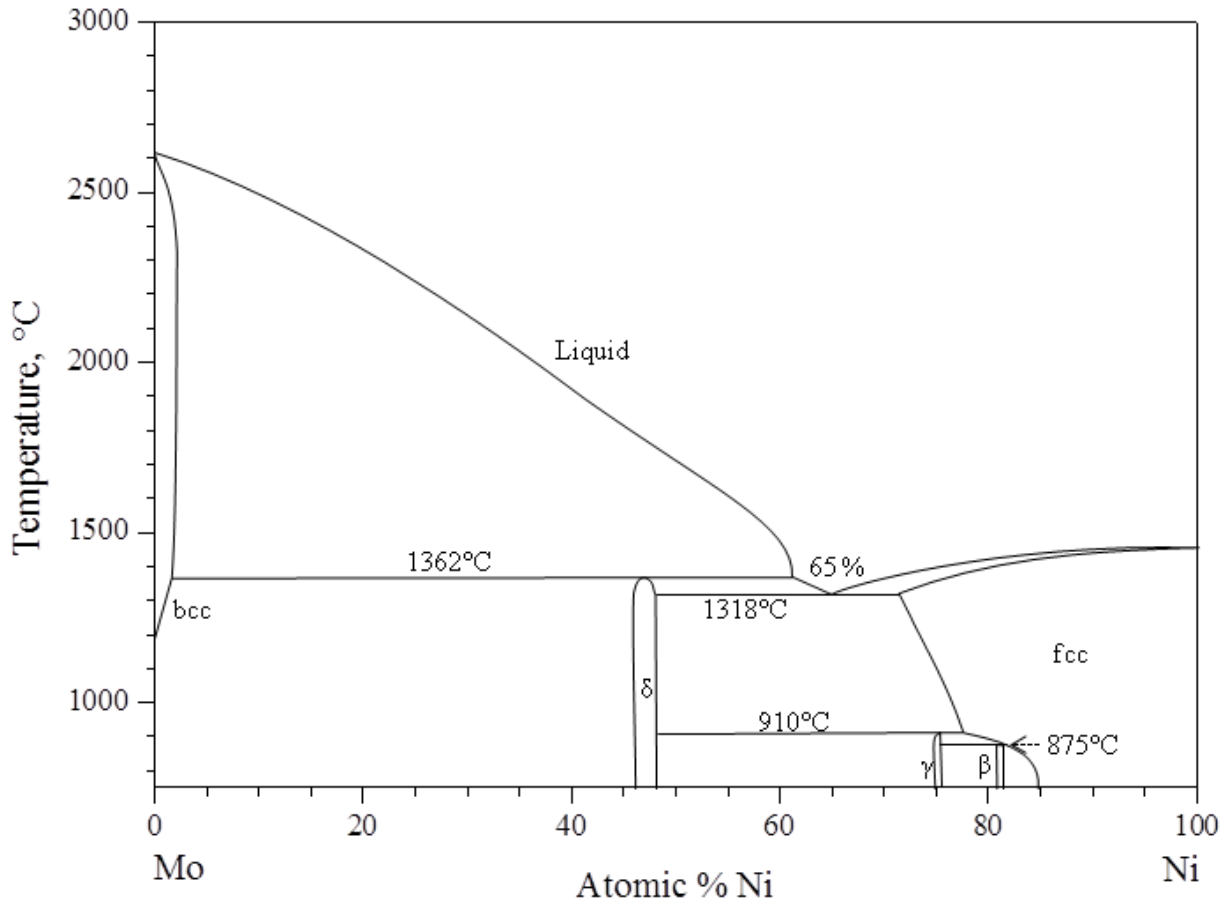


Figure 1-3: Mo-Ni phase diagram proposed by Casselton et al. [26].

As illustrated in the Figure 1-3, the Mo-Ni system is characterized by the presence of four reactions.

- Peritectic reaction:  $\text{Liquid} + \text{bcc} \rightleftharpoons \delta$
- Eutectic reaction:  $\text{Liquid} \rightleftharpoons \text{fcc} + \delta$
- Eutectoid reaction:  $\text{fcc} + \delta \rightleftharpoons \gamma$
- Eutectoid reaction:  $\text{fcc} + \gamma \rightleftharpoons \beta$

The liquidus curve on the Mo rich side was determined with the help of micro structural examination of the alloys quenched from successive temperatures whereas conventional thermal analysis was carried out for the determination of the solidus and liquidus curves on the Ni rich side. The temperature of the peritectic horizontal corresponding to the reaction,  $\text{bcc} + \text{Liquid} \rightleftharpoons \delta$ , was found to be 1362°C whereas eutectic reaction yielding fcc and  $\delta$  phases was reported at 1318°C and 65 at.% Ni. The eutectoid reactions resulting in the formation of  $\gamma$  and  $\beta$  phases take place at 910°C and 875°C respectively.

The phase boundaries of the Mo-Ni binary system were determined with the help of microscopic and X-ray methods. The maximum solubility of Mo in fcc was determined to be 28.4 at. % which was slightly greater than the value reported by Hansen [25]. On the other hand, homogeneity domain of bcc at low temperatures was very small at low temperatures, which increased to 1.8 at.% Ni at the peritectic horizontal. The homogeneity domain of the  $\delta$  phase was centered at about 47 at.% Ni. The width of the composition range of  $\delta$  phase was estimated to be 2-3 at.%. The homogeneity domain of  $\gamma$  phase was reported to be less than 1 at.% and includes exact atomic ratio  $\text{MoNi}_3$  whereas the phase field of the  $\beta$  phase lies in the region of 80.5-81 at.% Ni.

The experimental determination of the Mo-Ni system by Casselton et al. [26], was followed by several partial investigations. Heijwegen et al. [27] studied the Mo-Ni phase equilibria in the temperature range of 800°C to 1295°C by characterization of the diffusion couples and equilibrated arc melted alloys with the help of microscopic and electron probe microanalysis. The maximum solubility of Mo in Ni was reported to be 28 at.% Ni at 1318°C which is in agreement with the previous study by Casselton et al.[26] (28.4 at. % Ni). Similarly, the composition ranges of  $\gamma$  phase (75.6-76.1),  $\beta$  phase (80.1-81.6) and solubility limit of Ni in bcc at 1295°C (2 at. % Ni) were not very different from the data reported previously by Casselton et al.[26]. However Heijwegen et al. [27], reported a shift in the homogeneity domain of  $\delta$ -phase (47.8 at. % Ni - 51.8 at. % Ni) by 3 at.% towards rich Ni side. This shift in the composition range was also reported in a later investigation carried out by Meshkov et al. [28]. The phase field of bcc above the peritectic reaction was also investigated in more detail by Kang et al. [29]. A comparison of the partial investigations of the Mo-Ni binary system with the Mo-Ni phase diagram proposed by Casselton et al. [26] is shown in Table 1-3.

Table 1-3: Comparison of the previous investigations of the Mo-Ni system

Phases	Casselton et al. [26]	Heijwegen et al. [27]	Meshkov et al. [28]	Kang et al. [29]
bcc	0.3 (1200°C)		1.19(1200°C)	
	1.8 (1392°C)	1.1 (1000°C)	1.75 (1392°C)	1.43 (1392°C)
	1.9 (1512°C)	1.5 (1200°C)	1.92(1512°C)	1.96 (1512°C)
$\delta$	45-49%Ni	47.8 - 51.8	47.9-52.9	-
$\beta$	80.5-81%Ni	80.1-81.6	78.7-80	-
$\gamma$	75%Ni	75.6-76.1	74.2-75.7	-
fcc	15.7(800°C)%Mo	15.1 (800°C)	14.4(800°C)	
	26.8(1200°C)%Mo	25.9(1200°C)	25.2(1200°C)	-

As illustrated in Table 1-3, the reported homogeneity domain of Mo-Ni intermetallic phases except  $\delta$  phase lies within the experimental uncertainties. For  $\delta$  phase, a difference of around 3 at.% was observed in the position of its homogeneity domain. In addition, the reported solubility limits of the bcc and fcc phases also show small differences. Therefore it was concluded that some confirmation experiments are required to verify the position of the  $\delta$  phase field in the Mo-Ni binary system.

Although small differences were observed in the reported homogeneity domains, all the previous investigations agree in terms of types of intermetallic phases appearing in the Mo-Ni system. A brief introduction of the crystal structure of intermetallic phases appearing in the Mo-Ni system is provided in this section.

### The $\delta$ -phase

The presence of  $\delta$  phase in the Mo-Ni binary system was discovered by Ellinger [30] whereas shoemaker et al. [31] investigated its crystal structure with the help of an alloy of the composition  $\text{Mo}_{49}\text{Ni}_{51}$ . The  $\delta$  phase was reported to have an orthorhombic crystal structure. However, two of three cell dimensions are exactly equal so that the X-ray diffraction measurements indicate a strong pseudo-tetragonality. It has 56 atoms per unit cell which are distributed among 14 crystallographically different sites, all of which belong to the point set  $4a$ . The crystal structure information of the  $\delta$  phase is provided in Table 1-4.

Table 1-4: Crystallographic data of the  $\delta$  phase [31]

<b>Formula</b>	Mo <sub>7</sub> Ni <sub>7</sub>					
<b>Prototype</b>	Mo <sub>3</sub> (Mo <sub>0.8</sub> Ni <sub>0.2</sub> ) <sub>5</sub> Ni <sub>6</sub>					
<b>Pearson symbol</b>	oP56					
<b>Space Group</b>	P2 <sub>1</sub> 2 <sub>1</sub> 2 <sub>1</sub> (no.19)					
<b>Lattice Parameters</b>	$a = 9.108 \text{ \AA}$ , $b = 9.108 \text{ \AA}$ , $c = 8.852 \text{ \AA}$					
Site	Elements	Wyckoff Position	Coordination number	$x$	$y$	$z$
IV	Ni	4a	12	0.4519	0.1153	0.5322
VI	Ni	4a	12	0.4424	0.3662	0.5971
VIII	Ni	4a	12	0.3882	0.0523	0.2748
IX	Ni	4a	12	0.1337	0.0707	0.2157
X	Ni	4a	12	0.3768	0.4358	0.8567
XII	Ni	4a	12	0.0680	0.1442	0.9529
I	0.80Mo+0.20Ni	4a	14	0.2648	0.1993	0.7486
XIII	0.80Mo+0.20Ni	4a	14	0.3136	0.2464	0.0740
II	0.91Mo+0.09Ni	4a	14	0.0029	0.1969	0.6767
V	0.91Mo+0.09Ni	4a	14	0.1885	0.0157	0.4960
XI	0.58Mo+0.42Ni	4a	14	0.1031	0.4192	-0.0867
VII	Mo	4a	15	0.1763	0.4832	0.6425
XIV	Mo	4a	15	0.0338	0.3398	0.1807
III	Mo	4a	16	0.2289	0.2865	0.4098

### The $\gamma$ -phase

The crystal structure information of the  $\gamma$ -phase formed as a result of the eutectoid reaction between fcc and  $\delta$  phase in the Mo-Ni binary system was studied by Saito et al. [32]. It has orthorhombic crystal structure with 8 atoms per unit cell. The crystal structure details and average atomic positions of the Mo-Ni  $\gamma$  phase are listed in Table 1-5.

Table 1-5: Crystallographic data of the  $\gamma$ -phase [25]

<b>Formula</b>		MoNi <sub>3</sub>				
<b>Prototype</b>		Cu <sub>3</sub> Ti				
<b>Pearson Symbol</b>		oP8				
<b>Space group</b>		Pmmn (no. 59)				
<b>Lattice parameters</b>		$a=5.064 \text{ \AA}$ , $b=4.224 \text{ \AA}$ , $c=4.448 \text{ \AA}$				
Site	Elements	Wyckoff Position	Coordination number (CN)	$x$	$y$	$z$
<b>Mo</b>	Mo	2a	12	0.0	0.0	0.656
<b>Ni1</b>	Ni	2b	12	0.0	1/2	0.344
<b>Ni2</b>	Ni	4f	12	0.25	0.0	0.156

### The $\beta$ -phase

The crystal structure information of the Mo-Ni  $\beta$  phase formed as a result of the eutectoid reaction between fcc and  $\gamma$  phase was studied by Harker [33]. It has tetragonal unit crystal structure with 10 atoms per unit cell. The details about the crystal structure and average atomic positions of the  $\beta$  phase are given in Table 1-6.

Table 1-6: Crystallographic data of the  $\beta$ -phase [33]

Formula		MoNi <sub>4</sub>				
Prototype		MoNi <sub>4</sub>				
Pearson Symbol		tI10				
Space group		I4/m (no. 87)				
Lattice parameters		$a=5.720 \text{ \AA}$ , $c=3.564$				
Site	Elements	Wyckoff Position	Coordination number (CN)	$x$	$y$	$z$
Mo	Mo	2a	12	0	0	0
Ni	Ni	8h	12	0.2	0.4	0

### 1.6.2. The Ni-Re system

The phase equilibria study of the Ni-Re binary system has been the subject of several previous investigations. A brief summary of the previous studies carried out for determination of phase boundaries in the Ni-Re binary system is provided in this section.

The first attempt for complete experimental investigation of the Ni-Re binary system was carried out by Pogodin et al [34]. They studied phase equilibria in the Ni-Re binary system by using a combination of thermal, metallographic and X-ray methods and proposed a phase diagram which is shown in the Figure 1-4.

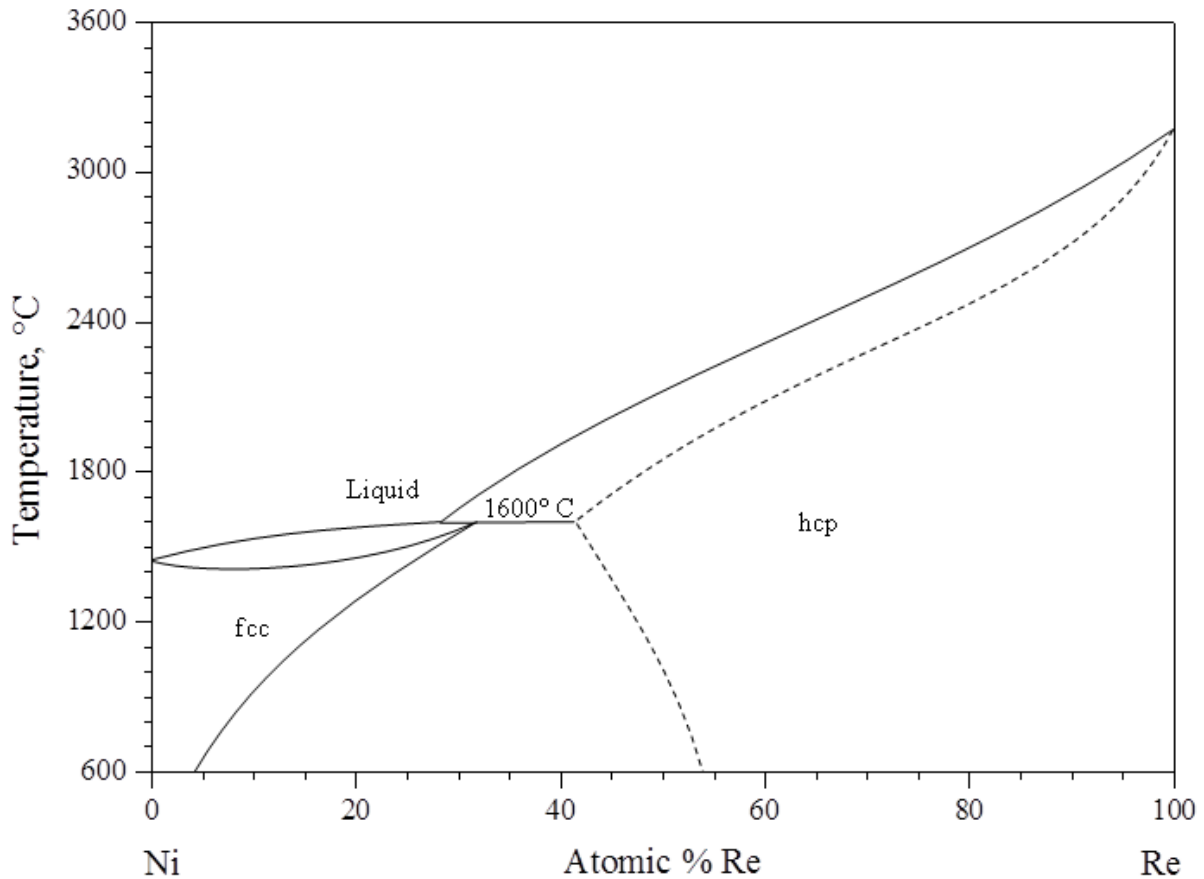


Figure 1-4: Ni-Re phase diagram suggested by Pogodin et al. [34].

As illustrated in the Figure 1-4, Pogodin et al. [34] reported the presence of a peritectic reaction at 1600°C and 29.8 at.% Re, resulting in the formation of Ni and Re solid solutions *i.e.* fcc and hcp respectively. They did not find presence of any intermetallic compound in the studied system. The maximum solid solubility of Re in fcc amount to 29.5 at.% Re at 1600°C which decreased rapidly with the temperature to 3.6 at.% Re at 600°C. The solubility limit of Ni in hcp at 1200°C and 1000°C was found out to be about 52.7 at.% Ni. The two phase field between fcc and hcp at 1200°C was reported to extend from 17.36 at.% Re to 47.29 at.% Re. However, the data reported by Pogodin et al. [34] for the liquidus and solidus of the fcc showed a minimum in the solidus, which is inconsistent with the phase rule.

The second complete study of the Ni-Re binary system was carried out by Savitskii et al. [35]. They investigated the structure and composition of annealed Ni-Re alloys with the help of

thermal, X-ray and microanalysis techniques. The Ni-Re phase diagram proposed by Savitskii et al. [35] is shown in the Figure 1-5.

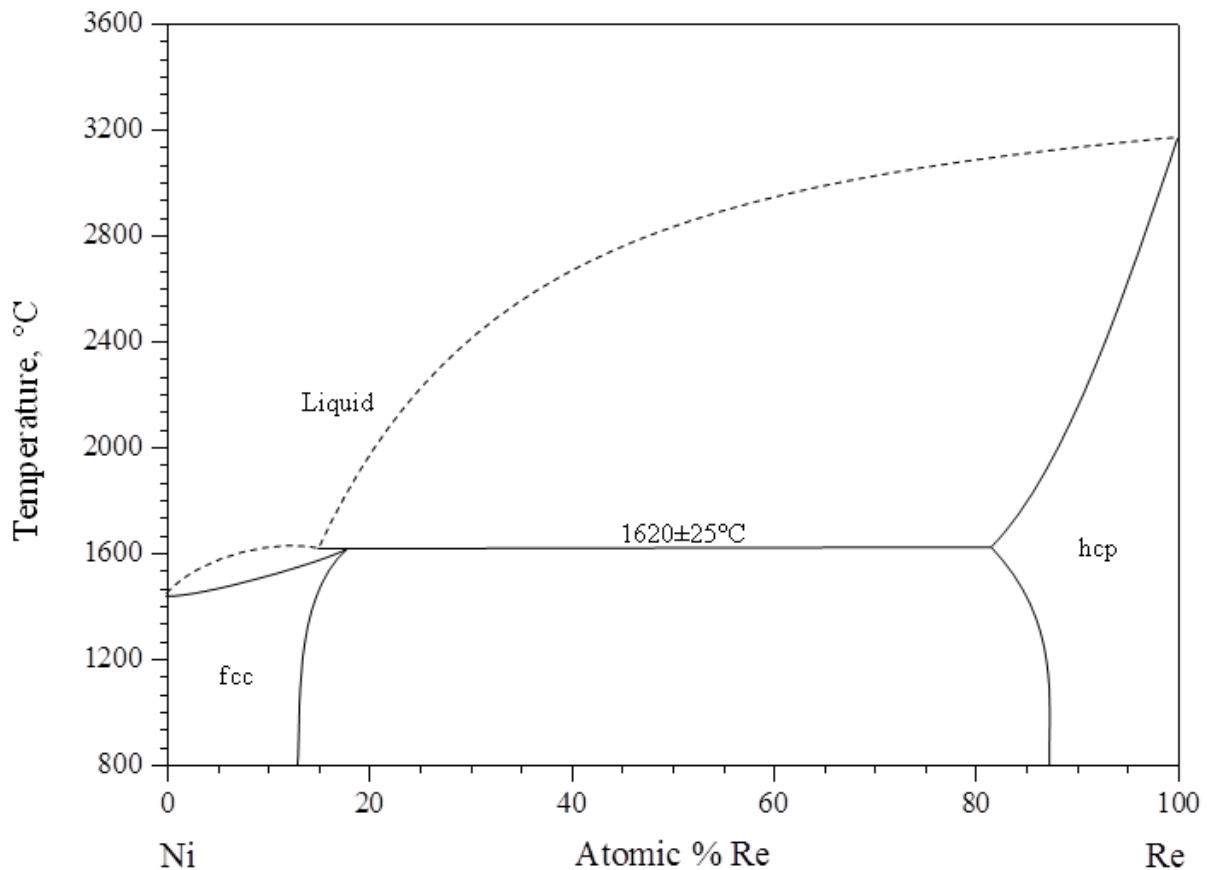


Figure 1-5: Ni-Re phase diagram suggested by Savitskii et al. [35].

The phase diagram proposed by Savitskii [35] showed presence of a peritectic reaction at  $1620^{\circ}\text{C} \pm 25^{\circ}\text{C}$ , with a peritectic composition of 17.4 at.% Re. The max solubility of Re in fcc was found at the peritectic reaction temperature which on cooling to  $800^{\circ}\text{C}$  decreased to 12.2 at. % Re. On the other hand, solubility of Ni in hcp was 13.3 at.% Ni and changed very little with the temperature. Savitskii et al. [35] did not evidence presence of any minimum in the solidus data.

In addition to the complete experimental determination, several partial investigations of the Ni-Re binary system were also carried out at  $1200^{\circ}\text{C}$  by Savitskii et al. [36], Hofmann et al. [37], and Solonin et al. [38]. The phase boundary data obtained from these investigations are plotted in the Figure 1-6.

Nash et al. [39] in 1985 critically reviewed the experimental information available on the Ni-Re system [34-36, 38, 40-46] specially the work carried out by Pogodin et al. [34] and Savitskii et al. [35]. They reported large differences in the phase boundaries indicated in the

two studies e.g., the maximum solubility of Re in fcc reported by Pogodin et al. was 12.1 at.% higher than the value indicated by Savitskii [34]. The only areas of agreement were found to be the absence of intermetallic compounds and the temperature of the peritectic reaction. Nash et al. preferred the data reported by Savitskii et al. [35] over the data reported by Pogodin et al. [34] because of the better materials, preparation techniques and the self consistency in the form of diagram and proposed a Ni-Re phase diagram which is shown in the Figure 1-6.

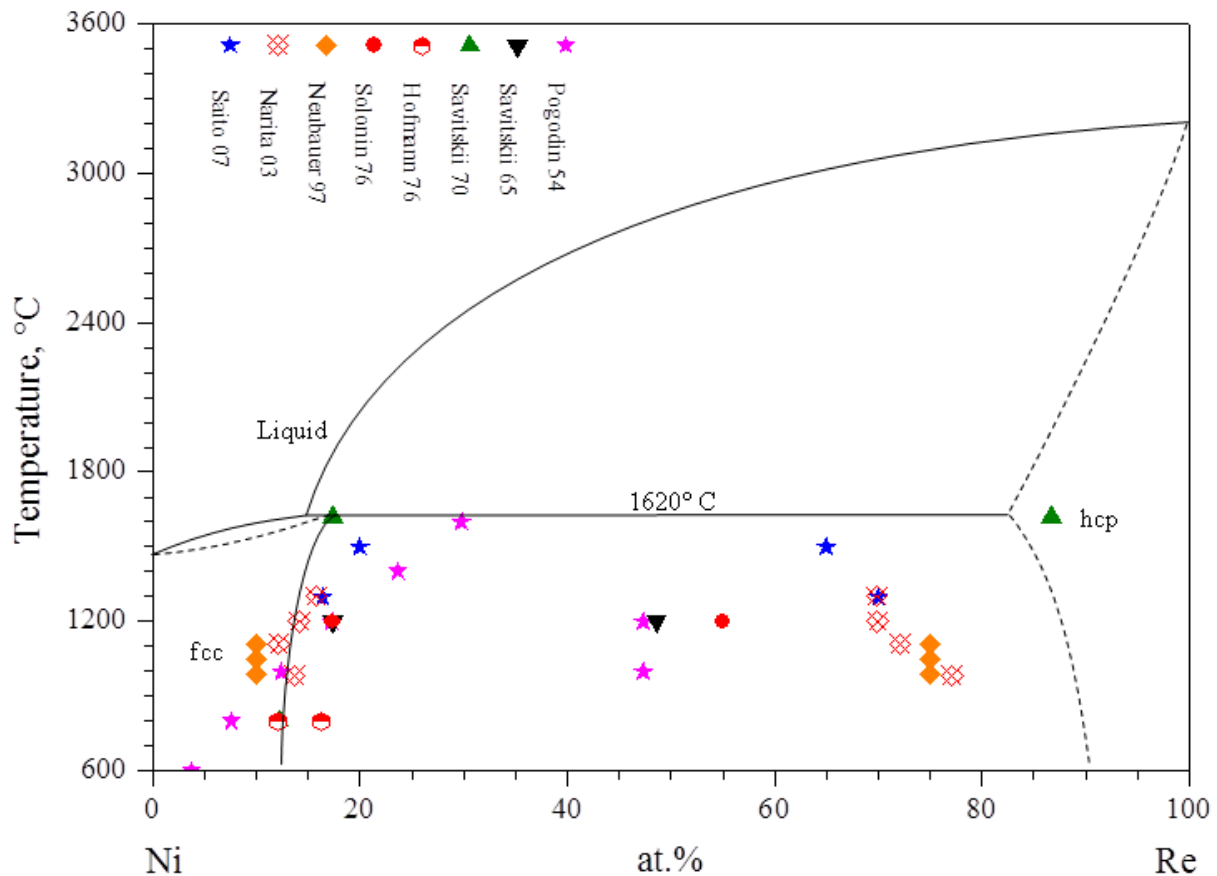


Figure 1-6: Ni-Re phase diagram proposed by Nash et al. and its comparison with other investigations.

The Ni-Re phase diagram proposed by Nash [39] has been previously considered as a reference. However, some of the recent partial investigations of the Ni-Re binary system by Neubauer et al. [47], Saito et al. [48] and Narita cited in [48], have placed question marks on the accuracy of the proposed phase diagram. A comparison of the phase boundaries reported in these recent investigations as well as the data reported previously with the phase diagram suggested by Nash [39] is also shown in the Figure 1-6. The Ni-Re phase diagram proposed by Nash [39] shows large disagreement not only with the recent studies but also with previous investigations particularly on the Re rich side. Most of the experimental results pointed out

much larger homogeneity domain of the hcp phase in comparison with the diagram proposed by Nash [39]. Similarly, considerable differences can also be seen on the Ni rich side. In addition, hcp phase fields in the Ni-Re phase diagram proposed by Nash *et al.* [39] also showed poor agreement with the related ternary isothermal sections such as Cr-Ni-Re [8, 49], Fe-Ni-Re [8, 50], Mn-Ni-Re [11], Mo-Ni-Re [8], Nb-Ni-Re [8, 49], Ni-Re-Ta [8], Ni-Re-Ti [8], Ni-Re-V [8, 49], Ni-Re-Zr [8].

Considering the large disagreements between the accepted Ni-Re phase diagram and reported data on the binary and related ternary system, it was concluded that the phase equilibria in this technologically important system is not well understood and requires a substantial experimental redetermination.

### 1.6.3. The Mo-Re system

The complete experimental determination of the Mo-Re binary system was independently carried out by Dickinson *et al.* [51], Knapton [52] and Savitskii *et al.* [53, 54] with the help of optical pyrometry, X-ray diffraction, and metallographic methods. Brewer *et al.* [55] reviewed the available experimental information related to the phase equilibria in the Mo-Re binary system and proposed a Mo-Re phase diagram which is shown in the Figure 1-7.

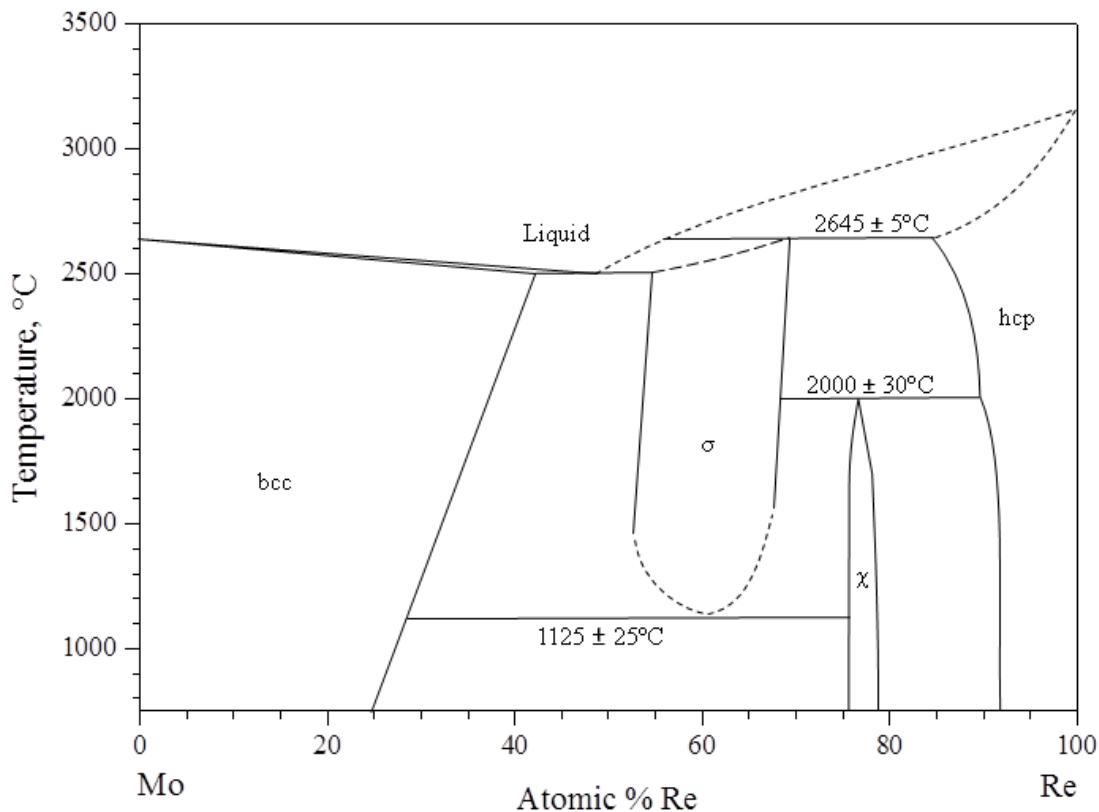


Figure 1-7: Mo–Re phase diagram assessed by Brewer *et al.* [55].

As illustrated in the Figure 1-7, the Mo-Re binary system is characterized by the presence of four invariant reactions.

- Peritectic reaction:  $\text{Liquid} + \text{hcp} \rightleftharpoons \sigma$
- Eutectic reaction:  $\text{Liquid} \rightleftharpoons \text{bcc} + \sigma$
- Peritectoid reaction:  $\sigma + \text{hcp} \rightleftharpoons \chi$
- Eutectoid reaction:  $\sigma \rightleftharpoons \text{bcc} + \chi$

The first three out of the four reactions i.e. peritectic, eutectic and peritectoid reactions, have been reported by Dickinson et al. [51], Knapton et al. [52] and Savitskii et al. [54]. However, temperatures reported in the work of Dickinson et al. [51] and Knapton et al. [52] showed considerable differences. Knapton [52], in a later discussion, agreed that the temperatures reported by Dickinson [51] are probably more accurate because of relatively lower temperature gradient in the furnace used in their work. Therefore, the temperatures of the eutectic and peritectic reactions temperatures reported by Dickinson [51] were preferred while proposing the phase diagram shown in the Figure 1-7. On the other hand, presence of the eutectoid reaction ( $\sigma \rightleftharpoons \text{bcc} + \chi$ ) was only evidenced by Knapton et al. [52]. They found that the  $\sigma$  phase is stable at temperatures higher than 1150°C. By combining different experimental results, Knapton [52] concluded that the eutectoid reaction in the Mo-Re binary system takes place between 1100°C and 1150°C. As annealing temperatures in both Dickinson et al. [51] and Savitskii et al. [54] studies were higher than 1100°C, therefore, they were not able to detect the eutectoid decomposition of the  $\sigma$  phase into bcc and  $\chi$ . The Mo-Re phase diagram, proposed by Brewer et al. [55], was found as being consistent with the previously reported data within the experimental uncertainties.

In the Mo-Re binary system suggested by Brewer et al. [55], the Mo based solid solution *i.e.* bcc, was found to have wide homogeneity domain. The solubility of Re in bcc varied with the temperature from about 42.4 at.% Re at the eutectic temperature to about 29.4 at% Re at 1200°C. On the other hand, the maximum solubility of Mo in hcp was taken to be about 18±3 at% Mo at the peritectic reaction temperature.

All the previous investigation indicated presence of two intermetallic phases *i.e.*  $\chi$  and  $\sigma$  phase, in the Mo-Re system. Both of these phases belong to the group of Frank-Kasper phases. In the Mo-Re binary system, the  $\chi$  phase is formed by a peritectoid reaction between hcp and  $\sigma$ -phase at 2000±30°C whereas the  $\sigma$ -phase is formed as a result of peritectic reaction

between hcp and liquid phase at  $2645\pm 5^\circ\text{C}$ . The homogeneity domain of the  $\chi$ -phase is narrow ranging from  $76\pm 1$  to  $79\pm 1$  at %Re at  $2000^\circ\text{C}$ . On the other hand, the  $\sigma$ -phase in the Mo-Re binary system was found to have wide homogeneity domain extending from  $52\pm 2$  at.% Re to  $70\pm 2$  at.% Re at  $2400^\circ\text{C}$ . However at low temperatures, the homogeneity domain of the  $\sigma$ -phase was not studied in detail in the previous investigations [51, 52, 54] and its position is rather uncertain. Therefore, it was shown as dashed line in the Figure 1-7. More experimental evidences are required to confirm the homogeneity domain of  $\sigma$  phase at low temperatures.

As the phase diagram of the Mo-Re binary system proposed by Brewer et al. [55] was found in agreement with the previous investigations within the experimental uncertainties, therefore, it was taken as a reference for the present study. However the homogeneity domain of  $\sigma$  phase at low temperatures needs to be determined.

The crystal structure information of the intermetallic phases present in Mo-Re binary system is provided in Table 1-7 and Table 1-8.

### **The $\sigma$ -phase**

The  $\sigma$  phase belongs to the group of TCP phases. It was originally found in the Fe-Cr system. Now its presence has been reported in 41 binary and several ternary systems. A detailed review of the crystal chemistry, general features like homogeneity ranges, electron concentrations, and modeling of  $\sigma$  phase with the help of the Calphad method has been carried out by Joubert et al. [22]. The crystal structure of the  $\sigma$  phase was previously elucidated by Shoemaker et al. [56] and Bergman et al.[57]. It has a tetragonal unit cell and is now commonly described with the space group  $P4_2/mnm$ . The  $\sigma$  phase contains 30 atoms per unit cell distributed among 5 different sites, the coordinates of which are given in Table 1-7.

Table 1-7: Crystallographic data of the  $\sigma$ -phase [58]

<b>Phase formula</b>	$Mo_{0.404}Re_{0.596}$					
<b>Prototype</b>	$Cr_{0.49}Fe_{0.51}$					
<b>Pearson symbol</b>	$tP30$					
<b>Space Group</b>	$P4_2/mnm$ (no.136)					
<b>Lattice Parameters</b>	$a = 9.588 \text{ \AA}, c = 4.980 \text{ \AA}$					
<b>Site</b>	<b>Elements</b>	<b>Wyckoff Position</b>	<b>Coordination number</b>	<b><math>x</math></b>	<b><math>y</math></b>	<b><math>z</math></b>
<b>Re1</b>	0.08M+0.92Re	$2a$	12	0	0	0
<b>M1</b>	0.75Mo+0.25Re	$4f$	15	0.3993	0.3993	0
<b>M2</b>	0.48Mo+0.52Re	$8i_1$	14	0.4652	0.1313	0
<b>Re2</b>	0.12Mo+0.88Re	$8i_2$	12	0.7393	0.0657	0
<b>M3</b>	0.52Mo+0.48Re	$8j$	14	0.1828	0.1828	0.2477

One of the main features of the  $\sigma$  phase is its non stoichiometry which is accommodated by substitutions on one or several sites of crystal structure [22]. The site occupancies of Mo-Re  $\sigma$  phase have been studied as a function of composition by Farzadfar et al. [58]. All sites have been found to be disordered but a clear preference is observed for Mo, the larger atom to occupy the high CN sites.

### The $\chi$ -phase

The  $\chi$  phase also belongs to the group of TCP phases. It was originally found in ternary Cr-Mo-Fe alloys [59, 60]. Now its presence has been observed in various binary and ternary systems. The crystal structure of the  $Cr_{12}Mo_{10}Fe_{36}$  alloy was determined by Kasper [61] by using both the X-ray and neutron diffraction methods. The  $\chi$  phase is isostructural with  $\alpha$ -Mn and has a body centered cubic structure with 58 atoms per unit cell [62]. It belongs to the space group  $I\bar{4}3m$ . The details about the crystal structure and atomic positions of the  $\chi$  phase are given in Table 1-8.

Table 1-8: Crystallographic data of the  $\chi$ -phase [58]

<b>Formula</b>	Mo <sub>0.21</sub> Re <sub>0.79</sub>					
<b>Prototype</b>	Mn					
<b>Pearson symbol</b>	cI58					
<b>Space Group</b>	$\bar{I}4\ 3m$ (no.217)					
<b>Lattice Parameters</b>	$a=9.582\ \text{\AA}$					
<b>Site</b>	Elements	Wyckoff Positions	Coordination number	$x$	$y$	$z$
<b>M1</b>	0.73Mo+0.27Re	2a	16	0	0	0
<b>M2</b>	0.64Mo+0.36Re	8c	16	0.3232	0.3232	0.3232
<b>M3</b>	0.21Mo+0.79Re	24g <sub>1</sub>	13	0.3583	0.3583	0.0435
<b>M4</b>	0.02Mo+0.98Re	24g <sub>2</sub>	12	0.0914	0.0914	0.2838

The site occupancies of the Mo-Re  $\chi$  phase as a function of composition have been studied by Farzadfar et al. [58] whereas details about the general crystal chemistry of the  $\chi$  phase can be found in detailed review by Joubert et al. [24]. As for the  $\sigma$  phase, mixed occupancy is observed on all sites with a preference of Mo for high CN sites.

#### 1.6.4. The Mo-Ni-Re system

Considering its commercial importance for the development of the Ni based superalloys, the Mo-Ni-Re system has been the subject of several previous investigations. A brief summary of the previous work conducted on the Mo-Ni-Re ternary system is presented in this section.

The preliminary investigation of the Mo-Ni-Re system in the Ni rich corner was carried out by Burhanov et al. [63] and Savitskii et al. [64]. They determined composition range of the Ni based solid solution i.e. fcc, in the Ni-Re, Mo-Ni, and Mo-Ni-Re system with the help of microstructural and X-ray analysis of the alloys annealed at 1200°C for 100 hours. The fcc phase was reported to extend up to 13.44 at.% Re (33 wt% Re) in the Ni-Re and 24.8 at.% Mo (35 wt% Mo) in the Mo-Ni system whereas the line defining the phase boundary of fcc in the ternary region extends toward the Mo-Re side and reaches 18.7 at.% Mo and 9.6 at. % Re. They also indicated that the Ni-based solid solution was found in equilibrium with Re-based

solid solution and Mo-Ni  $\delta$  phase. The results obtained by Burhanov et al. [63] are shown in Figure 1-8.

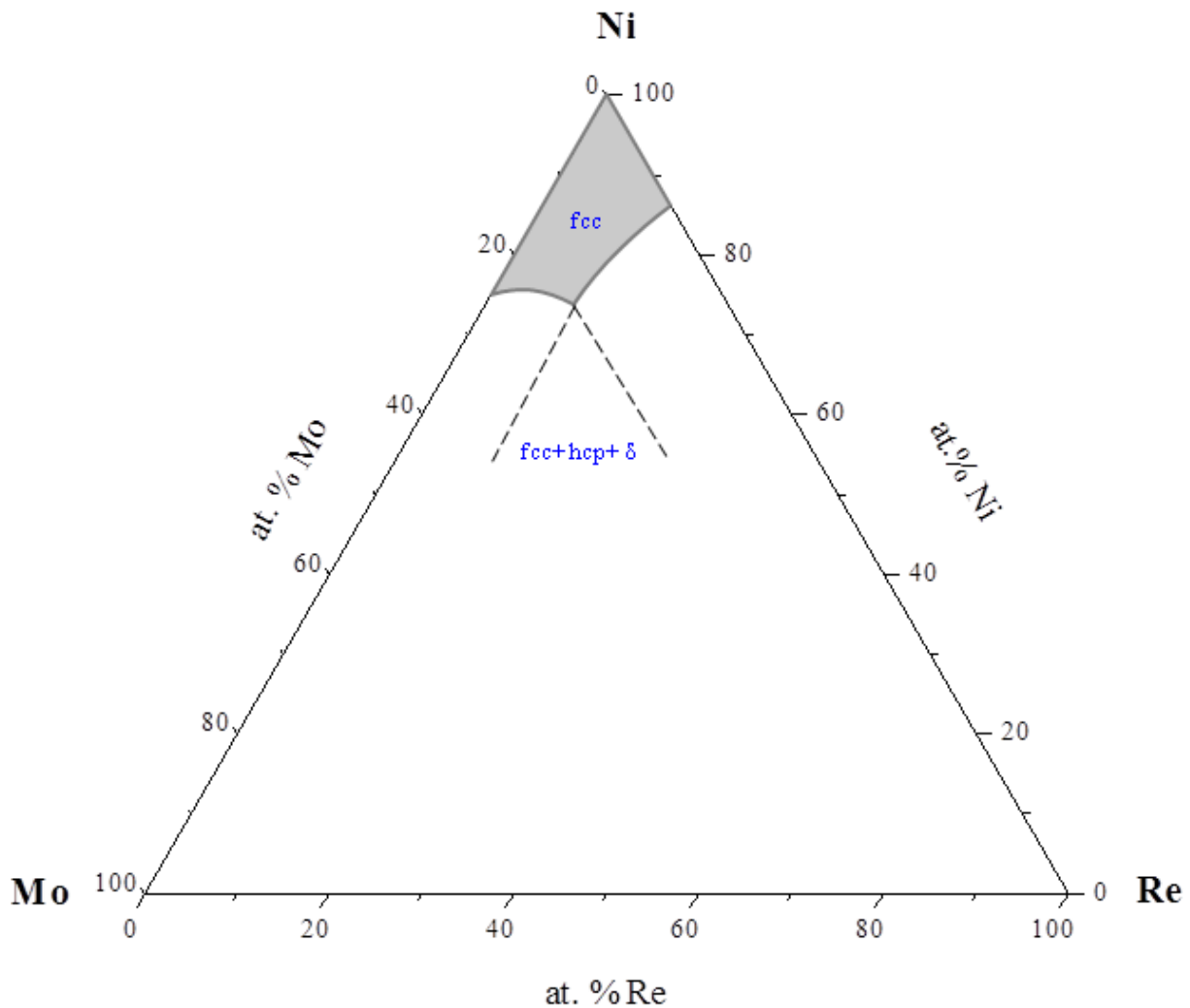


Figure 1-8: Preliminary investigation of Mo-Ni-Re system at 1200°C by Burhanov et al. [63].

The first attempt for determination of the Mo-Ni-Re phase diagram over the entire composition range was carried out by Kodentsov et al. [6]. They determined the isothermal section of Mo-Ni-Re system at 1152°C by means of diffusion couple and electron probe microanalysis. The isothermal section of the Mo-Ni-Re system proposed by Kodentsov et al. [6] is shown in Figure 1-9.

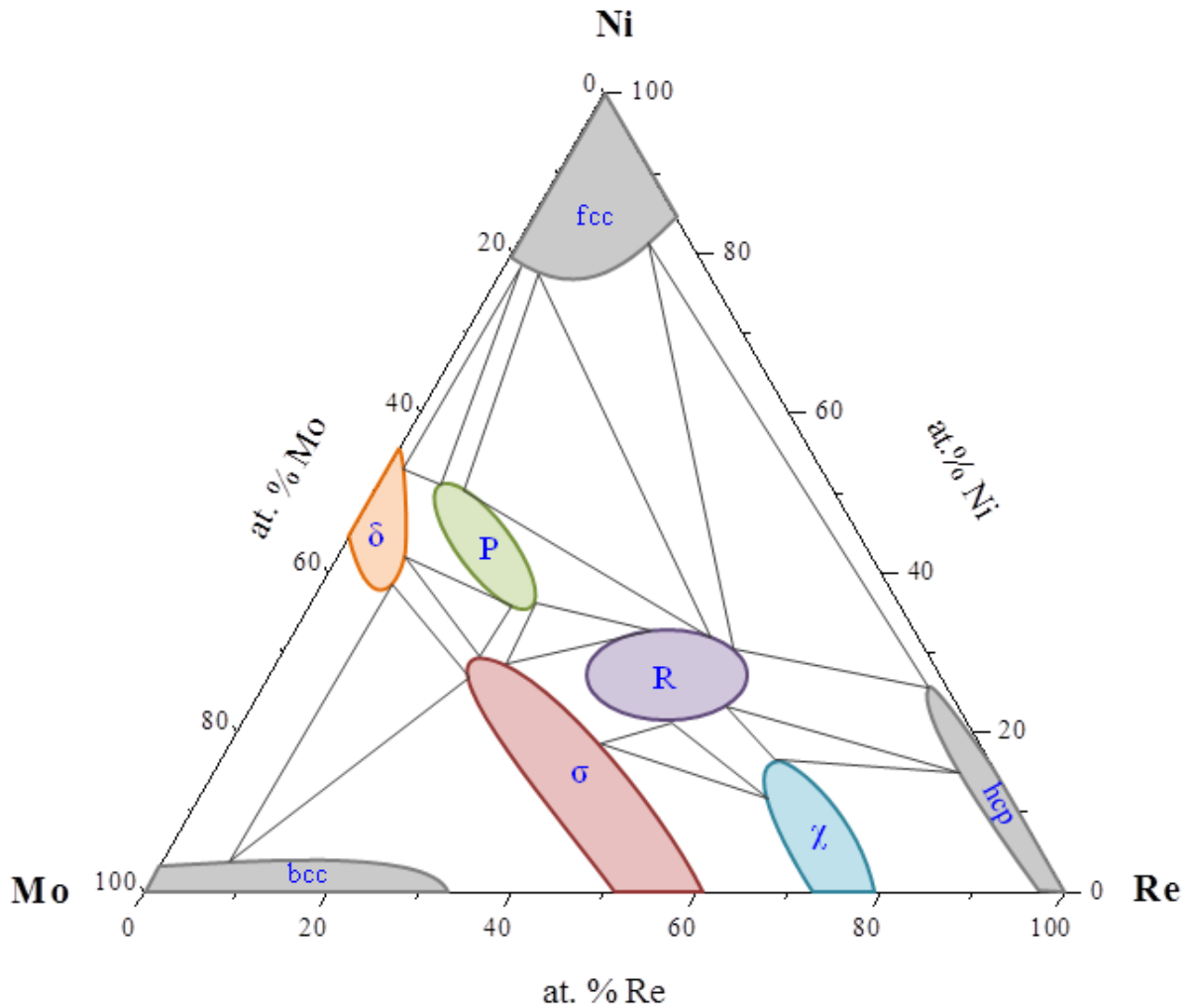


Figure 1-9: Isothermal cross-section of the Mo-Ni-Re system at 1152°C proposed by Kodentsov et al. [6].

As illustrated in Figure 1-9, the isothermal section of Mo-Ni-Re system at 1152 °C is characterized by the presence of three solid solutions: bcc; fcc; and hcp, five intermetallic compounds:  $\sigma$ ;  $\chi$ ;  $\delta$ ; P and R, and eight three phase equilibria. The binary phases of Mo-Re system i.e.  $\sigma$  and  $\chi$ , were found to have considerable extension into the ternary region. The maximum solubility of nickel in  $\sigma$  and  $\chi$  phases was reported to be 29.5 at % and 19 at % respectively. The  $\delta$ -phase, binary phase of Mo-Ni system, was found to extend into the ternary domain to about 7 at.% Re. In addition to the considerable extension of binary intermetallic compounds of the Mo-Re and Mo-Ni binary systems, Kodentsov et al. reported presence of two previously unknown ternary intermetallic compounds. The XRD measurements to find out the crystal structure of these ternary phases were not possible as Kodentsov et al. [6] used only diffusion couples for investigation of the isothermal sections. The Mo-Ni-Re ternary phases were therefore tentatively assigned as P and R only by analogy with other systems such as Cr-Mo-Ni [65], Co-Mn-Mo [66], Fe-Mo-Ni [67] in which these

phases were evidenced. In the previous investigation by Burhanov et al. [63] and Savitskii et al. [64], Ni based solid solution was only found in equilibrium with hcp and  $\delta$  phase. However Kodentsov et al. [6] reported that Ni based solid solution is also present in equilibrium with the ternary phases appearing in the Mo-Ni-Re system.

A more detailed study of the phase equilibria in Mo-Ni-Re system was carried out by Borisov et al. [7] and Slyusarenko et al. [8]. They determined isothermal section of the Mo-Ni-Re system at 1152°C with the help of diffusion couples and arc melted alloys. The structure of diffusion zones, concentration distribution of elements in the diffusion layers and phases of annealed arc melted alloys were investigated by using scanning electron microscopy (SEM), electron probe microanalysis (EPMA) and X-ray analysis. By combining the results obtained from the characterization of the diffusion couples and equilibrated arc melted alloys, 1152°C isothermal section of the Mo-Ni-Re system was proposed which is shown in the Figure 1-10.

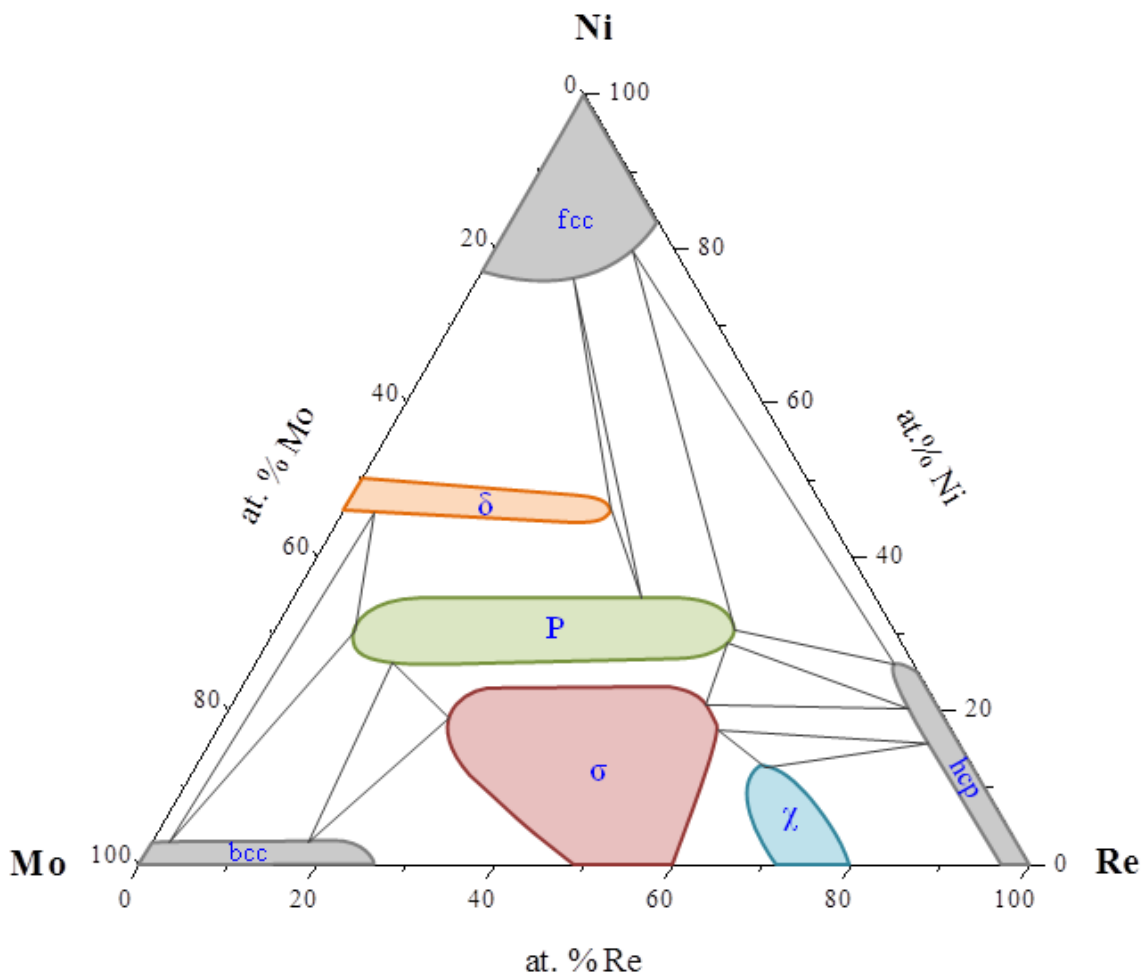


Figure 1-10: Isothermal cross-section of the Mo-Ni-Re system at 1152°C proposed by Borisov et al. and Slyusarenko et al. [7, 8].

As shown in the Figure 1-10, the Mo-Re  $\sigma$  and Mo-Ni  $\delta$  phase were found to have considerable extension in the ternary region. The maximum solubility of Re in  $\delta$ -phase was reported to be 28 at.%, whereas the  $\sigma$ -phase was found to have a homogeneity region up to 22 at.% Ni, 20-60 at.% Re and 22-60 at.% Mo. The extension of  $\chi$ -phase into the ternary was limited to about 13 at.% Re. Borisov et al. [7] observed the presence of only one ternary compound in the studied isothermal section. This ternary compound was tentatively assigned to the P-phase type. The homogeneity domain of the P-phase was reported to range from 7 at.% Re to 50 at.% Re. Contrary to the previous investigation by Kodentsov et al. [6], presence of R-phase and equilibrium between  $\sigma$  and  $\delta$  was not evidenced. The authors reported that the results obtained during their investigation of the Mo-Ni-Re system were consistent with the phase diagrams of systems of Ni and Re with bcc transition metals.

The most recent attempt for study of Mo-Ni-Re system, was carried out by Feng et al. [9]. They investigated phase equilibria of Mo-Ni-Re system at 1200°C by means of diffusion triple and electron probe microanalysis (EPMA). The 1200°C isothermal section of the Mo-Ni-Re system proposed by Feng et al. [9] is shown in the Figure 1-11.

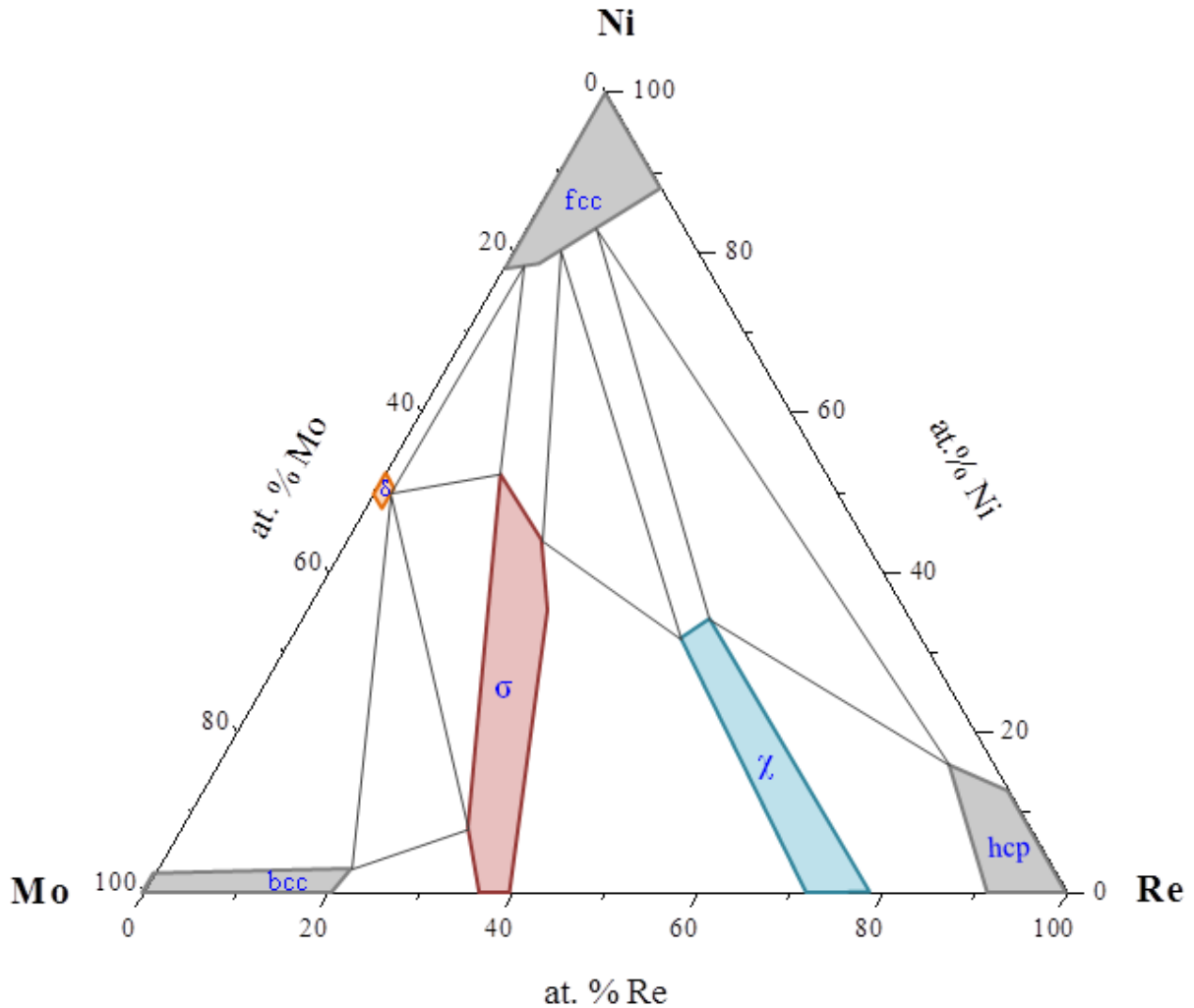


Figure 1-11: Isothermal cross-section of the Mo-Ni-Re system at 1200°C proposed by Feng et al. [9].

As shown in the Figure 1-11, presence of no ternary compound was evidenced in the studied isothermal section. Binary intermetallic compound of Mo-Re system were found to have large extension in to the ternary region. The maximum solubility of nickel in  $\sigma$  and  $\chi$  phase was reported to be 52.28 at.% and 33.96 at.% respectively. The extension of  $\delta$ -phase in the ternary section to was limited to only 2.04 at.% Re.

Unlike previously reported isothermal sections by Kodentsov et al. [6] and Borisov et al. [7], Feng et al. [9] did not report presence of any ternary phase in the studied isothermal. The three phase regions shown in the Figure 1-11 were also not established through EPMA analysis of three phase samples and their locations are rather tentative.

A comparison of the previous attempts made for the determination of phase equilibria in Mo-Ni-Re system shows that the determined isothermal sections not only contradict each other in

terms of number of ternary compounds present in the studied system but also none of the previous investigations carried out phase identification of ternary compounds. In addition previous investigation show large differences in terms of homogeneity domains of different phases. A comparison of the previous attempts made for the determination of isothermal section of Mo-Ni-Re is presented in Table 1-9.

*Table 1-9: Comparison of different investigations of the Mo-Ni-Re system*

Ternary phases	Extension in the ternary region								Ref	
	$\sigma$	$\chi$	$\delta$	fcc		bcc		hcp		
	(% Ni)	(% Ni)	(% Re)	%Mo	%Re	%Ni	%Re	%Mo		%Ni
-	-	-	-	18.7	9.6	-	-	-	-	[63] [64]
P, R	29.0	14.9	8.9	24.4	16.5	4.1	38.4	5.6	21.4	[6]
P	23.4	13.1	29.9	22.7	16.5	3.0	16.9	3.5	25.7	[8]
No phase	52.3	34.0	2.0	20.6	11.9	3.1	21.5	8.6	16.0	[9]

In addition to the contradictions mentioned in Table 1-9, the boundaries of the three phase regions, in all the previous attempts, were not determined through the EPMA analysis of three phase samples and their positions were rather tentative. Moreover, agreement of the previously determined isothermal sections with accepted binary data was also not satisfactory. Therefore it was concluded that Mo-Ni-Re system required further study.

## 1.7. Objectives of present work

The detrimental effects of TCP phases on the mechanical properties of Ni based superalloys have already been discussed in the section 1.1.5. To avoid the TCP phase precipitation resulting from higher concentrations of Mo and Re, experimental investigation and thermodynamic modeling of the Mo-Ni-Re system is required. Once the Mo-Ni-Re system has been modeled, its thermodynamic description can be combined with description of other subsystems and phase equilibria in the Ni based superalloys can be predicted. The prediction of phase equilibria would ultimately help in selection of suitable alloy composition to avoid precipitation of the TCP phases.

During the present study, a complete experimental redetermination of the Mo-Ni-Re followed by its thermodynamic modeling with the help of the Calphad method was planned to be carried out. However, prior to the investigation of the ternary system, it is important that the phase boundaries in the constituent binary systems should be well established. The bibliographic research carried out during the present study revealed that the phase diagrams of the Mo-Ni and Mo-Re binary system are well determined except some uncertainties in the homogeneity domain of some phases. Therefore, verification of the phase boundaries in the related binary systems at least at the temperatures selected for the present investigation of the Mo-Ni-Re system was required and was planned to be carried out during the present study. On the other hand, large uncertainties in the previously reported Ni-Re binary data necessitated complete experimental redetermination of the Ni-Re binary system. During the present study, the Ni-Re binary system was planned to be first studied experimentally, and then modeled thermodynamically with the help of new experimental information.

The literature review of the Mo-Ni-Re system presented in the section 1.6.4 revealed contradictory results in terms of homogeneity domains, presence of ternary compounds, crystal structure of ternary compounds, and agreement with the related binary systems. Therefore, in order to develop better understanding of the phase equilibria, redetermination of the Mo-Ni-Re system was planned to be carried out with the following objectives:

- Phase equilibria investigation of the Mo-Ni-Re system
- Structural characterization of phases
- Thermodynamic modeling of the Mo-Ni-Re system by using the Calphad method

Contrary to the previous studies, phase equilibria investigation of the Mo-Ni-Re system will be carried out exclusively by use of the equilibrated alloys. The refractory nature of the constituent elements demands higher annealing times and temperatures to achieve equilibrium. Therefore, during the present study, isothermal sections of the Mo-Ni-Re system will be studied at 1200°C for 1680 hours and at 1600°C for 9 hours. One of the reasons to study 1200°C isothermal section is to be able to compare the results with the previous studies of the Mo-Ni-Re system. The determination of 1600°C isothermal section in addition to the 1200°C isothermal section will help in studying the variation of homogeneity domains of constituent phases as a function of temperature.

One of the key objectives of multi-component phase diagram determination is to find and identify new phases. In the previous investigations of the Mo-Ni-Re system, the crystal structures of ternary phases were not identified with the help of diffraction techniques. They were tentatively assigned as P and R phases only from the analysis of the literature information. Therefore, crystal structure identification of the ternary phases (if present in the Mo-Ni-Re system) with the help of diffraction techniques was set as one of goals for the present study. In addition to the phase identification, the information such as site occupancies plays an important role in selection of a suitable thermodynamic model. The structural characterization of the selected phases with particular emphasis on determination of site occupancies will also be carried out.

Finally, the experimental information gathered from the first two steps will be used as input data and thermodynamic assessment of the Mo-Ni-Re system will be carried out with the help of the Calphad method. In addition to the experimental information, the results of the DFT calculations made by Jean-Claude Crivello will also be used.

The details about experimental techniques selected for the present study are provided in the chapter 2 whereas the Calphad approach used for thermodynamic assessment of the Mo-Ni-Re system is introduced in the chapter 3. The experimental results obtained during the present study are described in chapter 4 to chapter 7 while thermodynamic modeling of the Mo-Ni-Re is discussed in detail in chapter 8.

**References**

- [1] R. C. Reed, *The Superalloys Fundamentals and Applications*, 1, Cambridge University Press, New York, (2008).
- [2] M. J. Donachie, S. J. Donachie, *Superalloys: A technical guide*, ASM International, (2002).
- [3] <http://www.onera.fr/photos-en/materials-structures/nickel-based-superalloy.php>
- [4] C. M. Rae, R. C. Reed, *Acta Mater.*, 49 (2001) 4113-4125
- [5] H. Okamoto, *J. Phase Equilib.*, 21 (2000) 497
- [6] A. A. Kodentsov, S. F. Dunaev, E. M. Slyusarenko, E. M. Sokolovskaya, A. N. Priimak, *Vestn. Mosk. Univ., Ser. 2., Khim.*, 28 (1987) 153-158
- [7] V. A. Borisov, A. I. Yaschenko, E. M. Slyusarenko, S. F. Dunaev, *Moscow University Chemistry Bulletin*, 47 (1992) 76-79
- [8] E. M. Slyusarenko, A. V. Peristy, E. Y. Kerimov, M. V. Sofin, D. Y. Skorbov, *J. Alloys Compd.*, 264 (1998) 180-189
- [9] Y. Feng, R. Wang, K. Yu, D. Wen, *Rare Met.*, 27 (2008) 83-88
- [10] M. Kikuchi, M. Kajihara, H. Usuki, Y. Kadoya, R. Tanaka, *Proc. of the High-Temperature Alloys: Theory and Design*, Bethesda, Maryland, USA (1984), 359-379.
- [11] E. M. Slyusarenko, A. V. Peristy, E. Y. Kerimov, I. L. Guzei, M. V. Sofin, *J. Alloys Compd.*, 256 (1997) 115-128
- [12] D. C. Cox, C. M. F. Rae, R. C. Reed, in *Life assessment of hot section gas turbine components*, R. Townsend, Editor, 2000, The institute of materials: London, UK.
- [13] J. Emsley, *Nature's Building Blocks: An A-Z Guide to the Elements*, Oxford University Press Inc., New York, (2003).
- [14] T. B. Massalski, *Binary alloys phase diagrams*, second ed., ASM International, Materials Park, Ohio, (1990).
- [15] S. H. Avner, *Introduction to Physical Metallurgy*, McGraw-Hill, (1974).
- [16] J.-C. Zhao (Editor), *Methods for phase diagram determination*, Elsevier, (2007).
- [17] H. L. Lukas, S. G. Fries, B. Sundman, *Computational thermodynamics, the Calphad method*, 313, Cambridge University Press, (2007).

- 
- [18] N. Saunders, A. P. Miodownik, *Calphad, calculation of phase diagrams, a comprehensive guide*, Pergamon Materials Series, (1998).
- [19] A. A. Kodentsov, G. F. Bastin, F. J. J. van Loo, *Journal of Alloys and Compounds*, 320 (2001) 207–217
- [20] A. A. Kodentsov, G. F. Bastin, F. J. J. van Loo, *Application of Diffusion Couples in Phase Diagram Determination*, in *Methods for phase diagram determination*, J.-C. Zhao, Editor, 2007, Elsevier.
- [21] C. P. Heijwegen, G. D. Rieck, *Metallurgical Transactions*, 4 (1973) 2159-2167
- [22] J.-M. Joubert, *Prog. Mater. Sci.*, 53 (2008) 528-583
- [23] J.-M. Joubert, J.-C. Crivello, *Applied sciences*, doi:10.3390/app2030669 (2012) 669-681
- [24] J.-M. Joubert, M. Phejar, *Prog. Mater. Sci.*, 54 (2009) 945-980
- [25] M. Hansen, *Constitution of binary alloys*, McGraw-Hill, (1958).
- [26] R. E. W. Casselton, W. Hume-Rothery, *Journal of the less-common metals*, 7 (1964) 212-221
- [27] C. P. Heijwegen, G. D. Rieck, *Z. Metallkde.*, 64 (1973) 450-453
- [28] L. L. Meshkov, L. S. Guzei, E. M. Sokolovskaya, *Russian Journal of Physical Chemistry*, 49 (1975) 1128-1129
- [29] S.-J. L. Kang, Y.-D. Song, W. A. Kaysser, H. Hofmann, *Z. Metallkde.*, 75 (1984) 86-91
- [30] F. H. Ellinger, *Trans. ASM*, 30 (1942) 607
- [31] C. B. Shoemaker, D. P. Shoemaker, *Acta Crystallogr.*, 16 (1963) 997-1009
- [32] S. Saito, P. A. Beck, *Trans. Metall. Soc. AIME*, 215 (1959) 938-941
- [33] D. Harker, *J. Chem. Phys.*, 12 (1944) 315-317
- [34] S. A. Pogodin, M. A. Skryabina, *Izvestiya Sektora Fiziko-Khimicheskogo Analyza, Institut Obshchei i Neorganicheskoi Khimii, Akademiya Nauk SSSR*, 25 (1954) 81-88
- [35] E. M. Savitskii, M. A. Tylkina, E. P. Arskaya, *Izvestiya Vysshikh Uchebnykh Zavedenii, Tsvetnaya Metallurgiya*, 13 (1970) 113-116

- [36] E. M. Savitskii, M. A. Tylkina, K. B. Povarova, Proc. of the Moscow (1965).
- [37] U. Hofmann, *physica status solidi (a)*, 33 (1976) 119-123
- [38] S. M. Solonin, *Sov. Powder Metall. Met. Ceram.*, 15 (1976) 270-272
- [39] A. Nash, P. Nash, *Bull. Alloy Phase Diagr.*, 6 (1985) 348-350
- [40] K. Moers, *Z. Anorg. Allg. Chem.*, 196 (1931) 147-150
- [41] C. G. Fink, P. Deren, *Trans. Electrochem. Soc.*, 66 (1934) 471-474
- [42] C. B. F. Young, *Met. Ind.*, 34 (1936) 176-177
- [43] L. E. Netherton, M. L. Holt, *J. Electrochem. Soc.*, 98 (1951) 106-109
- [44] P. I. Kirichenko, V. E. Mikryukov, *High Temp. Sci.*, 2 (1964) 176-180
- [45] E. M. Savitskii, M. A. Tylkina, E. P. Arskaya, Proc. of the Splyav Tsvetnykh Metallov, (1972).
- [46] A. A. Katsnelson, E. M. Savitskii, A. M. Silonov, E. P. Arskaya, V. M. Silonov, A. S. Savichev, Proc. of the Fiz.-Khim. Svoistva Splyavov Reniya, Moscow (1979), 103-110.
- [47] C. M. Neubauer, D. Mari, D. C. Dunand, *Scr. Metall. Mater.*, 31 (1994) 99-104
- [48] S. Saito, K. Kurokawa, S. Hayashi, T. Takashima, T. Narita, *J. Jpn. Inst. Met.*, 71 (2007) 608-614
- [49] I. V. Ametov, S. F. Dunaev, E. M. Slyusarenko, A. V. Peristy, *Vestn. Mosk. Univ., Ser. 2., Khim.*, 31 (1990) 47-52
- [50] I. V. Ametov, S. F. Dunaev, E. M. Slyusarenko, A. V. Peristy, *Mosc. Univ. Chem. Bull.*, 45 (1990) 49-52
- [51] J. M. Dickinson, L. S. Richardson, *Trans. ASM*, 51 (1959) 1055-1071
- [52] A. G. Knapton, *J. Inst. Met.*, 87 (1958-59) 62-64
- [53] E. M. Savitskii, M. A. Tylkina, *Zh. Neorganich. Khim.*, 3 (1958) 820-837
- [54] E. M. Savitskii, M. A. Tylkina, K. B. Povarova, *Russ. J. Inorg. Chem.*, 4 (1959) 190-195
- [55] L. Brewer, R. H. Lamoreaux, *At. Energy Rev., Spec. Issue 7* (1980) 195-356

- [56] D. P. Shoemaker, G. Bergman, *J. Am. Chem. Soc.*, 72 (1950) 5793
- [57] G. Bergman, D. P. Shoemaker, *Acta Crystallogr.*, 7 (1954) 857-865
- [58] S.-A. Farzadfar, M. Levesque, M. Phejar, J.-M. Joubert, *Calphad: Comput. Coupling Phase Diagrams Thermochem.*, 33 (2009) 502-510
- [59] K. W. Andrews, *Nature*, 164 (1949) 1015
- [60] K. W. Andrews, P. E. Brookes, *Met. Treatment Drop Forging*, July (1951) 301
- [61] J. S. Kasper, *Acta Metall.*, 2 (1954) 456-461
- [62] A. J. Bradley, J. Thewlis, *Proc. R. Soc. (London)*, A115 (1927) 459-471
- [63] G. S. Burhanov, E. P. Arskaya, I. V. Burov, A. V. Kopyl, *Arch. Metall.*, 34 (1989) 33-39
- [64] E. M. Savitskii, M. A. Tylkina, E. P. Arskaya, *Issled. Primen. Splavov Reniya, (Dokl. Vses. Soveshch. Probl. Reniya)*, 4th (1973 (1975)) 58-61
- [65] S. Rideout, W. D. Manly, E. L. Kamen, B. S. Lement, P. A. Beck, *Trans. AIME*, 191 (1951) 872-876
- [66] B. N. Das, P. A. Beck, *Trans. Metall. Soc. AIME*, 218 (1960) 733-737
- [67] D. K. Das, S. P. Rideout, P. A. Beck, *J.o.M.*, 4 (1952) 1071-1075
- [68] C. Brink, D. P. Shoemaker, *Acta Crystallogr.*, 8 (1955) 734-735
- [69] D. P. Shoemaker, C. B. Shoemaker, F. C. Wilson, *Acta Crystallogr.*, 10 (1957) 1-14
- [70] Y. Komura, D. P. Shoemaker, C. B. Shoemaker, *Acta Crystallographica*, 10 (1957) 774-775
- [71] Y. Komura, W. G. Sly, D. P. Shoemaker, *Acta Crystallogr.*, 13 (1960) 575-585

# **Chapter 2**

## **Experimental Techniques**



## **2. Experimental Techniques**

During the present study, experimental investigation of the selected alloy systems was carried out with the help of equilibrated alloy method. Samples of different alloy compositions were prepared by arc melting, annealed at high temperatures for suitable periods of times and characterized mainly with the help of X-ray diffraction (XRD), electron probe microanalysis (EPMA) and differential thermal analysis (DTA) techniques. However, in some cases single crystal and neutron diffraction (ND) techniques were also used for the purpose of phase identification and structural characterization respectively. The working principle of above mentioned experimental techniques and their importance in the context of present study has been described briefly in this chapter which has been divided into the following three parts.

- Alloy preparation
- Homogenization heat treatment and quenching
- Characterization

### **2.1. Alloy preparation**

The alloy preparation is a key step for the investigation of phase equilibria in a multi-component system. The purity of the starting materials is also very important as very small amount of extraneous components may render significant modifications in the results. Therefore, high purity metal powders (Mo: Sigma Aldrich, <150 $\mu$ m, 99.99 %; Ni: Alfa Aesar, <125 $\mu$ m, 99.996 %; Re: Alfa Aesar, <44 $\mu$ m, 99.99 %) were used as the starting materials for the present study. Samples of desired composition were prepared by mixing and compacting pure metal powders into pellets (Diameter: 8 mm, Applied force: 4000 Kg) and subjecting them to melting under argon atmosphere. Considering the high melting temperature of the constituent elements, electric arc furnace was used for melting. The schematic and photograph of the electric arc furnace employed during the present study for sample preparation is shown in the Figure 2-1.

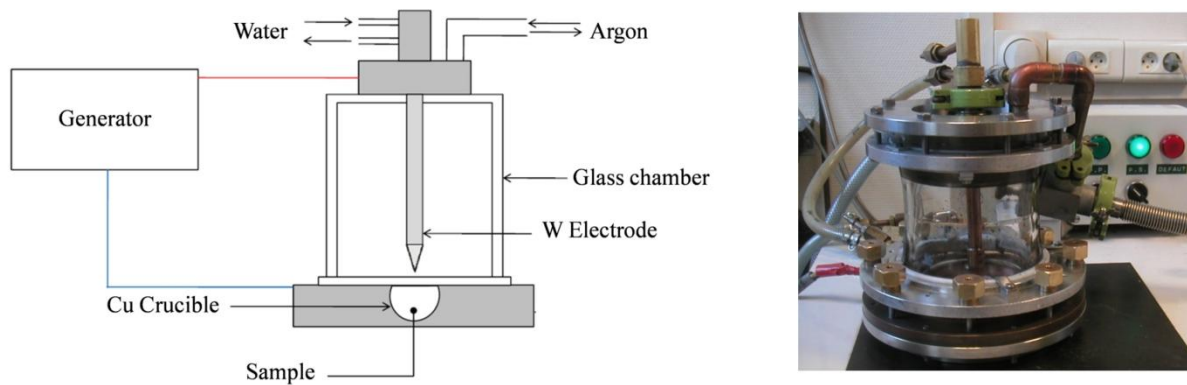


Figure 2-1: Schematic (left) and photograph (right) of the electric arc furnace used for the alloy preparation during the present study

As illustrated in the Figure 2-1, the electric arc furnace used during the present study consists of a non-consumable tungsten electrode serving as a cathode and a water cooled copper crucible that acts as a sample holder and as a part of the anode. For the alloy preparation, pellet to be melted was placed in the copper crucible, chamber of the furnace was closed and a secondary vacuum of  $2 \times 10^{-9}$  bar was applied in order to remove atmospheric gases that may cause oxidation during melting. Once the required value of the vacuum is achieved, high purity argon was inserted to avoid the evaporation of high vapor pressure components *i.e.* Ni in the present case, during melting. The insertion of argon in the chamber also made possible the movement of the tungsten electrode and striking of electric arc. After insertion of argon, arc was struck by moving the tungsten electrode towards the copper platform. As soon as, the arc is struck, a current of high intensity appears which ionizes the argon atoms present in the furnace chamber. The electrode is then moved towards the pellet, which in contact with the copper crucible acts like a second electrode and as a result strong current passes through them. Melting of the pellet takes place in few seconds. After melting, electrode is moved toward the border of the crucible and arc is turned off. The alloys obtained after melting are in the shape of buttons. The melted alloys should have a homogeneous composition because the macro-inhomogeneities left during melting are difficult to remove during subsequent annealing treatments. Therefore, in order to achieve a homogeneous distribution of the constituent elements in the alloys, the alloys were flipped over after melting and melted again. This process was repeated five times in order to achieve maximum homogenization. The weight of each sample was measured before and after melting to keep a record of the weight losses during sample preparation. In most of the cases, the weight loss during melting was less than 1 %.

The arc melting facility available in the lab is best suited for the small samples (mass around 3g). In case of the big samples, relatively large surface of the sample will be in contact with the water cooled copper crucible and as a result complete melting of the pellet may be difficult which can cause homogeneity problems. In most of the cases, weight of our sample was less than 1g. However sample weighing around 9 g were required for the neutron diffraction measurements. In that case, three samples (weighing 3 g each) of the same composition were initially prepared. Each sample was melted five times. Finally all the three samples were put together and melted again. The combined melting was also carried out five times. The chemical and structural homogeneity of these samples was later confirmed by XRD and EPMA measurements.

## **2.2. Homogenization heat treatment and quenching**

In order to remove the concentration gradient that may appear during solidification due to segregation and to obtain thermodynamic equilibrium at a particular temperature, annealing treatment is necessary. During the process of annealing, homogenization of the samples is achieved through diffusion; therefore, annealing time and temperature are two important factors. The diffusion of rhenium and molybdenum atoms is very slow by virtue of their refractory nature; therefore, high annealing temperatures and long annealing times may be required to attain equilibrium. During the present study, annealing of the samples was carried out either at 1200°C or at 1600°C. Few hours of annealing were sufficient at 1600°C whereas several weeks were required to attain thermodynamic equilibrium at 1200°C.

### **2.2.1. Annealing at 1200°C**

The annealing of the samples at 1200°C was carried out with the help of resistance furnace. Prior to the annealing at 1200°C, the arc melted alloys were wrapped in tantalum sheets and sealed in the silica (SiO<sub>2</sub>) capsules under argon atmosphere. The wrapping of the samples in the tantalum sheets was meant to avoid their oxidation which may occur during annealing due to their contact with silica tube. On the other hand, tantalum being a refractory metal with a very high melting point (3017°C) will remain solid at the annealing temperature and would minimize the risk of its reaction with the samples to be annealed. The insertion of argon gas inside the silica capsule was carried out to avoid the evaporation of Ni and collapsing of silica capsules at 1200°C during annealing. The pressure of argon inside the silica capsule at room temperature was so calculated that it becomes 1 bar at annealing temperature. After sealing,

silica capsules were placed in a preheated resistance furnace for duration of 10 weeks (1680 hours). An example of the silica capsule containing samples under argon atmosphere and of a resistance furnace used for the present study is shown in the Figure 2-2.



*Figure 2-2: Alloys encapsulated in silica tubes under argon atmosphere (left) and resistance furnace used for annealing (right)*

Once the annealing is over, samples should be rapidly cooled to freeze the homogenization temperature equilibrium microstructure to room temperature. Therefore to achieve rapid cooling, silica tubes containing samples were quenched in water. As a result, cooling of the samples from the annealing temperature to room temperatures took place in few seconds and annealing temperature microstructure was assumed to be retained at room temperature.

### **2.2.2. Annealing at 1600°C**

The annealing of the samples at 1600°C was carried out with the help of a high frequency induction furnace. The principle of induction heating is the following: passage of a high frequency current through the coil generates a very intense and rapidly changing magnetic field in the space within the coil. The sample to be annealed is placed within this intense alternating magnetic field. The alternating magnetic field induces a current flow, also known as Foucault or eddy current, in the sample. Since the sample to be annealed presents non-zero electrical resistivity, the heat energy which is proportional to the square of the induced intensity, will be dissipated by the joule effect ( $P = R \times I^2$ ) at each point for the sample and as a result temperature of the sample will increase. The schematic and photograph of a high frequency induction furnace used during the present study is shown in the Figure 2-3.

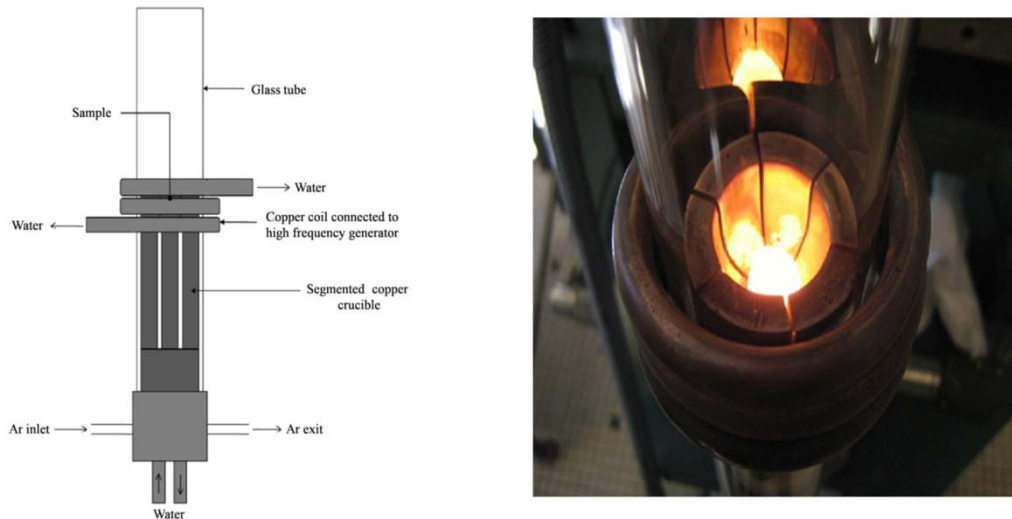


*Figure 2-3: Schematic (left) and photograph (Right) of the high frequency induction furnace used for annealing at 1600°C*

For annealing at 1600°C, samples were placed in a copper crucible specially designed for avoiding appearance of induction current in the crucible. A silica tube was placed on the crucible and secondary vacuum of  $2 \times 10^{-9}$  bar was applied. The sample at the start of the annealing was heated under vacuum for thermal desorption of the gas molecules adsorbed on the surface of sample. However, after some time, annealing of the sample was carried out under argon atmosphere. The samples were annealed at 1600°C for 9 hours. Once the annealing is over, the induction heating was switched off and rapid cooling of the sample took place due to its contact with water-cooled copper crucible.

The temperature of the sample during annealing was measured with help of the electronic pyrometer, Minolta-Cyclops 1.52A, which analyses emission spectrum of the hot body for measuring its temperature.

## **2.3. Characterization of alloys**

After annealing, investigation of the studied alloys compositions was carried out with the help of different characterization techniques. This section provides information about their working principle and interpretation of obtained results for the phase diagram determination.

### **2.3.1. X-ray diffraction (XRD)**

XRD is a non destructive material characterization technique used for identification of phase present in equilibrium, determination of their lattice parameter, quantitative phase analysis, and structural characterization [1]. The information gathered from the XRD measurements

can also be used for the determination/verification of phase boundaries in a multi-component phase diagram.

X-rays are basically electromagnetic in nature having a wavelength between 0.2 and 2 Å. When a monochromatic beam of X-rays is impinged on the sample, the X-rays-sample interaction causes oscillation of the electronic cloud of the atoms. This oscillation results in the emission of new radiations that have the same phase and wavelength as that of the incident beam (elastic scattering). This phenomenon is called as Thomson scattering. The nucleus bearing the positive charge might also be expected to take part in the coherent scattering. According to the Thomson equation, intensity of the coherent scattering is inversely proportional to the square of the mass of the scattering particle; therefore, nucleus because of its extremely large mass will not participate in the coherent scattering. Consequently, the coherent scattering by an atom is only due to the electrons present in that atom [2]. The radiations emitted by different atoms interact and the directions in which there is a constructive interference, diffracted beams are observed. The intensity of the diffracted beam is recorded as a function of incident angle by a detector.

According to the Bragg's law, constructive interference occurs only when the path difference between the rays scattered from parallel set of planes is an integer multiple of the wavelength of the radiation.

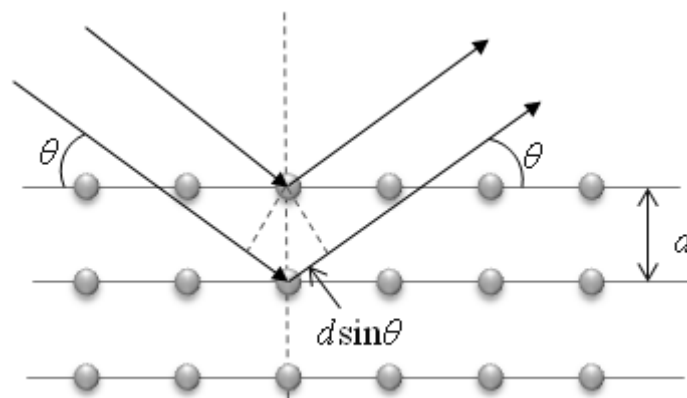


Figure 2-4: Bragg's Law

According to the Bragg's law

$$n\lambda = 2d_{hkl}\sin \theta_{hkl} \quad \text{Equation 2-1}$$

In the Equation 2-1,

- $n$  is an integer and corresponds to the order of diffraction
- $\lambda$  is the wavelength of the incident beam
- $h$ ,  $k$ , and  $l$  are miller indices
- $d_{hkl}$  is the distance between two planes of indices  $h$ ,  $k$  and  $l$
- $\theta_{hkl}$  is the angle between the incident beam and surface of the sample

In case of cubic unit cell, distance between two parallel planes is given by the following relation:

$$d_{hkl} = \frac{a}{\sqrt{h^2 + k^2 + l^2}} \quad \text{Equation 2-2}$$

In the Equation 2-2,

- $a$  represents lattice parameter of a cubic unit cell

The intensity diffracted by a set of planes of indices  $hkl$  is proportional to the squared modulus of the structure factor.

$$F_{hkl} = \sum_j n_j f_j \left( \frac{\sin \theta_{hkl}}{\lambda} \right) e^{2\pi i(hx + ky + lz)} e^{-B(T) \left( \frac{\sin \theta_{hkl}}{\lambda} \right)^2} \quad \text{Equation 2-3}$$

In the Equation 2-3,

- $n_j$  represents site occupancies
- $f_j$  is the atomic scattering factor of the atom  $j$
- $B(T)$  is Debye-Waller factor, it takes into account thermal agitation

Since, it is only the electrons that contribute to the diffraction of X-rays; therefore, contribution of light elements containing less number of electrons to the diffracted intensity will be weaker than that of heavy atoms possessing more electrons. As a result atoms with

remote atomic numbers can be differentiated. However it is difficult to distinguish the elements with close atomic numbers.

During the present study, XRD measurements were performed on a Bruker D8 advance diffractometer (Bragg-Brentano geometry: X-ray tube and detector makes an angle  $\theta$  with the sample) equipped with Cu  $K\alpha$  radiation and a rear graphite monochromator. Sample preparation for the XRD measurements involved crushing the sample in a mortar to obtain fine powder, sprinkling it on a double-sided tape applied on a plexi-glass sample holder, and flattening it with the help of a glass slide to obtain a smooth surface. The crushing of the sample prior to the XRD measurements helps to obtain random orientation of the grains with respect to the incident beam and avoids preferential orientation that may cause intensity variations during XRD measurements. Most of the samples investigated during the present study were easily reduced to the fine powder because of their high brittleness. In case of the alloy compositions that were difficult to crush, samples were cut from the center and polished before subjecting them to the XRD measurements.

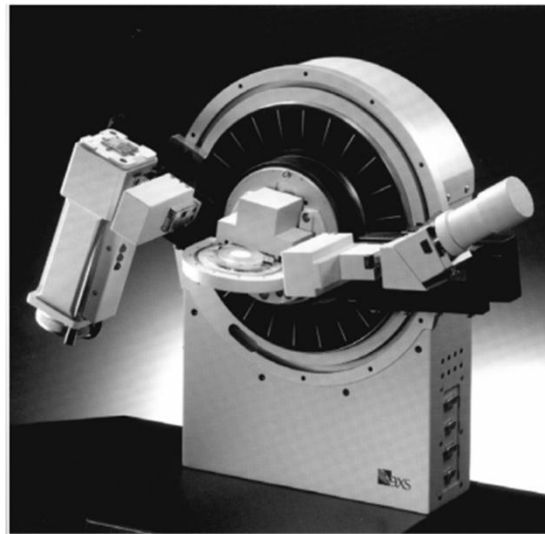


*Figure 2-5: Bruker D8 advance diffractometer*

### **2.3.2. Neutron diffraction (ND)**

The structural characterization of a ternary phase requires at least two diffraction datasets with large scattering contrast among the constituent elements in each dataset and different scattering contrast among the elements in two datasets. The constituent elements of the studied system (Mo-Ni-Re) present large and opposite scattering contrast in the X-ray and neutron diffraction (ND) techniques. Therefore ND measurements were also carried out in

addition to the XRD measurements for structural characterization of the selected Mo-Ni-Re compositions.

Neutron diffraction is also a non destructive technique that is used to probe atomic structure of the material. The sample to be studied is placed within a neutron beam and the angles at which the neutrons are deflected or scattered by the material are recorded to generate a diffraction pattern. Contrary to the X-rays that interact primarily with the electron cloud surrounding each atom, the neutrons interact directly with the nucleus of the atom. Due to their interaction directly with the nucleus of an atom, contribution to the diffracted intensity is different for each isotope; for example, regular hydrogen and deuterium. As a result atomic position of lighter elements and also of their isotopes can be determined even in the presence of heavier elements. In addition two elements situated very close in the periodic table such as iron and cobalt can also be differentiated with the help of this technique.

During the present study, ND measurements were carried out at Laboratoire Léon Brillouin (LLB; common laboratory CEA-CNRS), Saclay, France, using a 3T2 instrument. The schematic of a 3T2 instrument is shown in the Figure 2-6. It uses a beam of thermal neutrons that passes through a collimator and is deflected by a vertical germanium monochromator on the sample. The intensity of the scattered beam is measured in the angular range of  $5^\circ$  to  $122^\circ$  with the help of a multidetector.

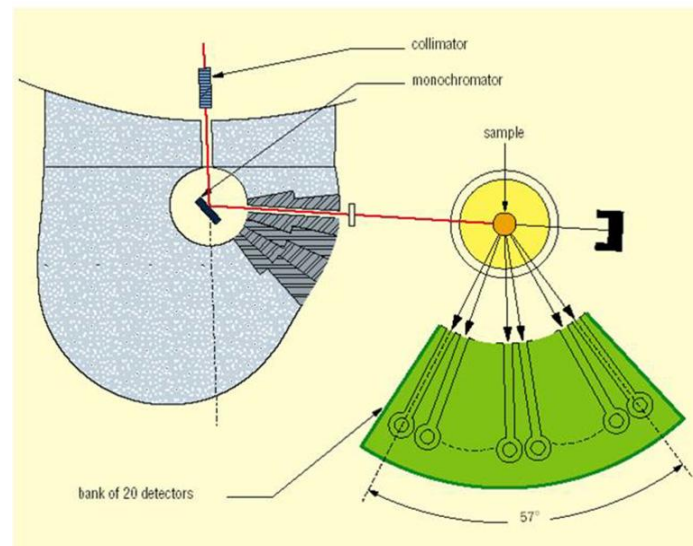


*Figure 2-6: Schematic of the LLB 3T2 diffractometer*

### 2.3.3. Analysis of the diffraction data

After the XRD and ND measurements, diagrams representing the intensity of diffracted rays measured by the detector as a function of its angular position are obtained.

The X-ray and neutron diffraction patterns were initially subjected to a crystallographic database PDF2 (Powder diffraction file) containing a large number of experimental and calculated diffraction patterns with the help of the software called DIFFRACPLUS Eva. This software by comparing the number, position and intensity of peaks in observed and stored diffraction patterns helps in identification of the phases present in the studied material. In addition, a rough idea about the lattice parameters of the phases present in the studied material can be obtained by manually adjusting lattice parameters of the phases stored in the database with the help of this software. The preliminary information obtained from this step serves as a basis for the refinement of the diffraction data.

For accurate determination of lattice parameters and structural characterization of the constituent phases, XRD and ND data was later refined by the Rietveld method. It is a method of calculating a theoretical diagram with the help of known structure information such as nature of phases in the sample, atomic positions, nature of atoms at each site, approximate line width, lattice parameters etc. and adjusting the values of these parameters by least square method to obtain the best possible agreement between the observed and calculated pattern.

During the present study, Rietveld method was implemented by using the FULLPROF program. The details about the FULLPROF program can be found in the manual [3]. The program uses the information provided by user about initial parameters and calculates intensity  $y_{\text{calc},i}$  for each observed point  $i$ , with the help of following formula:

$$y_{\text{calc},i} = \sum_{\varphi} S_{\varphi} \sum_h L_{\varphi,h} A_{\varphi,h} P_{\varphi,h} |F_{\varphi,h}|^2 \Omega_{\varphi,h}(\theta_i - \theta_{\varphi,h}) + b_i \quad \text{Equation 2-4}$$

In the Equation 2-4,

- $\varphi$  represents the phase present in the studied composition and varies between 1 and total number of phases.
- $S_{\varphi}$  is the scale factor of the phase  $\varphi$ . It varies according to the relative proportion of the present phases.

- $h$  represents the Bragg reflections ( $hkl$ ).
- $L_{\varphi,h}$  represents the Lorentz factor. It corrects the polarization due to the monochromator.
- $A_{\varphi,h}$  takes into account the microabsorption of the sample.
- $P_{\varphi,h}$  describes the preferential orientation that may appear during the sample preparation. It occurs when the orientation of the polycrystals of the sample is not random. This phenomenon becomes more important during analysis of a massive/bulk sample.
- $F_{\varphi,h}$  is the structure factor
- $\theta_i$  is the angle corresponding to the point  $i$
- $\theta_{\varphi,h}$  is the angle of reflection for the index  $h$  of the phase  $\varphi$
- $\Omega_{\varphi,h}$  describes the peak shapes and models the effects due to the instrument and also from the samples
- $b_i$  is the background intensity. It can be described either as a polynomial or by a list of points selected by the user

During the refinement of the diffraction data, values of the parameters entering into the calculation of  $y_{\text{calc},i}$  are optimized by successive iterations with the help of the FULLPROF program to minimize the following function.

$$\chi^2 = \sum_i \omega_i (y_{\text{obs},i} - y_{\text{calc},i})^2 \quad \text{Equation 2-5}$$

In the Equation 2-5,

- $y_{\text{obs},i}$  represents observed intensity at the point  $i$ .
- $y_{\text{calc},i}$  correspond to the calculated intensities at the point  $i$ .
- $\omega_i$  is the weight assigned to each intensity and is equal to

$$w_i = 1 / \sqrt{y_{\text{obs}}}$$

The Rietveld refinement of the diffraction data permits structural characterization of the constituent phases including accurate determination of their lattice parameters. In addition, it helps in detection of phases that may be present in the very small amounts in the studied alloy

compositions. From a structural point of view, in principle all the structural parameters involved in the structure factor may be determined. This includes atomic positions and displacement parameters, but in our work more emphasis was put on the determination of site occupancies, since it is a major feature of the TCP phases. In the case of ternary phases, if three elements mix on the same sites, combined Rietveld refinement of X-ray and neutron data should be used, as will be detailed in chapter 7.

### 2.3.4. Electron probe micro analysis (EPMA)

An electron probe micro analyzer (EPMA) is a non destructive analytical tool that combines the features of a scanning electron microscope (high magnification, high resolution imaging) with quantitative elemental analysis at the micron level. The foundations for quantitative analysis with the help of electron microprobe were laid by Raymond Castaing in 1948. Now-a-days, it is commonly employed for investigation of phase equilibria in a multi-component system.

During the EPMA measurement, a focused beam of high energy electrons (5 - 30 KeV [4]) is bombarded on the polished sample. These high energy electrons interact with the sample and knock out the inner shell electrons from atoms of the sample leaving them in the excited state. After a very short period of time (of order of nanoseconds), an electron jumps from the high energy level to fill the vacancy in the low energy level and the energy difference between the two levels results in the emission of characteristic X-rays. The principle of the EPMA measurement is shown in the Figure 2-7.

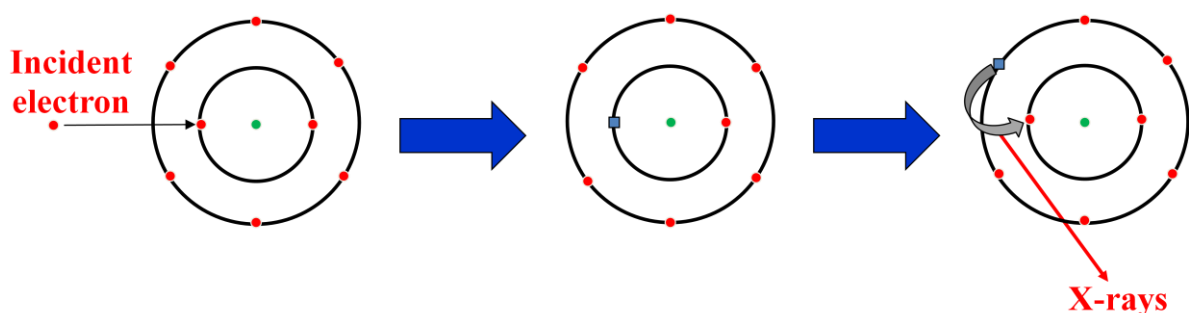


*Figure 2-7: Physical phenomena underlying the operation of electron probe micro analyzer*

The emitted X-rays are analyzed by wavelength dispersive X-ray spectroscopy (WDS or WDX) for the quantitative analysis. For the WDX analysis, the X-rays emitted from the sample are collimated and irradiate a known single crystal at a precise angle. The single crystal diffracts the photons according to the Bragg's law, which are collected by a detector.

Once the X-ray intensities of the constituent elements are measured at a specific beam current, their count rates are compared to those of pure elements (used as standards) for the quantitative analysis.

The EPMA technique can be used for detection of all the elements from beryllium to uranium. However, it cannot be used for light weight elements as they emit low energy X-ray photons which will be absorbed by the beryllium window protecting the detector. The elements from beryllium to fluorine have a tendency to de-excite by emission of Auger electrons: Emitted X-rays are intercepted by another electron of the atom which is also knocked out. Therefore quantitative analysis of these elements is very difficult with the help of EPMA. The interaction of incident electrons with electrons of the matrix (atomic number  $Z$ ) can adversely affect the quality of the results. Secondly, the X-rays once generated from a point within the specimen as a result of incident electron and target material interactions may encounter the materials of different chemical compositions and mass absorption coefficients while travelling to spectrometer. The absorption of the characteristic X-ray ( $A$ ) adversely affects the quality of the EPMA results [5, 6]. Thirdly, when the critical excitation energy of an atom species present in the diffusion zone is less than the energy of the primary X-rays being absorbed, fluorescence ( $F$ ) may take place. As a result X-ray signals of an element can be detected at a place where it is not present [5, 6]. However, corrections for such systematic deviations ( $Z$ ,  $A$ ,  $F$ ) are well developed and are usually employed.

The schematic of an EPMA (CAMECA SX100) used during the present study is shown in the Figure 2-8.

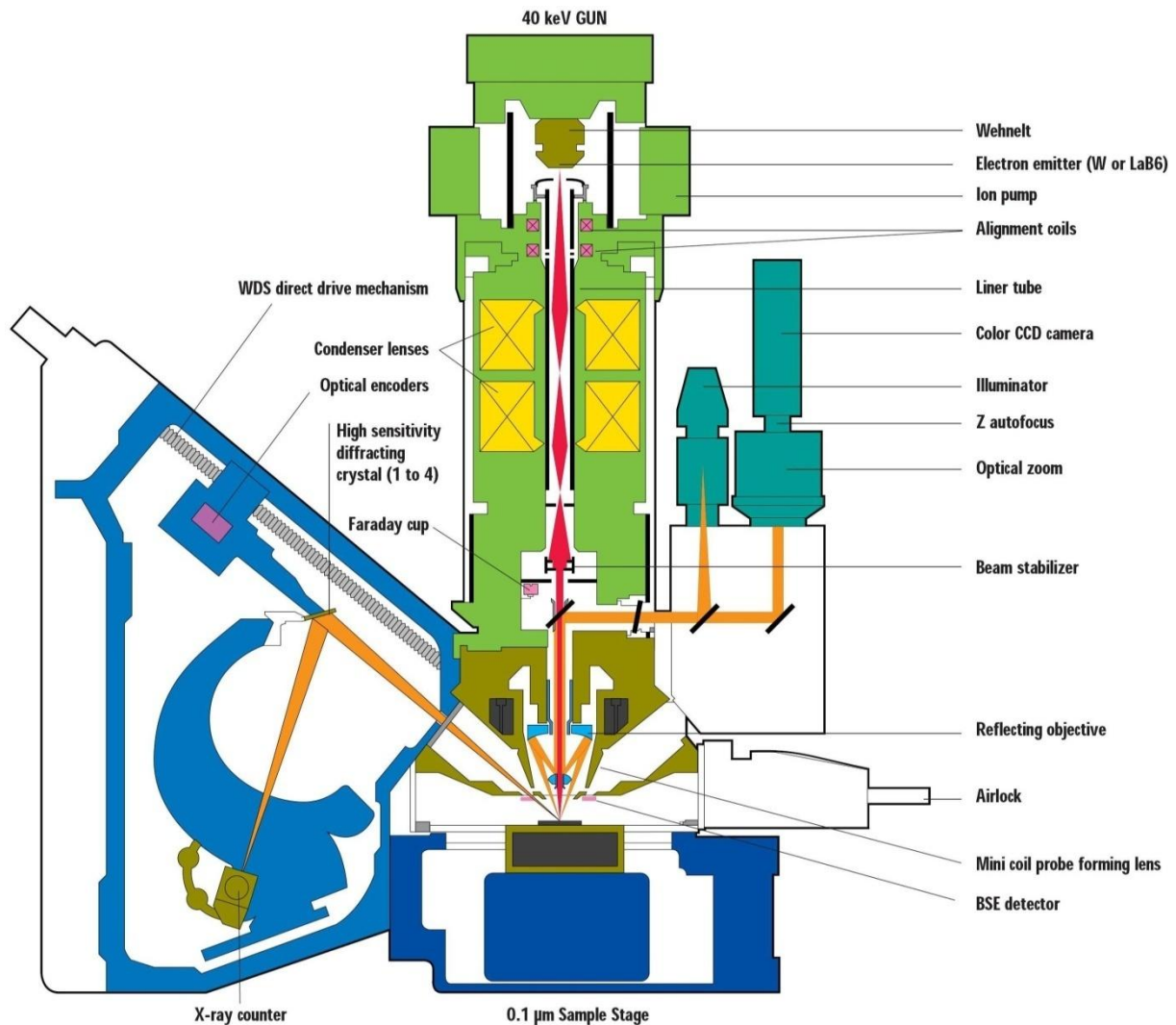


Figure 2-8: Schematic diagram of electron probe microanalyzer

During the present study, EPMA technique was employed to determine chemical composition of the phases present in equilibrium. The sample preparation for the EPMA measurement was carried out by using standard metallographic procedures. One part of the annealed sample was mounted in the wood alloy (Bismuth-50 w.t. %, lead-25 w.t. %, tin-12.5 w.t. % and cadmium-12.5 w.t. %) and subjected to a series of grinding and fine polishing steps. Silicon carbide sandpapers with decreasing content of abrasive material were used to produce a surface finish of about 5 microns. In order to produce a scratch-free mirror like surface, final polishing of the sample was carried out with the help of the diamond paste (3 and ½ microns) applied on a velvet cloth.

The polished sample was then subjected to the EPMA and quantitative analysis was carried out. To determine chemical composition of phases present in equilibrium, a large number of data points were measured on the grain of each phase. The results obtained from all the

EPMA data points were sorted in the increasing order of an element and are plotted on a graph. In case of the multi-phase samples, such a graph (Figure 2-9) shows different plateaus. Each plateau corresponds to the data points measured on a particular phase. The average and standard deviation of the data points on a particular plateau gives the composition and homogeneity of that phase respectively. On the other hand, points situated between different plateaus correspond to the data points that were unintentionally placed at the interface of the different phases. The main advantage of plotting the EPMA results in form of such a graph is that it helps in differentiating the points situated on a particular phase from the points located at the interface of different phases. These points located at the interphase interface were not taken into account while determining the phase composition. As a result chemical composition of the constituent phases can be determined more precisely.

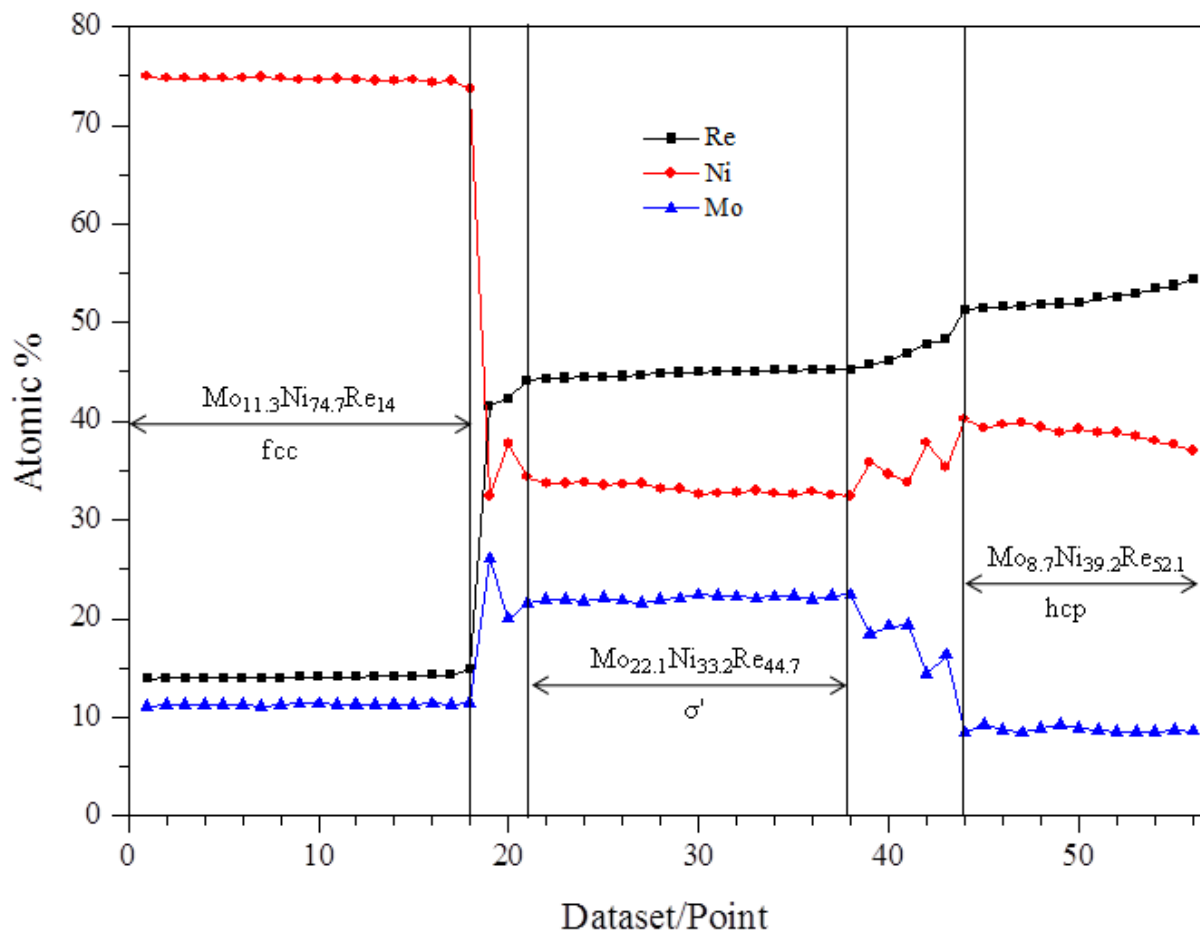


Figure 2-9: Sorting of EPMA data for determining phase composition

The EPMA measurement of two or three phase alloys helps in establishing the phase boundaries of a multi-component phase diagram. In case of a ternary system, the EPMA measurement requires only one alloy within the three-phase region to determine the position

of a tie triangle. On the other hand, techniques such as XRD would require number of alloys in single and two phase domains to determine the phase boundaries through the lattice constant vs. composition plot. Therefore EPMA is a more efficient technique for the determination of phase boundaries [4].

The size of the domain analyzed with EPMA is around  $1 \mu\text{m}^3$ . Therefore, if size of a phase is smaller than the zone irradiated by the beam of electrons, then it will not be possible to do point analysis only on that phase. As a result, such a phase may remain unnoticed during the graphical study discussed earlier. In addition, if two phases present in equilibrium have same electron density then it is not possible to distinguish them with the help of back-scattered electron images and as a result one of the phases may be ignored during the quantitative analysis.

### **2.3.5. Differential thermal Analysis (DTA)**

The information like phase transformation temperature is very important for determination of phase diagrams. The investigation of phase transformation temperatures is based on the fact that a phase transformation is usually accompanied by the enthalpy change (evolution or absorption of heat). Therefore, its temperature can be determined by studying the variation of the thermal properties as a function of temperature. The differential thermal analysis (DTA) is one of the most commonly employed techniques for determination of the phase transformation temperature. It consists in subjecting a test sample and a reference inert sample to the heating and cooling cycles under identical conditions and recording the temperature difference between them. The use of the DTA technique for the determination of phase transformation temperature has been discussed in detail by Boettinger *et al.* [7]

The schematic diagram of differential thermal analyzer used during the present study is shown in the Figure 2-10.

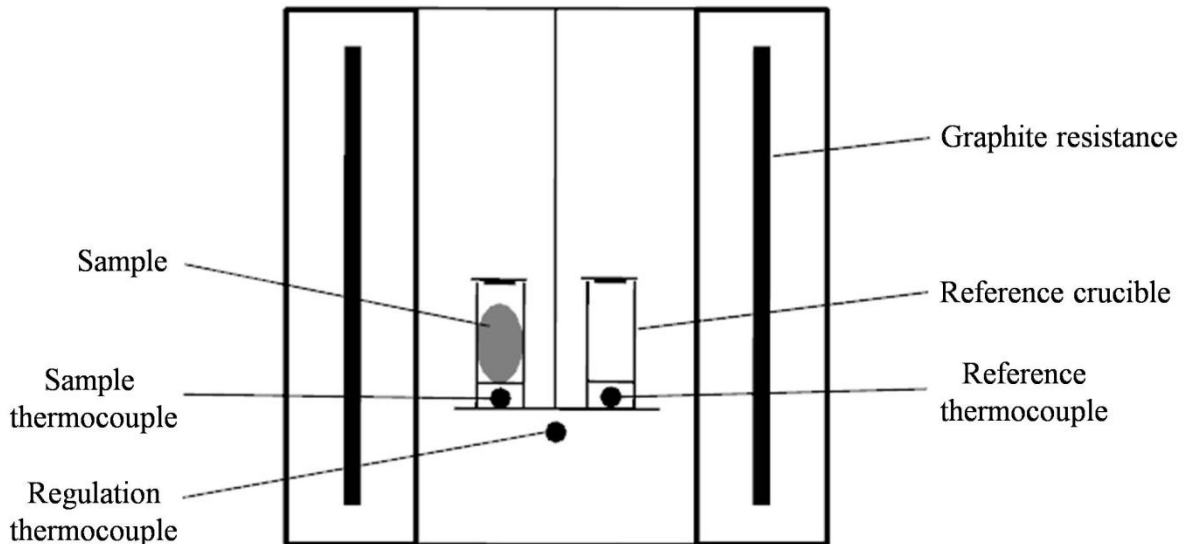


Figure 2-10: Schematic of the differential thermal analyzer

As illustrated in the Figure 2-10, the DTA assembly contains two crucibles. One of the crucibles is used for holding the test sample whereas other is used as a reference crucible. They are usually made of a material that does not undergo any phase transformation in the studied temperature range. During the present study alumina crucibles were used. A graphite resistance furnace surrounding the chamber is responsible for heating and is maintained under argon atmosphere to avoid its combustion. Measurement of the temperatures is carried out with the help of three thermocouples. One of the thermocouples regulates the temperature of the chamber whereas other two thermocouples give the difference in the temperature between sample and reference crucible.

For investigation of the phase transformation temperature, an alumina crucible containing the test sample in the powder form and an empty alumina crucible serving as a reference were inserted in an airtight chamber where they were heated and cooled under argon atmosphere. The temperature difference between sample and reference crucible was recorded as a function of time and temperature. When a phase transformation takes place in the test sample, its temperature rises or falls temporarily (depending on the nature of the transformation) in comparison with the reference sample and therefore results in a peak on the differential temperature vs. temperature or differential temperature vs. time plot. The onset temperature of this peak gives the phase transformation temperature. The experimental parameters such as heating/cooling rates can affect the DTA results. Low heating/cooling rates are generally preferred as they give higher resolution and sharp peaks [4]. During the present study, each alloy composition was investigated twice at the heating/cooling rates of 5°C/min and 10°C/min in the temperature range of 25-1600°C.

## 2.4. Conclusion of the chapter

Different experimental techniques employed during the present study have been discussed in detail. The first part of the chapter was dedicated to the sample preparation with the help of arc melting whereas the second part introduced annealing techniques along with experimental conditions. The techniques used for the phase equilibria investigation and structural characterization of the selected phases have been discussed in detail in the last part of the chapter.

The method used for thermodynamic modeling of the studied systems is presented in the chapter 3 whereas the results obtained by using experimental as well as computational methods are discussed in detail in chapter 4 to chapter 8.

### References:

- [1] J.-M. Joubert, Contribution of the Rietveld method to non-stoichiometric phase modeling. Part I : generalities, *Calphad* 26 (3) (2002) 419-425.
- [2] B. D. Cullity, *Elements of X-ray diffraction*, Addison-Wesley publishing company, 1978.
- [3] J. Rodríguez-Carvajal, Fullprof: a program for Rietveld refinement and pattern matching analysis, XV Congress of Int. Union of Crystallography, Satellite Meeting on Powder Diffraction (1990) 127.
- [4] Y. Z. Zhan, Y. Du, Y. H. Zhuang, *Determination of phase diagrams using equilibrated alloys*, in *Methods for phase diagram determination*, J.-C. Zhao, Editor, 2007, Elsevier, 108-150.
- [5] A. A. Kodentsov, G. F. Bastin, F. J. J. van Loo, The diffusion couple technique in phase diagram determination, *Journal of Alloys and Compounds* 320 (2001) 207–217.
- [6] A. A. Kodentsov, G. F. Bastin, F. J. J. van Loo, *Application of Diffusion Couples in Phase Diagram Determination*, in *Methods for phase diagram determination*, J.-C. Zhao, Editor, 2007, Elsevier.
- [7] W. J. Boettinger, U. R. Kattner, K.-W. Moon, J. H. Perepezko, *DTA and heat-flux DSC measurements of alloy Melting and freezing*, in *Methods for phase diagram determination*, J.-C. Zhao, Editor, 2007, Elsevier, 151-221.

# **Chapter 3**

## **The Calphad Method**



## 3. The Calphad Method

The Calphad method was introduced by Larry Kaufman more than 35 years ago. It was used during the present study for the thermodynamic modeling of the binary and ternary alloy systems. The details about the Calphad approach have been provided in different books (Kaufman et al. [1], Saunders et al. [2], Lukas et al. [3] whereas its history has been recently published by Spencer [4]. In this chapter, a brief introduction of the Calphad method in terms of selection of input data, available thermodynamic models, optimization principle and calculation of the phase diagrams, has been provided.

### 3.1. Principle

The Calphad method is based on the following principle: a phase diagram is a representation of the thermodynamic properties of a system, therefore if the thermodynamic properties of a system are known; it would be possible to calculate its phase diagrams. In the Calphad approach, Gibbs energy has been considered as the most appropriate state function for studying the chemical equilibrium and is described by using different mathematical models containing adjustable coefficients. The Calphad method makes use of experimental data to optimize the coefficients appearing in the Gibbs energy model of each phase and develop a self-consistent phase diagram. Therefore the Calphad has been considered as a semi-empirical method for calculation of phase diagrams.

The thermodynamic modeling of any system with the help of the Calphad method requires literature search, critical evaluation of the available experimental information, and selection of suitable data. The crystal structure information such as site occupancies of the constituent phases helps in selection of suitable thermodynamic models to describe their Gibbs energy. After selection of the input experimental information and thermodynamic models, the values of the model parameters are optimized by least square method with the help of commercial software to obtain a good fit with the input experimental data. Once the optimization of a system is done, it can be included in the already existing thermodynamic databases. By combining the reliable thermodynamic descriptions of the constituent lower order systems, the Calphad method permits prediction of phase equilibria in the complex multi-component systems such as quaternary or higher order systems. As a result, the Calphad method can significantly reduce the number of experiments required for investigation of phase equilibria

in a multi-component system. In addition, the Calphad method can also predict phase equilibria in the temperature or composition ranges that are difficult to investigate experimentally.

Different steps of the thermodynamic modeling are detailed in the coming paragraphs.

### 3.2. Selection of data

Thermodynamic modeling of a multi-component system requires information about presence of different phase in the system. In addition, Calphad is a semi-empirical method and requires input experimental data for optimization of the variables appearing in the Gibbs energy models of the constituent phases. Thus, literature search is the first step for the thermodynamic modeling of a system. The experimental information that can be useful for thermodynamic modeling of a system can be divided into the following categories:

- **Phase diagram data:** It includes the data related to the phase equilibria in a system such as liquidus temperatures, solidus temperatures, invariant reaction temperatures, invariant reaction compositions, tie lines, tie triangles, phase boundaries etc. The experimental techniques used for the characterization of phase equilibria in a multi-component system have already been discussed in the chapter **Error! Reference source not found.**
- **Thermodynamic data:** It includes the thermodynamic information such as enthalpy of mixing, enthalpy of transformation, enthalpy of formation, activity, chemical potential etc. The enthalpies of mixing at different compositions and temperatures and enthalpies of formation of the stable phases can be determined experimentally with the help of calorimetric measurements.
- **Crystallographic data:** The information related to the crystal structure of the constituent phases such as space group, site occupancies etc obtained from the structural characterization techniques such as X-ray or neutron diffraction, is very important in selection of the suitable thermodynamic models for the constituent phases.
- **Physical measurements:** It involves the data related to the specific heat or magnetism.
- **Calculated Data:** The information such as enthalpy of formation or enthalpy of mixing of different stable and metastable compounds can also be obtained with the

help of density functional theory (DFT) calculations and are very useful in thermodynamic modeling of a system.

The detailed literature survey provides a good overview of the system. However, it is not surprising that one may find contradictions between different experimental investigations in terms of temperatures of an invariant reaction, solubility limits of different phases, presence of intermetallic phases in a binary system etc. In such cases, one should critically evaluate the previously reported data in terms of

- Purity of the starting metals used. Sometimes a very small amount of impurities can significantly modify the results (either stabilize a non equilibrium phase or create nucleation barrier in the precipitation of an equilibrium phase).
- Sample preparation technique, annealing times and temperatures, characterization techniques, apparatus used, experimental conditions
- Standard deviation of results obtained by the same group
- Agreement between the data obtained from different groups

The first trials of the optimization can also help in detecting contradictory information and selection of the suitable data for optimization. Depending on the accuracy and reliability of the experimental information, one can assign different weights to different measurements during optimization. The experimental data which are more important and reliable can be assigned higher weights whereas less reliable data can have lower weights which in certain cases can be zero.

### **3.3. Selection of models**

After critical analysis of the available experimental information, next step is selection of suitable thermodynamic models for describing Gibbs energy of the constituent phases. In this section, a brief introduction of the mathematical models used during the present study is provided.

#### **3.3.1. Description of pure elements**

The Gibbs energy for the pure element in their stable structure was defined by the Scientific Group Thermodata Europe (SGTE) [5] in the following form:

$${}^{\circ}G_i^{\phi}(T) - {}^{\circ}H_i^{SER}(298.15\text{ K}) = f(T) \quad \text{Equation 3-1}$$

In the Equation 3-1,  ${}^{\circ}G_i^{\phi}(T)$  represent the molar Gibbs energy of the element  $i$  in the structure  $\phi$  at the temperature  $T$  whereas  ${}^{\circ}H_i^{SER}(298.15\text{ K})$  denotes the molar enthalpy of the element  $i$  in its stable element reference (SER) state. The term SER represents the state of element in its stable crystallographic structure at the temperature of 298.15 K and pressure of  $10^5$  Pa. For the ferromagnetic materials, it will be the paramagnetic state. The left hand side of the Equation 3-1 is defined as Gibbs energy of the element  $i$  in the structure  $\phi$  at the temperature  $T$  relative to the standard element reference (SER) state [5].

The temperature dependence of the molar Gibbs energy is given by the following equation.

$$G^{\phi}(T) = a + bT + cT\ln(T) + \sum_n d_n T^n \quad \text{Equation 3-2}$$

In the Equation 3-2,  $a$ ,  $b$ ,  $c$ ,  $d$  are the coefficients and  $n$  represents a positive or negative integer. In certain cases, other terms representing pressure dependent ( $G_{\text{pres}}$ ) or magnetic contribution ( $G_{\text{mag}}$ ) can be added to the Gibbs energy expression. However, the pressure dependence is generally not considered for the condensed phase.

From the Gibbs energy expression given in the Equation 3-2, other thermodynamic functions can be evaluated [5].

$$S = -b - c - c\ln(T) - \sum_n n d T^{n-1} \quad \text{Equation 3-3}$$

$$H = a - cT - \sum_n (n-1)d T^n \quad \text{Equation 3-4}$$

$$Cp = -c - \sum_n n(n-1)d T^{n-1} \quad \text{Equation 3-5}$$

**Lattice Stability:** The Calphad method is based on the principle of plotting Gibbs energy vs. composition curves for all the structure exhibited by the elements right across the whole alloy system. It requires extrapolation of Gibbs energy vs. composition curves of many phases in

the regions where they are either unstable or metastable. Therefore, relative Gibbs energies for unstable or metastable crystal structures of the pure elements of the system while referring to their stable state are required. By convention, these are called as lattice stabilities [2]. The concept of the lattice stability is shown in the Figure 3-1. The SER state of the element B is fcc. However, we may need the energy of this element when it is present in the hcp state. The difference between the Gibbs energy of two states of the element B (SER state and hcp state) is the lattice stability.

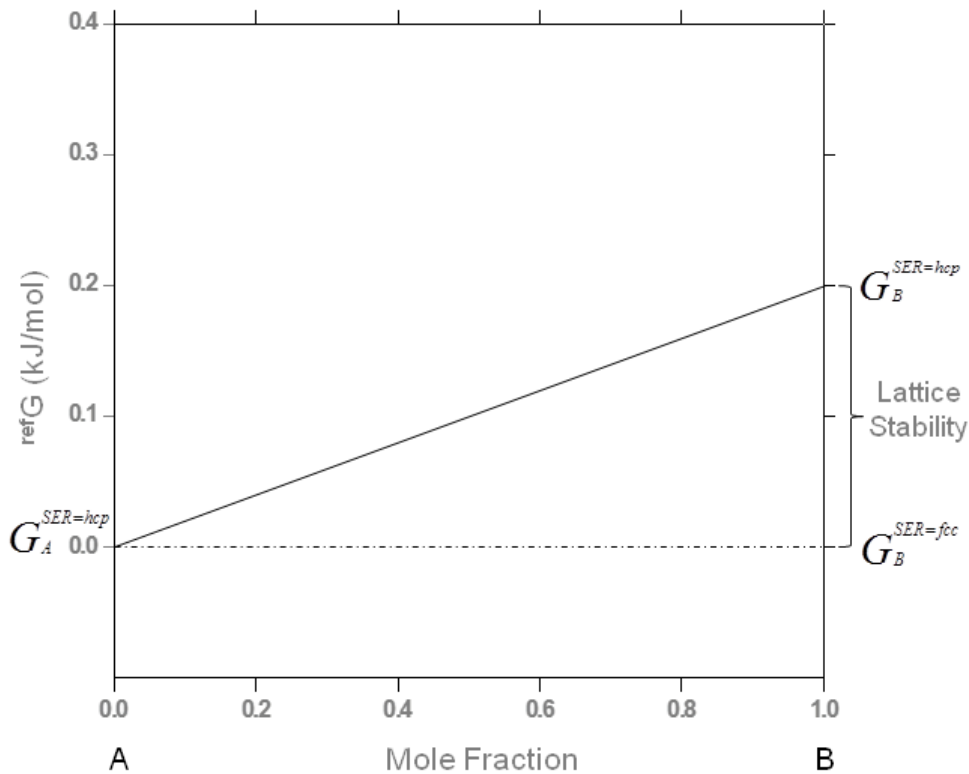


Figure 3-1: Reference Gibbs energy of the hcp phase in a binary system A-B when A and B has different SER states

### 3.3.2. Description of the stoichiometric compounds

Like pure elements, the Gibbs free energy of a stoichiometric compound is uniquely dependent on the temperature. According to the Kopp-Neumann rule, the heat capacity of a compound is the weighted sum of the heat capacity of the pure elements.

$$C_{p_{com}} = \sum_i a_i C_{p_i} \quad \text{Equation 3-6}$$

The heat capacity  $C_p$  of an element  $i$  is directly related to the Gibbs energy by the equation

$$\frac{\partial^2(^{\circ}G_i^{\phi}(T) - ^{\circ}H_i^{SER})}{\partial T^2} = -\frac{C_p}{T} \quad \text{Equation 3-7}$$

Based on the assumption of Kopp-Neumann, the molar Gibbs energy of a compound  $^{\circ}G_{comp}(T)$  is given by

$$^{\circ}G_{comp}(T) - ^{\circ}H_{comp}^{SER}(298.15 K) = a + bT + \sum_i a_i G_i^{SER}(T) \quad \text{Equation 3-8}$$

In the Equation 3-8, the term  $a$  corresponds to enthalpy of formation and  $b$  corresponds to the entropy of formation. The explanation of the term  $^{\circ}H_{comp}^{SER}(298.15 K)$  is given in the Equation 3-9.

$$^{\circ}H_{comp}^{SER}(298.15 K) = \sum_i a_i ^{\circ}H_i^{SER}(298.15 K) \quad \text{Equation 3-9}$$

In the above equations,  $a_i$  is the molar fraction of the element  $i$  in one mole of the compound;  $^{\circ}H_i^{SER}(298.15 K)$  represents the enthalpy of mechanical mixing of the pure elements in their SER state to obtain composition of a compound considered at 298.15 K.

### 3.3.3. Description of substitutional solutions

In case of substitutional solid solutions, probability of the constituent elements to occupy any site in a unit cell is the same. The molar Gibbs energy of a substitutional solution is described as a function of its atomic composition and modeled as sum of three terms (reference, ideal and excess). In case of the binary system A-B, the Gibbs energy of the substitutional solid solution phase  $\phi$  as a function of the mole fraction  $x_i^{\phi}$  of the element  $i$  is given by

$$G_m^{\phi} = {}^{ref}G^{\phi} + {}^{id}G^{\phi} + {}^{ex}G^{\phi} \quad \text{Equation 3-10}$$

In the Equation 3-10

$${}^{ref}G^\varphi = \sum_{i=A,B} x_i^\varphi G_i^\varphi \quad \text{Equation 3-11}$$

$${}^{id}G^\varphi = RT \sum_{i=A,B} x_i^\varphi \ln(x_i^\varphi) \quad \text{Equation 3-12}$$

$${}^{ex}G^\varphi = x_A^\varphi x_B^\varphi L_{A,B}^\varphi \quad \text{Equation 3-13}$$

The reference term, symbolized as  ${}^{ref}G^\varphi$ , corresponds to the Gibbs energy of the pure elements  $G_i^\varphi$  in structure of the phase  $\varphi$  weighted by their mole fractions. The importance of lattice stability (Figure 3-1) can be seen here as it is necessary to know the Gibbs energy of the pure elements in the states other than the SER state. The plot of the reference Gibbs energy is shown in the Figure 3-2(a). The Gibbs energy of the compound A and B are taken as zero for simplicity.

The ideal term, denoted by  ${}^{id}G^\varphi$ , corresponds to the contribution of configurational entropy to the Gibbs energy by considering random mixing of the elements also called as ideal mixing. It is shown in the Figure 3-2(b).

The excess Gibbs energy of the solution, symbolized as  ${}^{ex}G^\varphi$ , considers all contributions not included in the ideal part i.e., excess vibrational, excess configurational etc. by the interaction term  $L_{A,B}^\varphi$ . The interaction term is often modeled by the Redlich-Kister (RK) polynomial given in the Equation 3-14.

$$L_{A,B}^\varphi = \sum_v v L_{A,B}^\varphi (x_A^\varphi - x_B^\varphi)^v \quad \text{Equation 3-14}$$

A positive interaction term reflects repulsive nature of the constituent atoms and atoms of the same nature tend to group. As a result, one may find miscibility gaps in some systems in certain temperature ranges. A zero interaction term reflects random placement of atoms (ideal solution) whereas a negative interaction term shows an attractive tendency between atoms of different nature. In the latter case, different types of atoms tend to surround each other.

If only  ${}^0L$  is employed, the model is called regular solution model. In case when  ${}^1L$  or  ${}^2L$  are used, the models are called as sub-regular or subsubregular-solution models respectively. The excess Gibbs energy curves as a function of order of interaction terms ( ${}^0L$  to  ${}^3L$ ) are shown in the Figure 3-2(c). The value and sign of the interaction terms affect the total Gibbs energy.

The effect of different values of  ${}^0L$  on the total Gibbs energy is shown in the Figure 3-2(d). One should avoid using many interaction terms during optimization of a system.

During the present work  ${}^vL_{A,B}^\varphi$  was modeled in the form  ${}^v a^\varphi + {}^v b^\varphi T$ . The terms  ${}^v a^\varphi$  and  ${}^v b^\varphi$  represent the model parameters to be evaluated from the experimental data.

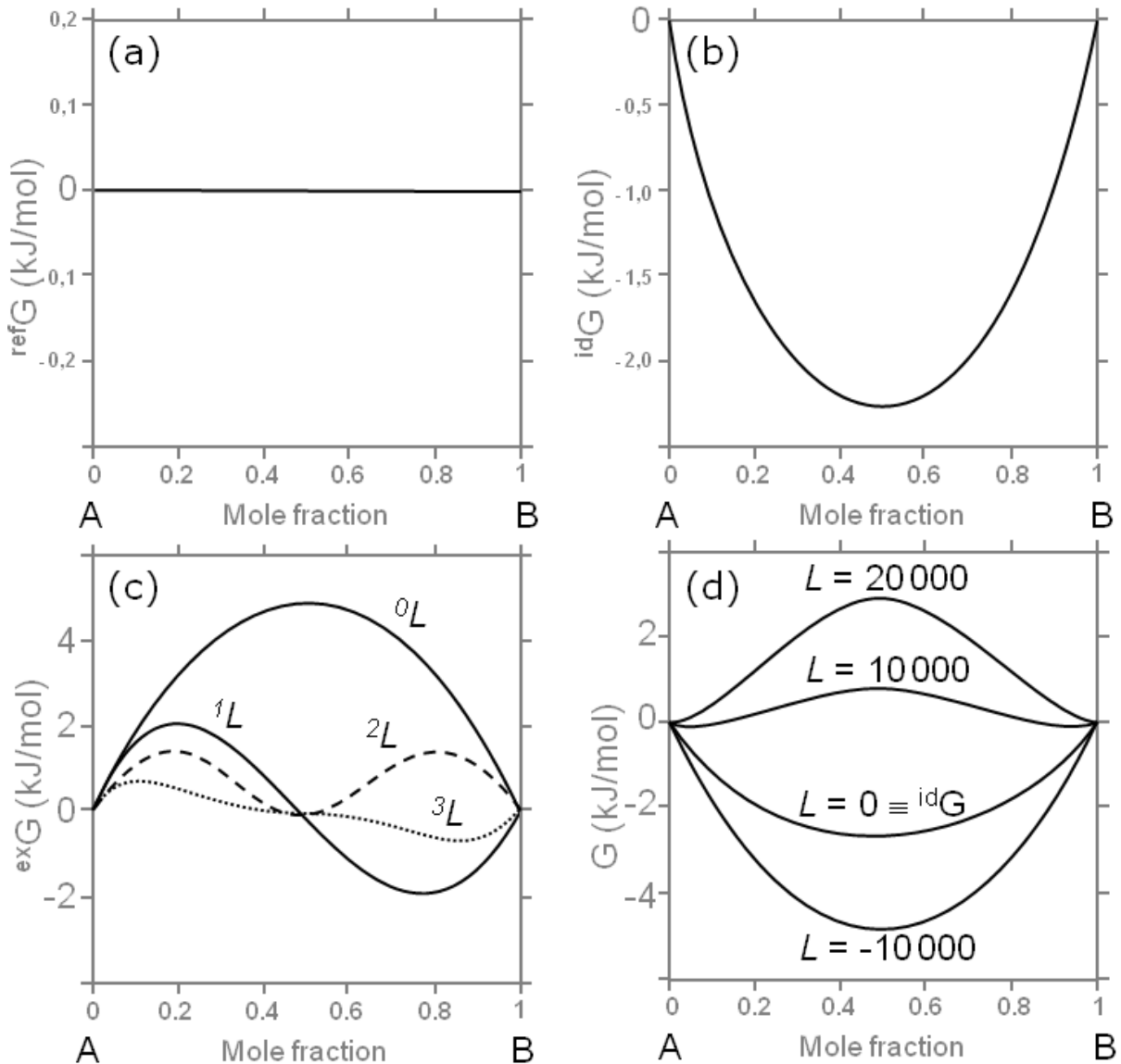


Figure 3-2: Plot of reference term (a), ideal term (b) and excess terms ( ${}^0L$  to  ${}^3L$ ) (c) and effect of different values of  ${}^0L$  term on the total Gibbs energy curve (d).

### 3.3.4. Sublattice model

The simplest approach to model long range order is to use sublattice model taking in to account which element enters in to which sublattices and assume random mixing in each sublattice. The sublattice model is therefore an extended form of substitutional solution model

which applies to each type of site within a crystallographic structure. It was generalized by Sundman and Ågren [6] and is a wide spread model in the thermodynamic modeling community. It is a flexible model and can account for interstitial solutions, carbides, nitrides, oxides, intermetallic phases such as  $\sigma$  and Laves phases which have wide homogeneity domains, and phases with order/disorder transformation [2].

The sublattices represent crystallographic sites and may contain the constituent atoms or vacancies. Each sublattice is symbolized by a pair of parentheses. These sublattices are assigned weights which are called multiplicity that denotes the size of the sublattice and are directly linked to the multiplicity of the represented crystallographic sites. The simple case of a sublattice model would be a two sublattice model with two constituents in each. Consider for example a two sublattice model  $(A,B)_m(C,D)_n$ . In this case, first sublattice contains the atoms A and B with the multiplicity  $m$  whereas the second sublattice contains the atoms C and D with the multiplicity  $n$ . In writing the Gibbs energy equations, different sublattices are separated by the punctuation “:” for example,  $G_{A:C}$  is the Gibbs energy of the compound  $A_mC_n$  consisting of the element A on the first sublattice and C on the second. If only one atom, ion or a vacancy is present at each sublattice, the model is equivalent to that of a stoichiometric compound. On the other hand, in case of one sublattice containing at least two elements, the model is identical to that of substitutional solution discussed earlier.

Like substitutional solution model, the Gibbs energy in the sublattice model is described as the sum of reference, ideal and excess term. However, these terms are significantly different. They are described by taking an example of a compound whose description is  $(A,B)_m(C,D)_n$ .

$${}^{ref}G^\varphi = y'_A y''_C \circ G_{A:C} + y'_A y''_D \circ G_{A:D} + y'_B y''_C \circ G_{B:C} + y'_B y''_D \circ G_{B:D} \quad \text{Equation 3-15}$$

$${}^{id}G^\varphi = RT[m[y'_A \ln(y'_A) + y'_B \ln(y'_B)] + n[y''_C \ln(y''_C) + y''_D \ln(y''_D)]] \quad \text{Equation 3-16}$$

$$\begin{aligned} {}^{ex}G^\varphi = & y'_A y'_B y''_C L_{A,B:C} + y'_A y'_B y''_D L_{A,B:D} + y'_A y''_C y''_D L_{A:C,D} \\ & + y'_B y''_C y''_D L_{B:C,D} + y'_A y'_B y''_C y''_D L_{A,B:C,D} \end{aligned} \quad \text{Equation 3-17}$$

In the above equations,  $y_i^s$  is the fraction of the sublattice  $s$  occupied by the specie  $i$ . It is the ratio of number of sites of the sublattice  $s$  occupied by the atoms of  $i$  and total number of sites of the sublattice

The Gibbs energy reference state is defined by the compounds generated when only pure components exist on the sublattice. These compounds are called end-members. In the Equation 3-15,  ${}^{\circ}G_{A:C}$ ,  ${}^{\circ}G_{B:D}$ ,  ${}^{\circ}G_{A:D}$ , and  ${}^{\circ}G_{B:C}$  correspond to the energies of four end-members formed by associating the four elements on two sublattices. The partial Gibbs energy of any end-member e.g., can be calculated by using Equation 3-18.

$$G_{A:D} = {}^{\circ}G_{A:D} + (1 - y'_A)(1 - y''_D)\Delta G + mRT\ln(y'_A) + nRT\ln y''_D \quad \text{Equation 3-18}$$

If enthalpies of formation of the end members are known by experimental methods or by DFT calculations, the values of their respective parameters can be fixed during optimization of the system.

### 3.4. Principle of optimization

Optimization adjusts the parameters entering into the Gibbs energy expressions by least square method to obtain a good fit with the experimental values. A good optimization on one hand depends on number of experimental data of good quality, coming from thermodynamic measurements and phase diagram data of the considered system (discussed in the section 3.2); and on the other hand on the selection of suitable thermodynamic model for each phase (discussed in the section 3.3). Depending on selection of the experimental dataset; weight assigned to different measurements, selection of model and its number of parameters, infinite numbers of optimizations of a system are possible.

The optimization of a system is carried out through specialized modules of commercial software such as Pandat [7], Factsage [8], MT-DATA [9] or Thermo-Calc [10]. During the present study, optimization of the studied system was carried out by using Parrot module of the Thermo-Calc software [10]. For that, selected experimental information is stored in a .pop file whereas mathematical models to describe Gibbs energy of different phases are entered in another file named as the setup file. The enthalpies of formation of different end-member known from the literature can be entered directly into the setup file whereas other parameters are considered as variables. The model variables are set free one by one and optimized by using parrot module in order to reproduce the entered experimental data. It is commonly accepted that a best optimization is the one that reproduces the entered experimental data as close as possible with minimum number of optimized variables.

### 3.5. Calculation of phase diagrams

The equilibrium calculation of a multi-component system consists in minimizing the total Gibbs energy of the system. The mathematical expressions for the molar Gibbs energy of the constituent phases are given in the section 3.3. The total Gibbs energy is derived by summing up the expressions given in the section 3.3 and multiplying by the fractions or amount of phases. Therefore calculation of equilibrium involves minimizing the sum given in the Equation 3-19 [3].

$$G = \sum_{i=1}^{n_p} n_i^\varphi G_i^\varphi \quad \text{Equation 3-19}$$

In the Equation 3-19,  $n_i^\varphi$  and  $G_i^\varphi$  represent number of moles and Gibbs energy of the phase  $\varphi$  respectively whereas  $n_p$  represents the total number of phases present in the system.

The term “driving force” is important to understand the relationship between stability of a phase and its Gibbs free energy. It is the smallest possible distance between Gibbs free energy curve and the plane joining the chemical potential of components of the system at equilibrium state. This plane is tangent to the Gibbs energy curves of the equilibrium phases and is called as the common tangent. The driving force of a stable phase is zero. The more the driving force of a phase will be negative; less stable the phase would be. In the Calphad method, Gibbs energies of all the constituent phases are calculated over entire composition and temperature range. The equilibrium between different phases at a particular temperature can be determined by plotting the common tangent between the Gibbs energy curves of different phases.

The concept is illustrated in the Figure 3-3 in which a binary system with a miscibility gap in the solid phase is considered. The Gibbs energy curves of the constituent phases at 200°C and 480°C are shown in the Figure 3-3(a) and Figure 3-3(b) respectively. The common tangents of the Gibbs energy curves show equilibrium between the two solid phases. The compositions of the phases obtained by common tangent construction represent the phase boundaries at their respective temperature and are used for plotting the phase diagram shown in the Figure 3-3(c) and Figure 3-3(d). In case of the Figure 3-3 (b), two common tangents can be drawn as the liquid phase is more stable than the solid phase in certain composition range. By using the

four compositions obtained by plotting of two common tangents in the Figure 3-3 (b), composition limits of the two phase domain at 650°C are obtained which is shown in the Figure 3-3(d).

The Thermo-Calc software [10] calculates equilibrium of a system by a procedure of minimization of the Gibbs energy and construction of the common tangent. As a result of these calculations, the software is capable of plotting not only the phase diagrams but also isopleths and other thermodynamic functions ( $C_p$ ,  $H$ ,  $S$ ) as a function of other variables. These thermodynamic calculations allow prediction of stable equilibrium as well as metastable equilibrium in a system.

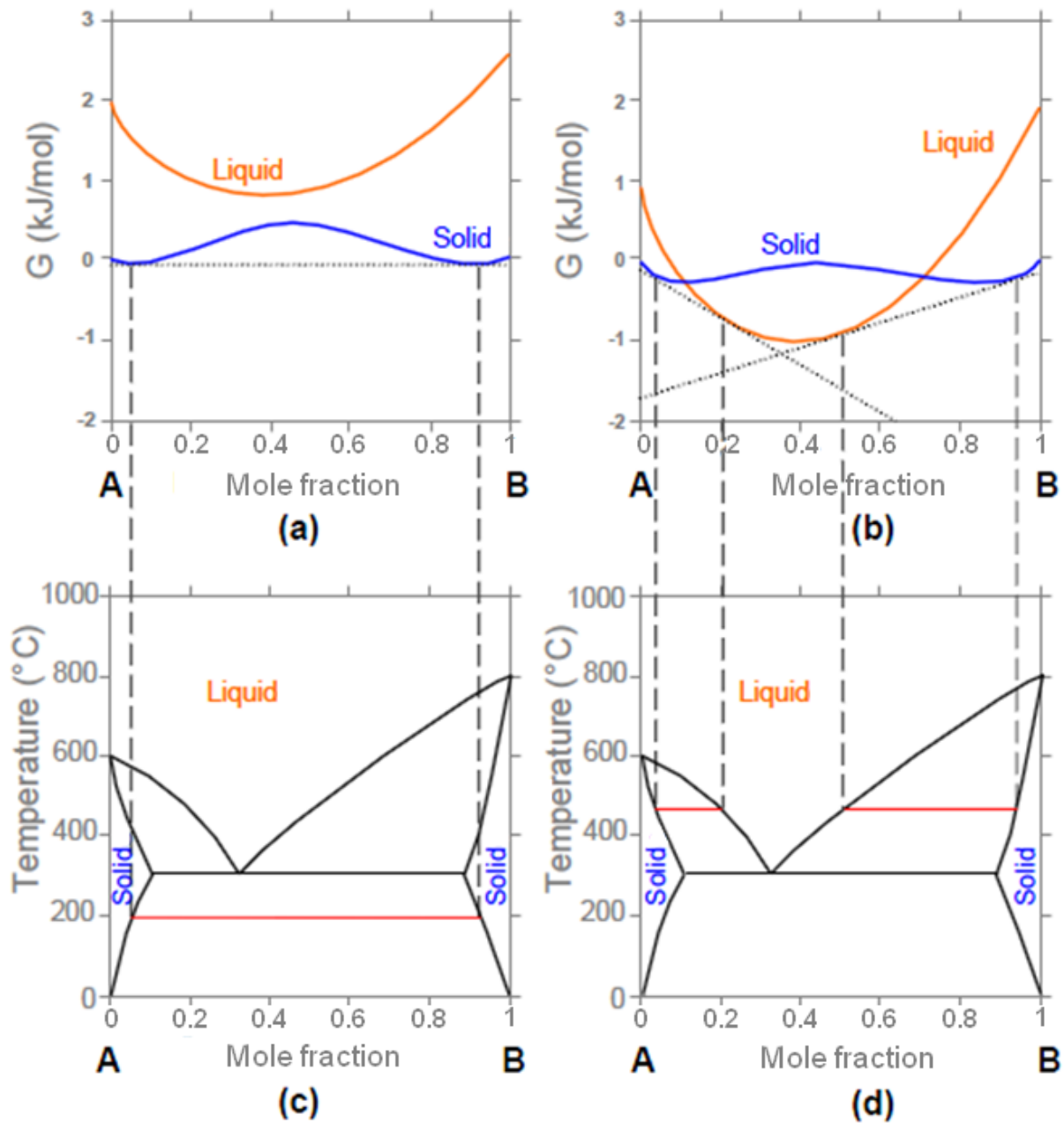


Figure 3-3: Phase diagram of the binary system A-B with their corresponding Gibbs energy curves at 200°C and 480°C.

### 3.6. Combination of phase diagrams and extrapolation

Once the lower order binary systems are optimized, their thermodynamic descriptions can be combined to predict phase equilibria in a higher order system. While combining any two assessments, it is necessary to use the same model for the phases that forms or may form a continuous solution from one binary system to another. It is obvious in case of terminal solid solutions, but some of the intermetallic phases such as  $\sigma$  phase, may also show continuous

homogeneity domain from one system to another. The Strukturbericht notations of the phases provide a great help in deciding whether two phases in different systems should be combined or not [3].

If the same phase has been described with different models in two different systems; then, prior to combining two assessments, reassessment of one of the binary system is required. An example of the model compatibility problem that required reassessment of one of the binary system is discussed in the section **Error! Reference source not found..**

Once the assessments with compatible models have been obtained, one can plot higher order systems. Typically, from a combination of A-B, B-C and A-C binary system, ternary system ABC can be plotted by extrapolation. For extension of binary phases in the ternary system, different models have been developed. These models are based on excess energy of a binary system. From the Equation 3-10, the value of excess term is given by,

$$exG^\varphi = G_m^\varphi - refG^\varphi - idG^\varphi$$

In addition,

$$exG^\varphi = bin,exG^\varphi + tern,exG^\varphi + high,exG^\varphi \quad \text{Equation 3-20}$$

In the above equation, the terms  $bin,exG^\varphi$ ,  $tern,exG^\varphi$  and  $high,exG^\varphi$  correspond to the excess Gibbs energy in a binary, ternary and higher order system respectively.

The Equation 3-20 has been derived in a geometrical way in order to consider three binary systems with same contribution. There are three different extrapolation models: Muggianu model [11], Kohler model [12] and Colinet model [13]. From the geometrical point of view, these models are same and the only difference is the reference points. Another model named as the Toop model [14] is an asymmetrical model which is used when one of the constituents behave differently from others. It is preferable to use Muggianu extrapolation model when Redlich-Kister polynomial is used.

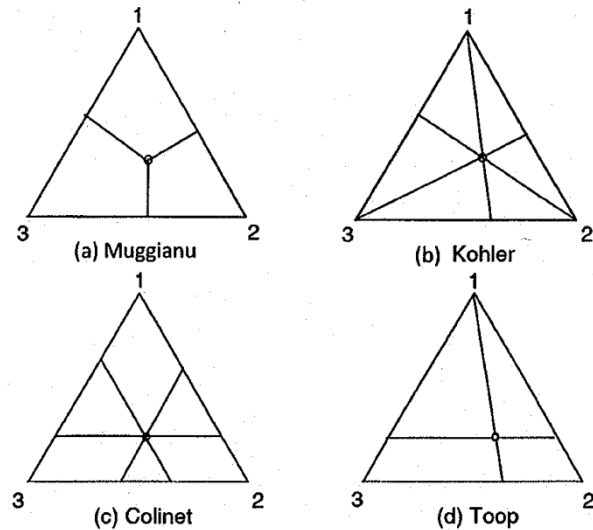


Figure 3-4: Ternary extrapolation methods presented graphically

### 3.7. Conclusion of the chapter

In this chapter, an introduction of the Calphad method that was employed during the present study for thermodynamic modeling of the Mo-Ni-Re and its constituent binary systems has been presented. The principle of the Calphad method and different steps involved in thermodynamic modeling of a system with the help of the Calphad method are introduced in the beginning of the chapter which have been detailed later. After introduction, importance of the literature search and critical analysis of the experimental information that can be used as input for thermodynamic modeling has been emphasized. Then different mathematical models that can be used for thermodynamic modeling are introduced. After selection of suitable experimental information and thermodynamic model, the optimization procedure and calculation of phase diagrams with the help of Calphad method have been discussed.

During the present study, the Calphad method was used for thermodynamic modeling of the Ni-Re, Mo-Ni and Mo-Ni-Re system. The results of the thermodynamic modeling of the Ni-Re binary system are discussed in the chapter 4 whereas thermodynamic modeling of the Mo-Ni and Mo-Ni-Re system are presented in the chapter 7.

**References**

- [1] L. Kaufman, H. Bernstein, Computer calculation of phase diagrams: with special reference to refractory metals, Academic Press Inc, 1970.
- [2] N. Saunders, A. P. Miodownik, Calphad, calculation of phase diagrams, a comprehensive guide, Pergamon Materials Series, 1998.
- [3] H. L. Lukas, S. G. Fries, B. Sundman, Computational thermodynamics, the Calphad method, Cambridge University Press, 2007.
- [4] P. Spencer, A brief history of Calphad, Comput. Coupling Phase Diagrams Thermochem. 32 (2008) 1-8.
- [5] A. T. Dinsdale, SGTE data for pure elements, Calphad 15 (4) (1991) 317-425.
- [6] B. Sundman, J. Ågren, A regular solution model for phases with several components and sublattices, suitable for computer applications, J. Phys. Chem. Solids 42 (1981) 297-301.
- [7] W. Cao, S.-L. Chen, F. Zhang, K. Wu, Y. Yang, Y. A. Chang, R. Schmid-Fetzer, W. A. Oates, PANDAT software with PanEngine, PanOptimizer and PanPrecipitation for multi-component phase diagram calculation and materials property simulation, Calphad: Comput. Coupling Phase Diagrams Thermochem. 33 (2) (2009) 328-342.
- [8] C. Bale, P. Chartrand, S. A. Degterov, G. Eriksson, K. Hack, R. Ben Mahfoud, J. Melancon, A. D. Pelton, S. Petersen, FactSage thermochemical software and databases, Calphad-Computer coupling of phase diagrams and thermochemistry 26 (2) (2002) 189-228.
- [9] R. H. Davies, A. T. Dinsdale, J. A. Gisby, J. A. J. Robinson, S. M. Martin, MTDATA - thermodynamic and phase equilibrium software from the national physical laboratory, Calphad-Computer coupling of phase diagrams and thermochemistry 26 (2) (2002) 229-271.
- [10] B. Sundman, B. Jansson, J. O. Andersson, The Thermo-Calc databank system, Calphad 9 (2) (1985) 153-190.
- [11] Y.-M. Muggianu, M. Gambino, J.-P. Bros, Enthalpies of formation of liquid bismuth-gallium-tin alloys at 723K. Choice of an analytical representation of integral and

- partial thermodynamic functions of mixing., *Journal de Chimie Physique et de Physico-Chimie Biologique* 72 (1975) 83-88.
- [12] F. Kohler, Estimation of the thermodynamic data for a ternary system from the corresponding binary systems, *Monatshefte für chemie* 91 (1960) 738-740.
- [13] C. Colinet, Estimation des grandeurs thermodynamiques des alliages ternaires, *Faculté des Sciences, Université de Grenoble, France* (1967).
- [14] G. W. Toop, Predicting ternary activities using binary data, *Trans. Metall. Soc. AIME* 233 (1965) 850-854.

# **Chapter 4**

## **The Ni-Re System**



## Introduction

The literature review of the Mo-Ni-Re and its related binary systems presented in the chapter 1 revealed that phase equilibria in the Ni-Re and Mo-Ni-Re system are not well-established and reinvestigation of these important systems is necessary. During the present study, prior to the complete experimental determination of the Mo-Ni-Re system, partial redetermination of the Ni-Re binary system was carried out with the following objectives:

- Investigation of the phase equilibria
- Determination of the solidus, liquidus and peritectic reaction temperatures

The investigation of the Ni-Re phase equilibria was carried out by chemical and structural characterization of equilibrated arc melted alloys with the help of electron probe microanalysis and X-ray diffraction techniques respectively whereas solidus, liquidus and invariant reaction temperatures were obtained with the help of differential thermal analysis measurements (DTA) on the as-cast arc melted alloys. The experimental techniques used during the present investigation of the Ni-Re binary system have already been previously discussed in detail in the chapter 2.

The experimental results obtained during the present study were found to be self-consistent. In addition, the phase boundaries determined during present study showed a very good agreement with the recent partial investigations of the Ni-Re binary system. By combining the phase equilibria and thermal analysis results obtained during the present study with the recent partial investigations of the Ni-Re binary system showing good agreement with the present study, a new phase diagram of the Ni-Re binary system was proposed.

The experimental results obtained during present study were considerably different from the previously accepted phase diagram in terms of:

- homogeneity domains of the Ni and Re solid solutions
- invariant reaction temperature
- freezing ranges of the solid solutions

Therefore, thermodynamic modeling of the Ni-Re binary system with new experimental information is necessary if the Mo-Ni-Re system is to be modeled completely. Thermodynamic modeling of the Ni-Re system was also carried out during the present study

with the help of the Calphad method. The calculated Ni-Re phase diagram showed a good agreement with the input experimental information.

The results obtained during the present study related to the experimental investigation and thermodynamic modeling of the Ni-Re binary system have recently been published in the “*Journal of Solid State Chemistry [K. Yaqoob, J.-M. Joubert, J. Solid State Chem., 196 (2012), 320-325]*” and are presented in this chapter in the article format. These results will be used later during experimental determination and thermodynamic modeling of the Mo-Ni-Re system discussed in the chapter 5 and chapter 8 respectively.



# Experimental determination and thermodynamic modeling of the Ni–Re binary system

Khurram Yaqoob, Jean-Marc Joubert \*

*Chimie Métallurgique des Terres Rares (CMTR), Institut de Chimie et des Matériaux Paris-Est (ICMPE), 2-8 rue Henri Dunant, 94320 Thiais Cedex, France*

## ARTICLE INFO

### Article history:

Received 2 May 2012

Received in revised form

20 June 2012

Accepted 23 June 2012

Available online 1 July 2012

### Keywords:

Ni–Re phase diagram

Differential thermal analysis

X-ray diffraction

Electron probe microanalysis

CALPHAD method

## ABSTRACT

The phase diagram of the Ni–Re binary system has been partially reinvestigated by chemical, structural and thermal characterization of the arc melted alloys. The experimental results obtained during the present investigation were combined with the literature data and a new phase diagram of the Ni–Re binary system is proposed. In comparison with the Ni–Re phase diagram proposed by Nash et al. in 1985 [1], significant differences in the homogeneity domains, freezing ranges and peritectic reaction temperature were evidenced. On the other hand, thermodynamic modeling of the studied system by using the new experimental information has also been carried out with the help of the CALPHAD method. The calculated Ni–Re phase diagram showed a good agreement with the selected experimental information.

© 2012 Elsevier Inc. All rights reserved.

## 1. Introduction

Considering its commercial importance for the development of Ni based superalloys, the Ni–Re binary system has been the subject of several investigations. Nash et al. [1] critically reviewed the available experimental information on the phase equilibria, crystal structure and magnetism of the Ni–Re binary system [2–11] and proposed a Ni–Re phase diagram which is shown in Fig. 1.

However, some of the recent measurements [12–14] have placed question marks on the accuracy of the phase diagram proposed by Nash et al. [1]. A comparison of these recent studies with the accepted Ni–Re phase diagram, showing poor agreement particularly on the Re rich side, is also presented in Fig. 1. All the recent investigations pointed out much larger homogeneity domain of the hcp phase in comparison with what was proposed previously. On the other hand, considerable differences were also evidenced on the Ni rich side. In addition to the disagreement with the recent binary data, the hcp phase field suggested by Nash et al. [1] also showed poor agreement with the related ternary isothermal sections e.g. Cr–Ni–Re [15,16], Fe–Ni–Re [15,17], Mn–Ni–Re [18], Mo–Ni–Re [15], Nb–Ni–Re [15,16], Ni–Re–Ta [15], Ni–Re–Ti [15], Ni–Re–V [15,16], Ni–Re–Zr [15]. The large disagreements between the accepted phase diagram and recent investigations on the binary and related ternary

systems necessitated the redetermination of the phase equilibria in the Ni–Re binary system.

During the present study, the phase equilibria in the Ni–Re binary system were investigated by the characterization of the equilibrated arc melted alloys with the help of electron probe microanalysis (EPMA) and X-ray diffraction (XRD) techniques. In addition to the phase equilibria determination, the solidus, liquidus and peritectic reaction temperatures were investigated with the help of differential thermal analysis (DTA). The results obtained during the present study were compared with the previous investigations and a new experimental phase diagram of the Ni–Re binary system is proposed. In addition, thermodynamic modeling of the studied system by incorporating the new experimental information was also carried out with the help of the CALPHAD method.

## 2. Experimental techniques

### 2.1. Sample preparation and annealing

The starting materials used for the present investigation consisted of high purity metal powders (Ni: Alfa Aesar, < 125 μm, 99.996%; Re: Alfa Aesar, < 44 μm, 99.99%). The Ni–Re binary alloys were synthesized by mixing and compacting raw materials into pellets of different compositions followed by arc melting under argon atmosphere. The alloy buttons were melted five times and turned around after each melting to achieve better homogeneity.

\* Corresponding author. Fax: +33 1 49 78 12 03.

E-mail address: [jean-marc.joubert@icmpe.cnrs.fr](mailto:jean-marc.joubert@icmpe.cnrs.fr) (J.-M. Joubert).

The alloys synthesized for the phase equilibria determination were subsequently annealed at 1200 °C, 1500 °C, and 1600 °C. For annealing at 1200 °C, the as-cast samples were encapsulated in silica tubes under an argon atmosphere, and placed in a preheated resistance furnace. The rapid cooling of the samples after annealing was reached by quenching the silica tubes in water. The annealing of the as-cast samples at temperatures higher than 1200 °C was conducted in a high-frequency induction furnace in a water-cooled copper crucible under an argon atmosphere, and the temperature of the sample was measured with the help of an optical pyrometer. After annealing, the induction heating was switched off and rapid cooling of the alloys took place by the water-cooled copper crucible.

## 2.2. Structural and chemical characterization

After annealing, chemical and structural characterization of the samples was carried out. For chemical characterization, part of each sample was polished using standard metallographic procedure and subjected to the electron probe microanalysis (EPMA; CAMECA SX100) calibrated with pure Ni and Re as standards. To determine the composition and homogeneity of the phases present in equilibrium, large number of data points were measured on each phase. The average of the point measurements performed on a particular phase gave composition of the phase whereas the calculated standard deviation of these measurements indicated phase homogeneity.

For structural characterization, the X-ray diffraction measurements were carried out on the polished samples with the help of a Bruker D8-Advance diffractometer equipped with CuK $\alpha$  radiation and a rear graphite monochromator. The lattice parameters of the constituent phases were determined by the Rietveld analysis of the XRD data with the help of FULLPROF program [19].

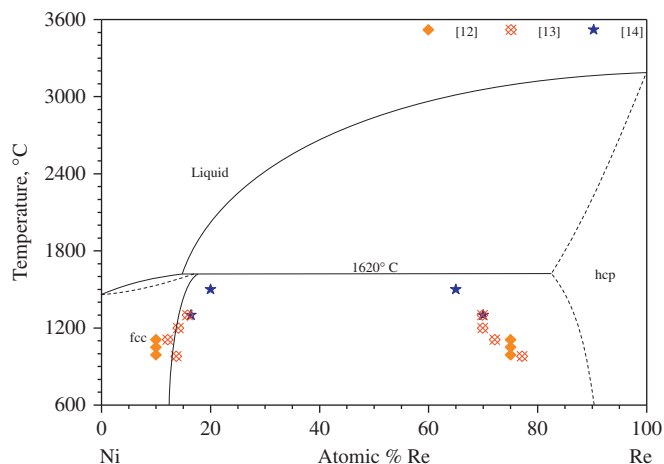


Fig. 1. Recently published experimental data superimposed on the Ni–Re phase diagram assessed by Nash [1].

**Table 1**  
Metallurgical characterization results of the equilibrated arc melted alloys.

Nominal composition	Annealing		Phases	EPMA composition		Lattice parameters	
	Temperature (°C)	Time (h)		Ni (at%)	Re (at%)	a	c
Ni <sub>68</sub> Re <sub>32</sub>	1200	1680	fcc	85.4(1)	14.6(1)	3.5902(6)	–
			hcp	29(1)	71(1)	2.7054(4)	4.3595(8)
Ni <sub>52</sub> Re <sub>48</sub>	1500	10	fcc	81(1)	19(1)	3.6034(3)	–
			hcp	35(1)	65(1)	2.6951(2)	4.3430(4)
Ni <sub>50</sub> Re <sub>50</sub>	1600	9	Liquid	–	–	–	–
			hcp	33.2(4)	66.8(4)	2.6937(3)	4.3391(6)

## 2.3. Thermal characterization

Prior to the thermal characterization of the selected compositions, the DTA apparatus (SETARAM-SETSIS Evolution) was calibrated by running DTA scan on the pure Ni. A good agreement was found between the measured (1451 °C) and reported value (1453 °C) of the melting temperature of Ni. For investigation of the phase transformation temperatures of the selected compositions, as-cast samples in powder form were loaded in alumina crucible and subjected twice to thermal cycles at 5 and 10 °C/min, under flowing argon atmosphere. The temperature of the invariant reaction was determined by the tangent construction method, whereas the temperatures corresponding to the first visible onset and offset of melting during the heating steps were considered as solidus and liquidus temperatures respectively.

## 3. Experimental results

The experimental results obtained during the present investigation can be divided into two main categories: (1) phase equilibria determination and (2) thermal analysis.

### 3.1. Phase equilibrium results

During the present investigation, the tie-lines of the studied system were investigated at 1200 °C, 1500 °C and 1600 °C. The nominal compositions of the samples synthesized for the phase equilibria determination together with measured compositions and lattice parameters of the constituent phases as determined by the EPMA and XRD measurements respectively, are listed in Table 1. The refractory nature of the constituent elements necessitated long annealing times and/or high temperatures. The annealing of the samples at 1200 °C was carried out for 1680 h whereas 9 and 10 h of annealing were sufficient at 1600 °C and 1500 °C respectively. The homogeneity of the phases was later confirmed by the EPMA measurement. The XRD results of the investigated compositions confirmed the absence of any intermetallic compound in the studied system.

During the present study, the phase boundaries at 1200 °C and 1600 °C were confirmed by EPMA analysis of more than one alloy composition. The diffraction pattern in the form of the Rietveld plot along with the back-scattered electron (BSE) image of the sample of composition Ni<sub>52</sub>Re<sub>48</sub> annealed at 1500 °C is shown in Fig. 2.

### 3.2. Thermal analysis results

The compositions selected for the investigation of the solidus, liquidus and invariant reaction temperatures together with the DTA results are listed in Table 2.

During the present study, each composition was investigated twice at two different heating/cooling rates, i.e. 5 °C/min and 10 °C/min. The DTA scans of the first thermal cycle were discarded.

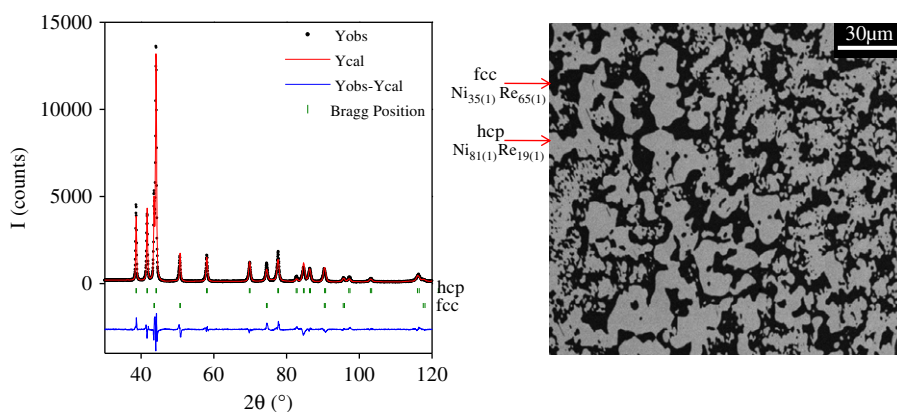


Fig. 2. XRD plot and BSE image of  $\text{Ni}_{52}\text{Re}_{48}$  annealed at  $1500\text{ }^{\circ}\text{C}$  for 10 h.

**Table 2**  
Thermal analysis results of the studied compositions.

Nominal composition		DTA results at		Extrapolation to $0\text{ }^{\circ}\text{C}/\text{min}$
		$10\text{ }^{\circ}\text{C}/\text{min}$	$5\text{ }^{\circ}\text{C}/\text{min}$	
$\text{Ni}_{95}\text{Re}_5$	Solidus	1459	1458	1457
	Liquidus	1517	1510	1503
$\text{Ni}_{90}\text{Re}_{10}$	Solidus	1465	1464	1463
	Peritectic reaction	1548	1546	1544
$\text{Ni}_{85}\text{Re}_{15}$	Solidus	1454	1454	1454
	Peritectic reaction	1540	1539	1538
$\text{Ni}_{80}\text{Re}_{20}$	Solvus	1473	1472	1471
	Peritectic reaction	1548	1546	1544
$\text{Ni}_{50}\text{Re}_{50}$	Peritectic reaction	1548	1546	1544

The phase transformation temperatures as determined from the heating steps at  $5\text{ }^{\circ}\text{C}/\text{min}$  and  $10\text{ }^{\circ}\text{C}/\text{min}$  were plotted against the heating rates and extrapolated to  $0\text{ }^{\circ}\text{C}/\text{min}$  for the determination of the exact value of the transformation temperature.

The presence of the peritectic reaction was evidenced in all the studied compositions except  $\text{Ni}_{95}\text{Re}_5$ . By combining results of the DTA scans on different compositions, the peritectic reaction temperature of the Ni–Re binary system was placed at  $1541 \pm 3\text{ }^{\circ}\text{C}$ . The DTA plots of a sample of composition  $\text{Ni}_{50}\text{Re}_{50}$  undergoing peritectic reaction and of  $\text{Ni}_{90}\text{Re}_{10}$  composition crossing solidus and peritectic line are shown in Figs. 3 and 4 respectively.

The DTA scans of the composition  $\text{Ni}_{95}\text{Re}_5$  were found to cross only solidus and liquidus line and no peritectic reaction was evidenced. The absence of the peritectic reaction in  $\text{Ni}_{95}\text{Re}_5$  composition indicated primary crystallization of the fcc phase whereas hcp phase was first to crystallize in  $\text{Ni}_{90}\text{Re}_{10}$  composition as indicated by the presence of the peritectic reaction ( $\text{L} + \text{hcp} \rightarrow \text{fcc}$ ) during DTA scans. The primary crystallization of fcc in  $\text{Ni}_{95}\text{Re}_5$  composition and hcp in  $\text{Ni}_{90}\text{Re}_{10}$  composition bracketed the boundary of fcc and hcp primary crystallization fields between 5 and 10 at% Re. To further narrow down the range of this boundary, an alloy of the composition  $\text{Ni}_{92}\text{Re}_8$  was prepared by arc melting and characterized with the help of X-ray diffraction and scanning electron microscope. The characterization results revealed primary crystallization of the fcc phase. Therefore, by combining the characterization results of  $\text{Ni}_{92}\text{Re}_8$  and  $\text{Ni}_{90}\text{Re}_{10}$  composition, the boundary between the freezing ranges of fcc and hcp phases was placed at  $9 \pm 1$  at% Re.

During the present study because of the experimental limitations of the DTA apparatus, each sample was heated to and cooled from  $1600\text{ }^{\circ}\text{C}$ . The fact that only  $\text{Ni}_{95}\text{Re}_5$  composition was found to cross the liquidus in the designed thermal cycles pointed out the presence of a very steep liquidus in the studied system.

The solidus temperature obtained from the DTA scans of the composition  $\text{Ni}_{85}\text{Re}_{15}$  was considered an outlier. The DTA results obtained during present study were used only for the determination of the solidus, liquidus and invariant reaction temperatures whereas the phase boundaries in the studied system were obtained from the characterization of the equilibrated alloys.

### 3.3. Discussion of the experimental results

The temperature of the peritectic reaction and absence of intermetallic compounds were the only areas of agreements among the previous studies on the Ni–Re binary system [1]. The absence of the intermetallic compounds is confirmed during the present study. However, the DTA scans conducted during the present investigation revealed that the peritectic reaction which was previously reported at  $1620\text{ }^{\circ}\text{C}$  [8] actually takes place at a much lower temperature, i.e.  $1541 \pm 3\text{ }^{\circ}\text{C}$ . The peritectic reaction temperature was obtained from the DTA scans on four different compositions and consistency of the obtained results confirmed the validity of the presently reported peritectic reaction temperature. In addition, our finding on the peritectic reaction temperature was close to a recent preliminary measurement (Ursula R. Kattner, Private communication) reporting  $1560 \pm 10\text{ }^{\circ}\text{C}$  as the peritectic reaction temperature. The primary crystallization field of the fcc phase, during the present study, was found up to  $9 \pm 1$  at% Re which is 5–6 at% Re less than the value suggested by Nash et al. [1]. On the other hand, freezing range of the hcp phase is also wider than the range suggested previously.

During the present study, the phase equilibria in the Ni–Re binary system were investigated at  $1200\text{ }^{\circ}\text{C}$ ,  $1500\text{ }^{\circ}\text{C}$  and  $1600\text{ }^{\circ}\text{C}$  with the help of arc melted alloys equilibrated for fairly long periods of time. As discussed in Section 3.1, 1680 h of annealing time was required to reach equilibrium at  $1200\text{ }^{\circ}\text{C}$ ; therefore the time necessary to reach equilibrium at lower temperatures may be prohibitive. This is the reason why the phase equilibria investigation during the present study was restricted to the higher temperatures. The phase boundaries determined during the present study at  $1200\text{ }^{\circ}\text{C}$  and  $1600\text{ }^{\circ}\text{C}$  were confirmed by several alloy compositions. Moreover, the phase boundaries obtained during the present study at the investigated temperatures were found to be self-consistent.

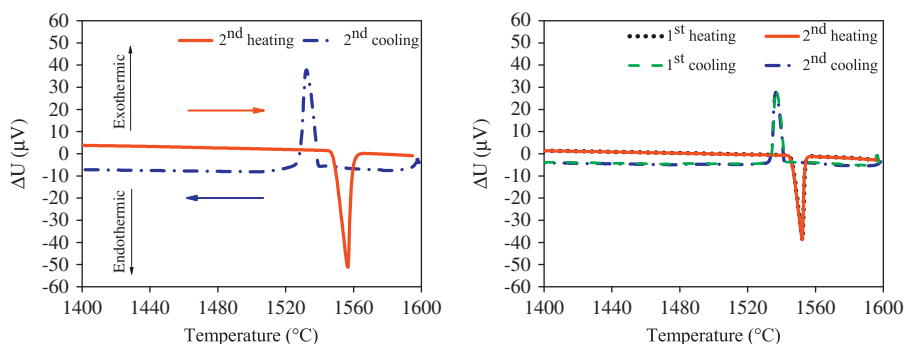


Fig. 3. DTA scans for Ni<sub>50</sub>Re<sub>50</sub> composition at 10 °C/min (left) and 5 °C/min (right).

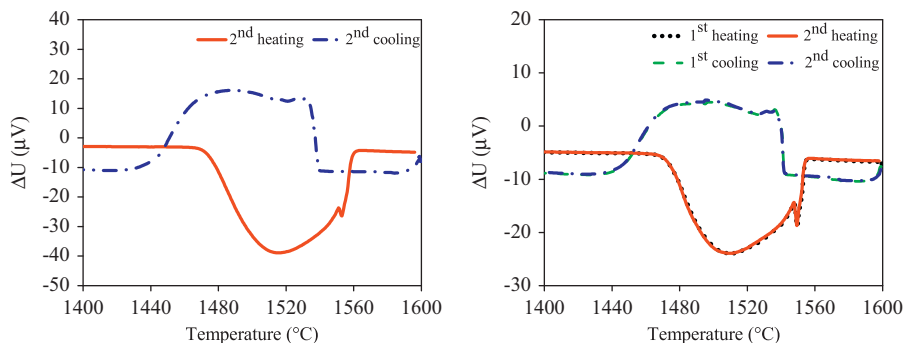


Fig. 4. DTA scans for Ni<sub>90</sub>Re<sub>10</sub> composition at 10 °C/min (left) and 5 °C/min (right).

A comparison of the present study with the recent investigations conducted for the phase equilibria determination in the Ni–Re binary system is presented below.

In general, the phase boundaries determined during the present study were found to be in good agreement with the most recent investigations [12–14]. The fcc and hcp phase boundary at 1200 °C were almost the same as reported by Narita [13], cited in [14]. Similarly, the EPMA results of the sample annealed at 1500 °C also showed good agreement with the solubility limits reported by Saito et al. [14]. The present investigation of the phase equilibrium at 1600 °C revealed two phase equilibrium between liquid and hcp phases which was in accordance with our reported peritectic reaction temperature. The maximum solubility of Ni in hcp phase at 1600 °C was found out to be 33.2 at%. No recent investigation has been carried out at this temperature. Considering the experimental uncertainties and rhenium strong tendency towards segregation, difference of about 1 at% observed with some of the recently reported data was accepted.

In addition to the investigated temperatures, a good agreement was also observed with recent investigations at other temperatures. The two-phase field between fcc and hcp phases at 1110 °C [13] and at 1300 °C [14] reported recently also showed good agreement with the present study. However, the phase equilibrium data obtained by Narita [13] at 980 °C was neither coherent with their own investigations at higher temperatures nor with the present study and was therefore considered an outlier. The phase equilibrium data proposed by Neubauer et al. presented a very steep solvus for both fcc and hcp phases which is rather unlikely. The data reported by Narita at 1110 °C [13] was preferred over the data reported by Neubauer et al. [12] at the same temperature.

By combining the metallurgical and thermal characterization results gathered during the present investigation with recently reported phase equilibrium data found consistent with our study, a new phase diagram of the Ni–Re system is proposed which is shown in Fig. 5.

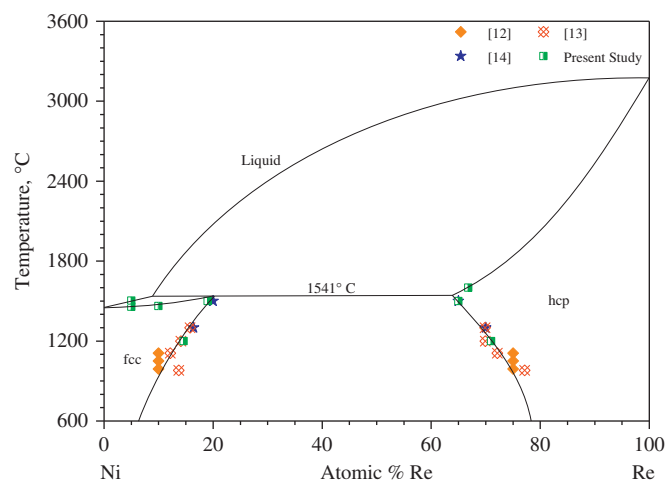


Fig. 5. Ni–Re phase diagram according to the present study.

A comparison of the phase diagram proposed during present study with the diagram suggested by Nash et al. [1] is shown in Fig. 6.

Contrary to the Ni–Re phase diagram suggested by Nash [1], a large increase in the homogeneity domain of the hcp phase producing a better agreement with the related ternary systems was observed. Some of the earlier investigations have shown even higher solubility of Ni in the hcp phase (52.7 at% [6] and 45 at% [10] at 1200 °C). However, the reported values presented large differences and were also inconsistent with the data at other temperatures. Therefore, the data obtained during the present measurement because of its self-consistency and consistency with other measurements conducted independently, was preferred in plotting the diagram shown in Fig. 5. In comparison with the phase diagram suggested by Nash [1], fcc solvus proposed

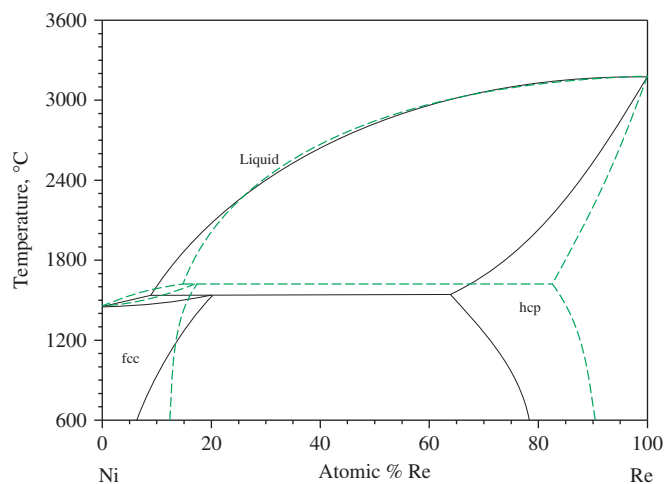


Fig. 6. Comparison of the present (solid) and previously (dashed) suggested experimental Ni–Re phase diagram [1].

during the present study was less steep and showed comparatively higher solubility of Re above 1200 °C.

#### 4. Thermodynamic modeling

The first attempt to model the Ni–Re binary system with the help of available experimental information was carried out by Nash et al. [1]. However, the result was a poor fit to the experimental data. The thermodynamic assessment of the Ni–Re binary system proposed by Nash et al. [1] was later corrected by Okamoto [20]. Huang et al. [21] by using different thermodynamic description of the pure elements [22] reassessed the Ni–Re binary system. Since all the previous assessments have used the experimental information (the peritectic reaction temperature and phase equilibria data) that during the present studies was found to be less accurate, reassessment of the studied system with more precise experimental information was needed and was carried out during the present study.

##### 4.1. Selection of data

The temperature of the invariant reaction has been considered as one of the most important experimental information for the thermodynamic assessment of a system. As discussed in Section 3.3, the peritectic reaction temperature obtained during the present study was confirmed by investigation of four different alloy compositions and was therefore preferred over the previously reported value. Similarly, the solidus and liquidus temperatures obtained from the DTA scans of Ni<sub>95</sub>Re<sub>5</sub> and Ni<sub>90</sub>Re<sub>10</sub> compositions, and the freezing ranges of the fcc and hcp phases obtained during the present study were also used as experimental inputs for thermodynamic assessment of the Ni–Re system. The phase boundaries of the studied system at 1200 °C, 1500 °C and 1600 °C obtained during present study because of their self-consistency and consistency with recently reported data [13,14] were preferred over the previously reviewed data [1]. As discussed in Section 3.3, the phase boundary data at 1110 °C reported by Narita [13] and at 1300 °C reported by Narita [13] and Saito et al. [14] were also found to be consistent with the present measurement and were also incorporated in the thermodynamic assessment of the system. In addition, the data reported by Neubauer et al. [12] at 990 °C was also used.

##### 4.2. Selection of model

As shown in Fig. 5, there are three solution phases in the Ni–Re binary system, i.e. fcc, hcp and liquid. The Gibbs energy in Joules per mole of atoms for a given phase was described by using substitutional-regular solution model.

$G_m^\varphi = x_{\text{Ni}} G_{\text{Ni}}^\varphi + x_{\text{Re}} G_{\text{Re}}^\varphi + RT(x_{\text{Ni}} \ln x_{\text{Ni}} + x_{\text{Re}} \ln x_{\text{Re}}) + {}^E G_m + \Delta^{\text{mag}} G_m^\varphi$  where  $x_{\text{Ni}}$  and  $x_{\text{Re}}$  represent the mole fractions of the element Ni and Re respectively,  $R$  is the Gas constant and  $T$  is the temperature. The quantities  $G_i^\varphi$  describe the molar Gibbs energy of the element  $i$  ( $i = \text{Ni}, \text{Re}$ ) in the phase  $\varphi$  ( $\varphi = \text{fcc}, \text{hcp}, \text{liquid}$ ) in the nonmagnetic state. In the present study, the values of  $G_i^\varphi$  were taken from the Pure4 database [23]. The term  $\Delta^{\text{mag}} G_m^\varphi$  represents the magnetic contribution to the Gibbs energy. The term with pre superscript “E” symbolizes the excess Gibbs energy and is expressed below:

$${}^E G_m = x_{\text{Ni}} x_{\text{Re}} \sum_{\nu=0}^n {}^\nu L_{\text{Ni}, \text{Re}}^\varphi (x_{\text{Ni}} - x_{\text{Re}})^\nu$$

During the present assessment of the Ni–Re binary system, one excess term was used for each phase, i.e.  $n=0$ .

The excess terms for fcc and hcp phases were made temperature dependent by using the following relationship:

$${}^\nu L_{\text{Ni}, \text{Re}}^\varphi = {}^\nu a_\varphi + {}^\nu b_\varphi T$$

where  ${}^\nu a_\varphi$  and  ${}^\nu b_\varphi$  represent the model parameters to be evaluated from the experimental information.

As available experimental information for the liquid phase was limited to a narrow temperature range, therefore, temperature independent interaction term was used for the liquid phase.

#### 5. Results and discussion

Thermodynamic assessment of the Ni–Re binary system was carried out with the help of PARROT module of the thermocalc software [24]. The values of the model parameters evaluated from the experimental information are listed in Table 3.

A comparison of the calculated phase diagram with the experimental data used during optimization process is presented in Fig. 7.

The Ni–Re phase diagram calculated after optimization of the model parameters well describes the selected experimental data.

#### 6. Conclusions

In the present study, new experimental and calculated phase diagrams of the Ni–Re binary system showing a large increase in the phase field of hcp, lower peritectic reaction temperature and different freezing ranges of fcc and hcp phases, were proposed. Contrary to the previously suggested experimental Ni–Re phase diagram [1], the diagram proposed during present study showed a better agreement with the related ternary systems close to the Ni–Re border. On the other hand, present thermodynamic assessment of the studied system based on the results either gathered

Table 3  
List of optimized parameters (J/mol of the formula unit).

Phase	Interaction parameters
Liquid	${}^\circ L_{\text{Ni}, \text{Re}}^{\text{Liq}} = 21,480.3$
fcc	${}^\circ L_{\text{Ni}, \text{Re}}^{\text{fcc}} = 5,054.5 + 8.29 * T$
hcp	${}^\circ L_{\text{Ni}, \text{Re}}^{\text{hcp}} = 9,968.6 + 7.60 * T$

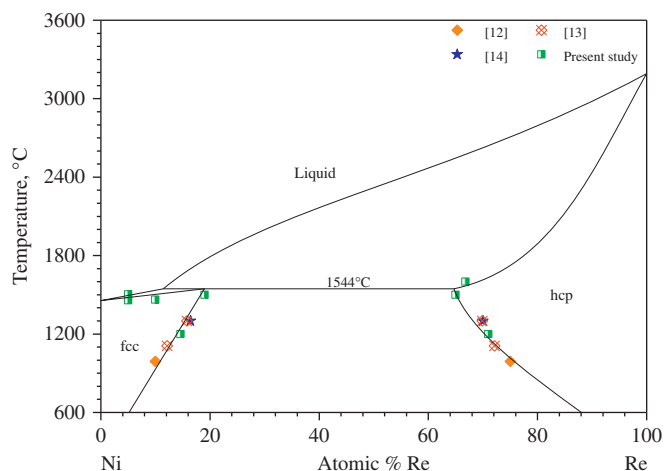


Fig. 7. Calculated Ni-Re phase diagram.

or reviewed during present study showed good agreement with selected experimental information. The use of the present thermodynamic description of the studied system, as it was based on more accurate experimental information, for thermodynamic assessment/reassessment of the related ternary and higher order systems is recommended.

#### Acknowledgments

Financial support from Agence Nationale de la Recherche (ANR) (project Armide 2010 BLAN 912 01) is acknowledged. The authors thank Jean-Marc Fiorani from Institut Jean Lamour for the useful discussion on the DTA scans, Ursula R. Kattner of National

Institute of Standards and Technology for sharing some of their unpublished results and Eric Leroy for EPMA measurements.

#### References

- [1] A. Nash, P. Nash, *Bull. Alloy Phase Diagr.* 6 (1985) 348–350.
- [2] K. Moers, *Z. Anorg. Allg. Chem.* 196 (1931) 147–150.
- [3] C.G. Fink, P. Deren, *Trans. Electrochem. Soc.* 66 (1934) 471–474.
- [4] C.B.F. Young, *Met. Ind.* 34 (1936) 176–177.
- [5] L.E. Netherton, M.L. Holt, *J. Electrochem. Soc.* 98 (1951) 106–109.
- [6] S.A. Pogodin, M.A. Skryabina, *Izv. Sekt. Fiz.-Khim. Anal. Inst. Obshch. Neorg. Khim. Akad. Nauk SSSR* 25 (1954) 81–88.
- [7] P.I. Kirichenko, V.E. Mikryukov, *High Temp. Sci.* 2 (1964) 176–180.
- [8] E.M. Savitskii, M.A. Tylkina, E.P. Arskaya, *Izv. Vyssh. Uchebn. Zaved., Tsvetn. Metall.* 13 (1970) 113–116.
- [9] E.M. Savitskii, M.A. Tylkina, E.P. Arskaya, *Proc. of the Splavy Tsvetnykh Metallov, Moscow, 1972*, pp. 220–229.
- [10] S.M. Solonin, *Sov. Powder Metall. Met. Ceram.* 15 (1976) 270–272.
- [11] A.A. Katsnelson, E.M. Savitskii, A.M. Silonov, E.P. Arskaya, V.M. Silonov, A.S. Savichev, *Proc. of the Fizicheskoi Khimii Svoistva Splavov Reniya, Moscow (1979)* 103–110.
- [12] C.M. Neubauer, D. Mari, D.C. Dunand, *Scr. Metall. Mater.* 31 (1994) 99–104.
- [13] S. Narita, Master's thesis, Graduate School of Hokkaido University, 2003.
- [14] S. Saito, K. Kurokawa, S. Hayashi, T. Takashima, T. Narita, *J. Jpn. Inst. Met.* 71 (2007) 608–614.
- [15] E.M. Slyusarenko, A.V. Peristy, E.Y. Kerimov, M.V. Sofin, D.Y. Skorbov, *J. Alloys Compd.* 264 (1998) 180–189.
- [16] I.V. Ametov, S.F. Dunaev, E.M. Slyusarenko, A.V. Peristy, *Vestn. Mosk. Univ., Ser. 2., Khim.* 31 (1990) 47–52.
- [17] I.V. Ametov, S.F. Dunaev, E.M. Slyusarenko, A.V. Peristy, *Mosc. Univ. Chem. Bull.* 45 (1990) 49–52.
- [18] E.M. Slyusarenko, A.V. Peristy, E.Y. Kerimov, I.L. Guzei, M.V. Sofin, *J. Alloys Compd.* 256 (1997) 115–128.
- [19] J. Rodríguez-Carvajal, XV Congress of International Union of Crystallography, Satellite Meeting on Powder Diffraction, 1990, p. 127.
- [20] H. Okamoto, *J. Phase Equilib.* 13 (1992) 335.
- [21] W. Huang, Y.A. Chang, *Mater. Sci. Eng. A259* (1999) 110–119.
- [22] A.T. Dinsdale, *CALPHAD* 15 (1991) 317–425.
- [23] B. Sundman, P. Shi, *SGTE Pure Element Database, version 4.4, Thermo-Calc Software, 2002*.
- [24] B. Sundman, B. Jansson, J.O. Andersson, *CALPHAD* 9 (1985) 153–190.

# **Chapter 5**

## **The Mo-Ni-Re System**



## Introduction

Mo-Ni-Re is an important subsystem for the development of Ni based superalloys. The literature review of the Mo-Ni-Re system and contradictions among previously reported isothermal sections of the Mo-Ni-Re system have been discussed in detail in the chapter 1. During the present study, complete experimental redetermination of the Mo-Ni-Re system along with verification of phase boundaries in the related binary systems was carried out. The experimental investigation of the Ni-Re phase diagram carried out during present study has already been discussed in the chapter 4. In this chapter, results of the partial investigations of the other constituent binary systems *i.e.* Mo-Ni and Mo-Re, and complete experimental determination of the Mo-Ni-Re system are presented. The main objectives of the present study include:

- verification of phase boundaries in Mo-Ni and Mo-Re binary system
- phase equilibria investigation of the Mo-Ni-Re system at 1200°C and 1600°C
- determination of primary crystallization fields of constituent phases

The phase equilibria investigation of the Mo-Ni-Re system was carried out by chemical and structural characterization of the equilibrated arc melted alloys with the help of EPMA and XRD techniques. The same experimental techniques were also used for investigation of phase boundaries in the Mo-Ni binary system at 1200°C and in Mo-Re binary system at 1200°C and 1600°C. The primary crystallization fields of the Mo-Ni-Re system were determined by characterization of the arc melted as-cast alloys with the help of scanning electron microscope and XRD techniques.

The phase boundary results of the Mo-Ni-Re system obtained during the present study were found to be self-consistent and also showed a good agreement with the phase boundaries in the related binary systems. By combining the binary and ternary phase equilibria results obtained during the present study, isothermal sections of the Mo-Ni-Re system at 1200°C and 1600°C have been proposed. The isothermal sections determined during present study showed a large extension of the Mo-Re  $\sigma$  phase whereas extension of Mo-Re  $\chi$  was restricted to few at. %. Considering large extension of  $\sigma$  phase, its structural characterization was also carried out. The results of structural characterization of  $\sigma$  phase are presented in chapter 7. In addition to large extension of the Mo-Re  $\sigma$  phase, the 1200°C isothermal section of Mo-Ni-Re system proposed during the present study also showed presence of two previously unknown

ternary compounds. One of the ternary phases has structural prototype  $\text{Mo}_3\text{CoSi}$  whereas the crystal structure identification of second ternary phase is presented in chapter 6.

The results of experimental determination of the Mo-Ni-Re system summarized above are provided in this chapter in the form of an article submitted recently to "*Acta Materialia*". They will be used later as input data for thermodynamic modeling of the Mo-Ni-Re system which is discussed in the chapter 8.

## Experimental investigation of phase equilibria in the Mo-Ni-Re system

*Khurram Yaqoob, Jean-Marc Joubert\**

Institut de Chimie et des Matériaux Paris-Est, CNRS, Université Paris-Est Créteil, 2-8 rue  
Henri Dunant 94320 Thiais Cedex, France

\*: Corresponding Author: Jean-Marc Joubert

E-mail address: jean-marc.joubert@icmpe.cnrs.fr

Telephone Number: +33 1 49 78 13 44

Fax Number: +33 1 49 78 12 03

### **Abstract:**

Isothermal sections of the Mo-Ni-Re system have been investigated at 1200°C and 1600°C by characterization of the equilibrated arc melted alloys with the help of electron probe micro analysis (EPMA) and X-ray diffraction (XRD) techniques. The 1200°C isothermal section proposed during the present study showed large extension of the Mo-Re  $\sigma$  phase and Mo-Ni  $\delta$  phase in the ternary region. In addition, presence of two previously unknown ternary phases (a phase with structure prototype  $\text{Mo}_3\text{CoSi}$  and another having a modulated  $\sigma$  structure) was also observed. The isothermal section of the Mo-Ni-Re system at 1600°C also showed large extension of  $\sigma$  phase in the ternary region whereas extension of Mo-Re  $\chi$  phase in both isothermal sections was restricted to only few at. % Ni. The presence of the ternary phases observed in the 1200°C isothermal was not evidenced in 1600°C isothermal sections. In addition to the phase equilibria investigation in the ternary system, partial determination of the phase equilibria in the Mo-Ni and Mo-Re systems, and of the liquidus projection of the Mo-Ni-Re system was also carried out. The liquidus projection of the Mo-Ni-Re system proposed during present study showed extended primary crystallization fields of the  $\sigma$  and (Re) phases.

Keywords: Isothermal section; Liquidus projection; X-ray diffraction (XRD); Scanning electron microscopy (SEM)

## 1. Introduction

Ni based superalloys are most commonly used for high temperature applications [1]. To further enhance their high temperature properties, several alloying additions are made. Molybdenum and rhenium are among the highly interesting elements for the development of Ni based superalloys. However, if their concentration is too large, topologically close packed phases also called as Frank-Kasper phases may form [2-5]. These are brittle intermetallic phases and have detrimental effect on the mechanical properties [6]. In order to avoid precipitation of Frank-Kasper phases and associated degradation in mechanical properties of Ni based superalloys, phase equilibria investigation of the Mo-Ni-Re system is necessary.

The Mo-Ni-Re system was previously investigated by Kodentsov *et al.* [2], Borisov *et al.* [3], Slyusarenko *et al.* [4] and Feng *et al.* [5]. Kodentsov *et al.* [2] studied the isothermal section of the Mo-Ni-Re system at 1152°C by using the diffusion couple method. In addition to the large extension of the binary phases in the ternary region, the presence of two ternary intermetallic compounds was also observed. A more detailed investigation of the Mo-Ni-Re system was later carried out by Borisov *et al.* [3] and Slyusarenko *et al.* [4]. They determined the isothermal section at 1152°C by using diffusion couples and equilibrated alloys. They studied homogeneity domains of different phases and reported the presence of only one ternary compound in the studied isothermal section. A more recent investigation of the Mo-Ni-Re system was carried out by Feng *et al.* [5]. They determined the isothermal section at 1200°C by using diffusion triple. They did not observe presence of any ternary intermetallic compound in the studied system. For comparison, the previously reported isothermal sections of the Mo-Ni-Re system are presented in Figure 1.

As illustrated in Figure 1, the previous studies of the Mo-Ni-Re system contradict not only in terms of number and homogeneity domains of ternary phases but significant differences were also observed in the reported extension of the binary phases in the ternary region. In addition, crystal structure identification of the ternary intermetallic compounds was not carried out and these compounds were tentatively assigned as P [7, 8] and R [9] phases only by the analysis of the literature information. The agreement of isothermal sections with previously accepted binary data was also not satisfactory. Moreover, boundaries of the three phase regions in previous investigations [2, 3] were not determined through the EPMA analysis of three phase samples and their positions were rather tentative. Therefore, in order to develop a better

understanding of the phase equilibria in Mo-Ni-Re system, a complete experimental redetermination of the Mo-Ni-Re system was necessary.

During the present study, isothermal sections of the Mo-Ni-Re ternary system have been investigated at 1200°C and 1600°C by characterization of equilibrated arc melted alloys with the help of electron probe micro analysis (EPMA) and X-ray diffraction (XRD) techniques. As the previously reported isothermal sections showed poor agreement with related binary systems, investigation of the phase boundaries in the Mo-Ni and Mo-Re binary systems was also carried out whereas phase boundaries data related to Ni-Re system was taken from our recent study [10]. By combining EPMA and XRD results of binary and ternary compositions investigated during the present study, isothermal sections of the Mo-Ni-Re system at 1200°C and 1600°C have been proposed. In addition to the phase equilibria determination, liquidus projection of the Mo-Ni-Re system was also studied and primary crystallization fields of different phases have been determined.

## **2. Experimental details**

### **2.1 Sample preparation**

The raw materials used for the present study consisted of pure metals powders (Mo: Sigma Aldrich, <150µm, 99.99 %; Ni: Alfa Aesar, <125µm, 99.996 %; Re: Alfa Aesar, <44µm, 99.99 %). These powders were mixed in the desired ratio in an agate mortar, compacted into pellets, and subjected to arc melting under argon atmosphere. The alloys were melted five times and flipped over after each melting to ensure the chemical homogeneity. Some of the Re rich compositions prepared during the present study showed higher weight losses during arc melting. The increase in weight loss for the Re rich samples was attributed to the evaporation of Ni because of its high vapor pressure at the extremely high melting temperature of the Re rich alloys (pure Re melts at 3186°C [11]).

### **2.2 Annealing**

To remove the concentration gradient appearing during solidification due to segregation and to attain thermodynamic equilibrium at the studied temperatures, annealing treatment was necessary. The refractory nature of the constituent elements required long annealing times and/or high temperatures. From a previous study of Mo-Re system at our lab it was concluded that 720 hours of annealing at 1200°C or 6 hours of annealing at 1600°C were not sufficient

to attain equilibrium. Therefore, during the present study, Mo-Ni-Re alloys were annealed for much longer periods of times i.e. 1680 hours at 1200°C or 9 hours at 1600°C, to attain equilibrium.

For annealing at 1200°C, as-cast samples were encapsulated in silica tubes under argon atmosphere and placed in a preheated resistance furnace for 1680 hours. The insertion of argon inside the silica capsule was meant to avoid the evaporation of high vapor pressure metal *i.e.* Ni in the studied system, and collapsing of silica capsule at annealing temperature (1200°C). The rapid cooling of the samples after annealing was carried out by quenching the silica tubes in water.

The annealing treatment of the as-cast samples at 1600°C was carried out in a high frequency induction furnace in a water cooled copper crucible under an argon atmosphere. The temperature of the samples was measured with the help of an optical pyrometer. After annealing, induction heating was switched off and the rapid cooling of the annealed sample took place due to its contact with water cooled copper crucible.

### **2.3 Chemical characterization**

In order to determine the composition of phases present in equilibrium, part of each sample was polished using standard polishing procedures and examined with the help of electron probe microanalysis (EPMA - CAMECA SX100) by using pure elements as standards. Large numbers of data points were measured on the grains of constituent phases. The chemical composition of each phase was determined by the average of the point measurements performed on that particular phase whereas the calculated standard deviation of these measurements indicated phase homogeneity.

### **2.4 Structural characterization**

To determine the crystal structure and lattice parameters of the phases present in equilibrium, powder X-ray diffraction measurements were carried on a Bruker D8-Advance diffractometer (Bragg-Brentano geometry) equipped with copper K $\alpha$  radiation and a rear graphite monochromator. Most of the samples by virtue of their high brittleness were easily reduced to fine powder. In case of ductile samples, XRD measurements were carried out on massive samples after cutting from the center and polishing. The XRD data was later refined by the Rietveld method with the help of the FULLPROF [12] program.

## **2.5 Scanning electron microscopy**

For micro structural characterization of the alloys prepared for the determination of the liquidus projection, alloys in their as-cast state were polished using standard polishing procedures and analyzed with the help of scanning electron microscope (SEM - LEO 1530) in the back scattered electron (BSE) mode.

## **3. Results**

During the present study, isothermal sections of the Mo-Ni-Re system at 1200°C and 1600°C have been investigated. In addition to the phase equilibrium study, partial determination of the liquidus projection of the studied system was also carried out. The experimental results obtained during the present study are divided into three main categories: (1) phase equilibria study at 1200°C, (2) phase equilibria study at 1600°C, and (3) determination of the liquidus projection.

### **3.1 Phase equilibria study at 1200°C**

To determine the isothermal section of the Mo-Ni-Re system at 1200°C, ternary samples of different alloy compositions were prepared by arc melting, annealed at 1200°C for 1680 hours and characterized with the help of XRD and EPMA techniques. In addition to the phase equilibrium study in ternary system, the phase boundaries in the Mo-Ni and Mo-Re binary system were also investigated at 1200°C. The nominal compositions of binary and ternary alloys along with measured compositions and lattice parameters of the constituent phases as obtained from the EPMA and Rietveld refinement of the XRD data respectively are listed in Table 1.

The chemical homogeneity of the constituent phases in studied alloy compositions (listed in Table 1) confirms that 1680 hours of annealing were sufficient to attain equilibrium at 1200°C. By combining the XRD and EPMA results summarized in Table 1, 1200°C isothermal section of the Mo-Ni-Re system is proposed, which is shown in Figure 2. The crystal structure information of the phases appearing in the 1200°C isothermal section of the Mo-Ni-Re system are listed in Table 2.

Among the samples annealed at 1200°C, composition 17, 27 and 37 showed higher weight losses during arc melting due to higher Ni evaporation. As a result, nominal composition of these samples (17, 27 and 37) does not lie on the observed tie line and in the observed tie

triangle. The shift in the nominal composition of these samples is represented with the help of arrows in Figure 2.

The identification of three phase equilibrium during the present study was carried out by XRD measurements whereas compositions of the phases present in equilibrium were determined with the help of EPMA measurements. However in some cases, the presence of a third phase was evidenced with the help of XRD measurements whereas its amount was so small that its composition cannot be determined accurately by the EPMA measurements. In that case, phase boundary was determined either from investigation of another composition located in the same three phase region or guessed from the nearby tie lines. The dashed lines in Figure 2 and Figure 4 correspond to the guessed compositions.

The back scattered electron (BSE) images of a two-phase (number 14 in Table 1) and a three-phase sample (number 18 in Table 1) annealed at 1200°C for 1680 hours are shown in Figure 3(a) and 3(b) respectively.

The 1200°C isothermal section of the Mo-Ni-Re system proposed during the present study showed a large extension of Mo-Re  $\sigma$  phase in the ternary region. The maximum extension of the Mo-Ni-Re  $\sigma$  phase towards Mo rich and Re rich side was found to be around 28.1 and 19 at.% Ni respectively. Similarly  $\delta$  phase, binary intermetallic compound of the Mo-Ni system, also showed a considerable extension in the ternary region. The maximum solubility of Re in the  $\delta$  phase was found out to be around 23.3 at. %. However, extension of the Mo-Re  $\chi$  phase in the 1200°C isothermal section of the Mo-Ni-Re system was restricted to only 3.3 at.% Ni.

In addition to the large extension of the binary intermetallic compounds ( $\sigma$  and  $\delta$ ), the phase equilibria investigation at 1200°C also revealed presence of two ternary phases. One of the ternary phases was found in equilibrium with (Mo),  $\sigma$ , and  $\delta$  phase. The crystal structure of this ternary phase was identified with the help of the powder XRD measurements. It has a body-centred tetragonal (BCT) crystal structure with a structure prototype of  $\text{Mo}_3\text{CoSi}$ . On the other hand, presence of another ternary phase found in equilibrium with (Ni), (Re),  $\delta$  and  $\sigma$  phase, was also evidenced. The identification of crystal structure of this phase has been the subject of our recent study in which determination of crystal structure of this phase was achieved with the help of X-ray and single crystal diffraction experiments [13]. The indexation of the single crystal diffraction pattern revealed that the average structure of this previously unknown ternary phase was very close to that of  $\sigma$  phase. However, critical

analysis of the reconstructed reciprocal lattice images showed some additional points which were neither indexed by  $\sigma$  nor by any kind of supercell of  $\sigma$ . Therefore, this phase was designated as modulated  $\sigma$  and was named as  $\sigma'$  because of its similarity with the  $\sigma$  phase. The determination of the modulation vector of  $\sigma'$  phase was not carried out due to the poor quality of the crystal [13]. On the other hand, microprobe analysis of one of the samples (number 21 in Table 1) during the present study showed two phase equilibrium between  $\sigma$  and  $\sigma'$ . Therefore, it was concluded that although  $\sigma$  and  $\sigma'$  phases have similar crystal structures; they are present in the Mo-Ni-Re system as distinct phases.

### 3.2 Phase equilibria study at 1600°C

The phase equilibria investigation of the Mo-Ni-Re system at a temperature higher than 1200°C was carried out for the first time. To determine the isothermal section of the studied system at 1600°C, arc melted alloys were annealed at 1600°C for 9 hours using high frequency induction furnace and characterized with the help of XRD and EPMA techniques. In addition to the investigation of the ternary compositions, phase boundaries in the Mo-Re binary systems were also studied. The nominal compositions of the binary and ternary alloys annealed at 1600°C along with their characterization results as obtained from EPMA and Rietveld refinement of the XRD data are listed in Table 3.

The chemical homogeneity of the constituent phases of the samples annealed at 1600°C (listed in Table 3) confirms that 9 hours of annealing were sufficient to attain equilibrium at 1600°C. From the XRD and EPMA results gathered in Table 3, isothermal section of the Mo-Ni-Re system at 1600°C is proposed which is shown in Figure 4.

Among the samples annealed at 1600°C, composition 17, 19 and 36 showed higher weight losses during arc melting. The shift in the nominal composition of these samples as a result of weight loss during melting is represented with the help of arrows in Figure 4.

The 1600°C isothermal section of the Mo-Ni-Re system proposed during the present study also exhibited a large extension of the Mo-Re  $\sigma$  phase in the ternary region. The maximum extension of the Mo-Ni-Re  $\sigma$  phase towards Mo rich and Re rich side was found to be around 28.5 and 30 at. % Ni respectively. On the other hand, extension of  $\chi$  phase in the 1600°C isothermal section was limited to 2.7 at.% Ni. The  $\delta$  phase, binary intermetallic compound of the Mo-Ni system, was not observed in the 1600°C isothermal section. The absence of  $\delta$

phase and establishment of two phase equilibrium between liquid and (Mo) is in accordance with the binary Mo-Ni phase diagram [14].

In addition, presence of ternary intermetallic compounds observed in the isothermal section at 1200°C was not evidenced in the 1600°C isothermal section. As a result of the absence of  $\delta$ , (Ni) and ternary phases, two phase equilibrium was established between the liquid and  $\sigma$ , (Mo) and (Re) phases. The presence of the liquid phase was also observed visually while annealing of some of the samples whereas a part of the sample remained solid. Back scattered electron image of a sample (number 15 in Table 3), containing liquid as one of its constituent phase at 1600°C is shown in Figure 3(c).

The experimental determination of composition of the liquid phase with the help of EPMA was quite difficult as it transformed into other phases during quenching. Therefore liquid phase boundary proposed in Figure 4 is tentative and was guessed from the analysis of the EPMA composition of quenched phase, amount of the phases and nominal composition of the samples. The uncertainty in the proposed liquid phase boundary can be as high as 5 at.% Ni and is therefore indicated as dashed line.

### **3.3 Liquidus projection**

During the present study, partial investigation of the liquidus surface projection of the Mo-Ni-Re system was also carried out. To determine liquidus surface projection of the studied system, samples of different compositions were prepared by arc melting. After melting, the as-cast alloys were cut in half. One half of the sample was polished and micro structural investigation was carried out with the help of scanning electron microscope in the backscattered electron mode. The other half of the sample was either crushed to fine powder or polished and subjected to X-ray diffraction for identification of crystal structure of the phases. The X-ray diffraction measurement of most of samples used for determination of liquidus projection was carried out on massive polished samples.

The nominal compositions of the samples used for the determination of the liquidus surface projection are shown in Figure 5. The alloys containing more than 50 at. % Ni and less than 20 at.% Re showed a weight loss of less than 0.5 wt.% during melting whereas remaining compositions showed weight loss of around 1 wt.% except composition 11 and 4 in which the weight loss was 3.1 and 3.9 w.t % respectively. As discussed in the section 2.1, weight losses during melting were attributed to the evaporation of Ni because of its high vapor pressure.

During the present study, primary crystallization fields of the Mo-Ni-Re phases were determined from micro structural study and XRD analysis. As an example, the BSE image of a sample of nominal composition  $\text{Mo}_{30}\text{Ni}_{60}\text{Re}_{10}$  named as 24 in Figure 5 is shown in Figure 3(d). The brighter phase because of its morphology was considered as primary crystallization phase. On the other hand, XRD analysis of the sample 24 showed presence of  $\sigma$  and (Ni) phase. The  $\sigma$  phase because of its higher electron concentration corresponds to the brighter phase in the BSE image and was designated as primary crystallization phase in the sample 24. Similarly primary crystallization phase of other compositions was determined. Different samples showing primary crystallization of a particular phase are represented with same symbols in Figure 5. The binary invariant reactions in the Mo-Ni, Mo-Re and Ni-Re binary systems serving as starting points for liquidus monovariant lines in the Mo-Ni-Re system were taken from the phase diagrams proposed by Casselton *et al.* [14], Brewer *et al.* [15] and Yaqoob *et al.* [10] respectively and are presented as half-filled green squares in Figure 5. By combining the primary solidification phase relationship determined during the present study with the binary data from the literature [10, 14, 15], liquidus projection of the Mo-Ni-Re system was proposed which is shown in Figure 5.

#### **4. Discussion**

The discussion part has been divided into two main sections. In the first sections the results obtained during present study are discussed whereas the second section deals with the comparison of the 1200°C isothermal section proposed during the present study with previous investigations.

##### **4.1 Present study**

###### **4.1.1 Phase boundaries in the Mo-Ni and Mo-Re system**

The literature survey on the Mo-Ni binary system revealed that homogeneity domain of  $\delta$  phase was previously reported at different compositions (46-48 at.% Ni [14], 48-52 at.% Ni [16], 49-53 at.% Ni [17]). Therefore, verification of the phase boundaries in the Mo-Ni binary system was necessary and was also carried out during the present study. The phase boundaries of the  $\delta$  phase determined during the present study (48-52 at.% Ni) were found to be in very good agreement with the recent investigation by Heijwegen *et al.* [16]. The previous investigations of the Mo-Re binary system were reviewed by Brewer *et al.* [15]. The phase boundaries of the Mo-Re binary system determined during the present study at 1200°C, showed a good agreement with the values suggested by Brewer *et al.* [15] for the (Re) phase boundary and boundary of the  $\chi$  phase on the Re rich side. However, the  $\chi$  phase boundary

towards  $\sigma$  phase determined during present study was neither consistent with the previous studies nor with our results at 1600°C and was therefore considered an outlier. In comparison with the homogeneity domain suggested by Brewer *et al.* (56.8 - 64.6 at.% Re) [15], present investigation of the Mo-Re binary system at 1200°C revealed much larger homogeneity domain of the  $\sigma$  phase (51.9 - 69.2 at. % Re). The homogeneity domain of Mo-Re  $\sigma$  phase determined during present study was found to be in a good agreement with our investigation of the Mo-Ni-Re  $\sigma$  phase. Moreover, larger homogeneity domain of Mo-Re  $\sigma$  phase was also pointed out in some of the previous investigations [18, 19]. Similarly, phase boundary investigation of the Mo-Re binary system was also carried out at 1600°C. The phase equilibrium results obtained during the present study showed a good agreement with the review of Mo-Re system by Brewer *et al.* [15]. The phase boundaries of the binary systems determined during the present study were used for plotting the isothermal proposed during the present study. The phase boundaries of the Ni-Re binary system were taken from our recent investigation [10]. The binary and ternary phase equilibrium data determined during the present study were found to be in good agreement.

#### **4.1.2 Comparison of 1200°C and 1600°C isothermal section**

The isothermal sections of the Mo-Ni-Re system, proposed during the present study, showed a large extension of  $\sigma$  phase in the ternary region. In comparison with the 1200°C isothermal section, homogeneity range of the  $\sigma$  phase at 1600°C was almost the same on the Mo rich side whereas an increase in the extension towards Re rich side was observed. The homogeneity domain of the Mo-Ni-Re  $\sigma$  phase at 1200°C as well as at 1600°C showed an extension towards binary Mo<sub>2</sub>Ni composition. This extension was predicted in a recent study involving determination of enthalpy of formation of the  $\sigma$  phase in the Mo-Ni, Mo-Re, Ni-Re and Mo-Ni-Re systems with the help of DFT calculations. As Mo<sub>2</sub>Ni was found to be the only  $\sigma$  phase configuration with negative enthalpy of formation in the Mo-Ni binary system, therefore, it was assumed that Mo-Re  $\sigma$  phase would show an extension towards Mo<sub>2</sub>Ni composition in the Mo-Ni-Re system [20]. During the present study, this assumption about the shape of the homogeneity domain of the Mo-Ni-Re  $\sigma$  phase has been verified experimentally. The ternary extension of  $\chi$  in the studied isothermal sections was restricted to few at.% Ni. However, solubility of Mo and Ni in the (Re) phase increased with increasing temperature and the phase field of (Re) at 1600°C showed considerably large extension in comparison with 1200°C isothermal section. The absence of the  $\delta$  phase and establishment of two phase equilibrium between liquid and (Mo) at 1600°C was in agreement with the Mo-Ni binary system [14]. In

addition, presence of ternary phases observed in the 1200°C isothermal section was not evidenced in the 1600°C isothermal section.

#### **4.1.3 Correlation between homogeneity domains and lattice parameters**

The large extension of  $\sigma$ ,  $\delta$  and (Re) phase in the 1200°C isothermal section and of  $\sigma$  and (Re) phase in the 1600°C isothermal sections was evident not only from the EPMA results but also from the unit cell volume of these phases obtained from lattice parameters after Rietveld refinement of the XRD data. The plots of unit cell volume of  $\sigma$ ,  $\delta$  and (Re) phase as a function of Ni or Re content in these phases are shown in Figure 6.

The variation of unit cell volume of ternary (Re) phase at 1200°C and 1600°C as a function of Ni content is shown in Figure 6(a) and 6(b) respectively. The unit cell volumes and compositions defining the phase boundaries of the (Re) phase in the Ni-Re binary system [10] are also plotted for comparison and are symbolized as half-filled green squares. As illustrated in Figure 6(a) and 6(b) the unit cell volume of the (Re) phase decreases linearly with increasing Ni content. This decrease in the unit cell volume was attributed to the substitution of Re by Ni because of its smaller atomic radii in comparison with the Re atoms. The fact that unit cell volume of (Re) phase in some of the ternary alloy compositions (35, 22 and 18 in Figure 6(a) and 18, 36, 22 and 13 in Figure 6(b)) is smaller than the unit cell volume of the (Re) phase in the Ni-Re binary system suggests that maximum solubility of Ni in (Re) in the Mo-Ni-Re system will be higher in comparison with the maximum solubility reported in the Ni-Re binary system and explains extension of (Re) phase in the studied isothermal sections. On the other hand, larger extension of (Re) phase at 1600°C in comparison with 1200°C isothermal section is also evident from the larger decrease in the unit cell volume of (Re) phase at 1600°C.

Similarly variation of the unit cell volume of  $\sigma$  phase at 1200°C and 1600°C as a function of Ni and of  $\delta$  phase as a function of Re content are shown in Figure 6(c), 6(d) and 6(e) respectively and are consistent with the homogeneity domain of these phases proposed during the present study with the help of EPMA results.

#### **4.1.4 Liquidus Projection**

The liquidus projection of the Mo-Ni-Re system proposed during present study revealed primary crystallization of  $\sigma$  and (Re) phases over large composition ranges. On the other

hand, analysis of compositions situated close to the Mo-Ni border in the Mo-Ni-Re system revealed absence of  $\delta$  as primary phase. Therefore, it was concluded that primary crystallization range of  $\delta$  in the Mo-Ni-Re system will be restricted to a narrow composition range. The primary crystallization field of  $\delta$  phase shown in Figure 5 is rather tentative. In addition, present study also showed absence of the ternary compounds as primary phase. As no DTA experiments were carried out during present study, therefore determination of the temperature descending direction of the liquidus monovariant lines and nature of ternary invariant reactions was not possible

## **4.2 Comparison of the 1200°C isothermal section with previous investigations**

### **4.2.1 Comparison with the studies by Kodentsov et al. [2] and Feng et al. [5]**

The isothermal sections of the Mo-Ni-Re system proposed by Kodentsov *et al.* [2] and Feng *et al.* [5] shows poor agreement with the present study. Although presence of two ternary phases was reported by Kodentsov *et al.* [2] but positions and homogeneity ranges of these ternary phases were considerably different from the results obtained during the present study. In addition, these ternary phases were designated as P and R phase by analogy with other systems such as Cr-Mo-Ni [21], Co-Mn-Mo [22], Fe-Mo-Ni [23]. The present study revealed that neither P nor R phase was stable in the studied isothermal section. On the other hand, Feng *et al.* [5] did not observe the presence of any ternary compound in the studied isothermal section. However, superimposing the EPMA results obtained by Feng *et al.* [5] on the isothermal section proposed during the present study in Figure 7(b) provided some interesting information. The positions of some of the EPMA results named as 1, 2 and 3 are more or less the same as the phase boundary of the ternary ( $\sigma'$ ) phase determined during the present study. Therefore, it is probable that Feng *et al.* [5] observed the presence of ternary phase but were not able to distinguish it from binary phases as they were not using any phase identification technique. Similarly another EPMA result named as “4” in Figure 7(b) may possibly correspond to the  $\delta$  phase boundary. In this case, absence of phase identification technique can be considered as one of the possible reasons for proposing different isothermal section.

### **4.2.2 Comparison with the study by Borisov et al. [3]**

The isothermal section of the Mo-Ni-Re system proposed by Borisov *et al.* [3] was based on the examination of equilibrated arc melted alloys and diffusion couples. Among the previous studies on the Mo-Ni-Re system, it shows relatively better agreement with the present study in

terms of the shapes of homogeneity domains of different phases. However, considerable differences in the limits of extension of some binary phases such as  $\delta$ ,  $\chi$ , and (Re) phase were observed. In addition, Borisov *et al.* [3] reported presence of only one ternary compound in the studied isothermal section. The homogeneity domain of this ternary phase (tentatively assigned as P phase) is closer to the combined homogeneity domains of two ternary phases ( $\sigma'$  and phase with prototype  $\text{Mo}_3\text{CoSi}$ ) observed during the present study. As Borisov *et al.* [3] did not carry out identification of the ternary phase, therefore it is possible that they were not able to distinguish between the two ternary phases and as a result attributed the homogeneity domains of two ternary phases to only one ternary phase.

A comparison of the EPMA results of equilibrated alloys reported by Borisov *et al.* [3] with the present study is shown in Figure 7(a). The alloys containing less than 50 at.% Re showed excellent agreement with the present study whereas significant differences were observed on the Re rich side i.e.  $\chi$  and (Re) phase boundary. The poor agreement between the two studies on the Re rich side can be attributed to annealing time which becomes more important at higher Re content due to its refractory nature. The alloys investigated by Borisov *et al.* [3] were annealed for 800 hours and perhaps required more time to attain thermodynamic equilibrium. On the other hand, annealing time during the present study was more than two times higher i.e. 1680 hours. Much longer annealing times during the present study made it possible to obtain consistent results even on the Re rich side.

The tie line between (Re) and ternary phase, (number 16 in Figure 7 (a)), also showed good agreement with the present study whereas (Re) phase field proposed by Borisov *et al.* [3] was considerably different. This difference in the (Re) phase fields was due to diffusion couples results which were different from the equilibrated alloys results and were preferred by Borisov *et al.* [3] while proposing the (Re) phase boundary.

Despite of having a very good agreement with the results obtained from equilibrated arc melted alloys, the isothermal sections proposed by Borisov *et al.* [3] was significantly different from the present study. The differences observed in the proposed isothermal sections can be attributed to absence of structural characterization of the ternary phases, some of the diffusion couple results, shorter annealing time and slightly lower annealing temperatures (1152°C) in the study by Borisov *et al.* [3].

#### **4.2.3 Summary**

Contrary to all the previous investigations, the present investigation of the Mo-Ni-Re system was carried out exclusively by investigation of large number of equilibrated arc melted alloys. The use of equilibrated alloys coupled with phase identification techniques is a standard way for the phase equilibria determination and has relatively less sources of error in comparison with the diffusion couple method. The good agreement between present study and previous investigation by Borisov *et al.* [3] can be attributed to the use of equilibrated alloys in both studies. The absence of phase identification technique in the previous investigations became a possible source of misinterpretation of some of their results. However during the present study each alloy composition was characterized by XRD measurements followed by refinement of the data with the help of Rietveld method. The refinement of the XRD data by Rietveld method permits detection of phases present even in very small amounts and also accurate determination of their lattice parameters. The Rietveld refinement of the XRD data confirmed absence of previously reported ternary compounds (P and R) in the studied system. In addition, investigation of large number of equilibrated alloy compositions during the present study with the help of EPMA and XRD techniques made possible the accurate determination of most of the three phase regions. In comparison with the previous investigations by Kodentsov *et al.* [2] and Feng *et al.* [5], the purity of raw materials used during present study was also higher. Borisov *et al.* [3] did not mention the purity of the used raw materials. Because of the better quality of starting materials, longer annealing times and characterization techniques, the Mo-Ni-Re phase equilibria results obtained during the present investigation were consistent and have higher accuracy in comparison with the previous investigations.

## 5. Conclusion

A complete experimental redetermination of the phase equilibria in the Mo-Ni-Re was carried out and isothermal sections at 1200°C and 1600°C have been proposed. The isothermal section at 1200°C showed presence of two ternary compounds whereas none of these compounds was stable at 1600°C. The extension of  $\sigma$  in the studied isothermal sections was quite large whereas homogeneity domain of  $\chi$  phase in both isothermal sections was restricted to few at. % Ni. A comparison of the 1200°C isothermal section proposed during present study with the previous investigations helped in finding out the possible errors/misinterpretations in the previous studies. In addition, partial investigation of liquidus projection of the Mo-Ni-Re system was also carried out which showed largely extended primary crystallization fields of  $\sigma$  and (Re) phases.

## Acknowledgement

Financial support from Agence Nationale de la Recherche (ANR) (Armide 2010 BLAN 912 01) is acknowledged. The authors are grateful to Jean-Marc Fiorani from Institut Jean Lamour and Nathalie Dupin from *Calcul Thermodynamique* for useful discussions and careful reading of the manuscript. The authors also thank Eric Leroy for EPMA measurements and Pierre Joubert for proofreading.

## References

- [1] Reed RC. The Superalloys Fundamentals and Applications, Cambridge University Press, New York, 2008.
- [2] Kodentsov AA, Dunaev SF, Slyusarenko EM, Sokolovskaya EM, Priimak AN. Vestn. Mosk. Univ., Ser. 2., Khim. 1987;28:153.
- [3] Borisov VA, Yaschenko AI, Slyusarenko EM, Dunaev SF. Moscow University Chemistry Bulletin 1992;47:76.
- [4] Slyusarenko EM, Peristyí AV, Kerimov EY, Sofin MV, Skorbov DY. J. Alloys Compd. 1998;264:180.
- [5] Feng Y, Wang R, Yu K, Wen D. Rare Met. 2008;27:83.
- [6] Rae CM, Reed RC. Acta Mater. 2001;49:4113.
- [7] Brink C, Shoemaker DP. Acta Crystallogr. 1955;8:734.
- [8] Shoemaker DP, Shoemaker CB, Wilson FC. Acta Crystallogr. 1957;10:1.
- [9] Komura Y, Sly WG, Shoemaker DP. Acta Crystallogr. 1960;13:575.
- [10] Yaqoob K, Joubert J-M. J. Solid State Chem. 2012;
- [11] Massalski TB. Binary alloys phase diagrams, second ed., ASM International, Materials Park, Ohio, 1990.
- [12] Rodríguez-Carvajal J. XV Congress of Int. Union of Crystallography, Satellite Meeting on Powder Diffraction 1990;127.
- [13] Yaqoob K, Guénée L, Cerný R, Joubert J-M. To be published.
- [14] Casselton REW, Hume-Rothery W. Journal of the less-common metals 1964;7:212.
- [15] Brewer L, Lamoreaux RH. At. Energy Rev. 1980;Spec. Issue 7:195.

- [16] Heijwegen CP, Rieck GD. *Z. Metallkde.* 1973;64:450.
- [17] Meshkov LL, Guzei LS, Sokolovskaya EM. *Russian Journal of Physical Chemistry* 1975;49:1128.
- [18] Dickinson JM, Richardson LS. *Trans. ASM* 1959;51:1055.
- [19] Farzadfar S-A, Levesque M, Phejar M, Joubert J-M. *Calphad: Comput. Coupling Phase Diagrams Thermochem.* 2009;33:502.
- [20] Yaqoob K, Crivello J-C, Joubert J-M. *Inorg. Chem.* 2012;51:3071.
- [21] Rideout S, Manly WD, Kamen EL, Lement BS, Beck PA. *Trans. AIME* 1951;191:872.
- [22] Das BN, Beck PA. *Trans. Metall. Soc. AIME* 1960;218:733.
- [23] Das DK, Rideout SP, Beck PA. *J.o.M* 1952;4:1071.
- [24] Gladyshevskii EI, Kripyakevich PI, Skolozdra RV. *Sov. Phys. - Dokl* 1968;12:755.
- [25] Joubert J-M. *Prog. Mater. Sci.* 2008;53:528.
- [26] Joubert J-M, Phejar M. *Prog. Mater. Sci.* 2009;54:945.
- [27] Shoemaker CB, Shoemaker DP. *Acta Crystallogr.* 1963;16:997.

## Tables

Table 1: Characterization results of the samples annealed at 1200°C. Standard deviation of the last significant digit is indicated in parentheses.

Sample Number	Nominal Composition (at. %)	Phases	Measured Composition (at. %)			Lattice parameters (Å)		
			Mo	Ni	Re	<i>a</i>	<i>b</i>	<i>c</i>
2	Mo <sub>37</sub> Ni <sub>56</sub> Re <sub>7</sub>	(Ni)	22.5(2)	75.2(3)	2.2(1)	3.6319(3)	-	-
		δ	42.5(1)	48.3(1)	9.3(1)	8.8243(5)	9.1330(9)	9.1349(9)
3	Mo <sub>25</sub> Ni <sub>55</sub> Re <sub>20</sub>	(Ni)	16.2(1)	76.4(2)	7.4(1)	3.6262*	-	-
		σ'	32.3(2)	34.2(3)	33.5(2)	-	-	-
4	Mo <sub>60</sub> Ni <sub>20</sub> Re <sub>20</sub>	(Mo)	>79.7	<3.9	<16.4	3.1349(2)	-	-
		σ	55.2(3)	23.4(5)	21.4(7)	9.3767(6)	-	4.9022(4)
5	Mo <sub>62.5</sub> Ni <sub>32.5</sub> Re <sub>5</sub>	(Mo)	89.2(3)	2.1(3)	8.7(5)	3.1405(2)	-	-
		δ	50.1(1)	45.9(1)	4.0(1)	8.855(1)	9.159(4)	9.170(4)
		Mo <sub>3</sub> CoSi	58.1(2)	36.0(3)	5.9(2)	12.667(2)	-	4.808(1)
6	Mo <sub>35</sub> Ni <sub>40</sub> Re <sub>25</sub>	δ	33.0(1)	43.6(2)	23.3(1)	8.831(2)	9.163(9)	9.159(9)
		σ'	36.6(1)	33.1(4)	30.3(3)	-	-	-
10	Mo <sub>24</sub> Ni <sub>19</sub> Re <sub>57</sub>	(Re)	6.5(6)	18.2(3)	75.3(6)	2.7276(3)	-	4.4017(7)
		σ	26.8(3)	19.0(7)	54.2(5)	9.3567(5)	-	4.9120(3)
11	Mo <sub>30</sub> Ni <sub>30.5</sub> Re <sub>39.5</sub>	σ'	29.4(2)	31.5(4)	39.1(4)	-	-	-
12	Mo <sub>60</sub> Ni <sub>7</sub> Re <sub>33</sub>	(Mo)	>65.5	<4.6	<29.9	3.1324(1)	-	-
		σ	51.1(5)	9.8(3)	39.1(6)	9.5105(5)	-	4.9542 (3)
13	Mo <sub>15</sub> Ni <sub>55</sub> Re <sub>30</sub>	(Ni)	11.3(1)	74.7(1)	14.0(1)	3.6267*	-	-
		(Re)	8.7	<38.9	>52.4	-	-	-
		σ'	22.0(3)	33.3(6)	44.7(3)	-	-	-
14	Mo <sub>30</sub> Ni <sub>58</sub> Re <sub>12</sub>	(Ni)	20.2(1)	75.3(1)	4.5(0)	3.6324(5)	-	-
		δ	36.8(4)	45.9(5)	17.2(2)	8.827(1)	9.150(3)	9.146(3)
15	Mo <sub>45</sub> Ni <sub>30</sub> Re <sub>25</sub>	σ'	44.6(6)	31.1(9)	24.3(4)	-	-	-
		(Mo)	87.5(10)	2.2(4)	10.3(7)	3.1384(1)	-	-
16	Mo <sub>70</sub> Ni <sub>20</sub> Re <sub>10</sub>	Mo <sub>3</sub> CoSi	55.5(3)	33.8(3)	10.7(3)	12.6731(7)	-	4.8119(4)
		σ	58.5(6)	28.1(1)	13.4(6)	9.331(3)	-	4.831(2)
		(Re)	<13.3(12)	<5.9(8)	>80.8	2.7536(2)	-	4.4434(5)
17	Mo <sub>20</sub> Ni <sub>10</sub> Re <sub>70</sub>	χ	21.7(9)	3.3(8)	75.0(4)	9.5581(5)	-	-
		σ	>28.8	10.1	<61.2	9.450(1)	-	4.942(1)
		(Ni)	11.2	>71.1	<17.7	-----	-	-----
18	Mo <sub>15</sub> Ni <sub>35</sub> Re <sub>50</sub>	(Re)	8.2(4)	36.7(9)	55.2(10)	2.6862(4)	-	4.3461(9)
		σ'	22.0(1)	32.4(2)	45.6(1)	-----	-	-
19	Mo <sub>35</sub> Ni <sub>5</sub> Re <sub>60</sub>	σ	34.5(5)	2.6(6)	62.9(9)	9.5363(2)	-	4.9668(1)
21	Mo <sub>35</sub> Ni <sub>30</sub> Re <sub>35</sub>	σ	37.5(5)	23.5(4)	39.0(3)	9.298(4)	-	4.927(2)
		σ'	35.9(3)	29.6(3)	34.5(2)	-	-	-
22	Mo <sub>7.5</sub> Ni <sub>55</sub> Re <sub>37.5</sub>	(Ni)	9.0(1)	76.6(2)	14.4(1)	3.6236(3)	-	-
		(Re)	5.6(1)	32.8(5)	61.6(6)	2.6915(4)	-	4.3411(8)
23	Mo <sub>62.5</sub> Ni <sub>35</sub> Re <sub>2.5</sub>	(Mo)	93.8(5)	2.4(5)	3.8(5)	3.1417(1)	-	-
		δ	51.1(1)	46.8(1)	2.1(0)	8.8518(4)	9.156(2)	9.159(2)
24	Mo <sub>31</sub> Ni <sub>44</sub> Re <sub>25</sub>	(Ni)	18.8 (2)	74.4(2)	6.8(2)	3.6280*	-	-
		σ'	36.8(4)	33.3(4)	29.9(4)	-	-	-
25	Mo <sub>20</sub> Ni <sub>27.5</sub> Re <sub>52.5</sub>	(Re)	7.1(2)	24.8(3)	68.2(4)	2.708(1)	-	4.382(2)
		σ'	24.3(2)	27.8(4)	47.4(3)	-	-	-
26	Mo <sub>45</sub> Ni <sub>15</sub> Re <sub>40</sub>	σ	45.2(7)	14.3(11)	40.5(16)	9.4437(3)	-	4.9324(1)
		(Re)	<14.0	<5.8	>80.2	2.7511(3)	-	4.4400(6)
27	Mo <sub>25</sub> Ni <sub>10</sub> Re <sub>65</sub>	χ	20.6(7)	4.0(4)	75.5(4)	9.5568(4)	-	-
		σ	30.1(4)	10.1(2)	59.8(4)	9.4514(4)	-	4.9431(3)
28	Mo <sub>38.5</sub> Ni <sub>46.5</sub> Re <sub>15</sub>	(Ni)	22.0(0)	74.1(1)	3.9(0)	3.6297(8)	-	-
		δ	39.9(3)	45.4(3)	14.7(1)	8.8263(4)	9.1481(9)	9.1448(9)

<b>29</b>	Mo <sub>27</sub> Ni <sub>6</sub> Re <sub>67</sub>	χ	22.4(5)	2.3(2)	75.4(6)	9.5675(2)	-	-
		σ	29.6(5)	5.9(5)	64.5(4)	9.4937(2)	-	4.9574(2)
<b>31</b>	Mo <sub>25</sub> Ni <sub>25</sub> Re <sub>50</sub>	σ'	24.3(5)	26.1(14)	49.6(10)	-	-	-
<b>32</b>	Mo <sub>30</sub> Ni <sub>27.5</sub> Re <sub>42.5</sub>	σ'	29.3(4)	28.3(10)	42.4(6)	-	-	-
<b>33</b>	Mo <sub>50</sub> Ni <sub>40</sub> Re <sub>10</sub>	δ	46.1(2)	45.5(2)	8.4(1)	8.8510 (3)	9.1617(10)	9.1654(9)
		Mo <sub>3</sub> CoSi	52.7(2)	35.4(2)	11.9(1)	12.6615(3)	-	4.8052(1)
<b>34</b>	Mo <sub>22.5</sub> Ni <sub>45</sub> Re <sub>32.5</sub>	(Ni)	13.0(1)	76.2(2)	10.8(2)	3.6222*	-	-
		σ'	25.8(3)	32.7(4)	41.5(3)	-	-	-
<b>35</b>	Mo <sub>15</sub> Ni <sub>31</sub> Re <sub>54</sub>	(Re)	6.9(7)	30.8(11)	62.3(17)	2.697 (1)	-	4.364(2)
		σ'	21.7(2)	31.7(3)	46.6(3)	-	-	-
<b>36</b>	Mo <sub>19</sub> Ni <sub>24</sub> Re <sub>57</sub>	(Re)	6.3(8)	22.2(9)	71.5(14)	2.7201(4)	-	4.3898(8)
		σ'	23.9(2)	26.4(7)	49.7(5)	-	-	-
<b>37</b>	Mo <sub>13</sub> Ni <sub>12</sub> Re <sub>75</sub>	(Re)	7.4(17)	5.9(16)	86.7(3)	2.7453(2)	-	4.4364(3)
		σ	29.0(3)	12.6(2)	58.4(2)	9.441(1)	-	4.934(2)
<b>38</b>	Mo <sub>72.5</sub> Ni <sub>7.5</sub> Re <sub>20</sub>	(Mo)	78.6(6)	1.4(1)	20.1(6)	3.1358(1)	-	-
		σ	-	-	-	9.4140(7)	-	4.9150(5)
<b>39</b>	Mo <sub>49</sub> Ni <sub>34</sub> Re <sub>17</sub>	δ	43.2(4)	44.1(5)	12.7(2)	8.832(2)	9.150(3)	9.187(3)
		Mo <sub>3</sub> CoSi	48.3(1)	34.8(2)	16.8(1)	12.6612(3)	-	4.8021(1)
<b>40</b>	Mo <sub>40</sub> Ni <sub>60</sub>	(Ni)	25.6(1)	74.4(1)	0	3.6386(4)	-	-
		δ	48.0(2)	52.0(2)	0	8.828 (1)	9.124(6)	9.092(6)
<b>41</b>	Mo <sub>60</sub> Ni <sub>40</sub>	(Mo)	97.5(2)	2.5(2)	0	3.1450(1)	-	-
		δ	52.0(1)	48.0(1)	0	8.8497(3)	9.1474(6)	9.1550(6)
<b>42</b>	Mo <sub>52</sub> Re <sub>48</sub>	(Mo)	-	0	-	3.1319(1)	-	-
		σ	48.1(1)	0	51.9(1)	9.6089(3)	-	4.9880(2)
<b>43</b>	Mo <sub>27</sub> Re <sub>73</sub>	χ	20.0(3)	0	80.0(3)	9.5892(2)	-	-
		σ	30.8(5)	0	69.2(5)	9.5692(4)	-	4.9775(3)
<b>44</b>	Mo <sub>13</sub> Re <sub>87</sub>	(Re)	8.5(5)	0	91.5(5)	2.7651(3)	-	4.4724(8)
		χ	19.8(9)	0	80.2(9)	9.5826(8)	-	-

\* : Rietveld refinement not possible due to unknown crystal structure of σ' phase, lattice parameters obtained with the help of EVA software)

Table 2: Crystal structure information of the phases appearing in the 1200°C isothermal section of Mo-Ni-Re system

Phases	Pearson symbol	Prototype	Space group	Reference
Mo <sub>3</sub> CoSi	<i>tI56</i>	Mo <sub>4</sub> (Mo <sub>0.8</sub> Co <sub>0.2</sub> ) <sub>5</sub> (Co <sub>0.4</sub> Si <sub>0.6</sub> ) <sub>5</sub>	$\bar{I}4\ c2$	[24]
σ'	-	-	-	-
σ	<i>tP30</i>	Cr <sub>0.49</sub> Fe <sub>0.51</sub>	$P4_2/mnm$	[25]
χ	<i>cI58</i>	Mn	$\bar{I}4\ 3m$	[26]
δ	<i>oP56</i>	Mo <sub>3</sub> (Mo <sub>0.8</sub> Ni <sub>0.2</sub> ) <sub>5</sub> Ni <sub>6</sub>	$P2_12_12_1$	[27]
(Mo)	<i>cI2</i>	W	$Im\ \bar{3}\ m$	[11]
(Ni)	<i>cF4</i>	Cu	$Fm\ \bar{3}\ m$	[11]
(Re)	<i>hP2</i>	Mg	$P6_3/mmc$	[11]

Table 3: Characterization results of the samples annealed at 1600°C. Standard deviation of the last significant digit is indicated in parentheses. \* : Guessed liquid composition

Sample Number	Nominal Composition (at. %)	Phases	Measured Composition (at. %)			Lattice parameters (Å)	
			Mo	Ni	Re	a	c
1	Mo <sub>10</sub> Ni <sub>35</sub> Re <sub>55</sub>	(Re)	10.3 (11)	13.9(10)	75.8(7)	2.743(1)	4.425(1)
		σ	26.5(2)	14.4(2)	59.1(3)	9.415(5)	4.938(3)
3	Mo <sub>25</sub> Ni <sub>55</sub> Re <sub>20</sub>	Liquid*	20	67	13	-	-
		σ	32.4(1)	27.9(3)	39.7(3)	9.258(2)	4.874(1)
4	Mo <sub>60</sub> Ni <sub>20</sub> Re <sub>20</sub>	(Mo)	77.4(8)	3.5(3)	19.1(6)	3.1311(2)	-
		σ	55.3(4)	20.0(3)	24.8(6)	9.3758(5)	4.9023(3)
6	Mo <sub>35</sub> Ni <sub>40</sub> Re <sub>25</sub>	Liquid*	22.3	66.0	11.7	-	-
		σ	37.6(4)	29.1(9)	33.4(8)	9.288 (2)	4.876(1)
8	Mo <sub>15</sub> Ni <sub>5</sub> Re <sub>80</sub>	(Re)	9.4(5)	3.2(5)	87.4(9)	2.7542(2)	4.4549(4)
		σ	27.7(2)	7.9(2)	64.3(1)	9.464(2)	4.955 (1)
9	Mo <sub>29.5</sub> Ni <sub>10</sub> Re <sub>60.5</sub>	σ	29.8(3)	7.3(1)	63.0(4)	9.4816(2)	4.9520(1)
10	Mo <sub>24</sub> Ni <sub>19</sub> Re <sub>57</sub>	(Re)	11.1(8)	16.6(12)	72.4(10)	2.7221(3)	4.3995(8)
		σ	25.3(2)	17.4(9)	57.3(7)	9.3515(2)	4.9104(1)
11	Mo <sub>30</sub> Ni <sub>30.5</sub> Re <sub>39.5</sub>	Liquid*	17.3	67.6	15.1	-	-
		σ	30.7(2)	28.2(4)	41.1(3)	9.2643(3)	4.8746(2)
12	Mo <sub>60</sub> Ni <sub>7</sub> Re <sub>33</sub>	(Mo)	>61.2	<5.7	<33.1	3.1277(1)	-
		σ	51.4(5)	9.4(3)	39.2(3)	9.5123(4)	4.9562(2)
13	Mo <sub>15</sub> Ni <sub>55</sub> Re <sub>30</sub>	Liquid*	13.8	67.6	18.6	-	-
		(Re)	13.2(1)	47.1(8)	39.7(9)	2.6346(3)	4.2684(5)
14	Mo <sub>30</sub> Ni <sub>58</sub> Re <sub>12</sub>	Liquid*	25.6	64.6	9.8	-	-
		σ	40.9(2)	29.6(4)	29.5(3)	-	-
15	Mo <sub>45</sub> Ni <sub>30</sub> Re <sub>25</sub>	σ	46.2(1)	26.7(1)	27.2(1)	9.3179(3)	4.8850(2)
		Liquid*	29.1	62.4	8.5	-	-
16	Mo <sub>70</sub> Ni <sub>20</sub> Re <sub>10</sub>	(Mo)	83.5(8)	4.5(4)	12.0(5)	3.1294(2)	-
		Liquid*	47.4	47.4	5.2	-	-
17	Mo <sub>17</sub> Ni <sub>13</sub> Re <sub>70</sub>	σ	59.4(2)	28.5(11)	12.1(10)	9.336(1)	4.865(1)
		(Re)	9.5(4)	4.4(4)	86.1(2)	2.7572(4)	4.4623(8)
18	Mo <sub>15</sub> Ni <sub>35</sub> Re <sub>50</sub>	σ	27.7(1)	8.2(1)	64.1(1)	9.479(3)	4.955(2)
		(Re)	12.8(3)	35.6(4)	51.6(2)	2.6831(4)	4.3400(8)
19	Mo <sub>20</sub> Ni <sub>7</sub> Re <sub>73</sub>	σ	24.7(1)	25.0(1)	50.3(1)	9.281(4)	4.882(3)
		(Re)	<13.3	<1.9	>84.7	2.7619(4)	4.4707(10)
22	Mo <sub>10</sub> Ni <sub>65</sub> Re <sub>25</sub>	σ	28.3(2)	4.9(3)	66.9(3)	9.501(3)	4.963(2)
		χ	21.0(10)	2.7(7)	76.3(8)	9.5724(8)	-
23	Mo <sub>30</sub> Ni <sub>5</sub> Re <sub>65</sub>	(Re)	8.2(2)	45.1(11)	46.7(13)	2.633(2)	4.268(3)
		Liquid*	10.1	73.7	16.2	-	-
25	Mo <sub>70</sub> Ni <sub>30</sub>	σ	29.6(4)	3.9(3)	66.5(7)	9.5181(2)	4.9635(1)
		(Mo)	98.1(2)	1.9(2)	0	3.1424(1)	-
26	Mo <sub>60</sub> Re <sub>40</sub>	Liquid*	-	-	-	-	-
		(Mo)	66.4(6)	0	33.6(6)	3.1330(2)	-
28	Mo <sub>28</sub> Re <sub>72</sub>	σ	46.7(3)	0	53.3(3)	9.6258(10)	5.0001(8)
		χ	30.5(4)	0	69.5(4)	9.5641(2)	4.9761(1)
30	Mo <sub>22</sub> Ni <sub>40</sub> Re <sub>38</sub>	σ	-	-	-	9.5850(2)	-
		Liquid*	14.2	67.6	18.2	-	-
31	Mo <sub>69</sub> Ni <sub>6</sub> Re <sub>25</sub>	σ	24.5(3)	29.9(2)	45.6(4)	-	-
		(Mo)	71.9(2)	2.6(5)	25.5(4)	3.1280(1)	-
33	Mo <sub>18</sub> Re <sub>82</sub>	σ	>26.3	18.3	<55.47	9.461(2)	4.932(1)
		(Re)	<10.3	0	>89.7	2.7679(2)	4.4839(7)
34	Mo <sub>70</sub> Ni <sub>13</sub> Re <sub>17</sub>	χ	21.9(2)	0	78.1(2)	9.5885(7)	-
		(Mo)	79.5(4)	4.4(1)	16.1(4)	3.1271(1)	-
36	Mo <sub>18</sub> Ni <sub>42</sub> Re <sub>40</sub>	σ	57.8(2)	23.8(3)	18.4(3)	9.3611(5)	4.8959(3)
		(Re)	13.2(2)	45.4(5)	41.5(7)	2.6484(3)	4.2908(7)
		σ	25.2(3)	26.2(2)	48.6(4)	9.2690(8)	4.8814(5)

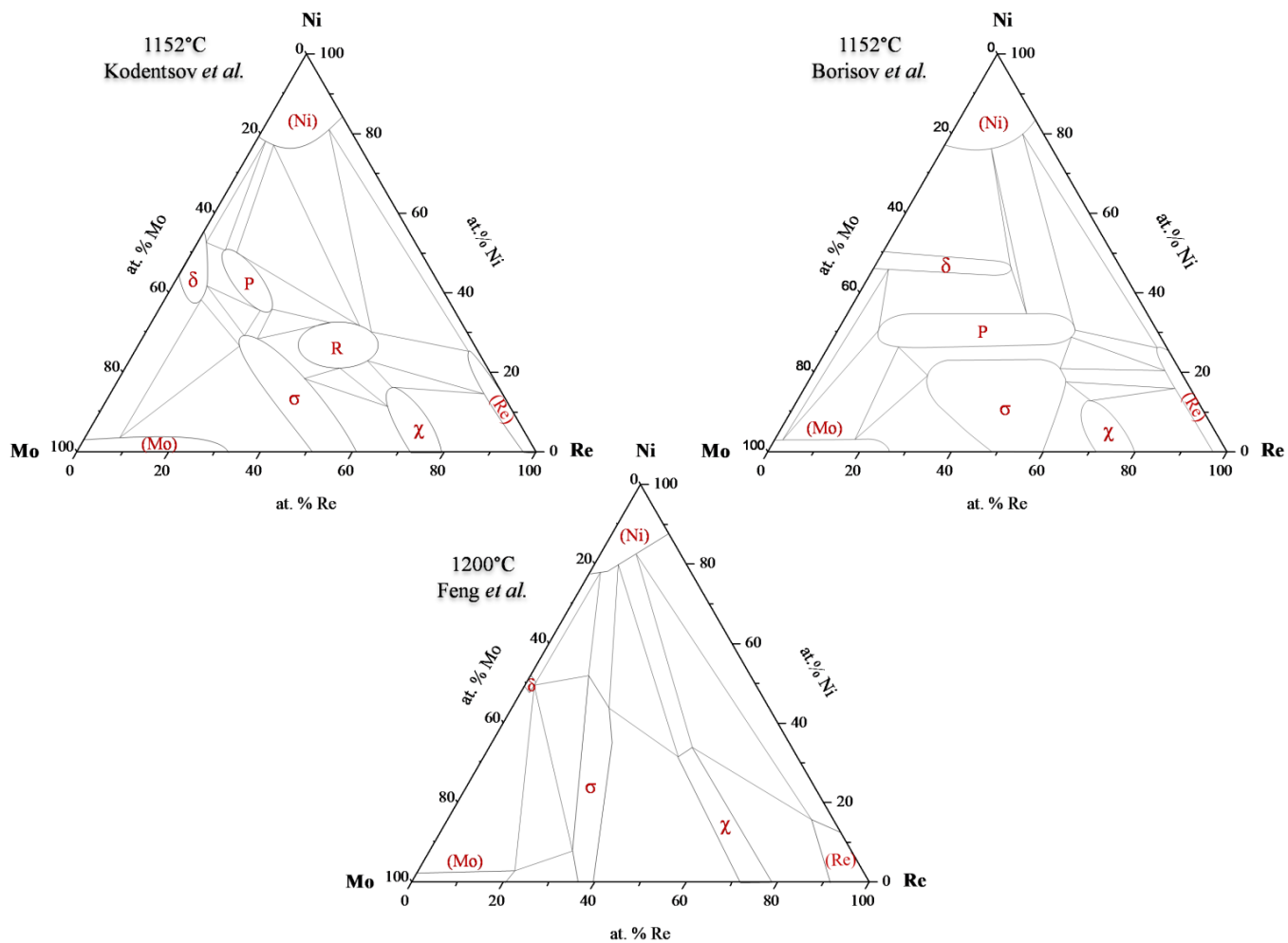


Figure 1: Previous investigations of the Mo-Ni-Re system: (a) Kodentsov *et al.* [2], (b) Borisov *et al.* [3], and (c) Feng *et al.* [5].

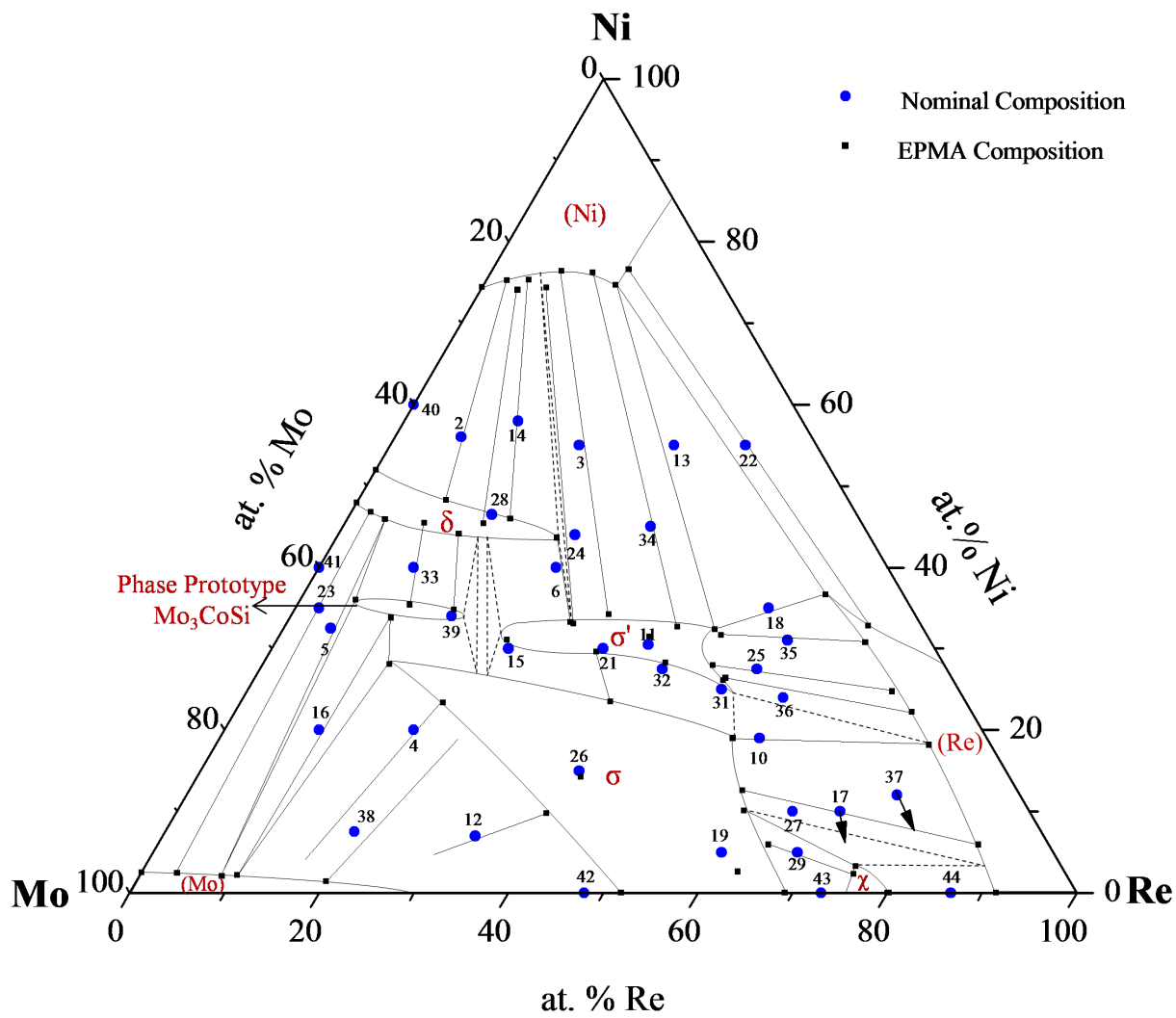
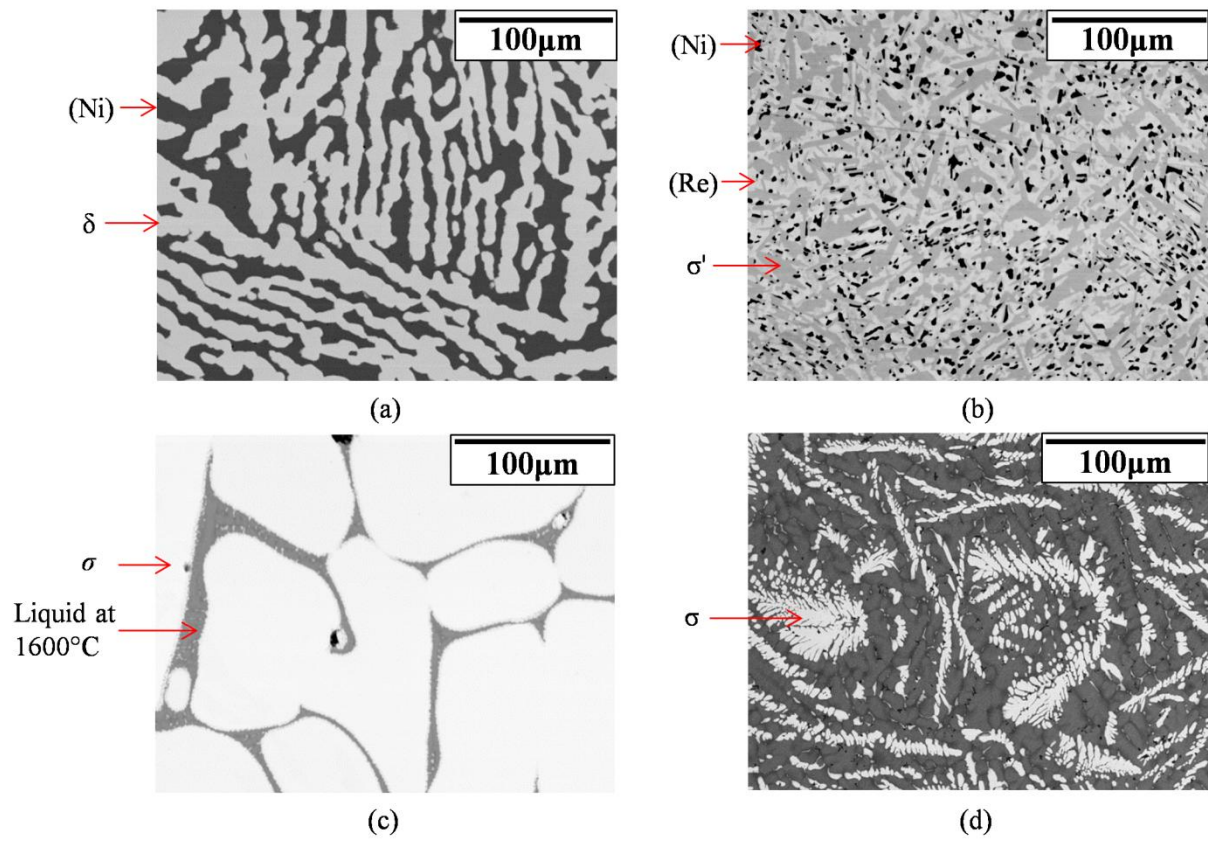


Figure 2: Isothermal section of the Mo-Ni-Re system at 1200°C proposed during the present study



*Figure 3: Back scattered electron images of (a) a two phase sample annealed at 1200°C (number 14 in Table 1), (b) a three phase sample annealed at 1200°C (number 18 in Table 1), (c) a two phase sample showing presence of liquid at 1600°C (number 15 in Table 3) (d) as-cast sample (number 24 in Figure 5).*

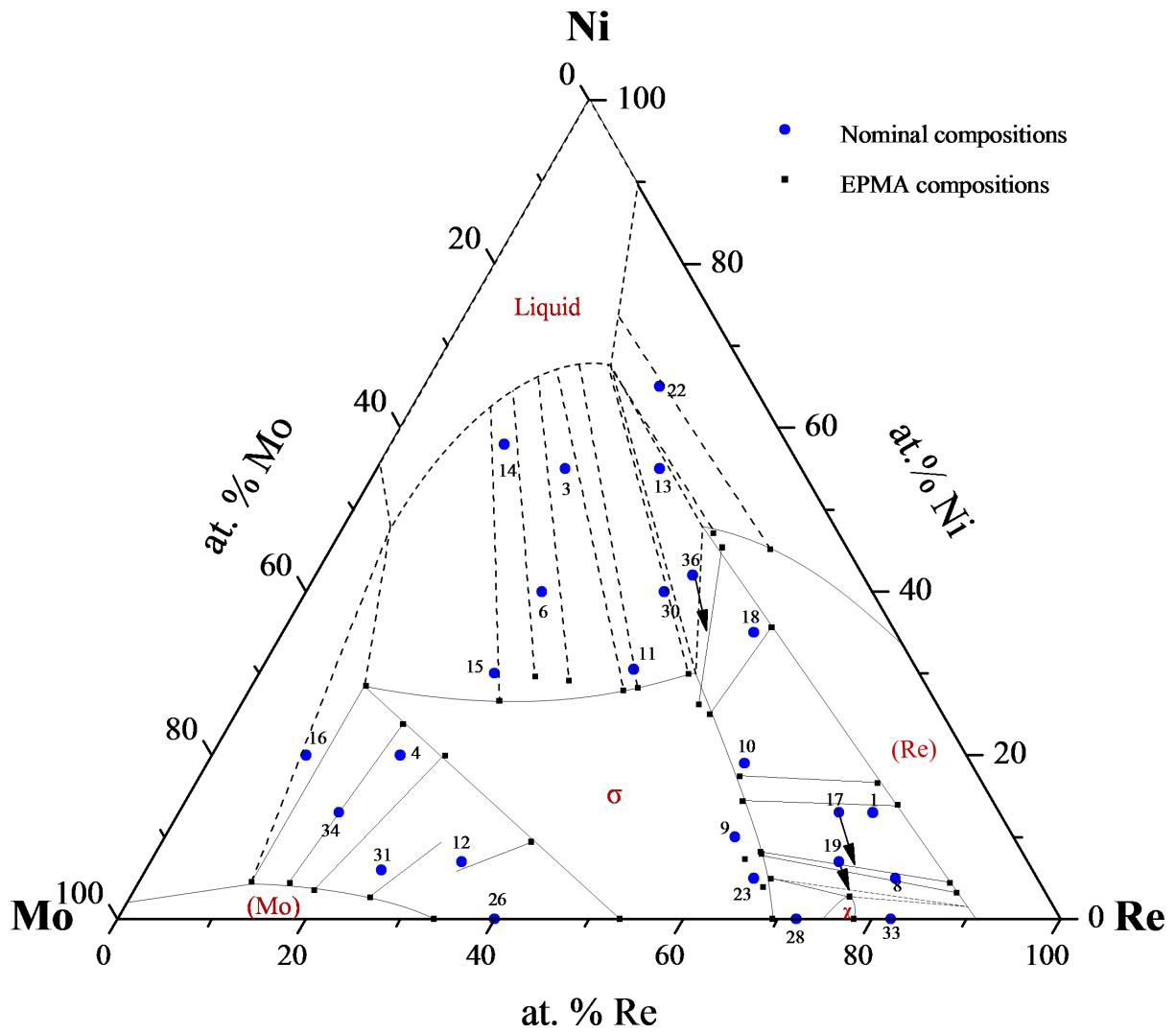


Figure 4: Isothermal section of the Mo-Ni-Re system at 1600°C proposed during the present study.

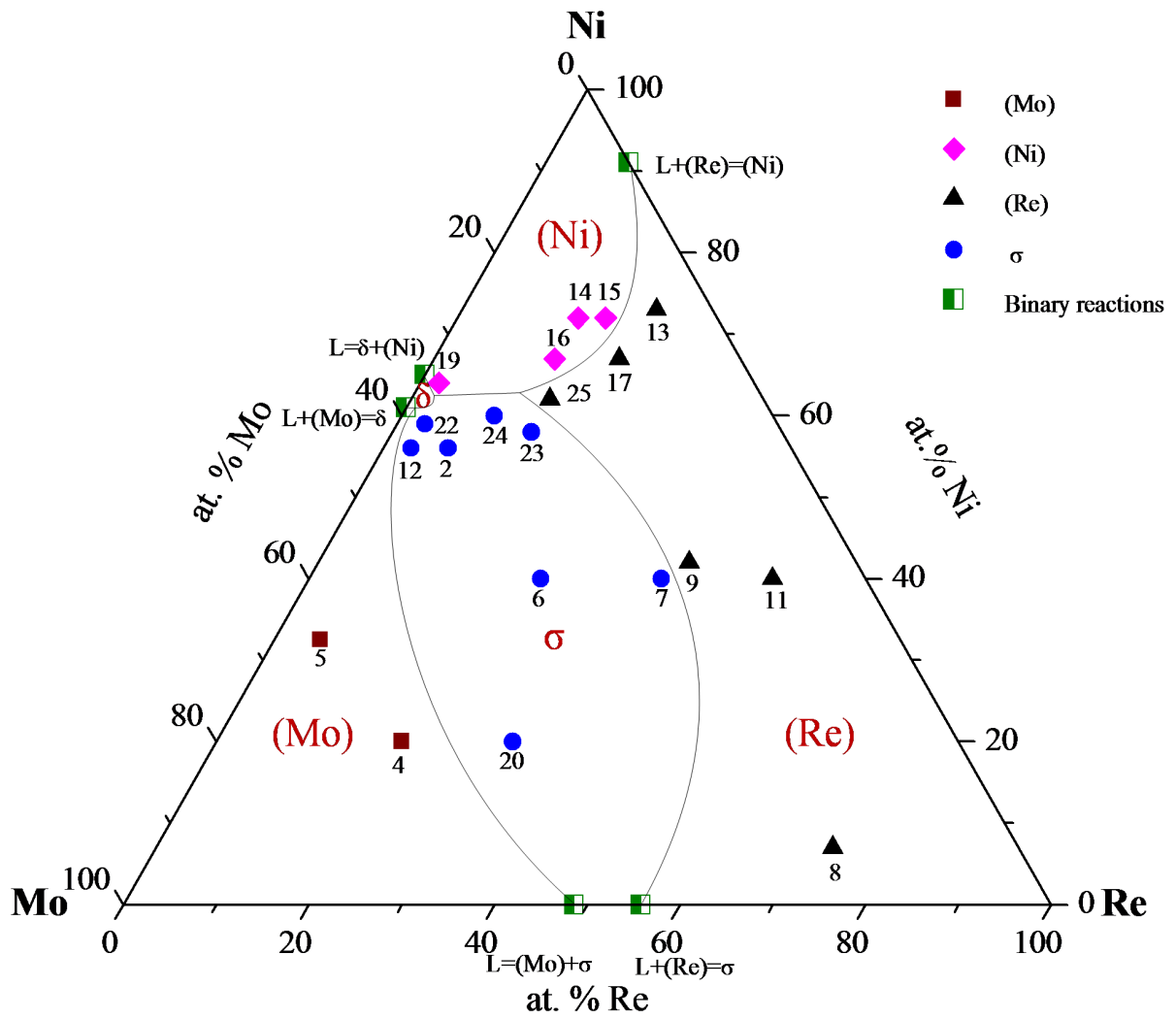


Figure 5: Partial liquidus projection of the Mo-Ni-Re system.

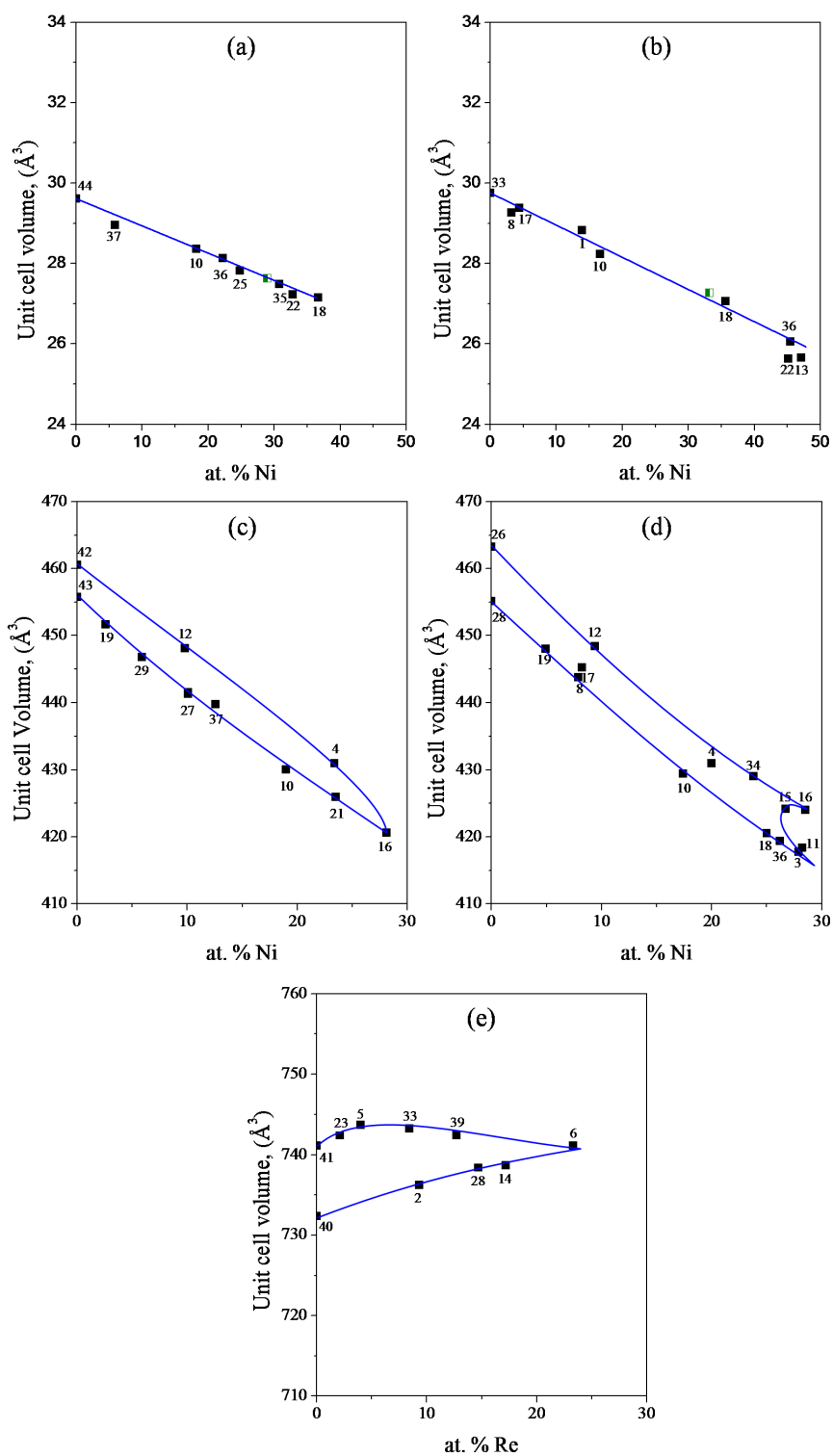


Figure 6: Variation of unit cell volume of (a) (Re) phase as a function of Ni content at 1200°C, (b) (Re) phase as a function of Ni content at 1600°C, (c)  $\sigma$  phase as a function of Ni content at 1200°C (d)  $\sigma$  phase as a function of Ni content at 1600°C (e)  $\delta$  phase as a function of Re content at 1200°C.

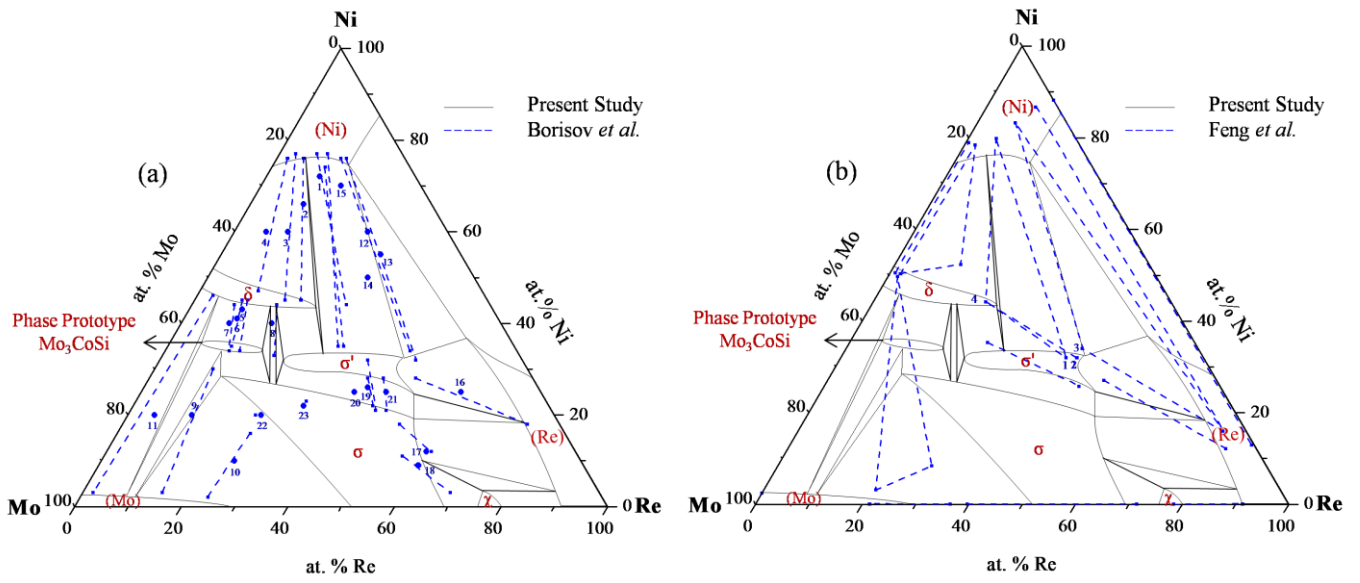


Figure 7: Comparison of the 1200°C isothermal section proposed during present study with the tie lines determined by (a) Borisov et al. [3], and (b) Feng et al. [5].



# **Chapter 6**

## **Structural Characterization of the Mo-Ni-Re $\sigma'$ Phase**



## Introduction

The phase equilibria investigation of the Mo-Ni-Re system presented in the chapter 5 showed presence of two ternary phases in the 1200°C isothermal section. The crystal structure identification of one of the ternary phases was achieved with the help of conventional powder XRD measurement whereas identification of the other ternary phase found in equilibrium with (Ni), (Re),  $\delta$  and  $\sigma$  phase was not possible due to poor quality of the X-ray diffraction pattern. The crystal structure identification of the second ternary phase is the subject of present chapter.

To improve quality of the X-ray diffraction pattern for identification of ternary phase crystal structure, different attempts were made which include

- Stress relieving annealing of the powder at 500°C and 800°C prior to the XRD measurement
- XRD measurement on the massive polished samples
- High temperature XRD at 100°C, 200°C, 300°C and 400°C
- XRD on the samples prepared with the help of spark plasma sintering

However, no improvement in the quality of the XRD pattern was observed. Finally, to identify crystal structure of the Mo-Ni-Re ternary phase, single crystal diffraction measurement was carried out. A comparison of the XRD and single crystal diffraction results revealed that this new ternary phase has a modulated  $\sigma$  structure. The ternary phase due to its similarity with  $\sigma$  phase was named as  $\sigma'$  phase. The details about crystal structure identification of the modulated  $\sigma$  phase are provided in the attached article submitted recently to the “*Intermetallics*” journal as a short communication.

Sample preparation, annealing, EPMA and XRD measurements for the present study were performed at our lab (ICMPE, CNRS, Thiais, France) whereas single crystal diffraction measurement was carried out at “*Laboratoire de Cristallographie, DPMC-MaNEP, Université de Genève, Switzerland*”, by coauthors of the attached article.



## **A modulated structure derived from the $\sigma$ phase in the Mo-Ni-Re system**

Khurram Yaqoob <sup>a</sup>, Laure Guénée <sup>b</sup>, Radovan Černý <sup>b</sup>, Jean-Marc Joubert <sup>a\*</sup>

<sup>a</sup>*Chimie Métallurgique des Terres Rares (CMTR), Institut de Chimie et des Matériaux Paris-Est (ICMPE), 2-8 rue Henri Dunant, 94320, Thiais Cedex, France*

<sup>b</sup>*Laboratoire de Cristallographie, DPMC-MaNEP, Université de Genève, 24, Quai Ernest-Ansermet CH-1211 Genève 4, Switzerland*

\* Corresponding Author. Tel.: +33 1 49 78 13 44; Fax: +33 1 49 78 12 03

E-mail address: jean-marc.joubert@icmpe.cnrs.fr

### **Abstract**

The crystal structure identification of a new Mo-Ni-Re phase was carried out. The chemical characterisation of the studied composition was performed with the help of electron probe microanalysis (EPMA) whereas X-ray diffraction (XRD) and single crystal diffraction techniques were used for structural characterisation. The characterisation results revealed that this new Mo-Ni-Re phase has a modulated  $\sigma$  phase structure.

### **Keywords**

A.  $\sigma$  phase, B. crystal chemistry of intermetallics, B. phase identification, F. diffraction (X-ray and single crystal), F. electron microprobe

## 1. Introduction

While investigating the isothermal section of the Mo-Ni-Re system at 1200°C by characterization of equilibrated arc melted alloys, a previously unknown ternary compound was found to exist in equilibrium with (Re), (Ni) and the ternary extensions of the Mo-Ni  $\delta$  and Mo-Re  $\sigma$  phase [1]. The present communication reports the attempts carried out to determine its crystal structure.

## 2. Experimental techniques

A sample of nominal composition  $\text{Mo}_{30.0}\text{Ni}_{30.5}\text{Re}_{39.5}$  was prepared by mixing and compacting pure metal powders (Mo: Sigma Aldrich, <150 $\mu\text{m}$ , 99.99 %; Ni: Alfa Aesar, <125 $\mu\text{m}$ , 99.996 %; Re: Alfa Aesar, <44 $\mu\text{m}$ , 99.99 %) followed by arc melting under an argon atmosphere. The as-cast sample was encapsulated in silica tube under an argon atmosphere and subsequently annealed at 1200°C for 1680 hours in a resistance furnace. After annealing, characterization of the sample was carried out with the help of electron probe microanalysis (EPMA; CAMECA SX100), X-ray diffraction (XRD; Bruker D8 Advance Diffractometer, Cu  $K\alpha$  radiation) and single crystal diffraction measurements (Supernova Agilent diffractometer with CCD camera, Mo  $K\alpha$  radiation). Single crystal measurements were performed on different crystals obtained after crushing the sample. Data collection and data processing (reciprocal lattice planes reconstruction and simulated powder pattern) were performed with CrysAlisPro software [2].

## 3. Results and discussion

The single phase character of the studied composition was confirmed by the EPMA and metallography. The composition of the studied phase as obtained from the EPMA was  $\text{Mo}_{29.2(2)}\text{Ni}_{31.8(5)}\text{Re}_{39.0(3)}$ . The powder XRD measurement of the studied composition presented few and rather broad peaks. As a result, it was not possible to resolve the crystal structure of this phase with the help of powder XRD pattern. At this step, we did not know whether the broad peaks were originating from cold working or from any kind of strains introduced while crushing the material. Therefore, in order to improve the quality of the powder XRD pattern several attempts were carried out, which include: stress relieving annealing of the powder at 500°C and 800°C for 24 hours, XRD measurement on massive sample after polishing and high temperature XRD measurement at 100°C, 200°C, 300°C and 400°C. In addition, another sample of the same composition was also prepared by the spark plasma sintering technique to avoid the solidification process of the material. However, no significant improvement in the

quality of the XRD pattern was observed. It could be indexed neither by powder recognition using the PDF database nor by *ab initio* indexing using TOPAS [3] and the problem of crystal structure identification remained unresolved.

The powder XRD pattern of this phase seems to be somewhat related to the  $\sigma$  phase (FeCr structure type,  $P4_2/mnm$ ) since many common features concerning the distribution and intensities of peaks have been observed. An attempt to refine its crystal structure with  $\sigma$  phase by using the FULLPROF [4] software is shown in the Figure 1. It is evident from the Figure 1 that the structures of the two phases are different. This should be understood not only in terms of peak broadening but also in terms of position and intensities of some peaks. Note in particular, presence of some additional peaks at  $26.0^\circ$ ,  $38.8^\circ$ ,  $44.6^\circ$  and  $45.6^\circ$ . In addition, our recent study of isothermal sections of the Mo-Ni-Re system [1] also revealed that this new phase can be present in equilibrium with  $\sigma$  phase and is therefore a distinct phase. It was also verified that this new phase is neither P nor R phase as was reported previously [5, 6].

Finally to investigate crystal structure of this new phase, single crystal diffraction experiment was carried out. The question whether selected crystal represented or not the bulk material was addressed by constructing a simulated powder pattern from the single crystal reciprocal lattice images. A comparison between the measured powder XRD pattern and powder pattern simulated from the single crystal reciprocal lattice images is shown in the Figure 2. The resemblance between the two patterns confirmed that the selected single crystal was a representative of the bulk material.

In the first attempt of indexing the single crystal diffraction data, a tetragonal cell ( $a=9.2851(19)$ ,  $c=4.912(3)$  Å) was found. Further structure solution and refinement yielded a crystal structure very close to that of the  $\sigma$  phase with structural parameters shown in Table 1. However, a closer look at the reconstructed reciprocal lattice images showed presence of some additional spots in the planes  $0kl$  and  $h1l$  (Figure 3), while the reciprocal lattice in the plane  $hk\bar{2}$  (Figure 4) corresponded well to the  $\sigma$  phase. The careful analysis of the spots showed that there is no obvious possibility to index the crystal structure with any superstructure of the  $\sigma$  phase (a modulation vector of  $0.2 c^*$  fail to index all the additional spots). In addition, as shown in the Figure 1, the powder pattern of this new phase could not be refined with the crystal structure of the  $\sigma$  phase. The differences between the  $\sigma$  phase and the new phase, shown in Figure 1, correspond indeed to the satellites generated by the

additional spots present in the Figure 3. Therefore, this new phase because of its resemblance with  $\sigma$  phase was named as the  $\sigma'$  phase.

#### 4. Conclusion

We have demonstrated that a new phase, not previously observed, is present in the Mo-Ni-Re system. A two phase domain between this new phase and  $\sigma$  phase was observed previously [1]. The characterisation results gathered during the present study revealed that this phase has a modulated structure characterized by incommensurate diffraction spots on reciprocal lattice images along the  $c^*$  axis of a tetragonal cell. The average structure of this phase is the  $\sigma$  phase, existing in the binary Mo-Re system [7] and extending far into the ternary composition field close to the homogeneity domain of  $\sigma'$  phase [1]. The single crystal diffraction data obtained during the present study was a representative of the whole bulk material as shown by the reconstruction of the powder pattern. However, due to the poor quality of the crystal (the  $\sigma'$  phase is not in equilibrium with the liquid) and in spite of numerous attempts to find a better one (after 1680 hours of annealing at 1200°C, it is difficult to improve the preparation of the sample), it was impossible to find the modulation vector and we could not go further with the structural characterization of this compound.

#### Acknowledgement

The authors would like to acknowledge the financial support from Agence Nationale de la Recherche (ANR) for funding the project (Armide 2010 BLAN 912 01).

#### References

- [1] Yaqoob K, Joubert J-M. To be published
- [2] Agilent (2012). CrysAlis PRO version 1.171.35.11. Agilent Technologies Y, England.
- [3] TOPAS, version 3, Bruker AXS, (1999).
- [4] Rodríguez-Carvajal J. XV Congress of Int. Union of Crystallography, Satellite Meeting on Powder Diffraction 1990;127
- [5] Kodentsov A A, Dunaev S F, Slyusarenko E M, Sokolovskaya E M, Priimak A N. Vestn. Mosk. Univ., Ser. 2., Khim. 1987;28:153-8
- [6] Slyusarenko E M, Peristyti A V, Kerimov E Y, Sofin M V, Skorbov D Y. J Alloys Comp 1998;264:180-9
- [7] Brewer L, Lamoreaux R H. At. Energy Rev. 1980;Spec. Issue 7:195-356

Table 1: Structural parameters of the average structure of  $\sigma'$  phase, s.g.  $P4_2nm$ ,  $a=9.2851(19)$ ,  
 $c=4.912(3)$  Å.

	$x$	$y$	$z$	$U_{iso}$ (Å <sup>2</sup> )	Occupancy
Ni2	0.0653(3)	0.2573(4)	0.0200(11)	0.0052(14)	0.45(2)
Mo2	0.0653(3)	0.2573(4)	0.9800(11)	0.0052(14)	0.55(2)
Re3	0.1315(3)	0.5358(3)	0.0200(11)	0.0059(11)	0.117(11)
Mo3	0.1315(3)	0.5358(3)	0.9800(11)	0.0059(11)	0.883(11)
Mo1	0.3162(2)	0.3162(2)	0.2536	0.0069(15)	1
Mo1a	0.3162(2)	0.3162(2)	0.7464	0.0020(15)	1
Mo4	0.3995(3)	0.6005(3)	-0.0114(12)	0.0035(11)	1
Mo5	0.0000	0.0000	-0.010(2)	0.005(3)	0.19(10)
Ni5	0.0000	0.0000	-0.010(2)	0.005(3)	0.81(10)

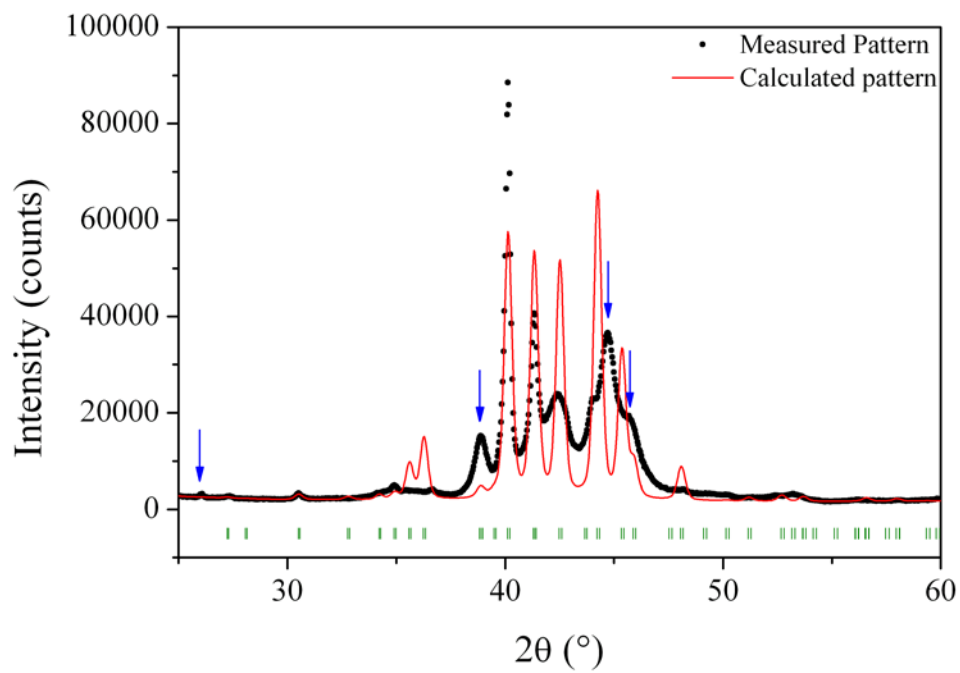
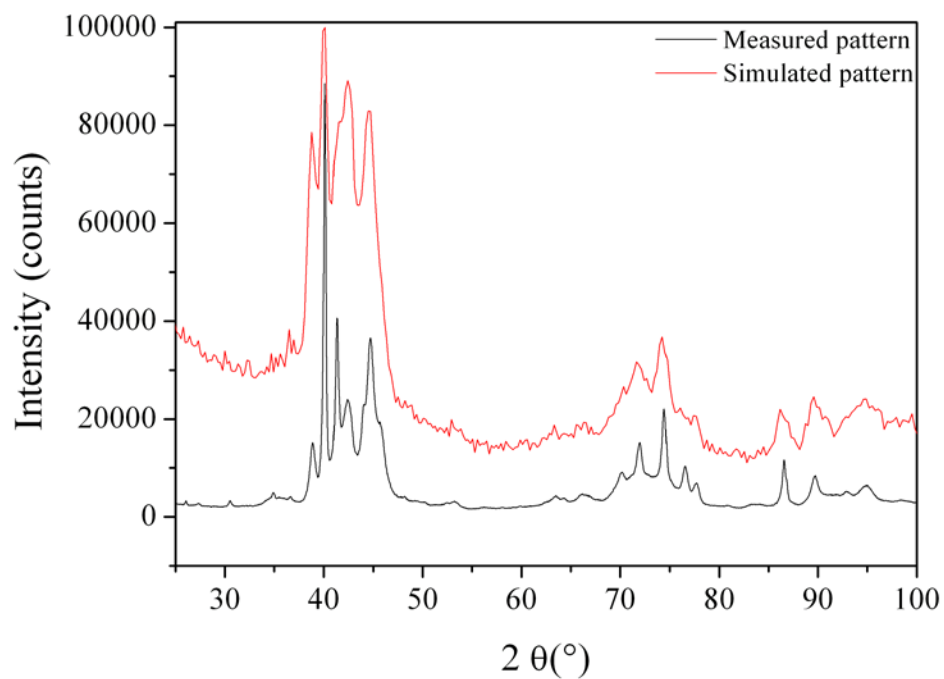


Figure 1: Rietveld refinement of the XRD pattern with  $\sigma$  phase.



*Figure 2: Comparison between the measured XRD powder pattern and that simulated from the single crystal XRD images.*

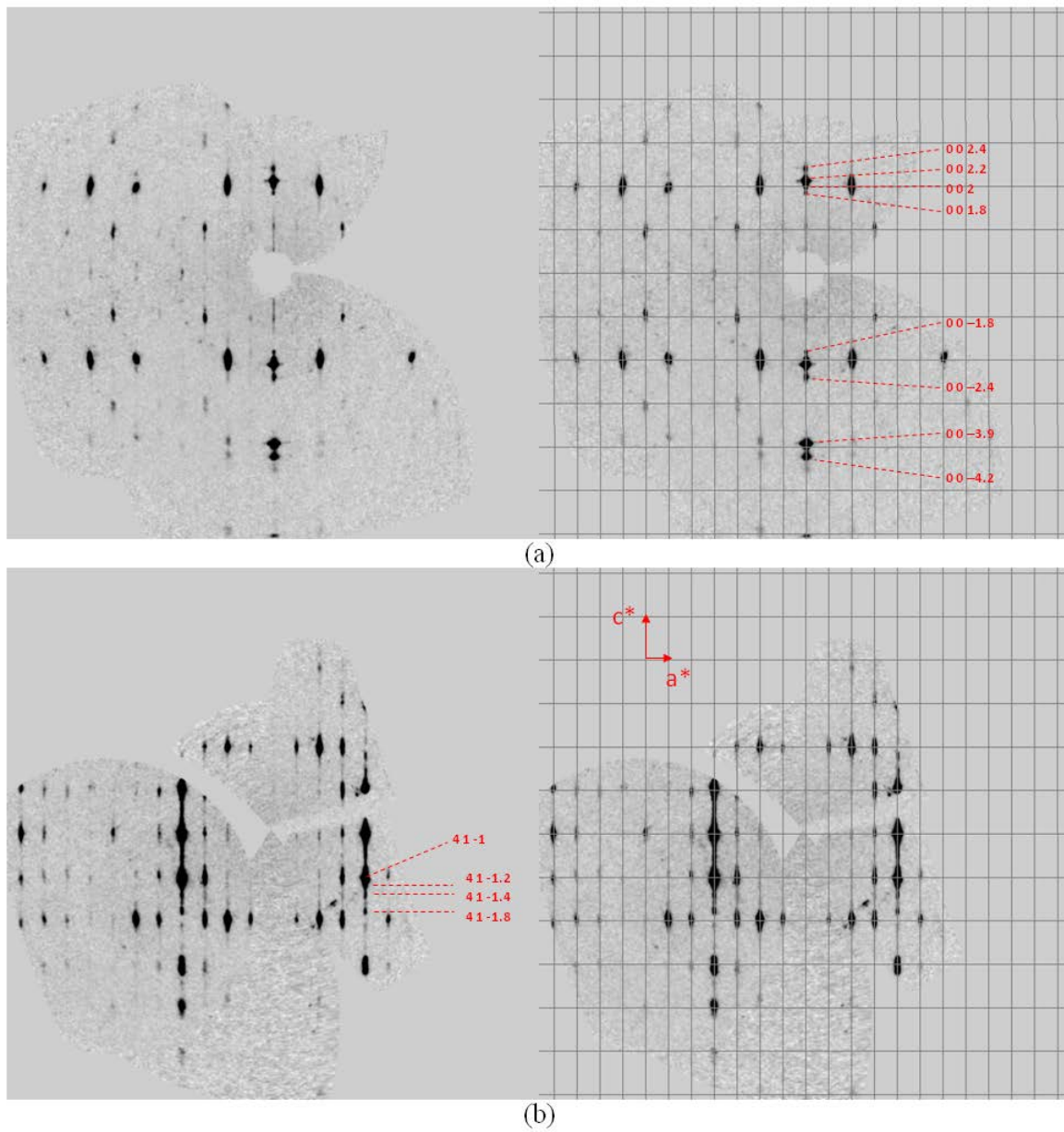
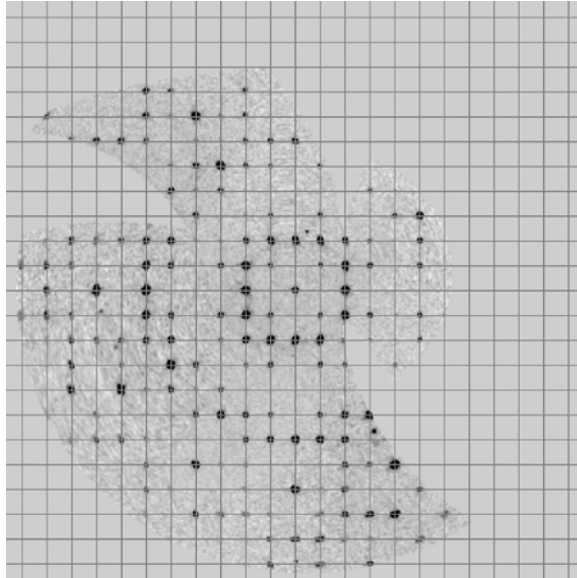


Figure 3: Reciprocal lattice of the  $\sigma'$  phase from the single crystal diffraction along two planes:  $0kl$  on (a) and  $hll$  on (b). Additional diffraction spots indexed approximately with a modulation vector  $0,0,0.2$  are indicated by dashed lines.



*Figure 4: Reciprocal lattice of the  $\sigma'$  phase from the single crystal diffraction along the plane  $hk\bar{2}$ .*



# **Chapter 7**

## **Structural Characterization of the Mo-Ni-Re $\sigma$ Phase**



## Introduction

The isothermal sections of the Mo-Ni-Re system presented in chapter 5 showed large extension of the Mo-Re  $\sigma$  phase in the ternary region. The  $\sigma$  phase pertains to the group of topologically closed packed (TCP) phases. In case of the binary TCP phases, it is well accepted that atoms with smaller atomic radii prefer occupying the crystallographic sites with low coordination number (CN) whereas larger atoms show preference for the high coordination number sites, though mixing occurs on all sites. However, the site occupancy trends in case of ternary TCP phases are not clear. During the present study, structural characterization of the Mo-Ni-Re  $\sigma$  phase was carried out by using experimental as well as calculation methods, with particular emphasis on the following:

- Determination of the site occupancies as a function of composition
- Comparison of the experimentally determined site occupancies with the ones obtained from DFT calculations

The experimental determination of site occupancies from a single diffraction dataset is not possible when three atoms occupy the same sites. This originates from the fact that, for example in the case of X-ray diffraction, only average electron density at each site may be obtained. When two elements share the site, site occupancies may be obtained, while if three elements are present another diffraction dataset for which the contrast between elements is different should be used. If neutron diffraction is used in addition to X-ray then both the average nuclear and electronic densities can be estimated and the two site occupancy unknowns can be obtained (the site occupancy of the third element is easily obtained if no vacancy is present). The usual procedure is then to use combined Rietveld refinement of both datasets for the data treatment which was done in the present work. In the case of Mo-Ni-Re system, this procedure works particularly well since the weaker scatterer for X-ray diffraction (Ni) is the strongest scatterer for neutron. Therefore during present study, experimental investigation of Mo-Ni-Re site occupancies was achieved by combined Rietveld refinement of X-ray and neutron diffraction data with good accuracy. Prior to the diffraction measurements, samples were annealed at 1600°C for 9 hours and their chemical homogeneity was confirmed with the help of EPMA measurements.

On the other hand, calculated site occupancies were obtained by using DFT calculations results of every ordered compound obtained by distribution of three atoms on the five sites of the crystal structure ( $3^5=243$ ). The DFT calculations of site occupancies for the present study

were carried out by Jean-Claude Crivello (our lab colleague and coauthor of the attached article). The calculated enthalpies of formation of  $\sigma$  phase are reported in the Annex 1 and will also be used during thermodynamic assessment of the Mo-Ni-Re system, discussed in chapter 8.

The site occupancy results of the Mo-Ni-Re  $\sigma$  phase obtained during the present study clearly showed preference of Ni and Mo atoms for sites with low and high coordination numbers (CN) respectively whereas Re having intermediate atomic size  $\{r_{\text{Ni}} (\sim 124 \text{ pm}) < r_{\text{Re}} (\sim 137 \text{ pm}) < r_{\text{Mo}} (\sim 139 \text{ pm})\}$  showed a dual behavior. The preference of Re depends on the composition proportion of the other two elements. The reversal of the Re site preference observed in the Mo-Ni-Re system originates from the fact that in metastable Ni-Re  $\sigma$  phase, it occupies the sites with higher CN due to its larger atomic radius while in Mo-Re it prefers occupying low CN sites. A comparison of the experimental and calculated site occupancies carried out during present study showed a very good agreement between the two data which confirmed the validity of both methods. The details about structural characterization of the Mo-Ni-Re  $\sigma$  phase summarized above are provided in the attached article published in the “*Inorganic chemistry [K. Yaqoob, J.-C. Crivello, J.-M. Joubert, Inorg. Chem., 51 (2012) 3071-3078]*” journal.

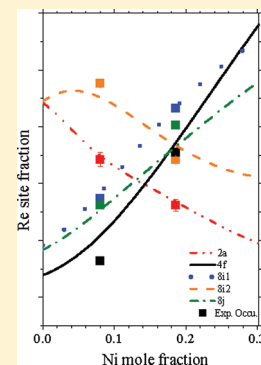
# Comparison of the Site Occupancies Determined by Combined Rietveld Refinement and Density Functional Theory Calculations: Example of the Ternary Mo–Ni–Re $\sigma$ Phase

Khurram Yaqoob, Jean-Claude Crivello, and Jean-Marc Joubert\*

Chimie Métallurgique des Terres Rares, Institut de Chimie et des Matériaux Paris-Est, CNRS, Université Paris-Est Créteil, 2–8 rue Henri Dunant, 94320 Thiais Cedex, France

## Supporting Information

**ABSTRACT:** The site occupancies of the Mo–Ni–Re  $\sigma$  phase have been studied as a function of the composition in the ternary homogeneity domain by both experimental measurements and calculations. Because of the possible simultaneous occupancy of three elements on the five sites of the crystal structure, the experimental determination of the site occupancies was achieved by using combined Rietveld refinement of X-ray and neutron diffraction data, whereas calculation of the site occupancies was carried out by using the density functional theory results of every ordered (i.e.,  $3^5 = 243$ ) configuration appearing in the ternary system. A comparison of the experimental and calculation results showed good agreement, which suggests that the topologically close-packed phases, such as the  $\sigma$  phase, could be described by the Bragg–Williams approximation (i.e., ignoring the short-range-order contributions). On the other hand, the atomic distribution on different crystallographic sites of the Mo–Ni–Re  $\sigma$  phase was found to be governed by the atomic sizes. Ni, having the smallest atomic size, showed a preference for low-coordination-number (CN) sites, whereas Mo, being the largest in atomic size, preferred occupying high-CN sites. However, the preference of Re, having intermediate atomic size, varied depending on the composition, and a clear reversal in the preference of Re as a function of the composition was evidenced in both the calculated and experimental site-occupancy results.



## INTRODUCTION

The determination of site-occupancy data for binary compounds by Rietveld refinement is a rather well-established procedure. However, obtaining the same types of data for sites in which three elements may be present simultaneously is a more challenging task. To solve this problem, one should use combined Rietveld refinement of different types of diffraction data in which the scattering contrast between the elements is different, for example, X-ray (XRD) and neutron diffraction (ND) data when the relative scattering in the two techniques is also adequate. On the other hand, density functional theory (DFT) calculations combined in the frame of the Bragg–Williams (BW) approximation may yield calculated site occupancies but are sometimes limited by the large number of configurations one has to calculate ( $3^s$  in the case of a ternary phase with  $s$  sites).

The crystal structure of the  $\sigma$  phase (structure type FeCr, space group  $P4_2/mnm$ , 30 atoms per unit cell, five inequivalent sites:  $2a$ ,  $4f$ ,  $8i_1$ ,  $8i_2$ ,  $8j$ ) is shown in Figure 1. It is a hard brittle intermetallic compound and has a deleterious effect on the mechanical properties of many technologically important systems. The main features of the  $\sigma$  phase include non-stoichiometry, which is accommodated by substitution on different sites of its crystal structure, and its ability to accept wide homogeneity ranges. Qualitatively, as usual for the Frank–Kasper phases, larger atoms show a preference for the sites with high coordination number (CN = 15 and 14), whereas smaller atoms occupy the sites with low coordination

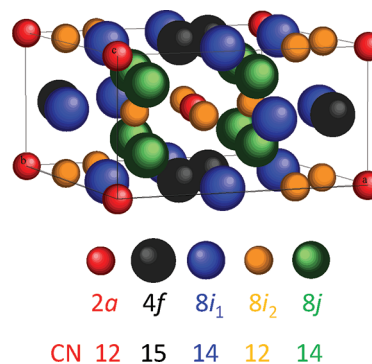


Figure 1. Crystal structure of the  $\sigma$  phase.

number (CN = 12).<sup>1</sup> However, determination of the actual exact site occupancies is important for thermodynamic modeling of the  $\sigma$  phase. Several investigations have been made for the quantitative determination of site occupancies in binary systems that have been summarized previously.<sup>1</sup> However, the work for determination of the site occupancies in ternary systems has recently been started and at present, according to our knowledge, it has been the subject of only one experimental<sup>2</sup> and two theoretical investigations.<sup>3,4</sup>

Received: November 21, 2011

Published: February 22, 2012

The study of the ternary  $\sigma$  phase is also of primary importance because it may offer the possibility studying a dual preference for the intermediate size atom depending on the composition proportion of the other two elements. This behavior was recently reported for Re in the Cr–Mo–Re  $\sigma$  phase.<sup>3</sup> One of the motivations for selecting the Mo–Ni–Re  $\sigma$  phase for the present study was to verify the dual preference of the intermediate size atom in the studied system. In addition, the large extension of the binary Mo–Re  $\sigma$  phase into the ternary region<sup>5</sup> permitting the study of the variation of the site occupancies as a function of the composition and the importance of the Mo–Ni–Re system for the development of Ni-based superalloys made it an interesting choice for the study of the ternary  $\sigma$  phase.

During the present investigation, a complete structural characterization of the ternary  $\sigma$  phase with particular emphasis on determination of the site occupancies as a function of the composition has been carried out. Unlike previous studies,<sup>2–4</sup> the site occupancies were determined by both experimental and theoretical methods. The reason for using two different approaches is to be able to compare their results and to check their validity. The experimental determination of site occupancies was accomplished by combined Rietveld analysis of XRD and ND data, whereas the theoretical approach for site-occupancy determination was based on the estimation of heats of formation by first-principles calculations. Finite temperature properties, such as site occupancies, were determined using the BW approximation, which ignores the short-range order within the defined sublattices. In spite of this simplification, the latter already gave excellent agreement with experimental studies on the  $\sigma$  phase of binary systems.<sup>6–8</sup> However, a comparison of the site occupancies determined experimentally with DFT predictions for the ternary  $\sigma$  phase has never been done before and is the subject of the present study.

## ■ EXPERIMENTAL DETAILS

**Sample Preparation and Annealing.** The materials used for the preparation of the ternary alloys consisted of pure metal powders (Mo, Sigma Aldrich, <150  $\mu\text{m}$ , 99.99%; Ni, Alfa Aesar, <125  $\mu\text{m}$ , 99.996%; Re, Alfa Aesar, <44  $\mu\text{m}$ , 99.99%). These powders were mixed in an agate mortar, compacted into pellets of different compositions, and subjected to arc melting under an argon atmosphere. The alloys were remelted five times and rotated upside down between each melting to achieve better homogenization. For the sake of reaching equilibrium, the alloys were annealed at 1873 K for 9 h. An annealing treatment of the samples was performed in a high-frequency induction furnace in a water-cooled copper crucible under an argon atmosphere, and the sample temperature was measured with the help of an optical pyrometer. After annealing, the samples were quenched by turning off

the induction heating and rapid cooling of the sample took place by the water-cooled copper crucible.

**Chemical Characterization.** Prior to the structural characterization, part of each sample was polished and investigated with the help of electron probe microanalysis (EPMA; CAMECA SX100) using pure elements as standards. Large numbers of data points were measured to determine the phase composition and homogeneity. The phase composition was averaged from the point measurements performed on that phase, and the calculated standard deviation of these measurements represented the phase homogeneity.

**Structural Characterization.** For structural characterization, XRD and ND measurements were performed by using a conventional powder method. All samples, by virtue of their high brittleness, were easily reduced to a fine powder (<63  $\mu\text{m}$ ).

Powder XRD measurements were performed at room temperature with Cu  $K\alpha$  radiation on a Bruker D8 Advance diffractometer (Bragg–Brentano geometry) equipped with a rear graphite monochromator. The X-ray data collection conditions include  $5^\circ \leq 2\theta \leq 120^\circ$ , a step size of  $0.04^\circ$ , and a total counting time of 63 h to obtain high data statistics.

ND measurements were performed at Laboratoire Léon Brillouin (LLB; common laboratory CEA-CNRS), Saclay, France, using a 3T2 instrument. The sample in powder form (7.5 g, <63  $\mu\text{m}$ ) was introduced into a sample holder consisting of a vanadium cylinder (diameter 6 mm) supported on a cadmium-protected aluminum cylinder. The measurement was performed at room temperature with the Debye–Scherrer geometry in the presence of five detectors. For each pattern, data were recorded in the angular range  $5^\circ \leq 2\theta \leq 121^\circ$  with a step size of  $0.05^\circ$  by using neutrons of wavelength 1.2253 Å.

To determine site occupancies, the combined Rietveld analysis of XRD and ND data was conducted using the *FULLPROF*<sup>9</sup> program in the multipattern mode. For refinement of the X-ray data, the background was interpolated between the peaks, whereas for the neutron data refinement, a polynomial background was used. The pseudo-Voigt function was used to define the peak shape in both XRD and ND patterns. Because Re presents the nonnegligible absorption coefficient for neutrons, an absorption correction was also applied by calculating the values of the absorption coefficient ( $\mu_r$ ) for each composition. To calculate the absorption coefficient, the density of noncompacted powders was estimated to be 40% of the density of the material. The values of absorption coefficients ( $\mu_r$ ) calculated for each composition are presented in Table 1.

## ■ COMPUTATIONAL DETAILS AND METHODOLOGY

The first-principles calculations were performed by using DFT, as implemented in the Vienna ab initio simulation package.<sup>10,11</sup> Previous calculations on binary Mo–Re<sup>8</sup> and Ni–Re  $\sigma$  phases<sup>12</sup> were done with the PW91 exchange–correlation energy functional,<sup>13</sup> but for the present work, every ordered Mo–Ni–Re  $\sigma$  ternary configuration i.e.,  $3^5 = 243$  configurations, was calculated with the PBE functional.<sup>14</sup> An energy cutoff of 400 eV was used for the plane-wave basis

**Table 1.** Rietveld Refinement Details of Experimentally Studied Compositions

	N <sub>1</sub>	N <sub>2</sub>	N <sub>3</sub>
nominal composition	Mo <sub>0.486</sub> Ni <sub>0.08</sub> Re <sub>0.426</sub>	Mo <sub>0.259</sub> Ni <sub>0.201</sub> Re <sub>0.540</sub>	Mo <sub>0.533</sub> Ni <sub>0.201</sub> Re <sub>0.266</sub>
EPMA composition	Mo <sub>0.49(2)</sub> Ni <sub>0.08(1)</sub> Re <sub>0.43(2)</sub>	Mo <sub>0.256(2)</sub> Ni <sub>0.186(6)</sub> Re <sub>0.558(6)</sub>	Mo <sub>0.52(1)</sub> Ni <sub>0.19(1)</sub> Re <sub>0.29(2)</sub>
space group	<i>P4<sub>2</sub>/mnm</i>	<i>P4<sub>2</sub>/mnm</i>	<i>P4<sub>2</sub>/mnm</i>
<i>a</i> (Å)	9.5262(2)	9.3392(2)	9.4018(4)
<i>c</i> (Å)	4.9605(1)	4.9072(1)	4.9134(2)
$\mu_r$ (ND)	0.2925	0.3825	0.2404
$R_B$ (XRD), $R_B$ (ND)	7.19, 3.32	4.95, 3.41	4.50, 2.76
profile parameters	4 for each pattern	4 for each pattern	4 for each pattern
intensity parameters	17	17	17

set, and a dense grid of  $k$  points in the irreducible wedge of the Brillouin zone ( $8 \times 8 \times 15$   $k$ -points meshing) was used with the sampling generated by the Monkhorst–Pack procedure.<sup>15</sup> For each of the 243 ordered configurations, successive relaxations (internal atomic coordinates and the lattice parameters, i.e.,  $a$  and  $c$ ) were done to fully relax the tetragonal cell structure. The final calculation was performed using the tetrahedron method with Blöchl corrections.<sup>16</sup> The self-consistent total energy calculations converged to less than 0.1 meV. From calculation of the pure elements in their stable element reference (SER) state, the heat of formation  $\Delta H_{ijklm}^{\text{for},\sigma}$  at 0 K of every ( $i, j, k, l, m = \text{Mo, Ni, Re}$ )  $\sigma$  configuration was obtained by the total energy differences written below. The fcc-Ni has been calculated in spin-polarized states.

$$\Delta H_{ijklm}^{\text{for},\sigma} = E_{ijklm}^{\sigma} - c_{\text{Mo}}E_{\text{Mo}}^{\text{bcc}} - c_{\text{Ni}}E_{\text{Ni}}^{\text{fcc,mag}} - c_{\text{Re}}E_{\text{Re}}^{\text{hcp}}$$

$c_{\text{Mo}}$ ,  $c_{\text{Ni}}$ , and  $c_{\text{Re}}$  are the mole fractions of the Mo, Ni, and Re elements, respectively.

On the basis of the compound energy formalism,<sup>17–19</sup> the five-sublattice model  $(i)_2(j)_4(k)_8(l)_8(m)_8$  is used, in conformity with the site multiplicities of the  $\sigma$ -crystal structure. The Gibbs energy  $G^{\sigma,\text{BW}}(\{x_i\}, T)$  is defined at a finite temperature  $T$  by using the BW approximation, i.e., considering only the configurational entropy and neglecting the entropy from

atomic correlations and excess interaction parameters within the sublattices:

$$G^{\sigma,\text{BW}}(\{x_i\}, T) = \sum_{i,j,k,l,m=\text{Mo,Ni,Re}} [y_i^{(2a)} y_j^{(4f)} y_k^{(8i_1)} y_l^{(8i_2)} y_m^{(8j)}] \times \Delta H_{ijklm}^{\text{for},\sigma} + RT \sum_s a^{(s)} \sum_{i=\text{Mo,Ni,Re}} y_i^{(s)} \ln(y_i^{(s)})$$

$R$  is the gas constant,  $a^{(s)}$  the multiplicity, and  $y_i^{(s)}$  the site fraction of element  $i$  on site  $s$ .

More details about the methodology can be found in previous papers.<sup>3,8</sup>

## EXPERIMENTAL RESULTS

The homogeneity domain of the  $\sigma$  phase in the 1873 K isothermal section of the Mo–Ni–Re system extends from the binary Mo–Re system, in which the homogeneity domain is  $52 \pm 2$ – $70 \pm 2$  atom % Re,<sup>20</sup> deeply into the ternary region. The exact location of the homogeneity domain of the Mo–Ni–Re  $\sigma$  phase will be published with complete determination of the phase diagram<sup>5</sup> but is shown only as indicative in Figure 2. To study the atomic distribution of the constituent elements, i.e., Mo, Ni, and Re, at the different crystallographic sites as a function of the composition, three compositions (named as  $N_1$ ,  $N_2$ , and  $N_3$ ) situated at the borders of the homogeneity domain of the  $\sigma$  phase and along the two lines  $\text{Mo}_2\text{Re}$ – $\text{Re}_2\text{Ni}$  and  $\text{MoRe}_2$ – $\text{Mo}_2\text{Ni}$  were prepared and characterized. As expected, EPMA and conventional powder XRD results confirmed the single-phase character of each sample. The small difference between the measured and nominal compositions reported in Table 1 was attributed to the evaporation of Ni during melting

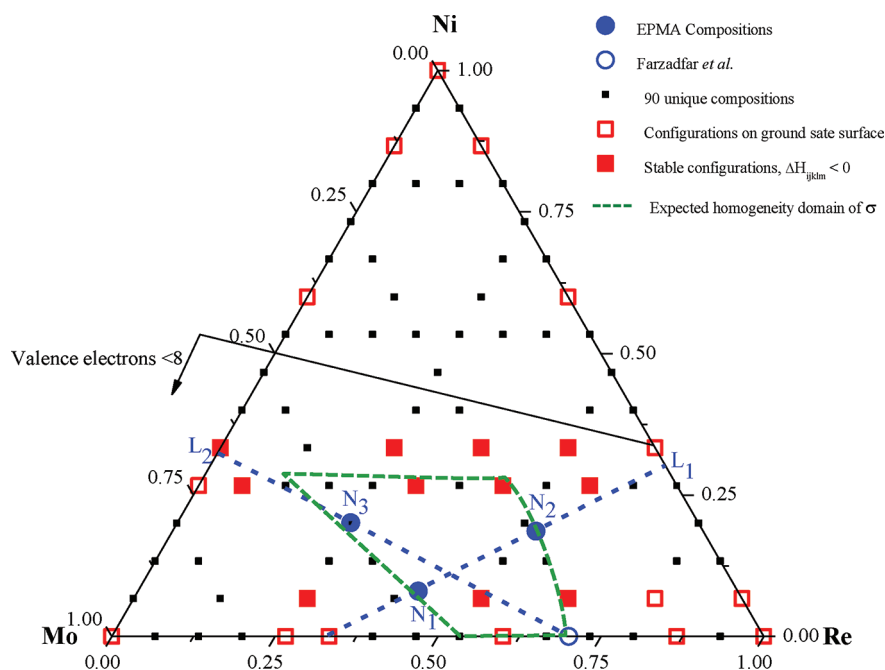


**Figure 2.** Plot of the compositions studied experimentally and by DFT calculations. The area surrounded by green dashed lines represents the indicative homogeneity domain of the Mo–Ni–Re  $\sigma$  phase at 1873 K. The positions of the experimentally studied compositions, named as  $N_1$ ,  $N_2$ , and  $N_3$ , are symbolized by blue filled circles, whereas the empty blue circle represents the composition studied previously.<sup>21</sup> The two blue dashed lines, i.e.,  $L_1$  and  $L_2$ , correspond to sections studied by DFT calculations. The 90 unique compositions generated during DFT calculations by the ordered distribution of three elements on the five sites of the  $\sigma$  phase are indicated by black squares. Among the 90 unique compositions, 26 compositions are located on the ground-state surface and are symbolized by red squares, whereas among 26 compositions, 11 compositions present negative heats of formation and are indicated by red filled squares.

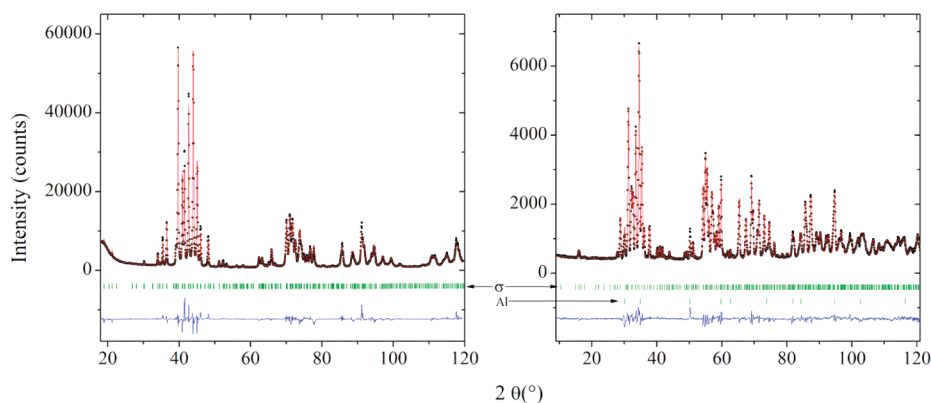


**Figure 3.** Combined Rietveld refinement of the XRD (left) and ND (right) patterns of the sample composition  $N_2$ . The experimental curves are symbolized as black dots, calculated ones as red lines, Bragg positions as vertical green marks, and the difference between the experimental and calculated curves is symbolized as a blue line situated under the vertical green marks.

because of its high vapor pressure at the extremely high melting temperatures of the alloys (the binary Mo–Re  $\sigma$  phase melts at 2918 K<sup>20</sup>). The positions of the measured compositions in the ternary section are represented by blue filled circles in Figure 2. In addition to the prepared compositions, the site-occupancy data of the binary Mo–Re  $\sigma$  phase of composition  $Mo_{0.299}Re_{0.701}$ , represented by the empty blue circle in Figure 2, were taken from the literature.<sup>21</sup>

The separate XRD refinement of the studied compositions yielded strongly negative values of displacement parameters ( $B$ ), indicating the presence of microabsorption phenomena in XRD measurements, because both are strongly correlated. Refinement of displacement parameters along with the microabsorption correction using one pattern refinement was not possible. However, during the combined refinement of the XRD and ND patterns, in which the value of  $B$  was also constrained by the ND pattern, microabsorption correction was applied. As a result, reasonable values of the displacement parameters were obtained. For the studied compositions, the site fractions of constituent elements at the five crystallographic sites of the  $\sigma$  phase were determined by combined Rietveld refinement of XRD and ND data. During the refinement, each pattern was assigned equal weights. The distribution of the elements was constrained in such a way that it reproduces the measured composition and full occupancy of all atom sites. As a result, there were two unknown occupancy factors per site on four sites, i.e., eight variables. The occupancy of the elements on the fifth site was constrained by the occupancies on the other four sites. The method for introducing such constraints in Rietveld refinement programs has been previously described.<sup>22–24</sup> For each composition, a total of 17 intensity parameters, including 7 coordinates, 2 displacement parameters (one for the sites with CN = 12 and the other for the higher CN sites), and 8 occupancy factors, were refined. The values of  $R_B$  considered as a measure of the quality of fit, along with other refinement details, are given in Table 1.

As an example, the diffraction patterns in the form of Rietveld plots of the sample composition  $N_2$  are presented in Figure 3.

The Rietveld analysis of all ND patterns disclosed the presence of several peaks not present in any of the XRD patterns. Investigation of these additional peaks revealed that these peaks correspond to the aluminum cylinder intercepting the neutron beam accidentally. Normally, the aluminum cylinder supporting the vanadium sample holder is very well protected

by cadmium, which does not appear to be the case in the present measurements, and as a result, we find peaks corresponding to aluminum in the ND patterns. These additional peaks were also taken into account during refinement of the ND patterns.

For the studied compositions, occupancy factors of the constituent elements at each site of the Mo–Ni–Re  $\sigma$  phase are presented in Table 2. The negative occupancy factors were

**Table 2.** Occupancy Factors for the Compositions  $N_1$ ,  $N_2$ , and  $N_3$

site	CN	element	occupancy (atom)		
			$N_1$ ( $Mo_{0.49(2)}Ni_{0.08(1)}Re_{0.43(2)}$ )	$N_2$ ( $Mo_{0.256(2)}Ni_{0.186(6)}Re_{0.558(6)}$ )	$N_3$ ( $Mo_{0.52(1)}Ni_{0.19(1)}Re_{0.29(2)}$ )
2a	12	Mo	0.18(9)	−0.15(10)	0.07(9)
		Ni	0.85	1.50	1.29
		Re	0.97(5)	0.65(4)	0.64(4)
4f	15	Mo	3.63(12)	1.82(13)	3.49 (12)
		Ni	−0.14	0.15	−0.12
		Re	0.51(6)	2.03(6)	0.63(6)
8i <sub>1</sub>	14	Mo	4.88(20)	2.86(19)	5.41(19)
		Ni	0.33	−0.19	0.08
		Re	2.79(10)	5.33(9)	2.51(8)
8i <sub>2</sub>	12	Mo	0.36(17)	0.04(17)	0.75(15)
		Ni	1.62	4.09	4.33
		Re	6.02(9)	3.87(9)	2.92(8)
8j	14	Mo	5.65	3.12	5.87
		Ni	−0.25	0.03	0.13
		Re	2.60	4.85	2.00

obtained at some sites that for comparison purposes were not constrained to be positive.

**DFT Calculation Results.** First of all, the results on the three binary systems are presented. In comparison with calculations of the Mo–Re<sup>8</sup> and Ni–Re<sup>12</sup> systems made with the PW91 functional, results obtained in PBE present very similar  $\Delta H_{ijklm}^{for,\sigma}$ . Differences are less than 1 kJ/mol of atoms and lead to insignificant modifications on the finite temperature properties, such as the site occupancies (found to be similar in both Mo–Re and Ni–Re systems). A more careful analysis on the relaxed crystal parameters shows that calculations with PBE are in slightly better agreement with the experimental results and confirms the choice of using this functional for the present

**Table 3. Energetic and Crystallographic Property Comparison between Experiments and Calculations with Two Different Functionals in the  $\text{Mo}_x\text{Re}_{1-x}$  System**

	$x \sim 0.33$			$x \sim 0.4$			ref
	$\Delta H$ (kJ/mol)	$V$ ( $\text{\AA}^3$ )	$c/a$	$\Delta H$ (kJ/mol)	$V$ ( $\text{\AA}^3$ )	$c/a$	
Exp		455.35	0.520		457.81	0.519	21
PW91	+5.29	460.76	0.513	+1.07	463.05	0.511	8
PBE	+5.42	459.41	0.513	+1.14	461.67	0.511	present work

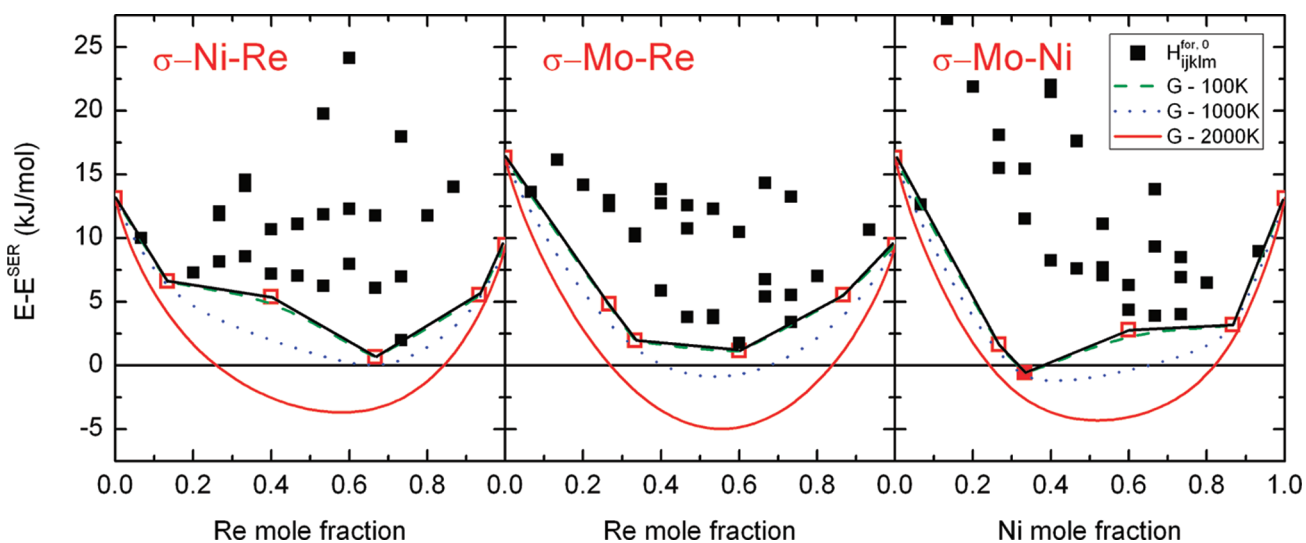


**Figure 4.** Calculated heats of formation  $\Delta H_{ijklm}^{for,\sigma}$  of the 32 configurations in the three binary Ni–Re, Mo–Re, and Mo–Ni  $\sigma$  phases with respect to SER states. The Gibbs energy lines obtained in the BW approximation are displayed at 100, 1000 and 2000 K.

work. As an example, a comparison is made for two compositions in the Mo–Re system and is given in Table 3.

The heat of formation calculation of the  $2^5 = 32$  configurations and the  $G^{\sigma,BW}(\{x_i\}, T)$  curves computed at  $T = 100$ , 1000, and 2000 K for the three binary systems are displayed in Figure 4.

As expected, the scatter of  $\Delta H_{ijklm}^{for,\sigma}$  points is more important in the Mo–Ni system because of the larger atomic radii difference between the Mo and Ni atoms, in comparison with Re–Ni and Mo–Re. All binary  $\Delta H_{ijklm}^{for,\sigma}$  are positive, except the  $(i,j,k,l,m) = \text{NiMoMoNiMo}$  configuration. The latter corresponds to the ideal  $\text{Mo}_2\text{Ni}$  composition with occupation of the low CN sites by Ni and high CN sites by Mo. For each system, the ground-state line is drawn. It is defined as the line joining the six most stable configurations obtained by a single atom permutation on every five sites. For the Mo–Re system, this line is convex and the following sequence is observed:  $\text{MoMoMoMoMo} \rightarrow \text{MoMoMoReMo} \rightarrow \text{ReMoMoReMo} \rightarrow \text{ReMoReReMo} \rightarrow \text{ReMoReReRe} \rightarrow \text{ReReReReRe}$ . On the contrary, a change of concavity is observed in both Mo–Ni and Ni–Re systems, yielding a miscibility gap. Only above  $T = 1000$  K, every Gibbs energy  $G^{\sigma,BW}(\{x_i\}, T)$  curve is convex and a single phase is stable in the whole concentration range.

From the  $3^5 = 243$  configurations generated in the ternary system, 90 are unique compositions, and among them, 26 configurations are on the ground-state surface. They are represented in Figure 2 by squares. In comparison with Cr–Mo–Re, it is interesting to note that the  $\sigma$  phase is more stable in the Mo–Ni–Re system with 11 negative  $\Delta H_{ijklm}^{for,\sigma}$  among the 26 ground-state configurations (versus the nonnegative formation enthalpy configuration and 19 on the ground-state surface for Cr–Mo–Re). These 11 configurations with negative  $\Delta H_{ijklm}^{for,\sigma}$  present a Ni composition of less than 33%. The most

stable configuration is with NiMoReNiMo ( $\text{Mo}_{0.40}\text{Ni}_{0.33}\text{Re}_{0.27}$ ). Because  $\text{Mo}_2\text{Ni}$  is the only stable binary composition with  $\Delta H_{ijklm}^{for,\sigma} < 0$ , it is expected that the  $\sigma$  phase, which exists experimentally in the binary Mo–Re system, would extend in the ternary region toward the  $\text{Mo}_2\text{Ni}$  direction. This assumption has been verified experimentally.<sup>5</sup>

In addition, as shown in Figure 2, both the suggested experimental phase field of  $\sigma$  and the calculated stable configurations are situated below the solid black line representing a valence electron concentration of 8. This result is in agreement with the empirical rule stating that the  $\sigma$  phase forms for an average electron concentration range between 5.5 and 8.<sup>1,25</sup>

The  $G^{\sigma,BW}(\{x_i\}, T)$  surface computed at  $T = 100$  K is represented in Figure 5. The change of concavity reveals the presence of miscibility gaps at this low temperature. The corresponding isocontour plot of this surface is also represented for the same temperature  $T = 100$  K and also for  $T = 1000$  K. At  $T = 1000$  K, the  $G^{\sigma,BW}(\{x_i\}, T)$  surface presents a single minimum, and accurate calculation shows that the miscibility gap disappears at  $T = 984$  K.

## DISCUSSION

Because the substitutional disorder in the ternary  $\sigma$  phase involves three elements, accurate experimental determination of the site occupancies required at least two diffraction data sets with large scattering contrast among the constituent elements in each data set and different scattering contrast among the elements in two data sets. The ternary system under study is well chosen because it obeys both conditions. The elements constituting the studied system give large scattering contrast in both XRD and ND techniques, as indicated by their atomic

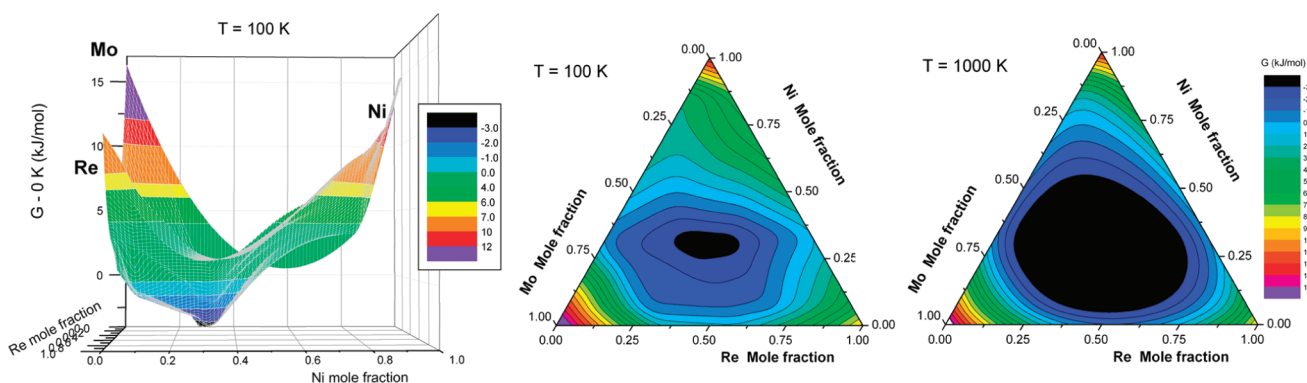


**Figure 5.** Gibbs energy surface of the Mo–Ni–Re  $\sigma$  phase obtained in the BW approximation displayed at 100 K. Corresponding isocontour plots at 100 and 1000 K are also presented.

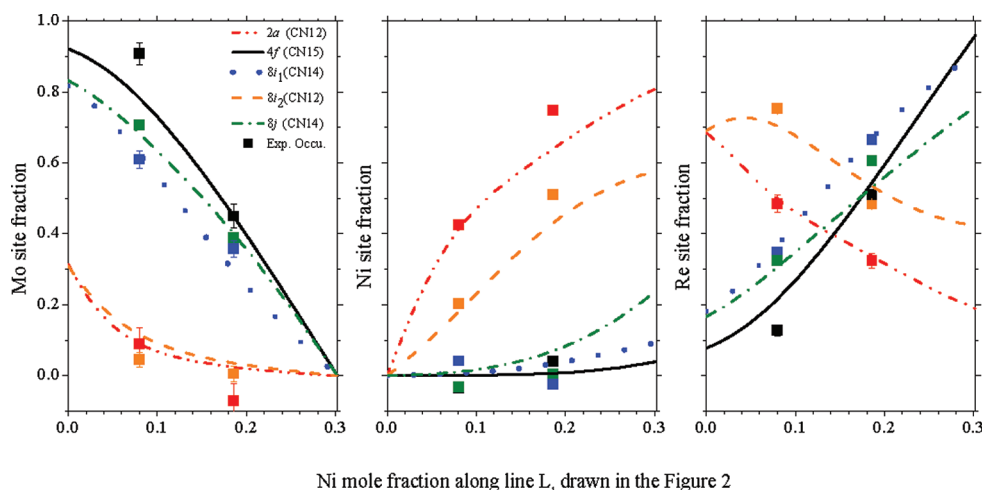


**Figure 6.** Comparison of the experimental and calculated site occupancies of the Mo–Ni–Re  $\sigma$  phase at 1873 K along the line  $L_1$  of Figure 2. The squares and lines correspond to the experimental ( $N_1$  and  $N_2$ ) and calculated site occupancies, respectively.

numbers ( $Z_{\text{Mo}} = 42$ ,  $Z_{\text{Ni}} = 28$ , and  $Z_{\text{Re}} = 75$ ) and Fermi lengths ( $b_{\text{Mo}} = 6.7$ ,  $b_{\text{Ni}} = 10.3$ , and  $b_{\text{Re}} = 9.2$  fm). On the other hand, they also present different scattering contrast in the two considered diffraction techniques; i.e., Ni is the weakest scattering element in the XRD experiment and the strongest in the ND experiment. The fulfillment of both conditions by the studied system made possible the accurate experimental determination of site occupancies.

To study the atomic distribution on different sites as a function of the composition, site occupancies were determined along the two lines named as  $L_1$  and  $L_2$  drawn in Figure 2. The line  $L_1$  has been chosen to pass from the ideal stoichiometry  $\text{Mo}_2\text{Re}$  to  $\text{ReNi}_2$ , whereas line  $L_2$  passes from close to the  $\text{MoRe}_2$  composition, i.e.,  $\text{Mo}_{0.299}\text{Re}_{0.701}$ ,<sup>21</sup> toward the calculated stable  $\text{Mo}_2\text{Ni}$  composition.

The site occupancies determined along the line  $L_1$  as a function of the Ni content are presented in Figure 6. As shown in the plot, the Mo and Ni site fractions in the Mo–Ni–Re  $\sigma$  phase along the line  $L_1$  show similar variations (either increase or decrease). Ni, whose atomic size is significantly smaller than Mo and Re, substitutes them mainly on the sites with low CN, i.e.,  $2a$  and  $8i_2$  (CN = 12). On the other hand, Mo atoms, being the largest in size, tend to occupy high-CN sites, i.e.,  $4f$ ,  $8i_1$ , and  $8j$  (CN = 15, 14, and 14), where they can find more space. Contrary to the behavior of Mo and Ni, the Re atoms, being intermediate in size [ $r_{\text{Ni}} (\sim 135 \text{ pm}) < r_{\text{Re}} (\sim 137 \text{ pm}) < r_{\text{Mo}} (\sim 139 \text{ pm})$ ], show dual preference depending on the

composition proportion of the other two elements. As can be seen from Figure 6, Re prefers occupying the low-CN sites at less Ni content. However, with increasing Ni content along the line  $L_1$ , a reversal in the behavior of Re was observed, and it exhibits a preference for occupying the sites with higher CN. This reversal in the preference of Re from the sites of low CN to the sites of high CN is evident not only from the calculated but also from the experimentally determined site occupancies. Therefore, it can be concluded that intermediate-size elements in any ternary  $\sigma$  phase depending on the composition proportion of the other two elements may have a dual preference. The same behavior of intermediate-size elements has also been recently reported in the Cr–Mo–Re  $\sigma$  phase.<sup>3</sup> However, unlike the present study, the dual preference of Re in the Cr–Mo–Re  $\sigma$  phase was evidenced only by DFT calculations, and no experimental investigation was carried out because of the unfavorable scattering factors of the constituent elements.

The plots of the experimental and calculated site occupancies along the line  $L_2$  as a function of the Ni content are presented in Figure 7. The Mo, Ni, and Re site fractions demonstrate either an increase or a decrease with increasing Ni content along the line  $L_2$ . The site occupancy results indicated that Mo, being the largest in atomic size, showed a preference for the high-CN sites, whereas Ni and Re atoms, being smaller in atomic size, preferred occupying the sites with low CN. In addition, the calculated site occupancies determined along the

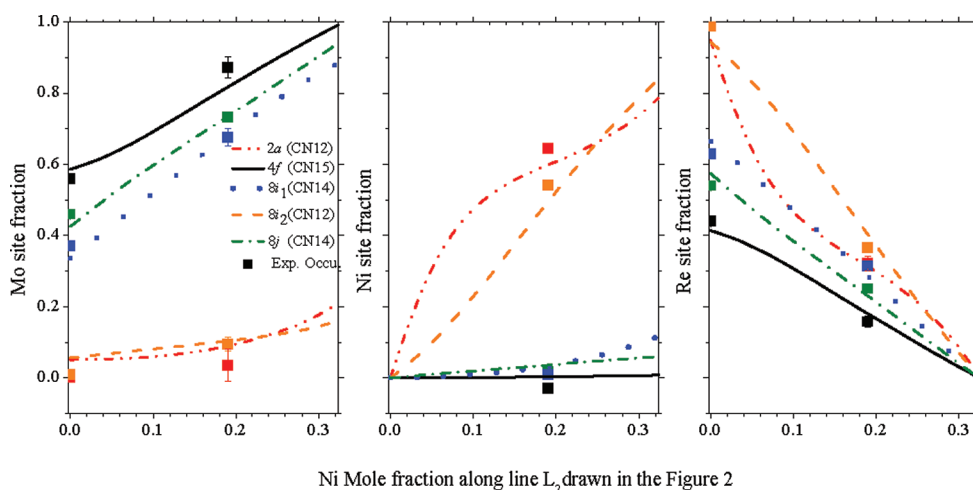


**Figure 7.** Comparison of the experimental and calculated site occupancies of the Mo–Ni–Re  $\sigma$  phase at 1873 K along the line  $L_2$  of Figure 2. The squares correspond to the experimental ( $N_3$  and experimental data from the literature<sup>21</sup>) site occupancies and the lines to the calculated site occupancies.

line  $L_2$  showed progressive advancement toward  $\text{Mo}_2\text{Ni}$  composition, as expected from the calculated stability of this particular binary composition, which was discussed earlier. This tendency of the  $\sigma$  phase toward ordering is also evident from the experimentally determined site occupancies of  $\sigma$  of composition  $N_3$  and of the  $\sigma$  phase of composition  $\text{Mo}_{0.701}\text{Re}_{0.299}$ .

In the Mo–Ni–Re  $\sigma$  phase, contrary to the Cr–Mo–Re  $\sigma$  phase in which the stability domain was parallel to the axis defined by the elements with the largest and smallest atomic radii, the stability line ( $L_2$ ) is orthogonal to the line in which Re reversal occurs ( $L_1$ ).

The comparison of the experimental and calculated site occupancies determined during the present investigation is presented in Figures 6 and 7. As can be seen from Figures 6 and 7, an appreciably good agreement was found between the two data, which confirms the validity of both the experimental and calculation techniques. In addition, because calculation of the site occupancies was carried out by using BW approximation, which ignores the short-range-order contributions, therefore, it can be concluded that calculation of the site occupancies even by using BW approximation can produce accurate results for topologically closed-packed phases such as the  $\sigma$  phase. Moreover, the site-occupancy data determined during the present investigation because of its reliability not only can be incorporated as an experimental input for the CALPHAD modeling of the Mo–Ni–Re system but also can be used in the selection of a suitable model for thermodynamic modeling of the  $\sigma$  phase by CALPHAD method. The site occupancies of the ternary  $\sigma$  phase determined during the present investigation, as shown in Figures 6 and 7, can be divided into two groups: one group corresponds to the sites with high CN and the other group corresponds to low-CN sites; which points to the fact that the  $\sigma$  phase can be well described even by using a 2-sublattice model, as was also suggested previously,<sup>1</sup> at least for the present system.

## CONCLUSIONS

In the present work, we have shown that it was possible to obtain accurate site occupancies for complex ternary intermetallic compounds not only experimentally by using the combined refinement of XRD and ND data but also by calculating, in the frame of the DFT, the complete set of

ordered configurations of the phase in the complete ternary range of composition. The agreement between these two kinds of determination has been found to be excellent. This may be considered as a confirmation of the validity of both techniques. Though difficult, making such a determination is particularly worthwhile for ternary systems in which the same element may play different roles regarding the two other elements and therefore show a reversal of its properties along the ternary existence range of the phase. Making more systematic studies on this subject is still an open field for future research.

## ASSOCIATED CONTENT

### Supporting Information

CIFs of the experimentally studied compositions and an additional table containing the complete list of calculated formation enthalpies and the crystallographic parameters of every relaxed Mo–Ni–Re-ordered configuration in the  $\sigma$ -phase structure. This material is available free of charge via the Internet at <http://pubs.acs.org>.

## AUTHOR INFORMATION

### Corresponding Author

\*E-mail: [jean-marc.joubert@icmpe.cnrs.fr](mailto:jean-marc.joubert@icmpe.cnrs.fr).

### Notes

The authors declare no competing financial interest.

## ACKNOWLEDGMENTS

Financial support from the Agence Nationale de la Recherche (Project Armide 2010 BLAN 912 01) is acknowledged. The authors thank Florence Porcher of LLB, Saclay, France, for carrying out ND experiments and Eric Leroy for EPMA measurements. DFT calculations were performed using HPC resources from GENCI-CINES (Grant 2011-96175).

## REFERENCES

- Joubert, J.-M. *Prog. Mater. Sci.* **2008**, *53*, 528–583.
- Tobola, J.; François, M.; Elkaim, E.; Joubert, J.-M.; Vilasi, M. *Intermetallics* **2010**, *18*, 781–790.
- Crivello, J.-C.; Palumbo, M.; Abe, T.; Joubert, J.-M. *CALPHAD: Comput. Coupling Phase Diagrams Thermochem.* **2010**, *34*, 487–494.
- Palumbo, M.; Taichi, A.; Fries, S. G.; Pasturel, A. *Phys. Rev.* **2011**, *B83*, 144109.

- (5) Yaqoob, K.; Joubert, J.-M. To be published.
- (6) Fries, S. G.; Sundman, B. *Phys. Rev.* **2002**, *B66*, 012203.
- (7) Korzhavyi, P. A.; Sundman, B.; Selleby, M.; Johansson, B. *Mater. Res. Soc. Symp. Proc.* **2005**, *842*, S4.10.11–16.
- (8) Crivello, J.-C.; Joubert, J.-M. *J. Phys.: Condens. Matter* **2010**, *22*, 035402.
- (9) Rodríguez-Carvajal, J. XV Congress of International Union of Crystallography, Satellite Meeting on Powder Diffraction, 1990; p 127.
- (10) Kresse, G.; Furthmüller, J. *Phys. Rev. B* **1996**, *54*, 11169–11186.
- (11) Kresse, G.; Joubert, D. *Phys. Rev. B* **1999**, *59*, 1758.
- (12) Palumbo, M.; Abe, T.; Kocer, C.; Murakami, H.; Onodera, H. *CALPHAD: Comput. Coupling Phase Diagrams Thermochem.* **2010**, *34*, 495–503.
- (13) Perdew, J. P.; Wang, Y. *Phys. Rev. B* **1992**, *45*, 13244–13249.
- (14) Perdew, J. P.; Burke, K.; Ernzerhof, M. *Phys. Rev. Lett.* **1997**, *78*, 1396.
- (15) Monkhorst, H. J.; Pack, J. D. *Phys. Rev.* **1976**, *B13*, 5188–5192.
- (16) Blöchl, P. E.; Jepsen, O.; Andersen, O. K. *Phys. Rev.* **1994**, *B49*, 16223.
- (17) Sundman, B.; Ågren, J. *J. Phys. Chem. Solids* **1981**, *42*, 297–301.
- (18) Ansara, I.; Dupin, N.; Sundman, B. *CALPHAD* **1997**, *21*, 535–542.
- (19) Ansara, I.; Burton, B.; Chen, Q.; Hillert, M.; Fernandez Guillermet, A.; Fries, S. G.; Lukas, H. L.; Seifert, H. J.; Oates, W. A. *CALPHAD* **2000**, *24*, 19–40.
- (20) Brewer, L.; Lamoreaux, R. H. *At. Energy Rev.* **1980**, No. Spec. Issue 7, 195–356.
- (21) Farzadfar, S.-A.; Levesque, M.; Phejar, M.; Joubert, J.-M. *CALPHAD: Comput. Coupling Phase Diagrams Thermochem.* **2009**, *33*, 502–510.
- (22) Joubert, J.-M.; Cerný, R.; Latroche, M.; Percheron-Guégan, A.; Yvon, K. *J. Appl. Crystallogr.* **1998**, *31*, 327–332.
- (23) Joubert, J.-M. *CALPHAD* **2002**, *26*, 419–425.
- (24) Joubert, J.-M. *CALPHAD* **2002**, *26*, 427–438.
- (25) Seiser, B.; Drautz, R.; Pettifor, D. G. *Acta Mater.* **2011**, *59*, 749–763.

# **Chapter 8**

## **Thermodynamic Modeling of the Mo-Ni-Re System**



## 8. Thermodynamic Modeling of the Mo-Ni-Re System

After experimental investigation of phase equilibria and structural characterization of the intermetallic phases, thermodynamic modeling of the Mo-Ni-Re system was carried out with the help of the Calphad method. Prior to the thermodynamic modeling of the Mo-Ni-Re system, thermodynamic assessment of the constituent binary systems is necessary. The Ni-Re system and Mo-Ni binary system were reassessed during the present study whereas thermodynamic description of the Mo-Re binary system was taken from literature [1]. The thermodynamic description of the Ni-Re binary system has already been discussed in Chapter 4. The thermodynamic reassessment of the Mo-Ni system, selection of thermodynamic assessment of the Mo-Re system and thermodynamic modeling of Mo-Ni-Re system by combining thermodynamic descriptions of constituent binary systems is the subject of the present chapter.

The results provided in this chapter have not been submitted to any journal and are not presented in the article format as the previous ones.

### 8.1. The Mo-Ni binary system

During the present study, thermodynamic reassessment of the Mo-Ni binary system was carried out to incorporate enthalpies of formation of intermetallic compounds and enthalpies of mixing in solid solutions, calculated recently at our lab by J.-C Crivello and A. Breidi [2]. Thermodynamic assessment of the Mo-Ni binary system was previously carried out by Karin Frisk [3], Cui et al. [4], Morishita et al. [5], and Zhou et al. [6]. An introduction to the previous thermodynamic assessments of the Mo-Ni binary system is provided before discussing the present thermodynamic assessment of the Mo-Ni binary system.

#### 8.1.1. Introduction

The first attempt for thermodynamic assessment of the Mo-Ni binary system was carried out by Karin Frisk [3]. Prior to the thermodynamic assessment, she critically reviewed the available experimental phase diagram data and thermodynamic data which were also used as a reference in the later assessments of the Mo-Ni system. Considering the restricted composition range (less than 1 at.%) of the low temperature intermetallic phases i.e.  $\beta$  and  $\gamma$ , Karin Frisk modeled them as stoichiometric compounds whereas the  $\delta$  phase because of its considerable homogeneity domain (around 4 at.%) was treated with three sublattice model

(Ni)<sub>24</sub>(Mo,Ni)<sub>20</sub>(Mo)<sub>12</sub>. The justification of using three-sublattice model for  $\delta$  phase is provided later in the section 8.1.3. The Mo-Ni phase diagram calculated by Frisk showed fairly good agreement with selected experimental information except for the  $\delta$  phase boundary on the rich Mo side and fcc phase boundary at low temperatures. The thermodynamic description of the Mo-Ni system suggested by Karin Frisk [3] was later modified by Cui et al. [4] during thermodynamic modeling of the Mo-Ni-Ta system. The  $\gamma$  (MoNi<sub>3</sub>) phase appearing in the Mo-Ni system and TaNi<sub>3</sub> phase appearing in the Ta-Ni system have similar crystal structure. The TaNi<sub>3</sub> phase was treated with two-sublattice model in the Ta-Ni system. Therefore, in order to have consistent models for both phases (MoNi<sub>3</sub> and TaNi<sub>3</sub>) for calculation of the Mo-Ni-Ta system, Cui et al. [4] reassessed the Mo-Ni system by using two sublattice model (Mo,Ni)<sub>3</sub>(Mo,Ni) for  $\gamma$  (MoNi<sub>3</sub>) phase. However, agreement of the calculated phase diagram with the experimental information for  $\delta$  phase and fcc phase was comparatively better in the previous thermodynamic assessment by Frisk [3]. Morishita et al. [5] also reassessed the Mo-Ni system during thermodynamic modeling of the B-Mo-Ni system. They used some additional thermodynamic data (enthalpy of mixing measured at their lab) to evaluate Gibbs energy functions of liquid, fcc and  $\delta$  phase of the Mo-Ni system whereas other compounds of the Mo-Ni system ( $\beta$ ,  $\gamma$ ) were not considered. In addition, they modeled  $\delta$  phase as a stoichiometric compound which is rather inconsistent with the experimental information. The most recent attempt for thermodynamic assessment was carried out by Zhou et al. [6] in which they took in to account the possible existence of MoNi<sub>2</sub> and MoNi<sub>8</sub> phases. They also used using enthalpies of formation of compounds calculated by Wang [7] by using VASP [8] and enthalpies of mixing in fcc and bcc calculated by using special quasirandom structures (SQS). They used the same Gibbs energy models for  $\delta$  and  $\beta$  phases as were used previously by Frisk [3] whereas  $\gamma$  phase was modeled with two-sublattice model (Mo,Ni)<sub>3</sub>(Mo,Ni)<sub>1</sub> as well as with three sublattice model (Mo,Ni)<sub>4</sub>(Ni)<sub>2</sub>(Mo,Ni)<sub>2</sub>. The calculated phase diagram was shown to have good agreement with selected experimental information. However, optimization was carried out with the help of too many fitting parameters ( ${}^0L_{Mo,Ni}^{Liquid}$ ,  ${}^1L_{Mo,Ni}^{Liquid}$ ,  ${}^2L_{Mo,Ni}^{Liquid}$ ,  ${}^0L_{Mo,Ni}^{fcc}$ ,  ${}^1L_{Mo,Ni}^{fcc}$ ,  ${}^2L_{Mo,Ni}^{fcc}$ ,  ${}^0L_{Mo,Ni}^{bcc}$ ,  ${}^1L_{Mo,Ni}^{bcc}$ ,  ${}^0L_{Ni:Mo,Ni:Mo}^{\delta}$ ,  ${}^1L_{Ni:Mo,Ni:Mo}^{\delta}$ ,  ${}^0L_{Mo,Ni:Mo}^Y$ ,  ${}^0L_{Ni:Mo,Ni}^Y$ ) which made it rather less suitable for extrapolation in ternary and higher order systems. Therefore, remodeling of the Mo-Ni system to obtain a good agreement with selected experimental information with less number of fitting parameters was required.

During the present study, thermodynamic assessment of the Mo-Ni system was carried out to incorporate recent data and obtain better agreement with experimental information by using minimum number of fitting parameters. The results of the present thermodynamic assessment of the Mo-Ni binary system are presented after providing a brief introduction to the selected input data and thermodynamic models of the constituent phases.

### 8.1.2. Selection of data

Thermodynamic modeling of a system starts with the selection of credible experimental information. The contradictions about homogeneity domain of  $\delta$  phase presented in the Chapter 1 were addressed during the present study by the partial reinvestigation of the Mo-Ni binary system. The experimental results obtained during present study (presented in Chapter 5) confirmed the  $\delta$  phase boundaries previously reported by Heijwegen et al. [9]. The phase diagram and thermodynamic data selected by Frisk [3] was used as a reference in the later assessments of the Mo-Ni binary system by Cui et al. [4] and Zhou et al. [6] and was also used during the present study. The enthalpies of formation of  $\delta$ ,  $\gamma$  and  $\beta$  phases obtained with the help of DFT calculations and enthalpies of mixing in fcc and bcc phases by using special quasirandom structures have been recently calculated at our lab by J.-C Crivello and A. Breidi [2]. These calculation results, given in the Table 8-1, were also used during the present thermodynamic assessment of the Mo-Ni binary system.

*Table 8-1: Calculated values of enthalpies of mixing (in bcc and fcc phases) and enthalpies of formation ( $\delta$ ,  $\gamma$  and  $\beta$  phases) used for thermodynamic modeling of the Mo-Ni system [2].*

Phase	Formula / End-members	DFT results $\Delta H$ (J/mole)
bcc	Mo <sub>25</sub> Ni <sub>75</sub>	5693
	Mo <sub>50</sub> Ni <sub>50</sub>	11541
	Mo <sub>75</sub> Ni <sub>25</sub>	10379
fcc	Mo <sub>25</sub> Ni <sub>75</sub>	-4620
	Mo <sub>50</sub> Ni <sub>50</sub>	-6152
	Mo <sub>75</sub> Ni <sub>25</sub>	-3508
$\delta$	Mo <sub>12</sub> :Ni <sub>20</sub> :Ni <sub>24</sub>	26880
	Mo <sub>12</sub> :Mo <sub>20</sub> :Ni <sub>24</sub>	-164024
$\gamma$	Mo:Ni <sub>3</sub>	-34052
$\beta$	Mo:Ni <sub>4</sub>	-37888

The uncertainty in the SQS values of enthalpy of mixing in bcc phase at 75 at. % Ni and in fcc phase at 25 at.% Ni can be very high because these compositions are very close to the dynamically unstable structures i.e. bcc Ni and fcc Mo. Therefore, these values were not used during optimization of the Mo-Ni binary system.

### 8.1.3. Selection of model

The literature review of the Mo-Ni system presented in the Chapter 1 revealed the presence of three intermetallic compounds ( $\gamma$ ,  $\beta$  and  $\delta$ ), two solid solutions (bcc, fcc) and liquid phase. In this section, thermodynamic models selected during the present study to describe Gibbs energy functions of the constituent phase are presented.

#### Liquid, fcc and bcc phases

The liquid phase and the two terminal solid solutions i.e. bcc and fcc were treated with the regular solution model:

$$G_m^\varphi = x_{\text{Mo}} \circ G_{\text{Mo}}^\varphi + x_{\text{Ni}} \circ G_{\text{Ni}}^\varphi + RT(x_{\text{Mo}} \ln(x_{\text{Mo}}) + x_{\text{Ni}} \ln(x_{\text{Ni}})) + x_{\text{Mo}}x_{\text{Ni}} {}^0L_{\text{Mo,Ni}}^\varphi \quad \text{Equation 8-1}$$

In the Equation 8-1,  $\varphi$  represents fcc, bcc and liquid phases.  $\circ G_i^\varphi$  ( $i=\text{Mo,Ni}$ ) correspond to the Gibbs energy of the pure element  $i$  in the structure  $\varphi$ . The Gibbs energies of the pure elements were taken from the Pure 4 database. The term  ${}^0L_{\text{Mo,Ni}}^\varphi$  corresponds to the interaction between Mo and Ni atoms in the phase  $\varphi$  and is expressed as  $a^\varphi + b^\varphi T$ . The values of  $a^\varphi$  and  $b^\varphi$  were evaluated from the input experimental data and calculated enthalpies of mixing in fcc and bcc phases listed in Table 8-1.

#### The $\delta$ phase

The crystal structure information such as site occupancies of an intermetallic phase plays a very important in selection of a suitable thermodynamic model. The crystal structure of the  $\delta$  phase has already been discussed in the section 1.6.1. It consists of 56 atoms distributed on 14 sites with coordination number 12, 14, 15 and 16. Each crystallographic site has a Wyckoff multiplicity of 4. The crystallographic model of  $\delta$  phase [10] shows that 6 sites with coordination number (CN) 12 are completely occupied by Ni (12 atoms), 5 sites with CN 14 are shared by Mo and Ni atoms (20 atoms), and 2 sites with CN 15 and a site with CN 16 are completely occupied by Mo (12 atoms). Ideally a thermodynamic model of  $\delta$  phase should consider 14 distinguishable types of sites. However such a model will produce numerous end-members. Considering the elemental site occupation preferences and coordination number,

different sites can be combined in one sublattice to reduce the total number of end-members. Thus, the crystallographic sites completely occupied by Ni (CN 12) can be grouped in one sublattice, the sites shared by Mo and Ni atoms (CN 14) on another sublattice and the sites completely occupied by Mo (CN 15 and CN 16) on the third sublattice. As a result, Gibbs energy of the  $\delta$  phase can be described by using three sublattice model  $(\text{Ni})_{24}(\text{Mo},\text{Ni})_{20}(\text{Mo})_{12}$  with only one sublattice with mixed occupancies. This three-sublattice model was previously used by Karin Frisk [3], Cui et al. [4] and Zhou et al. [6] to describe Gibbs energy of the  $\delta$  phase and was also used during the present thermodynamic assessment of the Mo-Ni binary system. The mathematical expression to describe Gibbs energy of the  $\delta$  phase with the above mentioned three-sublattice model is given in the Equation 8-2.

$$G_m^\delta = y_{\text{Mo}}^{\text{II}} \circ G_{\text{Ni:Mo:Mo}}^\delta + y_{\text{Ni}}^{\text{II}} \circ G_{\text{Ni:Ni:Mo}}^\delta + 20RT(y_{\text{Mo}}^{\text{II}} \ln y_{\text{Mo}}^{\text{II}} + y_{\text{Ni}}^{\text{II}} \ln y_{\text{Ni}}^{\text{II}}) + {}^{\text{ex}}G_m^\delta \quad \text{Equation 8-2}$$

In the Equation 8-2,  $y_i^{\text{II}}$  corresponds to the site fraction of the element  $i$  on the second sublattice whereas  $\circ G_{\text{Ni}:i:\text{Mo}}^\delta$  ( $i=\text{Mo},\text{Ni}$ ) represent the Gibbs energies of the end-members of the  $\delta$  phase and is given by the following equations:

$$\circ G_{\text{Ni:Mo:Mo}}^\delta = 24 \circ G_{\text{Ni}}^{\text{fcc}} + 20 \circ G_{\text{Mo}}^{\text{bcc}} + 12 \circ G_{\text{Mo}}^{\text{bcc}} + \Delta G_{\text{Ni}:i:\text{Mo}}^\delta \quad \text{Equation 8-3}$$

$$\circ G_{\text{Ni:Ni:Mo}}^\delta = 24 \circ G_{\text{Ni}}^{\text{fcc}} + 20 \circ G_{\text{Ni}}^{\text{fcc}} + 12 \circ G_{\text{Mo}}^{\text{bcc}} + \Delta G_{\text{Ni}:i:\text{Mo}}^\delta \quad \text{Equation 8-4}$$

In the above Equations,  $\circ G_{\text{Ni}}^{\text{fcc}}$  and  $\circ G_{\text{Mo}}^{\text{bcc}}$  represent Gibbs energies of the pure fcc Ni and bcc Mo respectively and were taken from the Pure 4 database. The term  $\Delta G_{\text{Ni}:i:\text{Mo}}^\delta$  corresponds to the Gibbs energy of formation of the end-members and is expressed as:

$$\Delta G_{\text{Ni}:i:\text{Mo}}^\delta = a_{\text{Ni}:i:\text{Mo}}^\delta + b_{\text{Ni}:i:\text{Mo}}^\delta T \quad \text{Equation 8-5}$$

In the Equation 8-5, the terms  $a_{\text{Ni}:i:\text{Mo}}^\delta$  and  $b_{\text{Ni}:i:\text{Mo}}^\delta$  represent enthalpy and entropy of formation of the  $\delta$  phase end-members. During the present study, the term  $a_{\text{Ni}:i:\text{Mo}}^\delta$  was assigned the values obtained with the help of DFT calculations whereas the term  $b_{\text{Ni}:i:\text{Mo}}^\delta$  was optimized to obtain a better fit with the selected experimental information. The term  ${}^{\text{ex}}G_m^\delta$  in the Equation 8-2 corresponds to the excess Gibbs energy of the  $\delta$  phase and is expressed in Redlich-Kister polynomial as:

$${}^{ex}G_m^\delta = y_{Ni}^I y_{Mo}^I \sum_{v=0}^n {}^vL_{Ni:Ni,Mo:Mo}^\delta (y_{Mo}^I - y_{Ni}^I)^v \quad \text{Equation 8-6}$$

In the Equation 8-6, the term  ${}^vL_{Mo,Ni}^\phi$  corresponds to the interaction parameter and is expressed as  ${}^v a^\phi + {}^v b^\phi T$ . The values of  ${}^v a^\phi$  and  ${}^v b^\phi$  were evaluated from the input experimental information.

### The $\gamma$ and $\beta$ phases

The  $\gamma$  and  $\beta$  phases because of their restricted homogeneity domains (less than 1 at.%) were treated as  $MoNi_3$  and  $MoNi_4$  stoichiometric compounds respectively. The Gibbs energy of these compounds was therefore described with the help of following mathematical expression:

$$G_m^{MoNi_i} = a^{MoNi_i} + b^{MoNi_i} T + i^\circ G_{Ni}^{fcc} + {}^\circ G_{Mo}^{bcc} \quad \text{Equation 8-7}$$

In the Equation 8-7, the terms  $a^{MoNi_i}$  correspond to the enthalpies of formation of  $\beta$  and  $\gamma$  phases and were fixed to the values listed in the Table 8-1 whereas the terms  $b^{MoNi_i}$  corresponding to their entropies of formation were optimized to obtain a good fit with the selected input information.

### 8.1.4. Results and discussion

During the present study, thermodynamic assessment of the Mo-Ni binary system was carried out by using parrot module of the Thermo-Calc software [11]. The terms corresponding to the enthalpies of formation of  $\delta$ ,  $\beta$  and  $\gamma$  phases in their respective Gibbs energy models were fixed to the DFT values listed in the Table 8-1. The Mo-Ni phase diagram calculated after introducing the DFT values for enthalpies of formation of intermetallic compounds but prior to the optimization of any other parameter is illustrated in the Figure 8-1. The calculated Mo-Ni phase diagram shows a very large extension of the bcc phase, absence of  $\delta$  phase and stability of  $\beta$  and  $\gamma$  phases at higher temperatures.

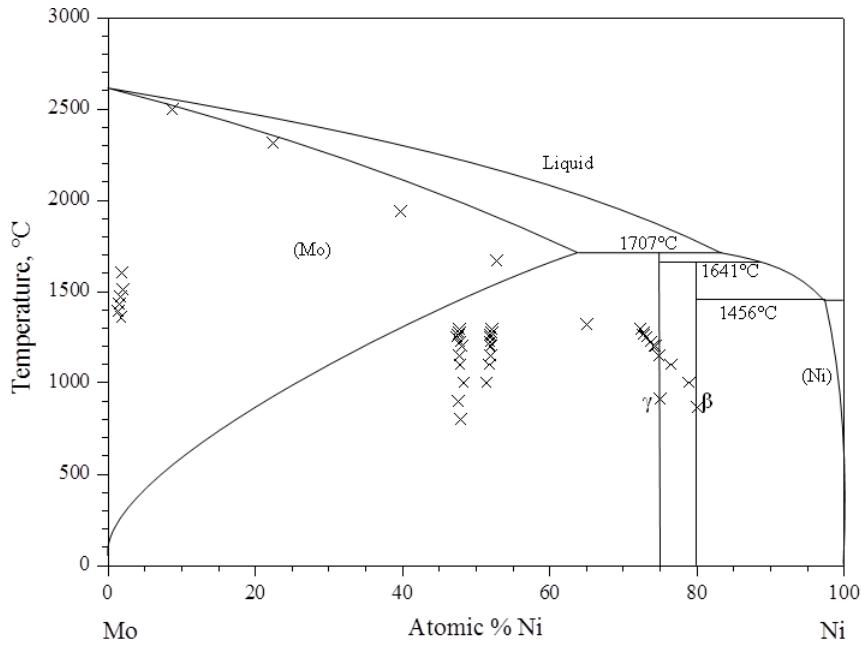


Figure 8-1: Comparison of calculated Mo-Ni phase diagram before optimization with experimental data

In order to match experimental phase diagram, it is necessary to reduce the composition range of bcc phase, temperature ranges of  $\beta$  &  $\gamma$  phases and to stabilize the  $\delta$  phase in the calculated Mo-Ni binary system. The calculated phase boundary of the bcc phase was shifted towards the experimental one by giving a strongly positive starting value to the composition dependent term of interaction parameter  ${}^0L_{Mo,Ni}^{BCC}$  whereas temperature ranges of  $\beta$  and  $\gamma$  phases were reduced to the experimental limits by giving positive values to the terms  $b^{MoNi_i}$  (Equation 8-7) corresponding to their entropy of formation. Decreasing the temperature range of  $\beta$  and  $\gamma$  close to the experimental limits also stabilized  $\delta$  phase in the calculated Mo-Ni phase diagram. Once all the constituent phases appear in the calculated Mo-Ni phase diagram, all the selected experimental information was taken into account and optimization of the Gibbs energy model parameters was carried out by using parrot module of the Thermo-Calc software [11]. In case of  $\beta$  and  $\gamma$  phases, only the terms corresponding to their entropy of formation were optimized whereas for  $\delta$  phase, optimization of the excess Gibbs energy terms was also required to obtain a good fit with the selected experimental information. The values of the Gibbs energy expression parameters obtained either after optimization or from the DFT calculations (in bold) are listed in Table 8-2.

Table 8-2: Thermodynamic parameters of the Mo-Ni binary system

Phase	Parameters (J/mole)
Liquid	${}^0L_{Mo,Ni}^{Liquid} = -20576.3 + 8.27 * T$
bcc	${}^0L_{Mo,Ni}^{BCC} = 50988.28$
fcc	${}^0L_{Mo,Ni}^{FCC} = -26399.36 + 16.52 * T$
	$\Delta G_{Ni:Ni:Mo}^{\delta} = +26880 + 85.92 * T$
$\delta$	$\Delta G_{Ni:Mo:Mo}^{\delta} = -164024 + 39.72 * T$
	${}^1L_{Ni:Mo,Ni:Mo}^{\delta} = -985076.5 + 892.6 * T$
$\gamma$	$\Delta G_{Mo:Ni}^{\gamma} = -34052 + 19.14 * T$
$\beta$	$\Delta G_{Mo:Ni}^{\beta} = -37888 + 20.82 * T$

A comparison of the Mo-Ni phase diagram calculated from the parameters listed in the Table 8-2 with selected experimental information is shown in the Figure 8-2.

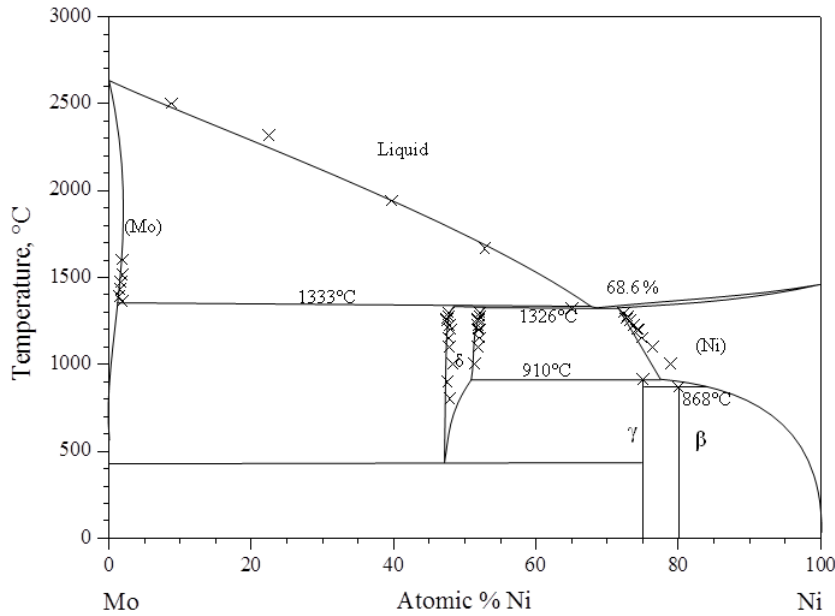


Figure 8-2: Comparison of calculated Mo-Ni phase diagram after optimization with experimental data [9, 12, 13]

The calculated Mo-Ni phase diagram illustrated in the Figure 8-2 reproduces well the selected experimental information with small number of optimized variables. In addition, it shows eutectoid decomposition of the  $\delta$  phase at around 425°C. No experimental investigation of the

Mo-Ni binary system has been carried out at such low temperatures. The decomposition of  $\delta$  and presence of  $\beta$  and  $\gamma$  phases at low temperatures is due to the ground state of the Mo-Ni system defined by the DFT calculations which is illustrated in Figure 8-3.

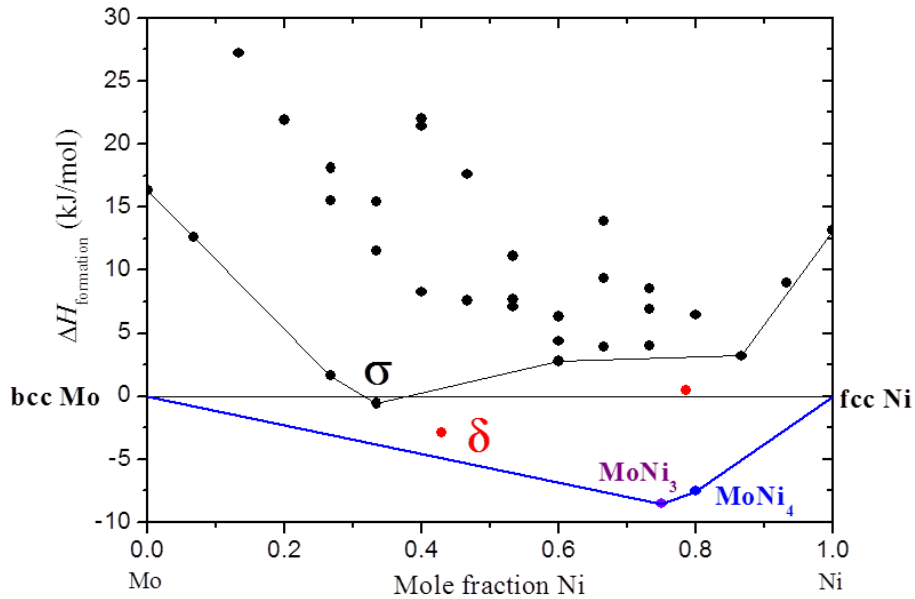


Figure 8-3: Mo-Ni ground state

The enthalpies of mixing in fcc and bcc phases listed in the Table 8-1 were also used as an input data for optimization. A comparison of SQS values of enthalpies of mixing in fcc and bcc phases with the ones calculated after optimization is shown in the Figure 8-4. The calculated enthalpies of mixing in the fcc as well as in the bcc phase shows good agreement with the SQS values. The SQS values of enthalpy of mixing in bcc phase at 75 at. % Ni and in fcc phase at 25 at.% Ni were not used during optimization because these compositions are very close to the dynamically unstable structures i.e. bcc Ni and fcc Mo. This is the reason why agreement between the SQS and calculated values of enthalpies of mixing is not as great as was observed for other compositions.

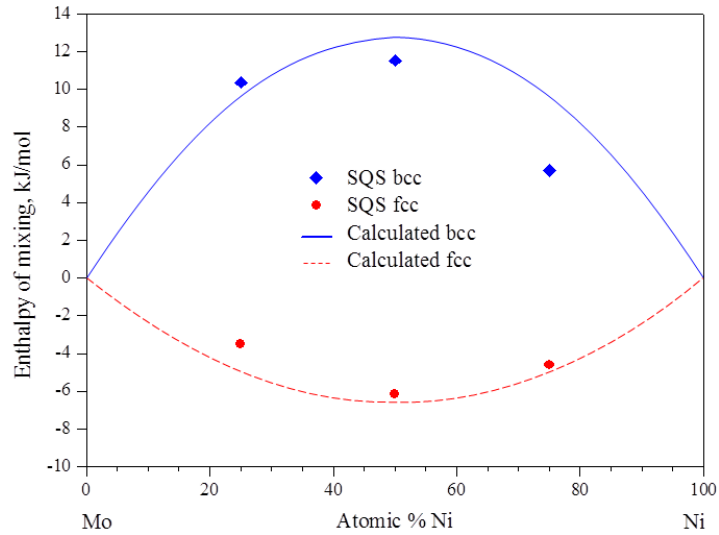


Figure 8-4: Comparison of calculated enthalpies of mixing of bcc referred to bcc-Ni and bcc-Mo and enthalpies of mixing of fcc referred to fcc-Ni and fcc-Mo with SQS values for bcc and fcc structure

A comparison of the activity values of Mo in the fcc phase reported in the literature [14-17] with the ones calculated after optimization of the Mo-Ni system is shown in the Figure 8-5. The calculated activities show fairly good agreement with the values reported by Katayama et al. [14].

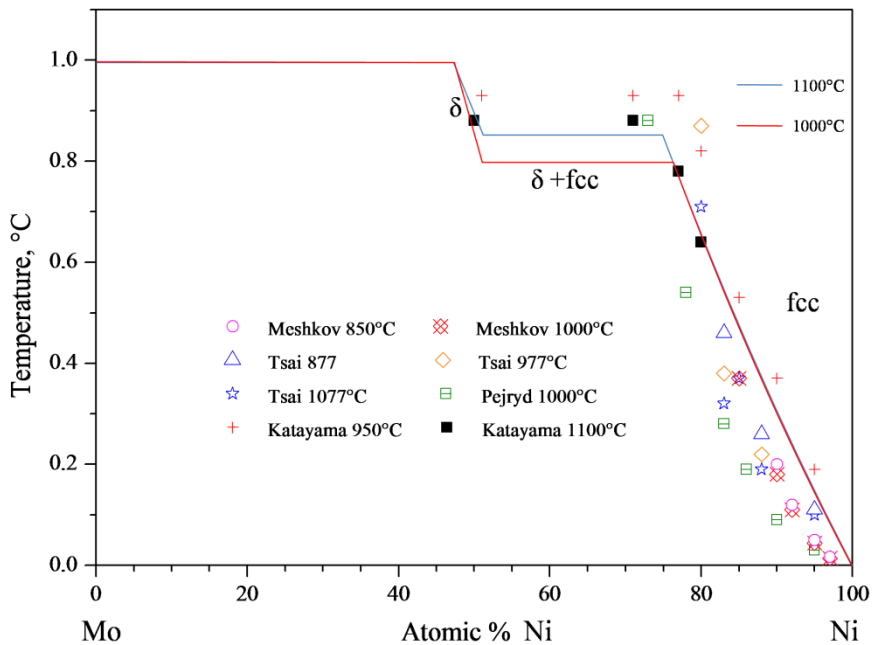


Figure 8-5: Comparison of calculated activity of Mo (in fcc and  $\delta$  phase) with experimental data

### **8.1.5. Conclusion**

Thermodynamic assessment of the Mo-Ni binary system was carried out by incorporating recently calculated enthalpy of formation of  $\beta$ ,  $\gamma$  and  $\delta$  phase and enthalpy of mixing in bcc and fcc calculated by using special quasirandom structures (SQS). Contrary to the recent thermodynamic modeling by Zhou et al. [6] in which a large number of fitting parameters were used, the Mo-Ni phase diagram calculated during present study showed a good agreement with the selected experimental as well as with the calculation data (Figure 8-2, Figure 8-4 and Figure 8-5) with very few optimizing variables. The calculated Mo-Ni phase diagram also showed eutectoid decomposition of  $\delta$  phase at around 495°C and stability of  $\beta$  and  $\gamma$  phases at room temperature which is a consequence of the ground state drawn with the help of DFT calculations. The thermodynamic description of the Mo-Ni binary system proposed during present study will be used in the thermodynamic modeling of the Mo-Ni-Re system discussed in the section 8.4.

### **8.2. The Ni-Re system**

The results of thermodynamic assessment of Ni-Re binary system carried out during present study have already been presented in the Chapter 4.

### **8.3. The Mo-Re system**

The thermodynamic assessment of the Mo-Re binary system has been previously carried out by Mao et al. [18], Farzadfar et al. [19] and Yang et al. [20]. The calculated Mo-Re phase diagrams in general showed a good agreement with the selected experimental information. The main difference among the previous assessments lies in thermodynamic models selected to describe  $\sigma$  and  $\chi$  phases. The thermodynamic models of  $\sigma$  and  $\chi$  used in the previous assessments are listed in the Table 8-3.

Table 8-3: Thermodynamic models for  $\sigma$  and  $\chi$  phases used in previous Mo-Re assessments [18-20].

$\sigma$	$\chi$	Reference
(Mo) <sub>4</sub> (Mo,Re) <sub>16</sub> (Re) <sub>10</sub>	(Re) <sub>24</sub> (Mo) <sub>10</sub> (Mo, Re) <sub>24</sub>	[18]
(Mo) <sub>4</sub> (Mo,Re) <sub>18</sub> (Re) <sub>8</sub>		
(Mo,Re) <sub>20</sub> (Mo,Re) <sub>10</sub>	(Mo,Re) <sub>10</sub> (Mo,Re) <sub>24</sub> (Re) <sub>24</sub>	[19]
(Mo,Re) <sub>4</sub> (Mo,Re) <sub>16</sub> (Re) <sub>10</sub>	(Mo,Re) <sub>10</sub> (Mo,Re) <sub>24</sub> (Re) <sub>24</sub>	[20]

In general, the  $\sigma$  and  $\chi$  phase have broad range of existence ( $\sigma$  exists from 10 at.% A in V–Mn to 85 at.% A in Ta–Ir). This existence range can be extended to pure elements since an allotropic form of U and  $\alpha$ -Mn has the structure of  $\sigma$  and  $\chi$  phase respectively. Therefore, thermodynamic models selected for these phase should be able to describe their entire composition ranges in all the systems in which they appear. This requires presence of all the constituent elements in each sublattice. Among the previous assessments of the Mo-Re system listed above, only the model used by Farzadfar [19] can describe entire composition range of  $\sigma$  phase.

A new thermodynamic description of the Mo-Re binary system by using different models for  $\sigma$  and  $\chi$  phase in which all the constituent elements are present in each sublattice has been proposed by Nathalie Dupin [1]. The thermodynamic models used by Nathalie Dupin for  $\sigma$  and  $\chi$  phase are listed in the Table 8-4.

Table 8-4: Thermodynamic models for  $\sigma$  and  $\chi$  phases used by Nathalie Dupin [1].

$\sigma$	$\chi$
(Mo,Re) <sub>2</sub> (Mo,Re) <sub>4</sub> (Mo,Re) <sub>8</sub> (Mo,Re) <sub>8</sub> (Mo,Re) <sub>8</sub>	(Mo,Re) <sub>2</sub> (Mo,Re) <sub>8</sub> (Mo,Re) <sub>24</sub> (Mo,Re) <sub>24</sub>
(Mo,Re) <sub>10</sub> (Mo,Re) <sub>4</sub> (Mo,Re) <sub>8</sub> (Mo,Re) <sub>8</sub>	(Mo,Re) <sub>10</sub> (Mo,Re) <sub>24</sub> (Mo,Re) <sub>24</sub>
(Mo,Re) <sub>10</sub> (Mo,Re) <sub>4</sub> (Mo,Re) <sub>16</sub>	(Mo,Re) <sub>10</sub> (Mo,Re) <sub>48</sub>
(Mo,Re) <sub>10</sub> (Mo,Re) <sub>20</sub>	-

Besides available experimental information, recently calculated enthalpies of formation of Mo-Re  $\sigma$  and Mo-Re  $\chi$  phase [21] were also used. Thermodynamic assessment was initially carried out by using the most complex possible models (five-sublattice model for  $\sigma$  and four-sublattice model for  $\chi$  phase), and then the effect of simplification of models on the excess

Gibbs energy terms was studied. The thermodynamic description proposed by using five-sublattice model for  $\sigma$  and four-sublattice model for  $\chi$  phase showed good agreement with experimental data without optimization of any of their excess Gibbs energy terms. It was therefore selected as a reference for the present thermodynamic assessment of the Mo-Ni-Re system.

## 8.4. The Mo-Ni-Re system

### 8.4.1. Selection of data

The results of phase equilibria investigation of the Mo-Ni-Re system, presented in the Chapter 5, were used as input information for thermodynamic modeling of the Mo-Ni-Re system. In addition, enthalpies of formation of intermetallic phases obtained by J.-C Crivello with the help of DFT calculations [21] were also used during the present study. The values of calculated enthalpies of formation of  $\delta$  phase and phase with prototype  $\text{Mo}_3\text{CoSi}$  are listed in Table 8-5 whereas those of  $\sigma$  and  $\chi$  phase are provided in Annex I and Annex II respectively.

*Table 8-5: Enthalpies of formation of  $\delta$  phase and phase with prototype  $\text{Mo}_3\text{CoSi}$  obtained with the help of DFT calculations [21].*

Phase	End-members	$\Delta H^{\text{for}}$ (J/mole)
$\delta$	$\text{Mo}_{12}:\text{Re}_{20}:\text{Ni}_{24}$	-329112
	$\text{Mo}_9:\text{Ni}_4:\text{Ni}$	-28056
$\text{Mo}_3\text{CoSi}$	$\text{Mo}_9:\text{Re}_4:\text{Ni}$	69748
	$\text{Re}_9:\text{Ni}_4:\text{Ni}$	-7812
	$\text{Re}_9:\text{Re}_4:\text{Ni}$	153020

### 8.4.2. Selection of model

The phase equilibrium investigation of the Mo-Ni-Re system presented in Chapter 5 showed presence of a liquid phase, three solid solutions (bcc, fcc, hcp) and five intermetallic phases ( $\delta$ ,  $\sigma$ ,  $\chi$ , phase with prototype  $\text{Mo}_3\text{CoSi}$ ,  $\sigma'$ ). Thermodynamic models selected for each phase along with their Gibbs energy expressions are given below.

### Liquid, bcc, fcc, hcp

The liquid phase and the three terminal solid solutions i.e. bcc, fcc and hcp, were treated with the regular solution model. The Gibbs energy of the phase  $\varphi$  ( $\varphi$  represents liquid, bcc, fcc and hcp phase) is expressed by the following expression:

$$G_m^\varphi = \sum_{i=\text{Mo,Ni,Re}} x_i {}^\circ G_i^\varphi + RT \sum_{i=\text{Mo,Ni,Re}} x_i \ln(x_i) + {}^{ex}G_m^\varphi \quad \text{Equation 8-8}$$

In the Equation 8-8, the term  ${}^\circ G_i^\varphi$  corresponds to the Gibbs energy of the pure element  $i$  in the structure  $\varphi$ .

### The $\delta$ phase

The  $\delta$  phase was treated with three-sublattice model  $(\text{Ni})_{24}(\text{Mo,Ni})_{20}(\text{Mo})_{12}$  in the Mo-Ni binary system. To account for its extension in the Mo-Ni-Re ternary system, the model was modified to  $(\text{Ni})_{24}(\text{Mo,Ni,Re})_{20}(\text{Mo})_{12}$ , in which the Re whose atomic size is between Mo and Ni was assumed to substitute them on the sites with coordination number 14 whereas the sites with CN 12 and CN 15,16 remain completely occupied by Ni and Mo atoms respectively. The three-sublattice model selected for the Mo-Ni-Re  $\delta$  phase yields the following Gibbs energy expression for one mole of formula units:

$$G_m^\delta = \sum_{(i=\text{Mo,Ni,Re})} y_i^{\text{II}} G_{\text{Ni}:i:\text{Mo}}^\delta + 20RT \sum_{(i=\text{Mo,Ni,Re})} y_i^{\text{II}} \ln(y_i^{\text{II}}) + {}^{ex}G_m^\delta \quad \text{Equation 8-9}$$

In the Equation 8-9,  $G_{\text{Ni}:i:\text{Mo}}^\delta$  represents Gibbs energy of end-members of  $\delta$  phase and  $y_i^{\text{II}}$  the site fraction of element  $i$  on the second sublattice. The positions of three end members of  $\delta$  phase defined by the selected three-sublattice model  $(\text{Ni})_{24}(\text{Mo,Ni,Re})_{20}(\text{Mo})_{12}$  are shown in the Figure 8-6.

### The $\sigma$ and $\chi$ phase

The availability of DFT values of enthalpies of formation of all the possible ordered configuration of  $\sigma$  and  $\chi$  phase [21, 22] has allowed us to use the most complex models to describe their Gibbs energy. Therefore, thermodynamic assessment of the Mo-Ni-Re system was carried out by using five-sublattice model for  $\sigma$  and four-sublattice model for  $\chi$  phase. Thermodynamic assessment of the Mo-Ni-Re system by using simpler models for  $\sigma$  and  $\chi$  phase can be carried out in later studies to see the effect of simplification of  $\sigma$  and  $\chi$  phase models on the excess terms and calculated Mo-Ni-Re ternary system. The possibility of

describing Mo-Ni-Re  $\sigma$  phase with a model as simple as two-sublattice has already been discussed in the Chapter 7.

**The  $\sigma$  phase:** To account for the ternary extension of Mo-Re  $\sigma$  phase in the studied isothermal sections of the Mo-Ni-Re system, the five-sublattice model used for the Mo-Re  $\sigma$  phase [1] was modified to  $(\text{Mo,Ni,Re})_2(\text{Mo,Ni,Re})_4(\text{Mo,Ni,Re})_8(\text{Mo,Ni,Re})_8(\text{Mo,Ni,Re})_8$ , in which Ni substitutes for Mo and Re on all the sublattices. The Gibbs energy of the Mo-Ni-Re  $\sigma$  phase was described by using the modified compound formalism.

$$G^\sigma = \sum_s a_s G^{\text{dis}-\sigma}(x) + \Delta G^{\text{ord}-\sigma}(y) \quad \text{Equation 8-10}$$

$$G^{\text{dis}-\sigma}(x) = \sum_{i=\text{Mo,Ni,Re}} x_i G_i^\sigma \quad \text{Equation 8-11}$$

$$\begin{aligned} \Delta G^{\text{ord}-\sigma}(y) = & \sum_{ABCDE=\text{Mo,Ni,Re}} y_A^{2a} y_B^{4c} y_C^{8i_1} y_D^{8i_2} y_E^{8j} \Delta G_{ABCDE}^\sigma \\ & + RT \sum_s a^{(s)} \sum_i y_i^{(s)} \ln(y_i^{(s)}) \end{aligned} \quad \text{Equation 8-12}$$

$$\Delta G_{ABCDE}^\sigma = E_{ABCDE}^\sigma - \sum_s a^{(s)} E_{iiii}^\sigma \quad \text{Equation 8-13}$$

$$G_i^\sigma - G_i^{\text{SER}} = \frac{G_{iiii}^\sigma}{\sum_s a^{(s)}} - G_i^{\text{SER}} = \frac{E_{iiii}^\sigma}{\sum_s a^{(s)}} - E_i^{\text{SER}} - T\Delta S_i^\sigma \quad \text{Equation 8-14}$$

In the above equations,  $G_{ABCDE}^\sigma$  represents Gibbs energy of end-members of  $\sigma$  phase, the terms  $y_A^{2a} y_B^{4c} y_C^{8i_1} y_D^{8i_2} y_E^{8j}$  correspond to the sublattice fraction of the constituent elements on five sublattices of  $\sigma$  phase and  $a^{(s)}$  indicate multiplicity of the sublattice  $s$ . The value of  $\Delta G^{\text{ord}-\sigma}(y)$  comes from the DFT values. During the present study, no excess term was optimized for  $\sigma$  phase. The only parameter assessed during present study was  $\Delta S_i^\sigma$ . The value of  $\Delta S_{\text{Mo}}^\sigma$  and  $\Delta S_{\text{Re}}^\sigma$  were taken from the assessment of the Mo-Re binary system performed by Nathalie Dupin [1] whereas  $\Delta S_{\text{Ni}}^\sigma$  was optimized during the present study.

The presence of 3 elements on five sublattices generates  $3^5=243$  end-members of the Mo-Ni-Re  $\sigma$  phase. Among 243 end-members of  $\sigma$ , 90 correspond to the unique composition. The positions of 90 unique compositions of Mo-Ni-Re  $\sigma$  phase have already been shown in Figure 2 of the Chapter 5.

**The  $\chi$  phase:** To model extension of the Mo-Re  $\chi$  phase observed in the studied isothermal sections of the Mo-Ni-Re system, the four-sublattice model of the Mo-Re  $\chi$  phase [1] was modified to  $(\text{Mo,Ni,Re})_2(\text{Mo,Ni,Re})_8(\text{Mo,Ni,Re})_{24}(\text{Mo,Ni,Re})_{24}$ , in which Ni substitutes for Mo and Re on all the sublattices. The Gibbs energy of the Mo-Ni-Re  $\chi$  phase was described by using the modified compound formalism.

$$G_m^\chi = \sum_s a_s G^{\text{dis}-\chi}(x) + \Delta G^{\text{ord}-\chi}(y) \quad \text{Equation 8-15}$$

$$G^{\text{dis}-\chi}(x) = \sum_{i=\text{Mo,Ni,Re}} x_i G_i^\chi \quad \text{Equation 8-16}$$

$$\begin{aligned} \Delta G^{\text{ord}-\chi}(y) = & \sum_{\text{ABCD}=\text{Mo,Ni,Re}} y_A^{2a} y_B^{8c} y_C^{24g_1} y_D^{24g_2} \Delta G_{\text{ABCD}}^\chi \\ & + RT \sum_s a^{(s)} \sum_i y_i^{(s)} \ln(y_i^{(s)}) \end{aligned} \quad \text{Equation 8-17}$$

$$\Delta G_{\text{ABCD}}^\chi = E_{\text{ABCD}}^\chi - \sum_s a^{(s)} E_{\text{iiii}}^\chi \quad \text{Equation 8-18}$$

$$G_i^\chi - G_i^{\text{SER}} = \frac{G_{\text{iiii}}^\chi}{\sum_s a^{(s)}} - G_i^{\text{SER}} = \frac{E_{\text{iiii}}^\chi}{\sum_s a^{(s)}} - E_i^{\text{SER}} - T\Delta S_i^\chi \quad \text{Equation 8-19}$$

During the present study, no excess terms was optimized for  $\chi$  phase. The value of  $\Delta G^{\text{ord}-\chi}(y)$  comes from the DFT values. The value of  $\Delta S_{\text{Mo}}^\chi$  and  $\Delta S_{\text{Re}}^\chi$  were taken from the assessment of the Mo-Re binary system performed by Nathalie Dupin [1] whereas  $\Delta S_{\text{Ni}}^\chi$  was optimized during the present study.

The ordered distribution of 3 elements on the four sublattices of the Mo-Ni-Re  $\chi$  phase defines  $3^4=81$  end-members. Out of 81 end-members, 54 correspond to the unique compositions. The positions of 54 unique ordered compositions of  $\chi$  phase are shown in the Figure 8-6.

### The $\sigma'$ phase

The  $\sigma$  and  $\sigma'$  phase observed in the 1200°C isothermal section of Mo-Ni-Re system are two distinct phases; therefore, a separate model is required for both phases. The selection of a thermodynamic model for  $\sigma'$  phase based on its crystallographic information was not possible. Therefore,  $\sigma'$  phase was defined as a line compound  $(\text{Mo,Re})_2(\text{Ni})$  by only

considering its experimental homogeneity domain which is parallel to the Mo-Re system at around 29-34 at.% Ni. The selected sublattice model yields the following mathematical expression of the Gibbs energy for one mole of formula units of  $\sigma'$  phase:

$$G_m^{\sigma'} = \sum_{(i=Mo,Re)} y_i^{II} G_{i:Ni}^{\sigma'} + 2RT \sum_{(i=Mo,Re)} y_i^{II} \ln(y_i^{II}) + {}^{ex}G_m^{\sigma'} \quad \text{Equation 8-20}$$

$${}^{\circ}G_{Mo:Ni}^{\sigma'} = 2 {}^{\circ}G_{Mo}^{bcc} + {}^{\circ}G_{Ni}^{fcc} + \Delta G_{Mo:Ni}^{\sigma'} \quad \text{Equation 8-21}$$

$${}^{\circ}G_{Re:Ni}^{\sigma'} = 2 {}^{\circ}G_{Re}^{hcp} + {}^{\circ}G_{Ni}^{fcc} + \Delta G_{Re:Ni}^{\sigma'} \quad \text{Equation 8-22}$$

In the Equation 8-20,  $G_{i:Ni}^{\sigma'}$  corresponds to the Gibbs energy of the end-members. The terms  ${}^{\circ}G_{Ni}^{fcc}$ ,  ${}^{\circ}G_{Mo}^{bcc}$  and  ${}^{\circ}G_{Re}^{hcp}$  in Equation 8-21 and Equation 8-22 represent Gibbs energies of the pure fcc Ni, bcc Mo and hcp Re respectively and their values were taken from the Pure 4 database. The terms  $\Delta G_{Mo:Ni}^{\sigma'}$  and  $\Delta G_{Re:Ni}^{\sigma'}$  corresponds to the Gibbs energy of formation of respective end-members and are expressed as:

$$\Delta G_{i:Ni}^{\sigma'} = a_{i:Ni}^{\sigma'} + b_{i:Ni}^{\sigma'} T \quad \text{Equation 8-23}$$

In the Equation 8-23, the terms  $a_{Ni:i}^{\sigma'}$  and  $b_{Ni:i}^{\sigma'}$  represent the enthalpy ( $\Delta H_{i:Ni}^{\sigma'}$ ) and entropy  $-\Delta S_{i:Ni}^{\sigma'}$  of formation of the  $\sigma'$  phase end-members respectively. During the present study,  $\Delta H_{i:Ni}^{\sigma'}$  and  ${}^{ex}G_m^{\sigma'}$  were optimized

The positions of the  $\sigma'$  phase end-members are shown in the Figure 8-6.

### Ternary phase with prototype $Mo_3CoSi$

The second ternary phase found in the 1200°C isothermal section of the Mo-Ni-Re system has structure prototype  $Mo_3CoSi$  which contains 56 atoms distributed on 6 sites with CN 10, 12, 14 and 15. Before describing thermodynamic model of the phase, its crystallographic model is presented. In the  $Mo_3CoSi$  phase [23], the sites with CN 10 and CN 12 are shared by smaller and intermediate size atom (Si and Co respectively), the sites with CN 14 are occupied by intermediate and larger atom (Co and Mo respectively) and the only site with CN 15 contains larger atom (Mo). The Rietveld refinement of the XRD pattern of the Mo-Ni-Re ternary phase with prototype  $Mo_3CoSi$  was initially carried out by replacing Si with Ni, and Co with Re in the crystallographic model of  $Mo_3CoSi$ . However, a better fit with the observed XRD pattern and EPMA composition of the phase was obtained by some modifications in the

crystallographic model which include removing the intermediate size atom (Re) from the site with CN 10 and putting it on the site with CN 15 along with Mo. In the modified model of the ternary phase with prototype Mo<sub>3</sub>CoSi, the sites with CN 14 and CN 15 are shared by Mo and Re atoms, the sites with CN 12 are occupied by Ni and Re, whereas the only site with CN 10 contains Ni.

By considering its crystal structure information, the Mo-Ni-Re ternary phase with structure prototype Mo<sub>3</sub>CoSi was described by using a three-sublattice model (Mo,Re)<sub>36</sub>(Ni,Re)<sub>16</sub>(Ni)<sub>4</sub> or (Mo,Re)<sub>9</sub>(Ni,Re)<sub>4</sub>(Ni). The first sublattice groups the sites with CN 14 and CN 15, the second sublattice combines the sites with CN 12 and the third contains the only site with CN 10. The mathematical expression to describe the Gibbs energy of the ternary phase with structure prototype Mo<sub>3</sub>CoSi is given in the Equation 8-24.

$$\begin{aligned}
 G_m^{\text{Mo}_3\text{CoSi}} = & \sum_{(i=\text{Ni,Re})} \sum_{(j=\text{Mo,Re})} [y_i^{\text{II}} y_j^{\text{III}}] G_{\text{Ni}:i:j}^{\text{Mo}_3\text{CoSi}} \\
 & + 16RT \sum_{(i=\text{Ni,Re})} y_i^{\text{II}} \ln(y_i^{\text{II}}) + 36RT \sum_{(j=\text{Mo,Re})} y_j^{\text{III}} \ln(y_j^{\text{III}}) \\
 & + \text{ex} G_m^{\text{Mo}_3\text{CoSi}}
 \end{aligned}
 \tag{Equation 8-24}$$

The term  $G_{\text{Ni}:i:j}^{\text{Mo}_3\text{CoSi}}$  corresponds to the Gibbs energy of the end-members, the positions of which have been shown in the Figure 8-6. During the present study, the terms corresponding to enthalpies of formation of all the end-members of phase with structural prototype Mo<sub>3</sub>CoSi were fixed to the DFT values listed in the Table 8-5 whereas terms corresponding to entropies of formation of end-members and excess Gibbs energy terms were optimized.

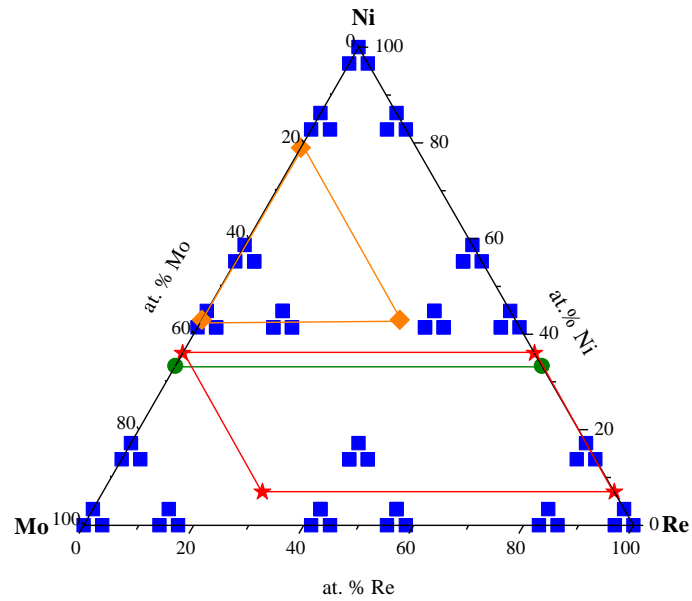


Figure 8-6: Position of end-members of  $\delta$  phase,  $\sigma'$  phase, phase with structural prototype  $\text{Mo}_3\text{CoSi}$  and unique configurations of  $\chi$  phase

### 8.4.3. Results and discussion

Thermodynamic descriptions of three related binary systems were combined. The enthalpies of formation of all the end-members of  $\sigma$ ,  $\chi$ ,  $\delta$  and phase with prototype  $\text{Mo}_3\text{CoSi}$  defined by their respective sublattice models were fixed to the DFT values. The enthalpies of formation of  $\delta$  and phase with prototype  $\text{Mo}_3\text{CoSi}$ , are listed in the Table 8-5 whereas enthalpies of formation of  $\sigma$  and  $\chi$  phase are provided in the Annex I and Annex II respectively. The 1200°C isothermal sections of the Mo-Ni-Re system calculated after combining the descriptions of related binary systems and introducing the DFT values for enthalpies of formation is illustrated in the Figure 8-7.

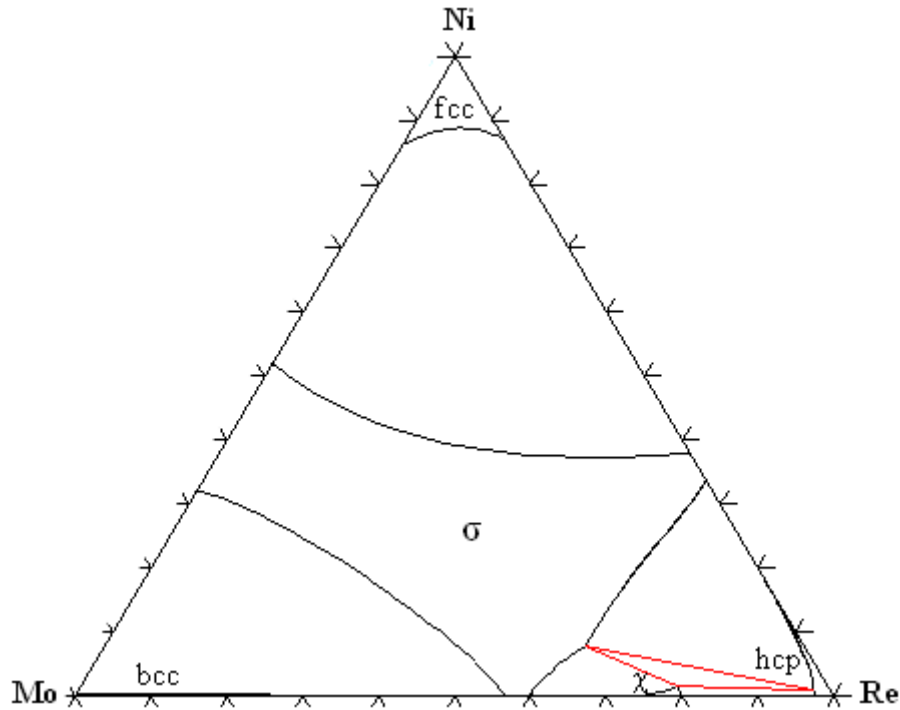


Figure 8-7: Calculated 1200°C isothermal section before optimization

The calculated 1200°C isothermal section illustrated in the Figure 8-7 shows very large homogeneity domain of the  $\sigma$  phase existing as a continuous phase in all the constituent binary systems whereas presence of  $\delta$  and two ternary phases was not evidenced in the Mo-Ni-Re isothermal sections. In order to reduce the homogeneity domain of the  $\sigma$  phase close to the experimental values, the entropy of Ni  $\sigma$  ( $\Delta S_{\text{Ni}}^{\sigma}$ ) was optimized. The optimization of  $\Delta S_{\text{Ni}}^{\sigma}$  reduced the ternary extension of  $\sigma$  phase. As a result, presence of  $\delta$  and ternary phase with structure prototype  $\text{Mo}_3\text{CoSi}$ , was evidenced in the 1200°C isothermal sections. Unlike other intermetallic phases whose enthalpies of formations were fixed to the DFT values, the enthalpies of formation of the  $\sigma'$  phase end-members and their excess Gibbs energy terms were optimized to make  $\sigma'$  phase stable in the 1200°C isothermal section. The parameters optimized during the assessment of the Mo-Ni-Re system are listed in the Table 8-6.

Table 8-6: Optimized parameters of the Mo-Ni-Re system

Phase	Parameters (J/mole)		
Solid Solutions	${}^0L_{\text{Mo,Ni,Re}}^{\text{fcc}} = -60549.3$	${}^0L_{\text{Mo,Ni,Re}}^{\text{hcp}} = 83286.9 - 72.9T$	${}^0L_{\text{Mo,Ni,Re}}^{\text{Liquid}} = -22580.2$
$\sigma$	$-\Delta S_{\text{Ni}}^{\sigma} = 8.1$		
$\chi$	$-\Delta S_{\text{Ni}}^{\chi} = 1.89$		
$\delta$	$-\Delta S_{\text{Ni:Re:Mo}}^{\delta} = 41.92$	${}^0L_{\text{Ni:Mo,Re:Mo}}^{\delta} = -152636.7$	
$\sigma'$	$\Delta H_{\text{Mo:Ni}}^{\sigma'} = -484.93$	$\Delta H_{\text{Re:Ni}}^{\sigma'} = 3985.9$	${}^0L_{\text{Mo,Re:Ni}}^{\sigma'} = -46223.26$
$\text{Mo}_3\text{CoSi}$	${}^0L_{\text{Mo,Re:Ni:Ni}}^{\text{Mo}_3\text{CoSi}} = -31738.74$	${}^1L_{\text{Mo,Re:Ni:Ni}}^{\text{Mo}_3\text{CoSi}} = -161544.1$	
	$-\Delta S_{\text{Mo:Ni:Ni}}^{\text{Mo}_3\text{CoSi}} = -\Delta S_{\text{Re:Ni:Ni}}^{\text{Mo}_3\text{CoSi}} = -\Delta S_{\text{Mo:Re:Ni}}^{\text{Mo}_3\text{CoSi}} - \Delta S_{\text{Re:Re:Ni}}^{\text{Mo}_3\text{CoSi}} = 2.04$		

A comparison of 1200°C and 1600°C isothermal sections of the Mo-Ni-Re calculated from the parameters listed in the Table 8-6, with experimentally determined isothermal sections is shown in the Figure 8-8 and Figure 8-9 respectively.

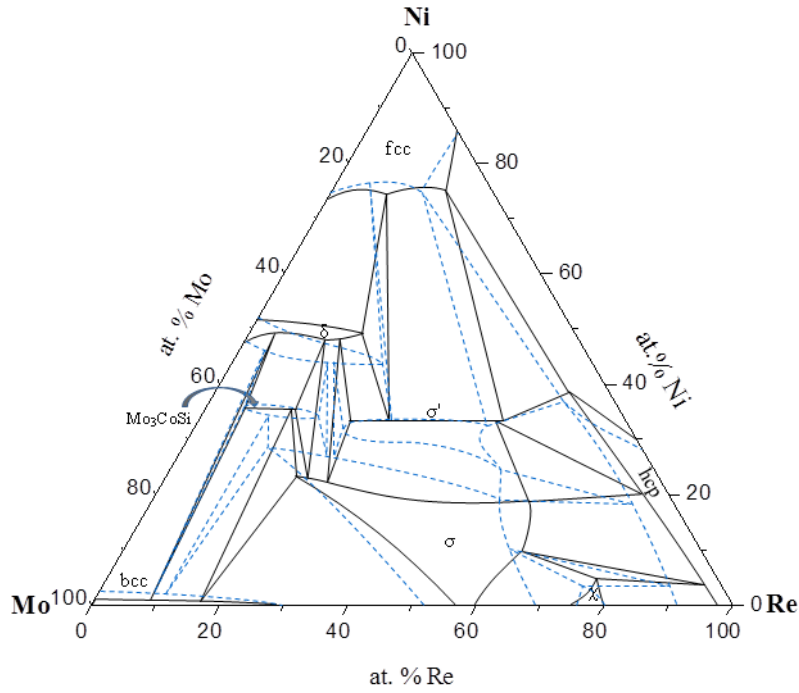


Figure 8-8: Comparison of experimental (blue dashed lines) and calculated 1200°C (solid black line) isothermal section after optimization

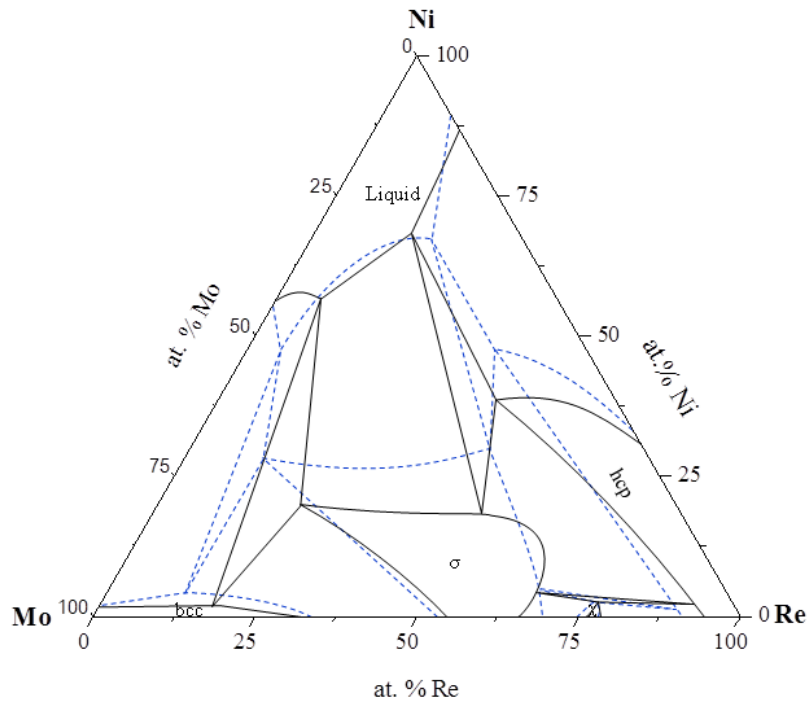


Figure 8-9: Comparison of experimental (blue dashed lines) and calculated 1600°C (solid black line) isothermal section after optimization

In case of solid solutions, only the ternary interaction term  ${}^0L_{\text{Mo,Ni,Re}}^\varphi$  ( $\varphi = \text{fcc, hcp, liquid}$ ) was optimized whereas interaction of Ni and Re in bcc structure was assumed equal to their interaction in liquid phase, the value of which was obtained during optimization of Ni-Re binary system. Similarly, the interaction of Mo and Re in the fcc phase and Mo and Ni in the

hcp phase, was assumed equal to their interaction in the hcp and fcc phase respectively which was obtained from optimization of the related binary systems. The agreement of the fcc and the liquid phase is fairly good whereas solubility of Mo and Ni in the hcp phase at 1200°C and 1600°C respectively is lower in the calculated phase diagrams. Since, the most complex models were used during the present study for  $\sigma$  and  $\chi$  phase yielding 243 and 81 end-members respectively; therefore it was decided not to take in to account any interaction parameter and optimize only the entropy of  $\sigma$  Ni ( $\Delta S_{Ni}^{\sigma}$ ) and  $\chi$  Ni ( $\Delta S_{Ni}^{\chi}$ ) in order to match the experimental homogeneity domains. The calculated homogeneity domain of the  $\chi$  phase in 1200°C as well as in 1600°C isothermal section showed good agreement with the input experimental information. On the other hand, calculated extension of  $\sigma$  phase in the Mo-Ni-Re system (shown in the Figure 8-8 and Figure 8-9) is underestimated. In the beginning of assessment, the parameter corresponding to  $-\Delta S_{Ni}^{\sigma}$  was optimized with the help of ThermoCalc software [11] which yielded a much better agreement between experimental and calculated  $\sigma$  phase homogeneity domains but it also inevitably stabilized the  $\sigma$  phase in the Mo-Ni binary system at around  $Mo_2Ni$  composition. The ground state of the Mo-Ni system (Figure 8-3) shows that  $Mo_2Ni$  is the only  $\sigma$  phase configuration with negative enthalpy of formation and is nearly stable in the Mo-Ni binary system. To avoid stabilizing the  $\sigma$  phase in the Mo-Ni binary and obtain better agreement in the ternary region, the Mo-Ni and Mo-Ni-Re phase diagram were calculated by assigning different values to  $-\Delta S_{Ni}^{\sigma}$ . The manual adjustment of the parameter showed that calculated and experimental Mo-Ni-Re  $\sigma$  phase homogeneity domains are in better agreement at lower values of  $-\Delta S_{Ni}^{\sigma}$  and the minimum value of  $-\Delta S_{Ni}^{\sigma}$  at which  $\sigma$  does not appear in the Mo-Ni system was found to be 8.1. Therefore, the term  $-\Delta S_{Ni}^{\sigma}$  was fixed to 8.1 during the present assessment of the Mo-Ni-Re system. In case of  $\delta$  phase, the parameter corresponding to entropy ( $-\Delta S_{Ni:Re:Mo}^{\delta}$ ) and excess Gibbs energy  ${}^0L_{Ni:Mo,Re:Mo}^{\delta}$  were optimized. However, the calculated homogeneity domain of the  $\delta$  phase lies at higher Ni content. Attempt were made to move the  $\delta$  phase homogeneity domain to higher Mo content in order to obtain a better fit with experimental information but all such attempts resulted change in ranges where fcc and phase with prototype  $Mo_3CoSi$  appear. The extension of phase with prototype  $Mo_3CoSi$  as well as the  $\sigma'$  phase which was modeled as a line compound showed good agreement with the experimental data.

By using the present thermodynamic description of the Mo-Ni-Re system, isothermal sections of the Mo-Ni-Re system were also calculated at the temperatures between 1200°C and 1600°C. The 1300°C isothermal section of the Mo-Ni-Re system illustrated in Figure 8-10

showed presence of all the phases evidenced in 1200°C isothermal section with slight changes in their homogeneity domains. The isothermal section of the Mo-Ni-Re system calculated at 1400°C, illustrated in Figure 8-11, showed presence of the liquid phase found in equilibrium with bcc, fcc and  $\sigma$  phase. The ternary phase with prototype  $\text{Mo}_3\text{CoSi}$  and  $\delta$  phase were not stable at 1400°C whereas the homogeneity domain of the  $\sigma'$  phase decreased with increase in the temperature. The presence of the  $\sigma'$  phase was not evidenced in the 1500°C isothermal section (Figure 8-12). The composition range of  $\chi$  and bcc phase changed very little with temperature whereas composition range of liquid and hcp phase increased with increase in the temperature.

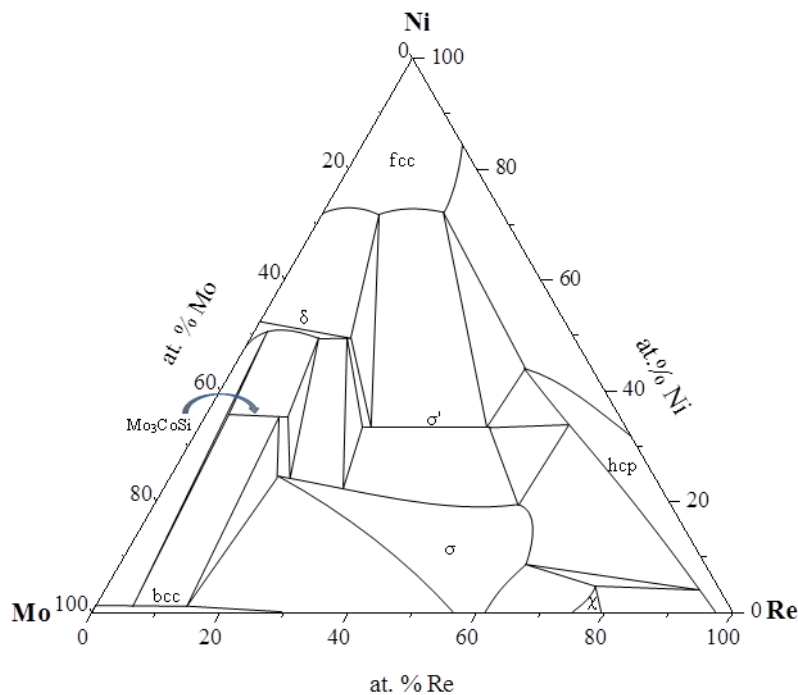


Figure 8-10: Calculated Mo-Ni-Re isothermal section at 1300°C

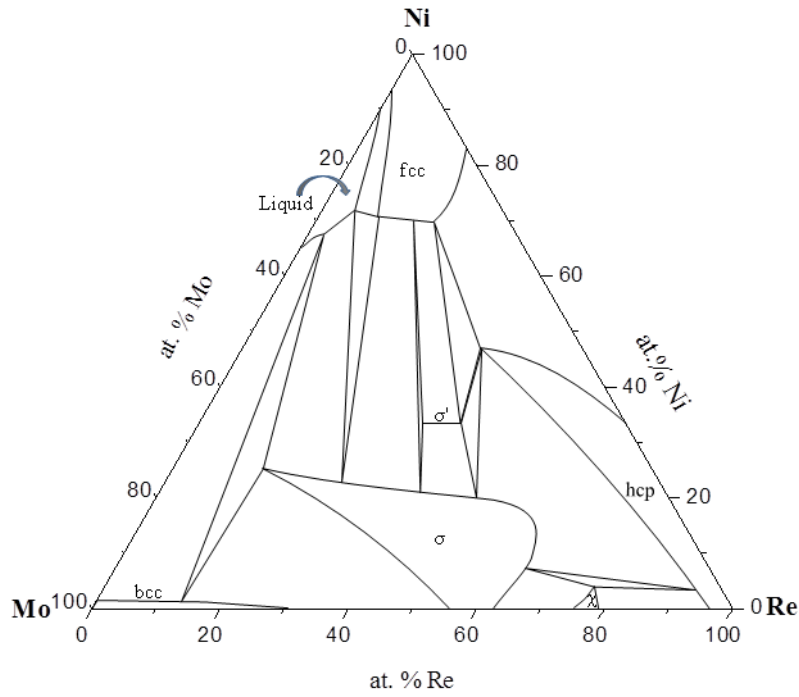


Figure 8-11: Calculated Mo-Ni-Re isothermal section at 1400°C

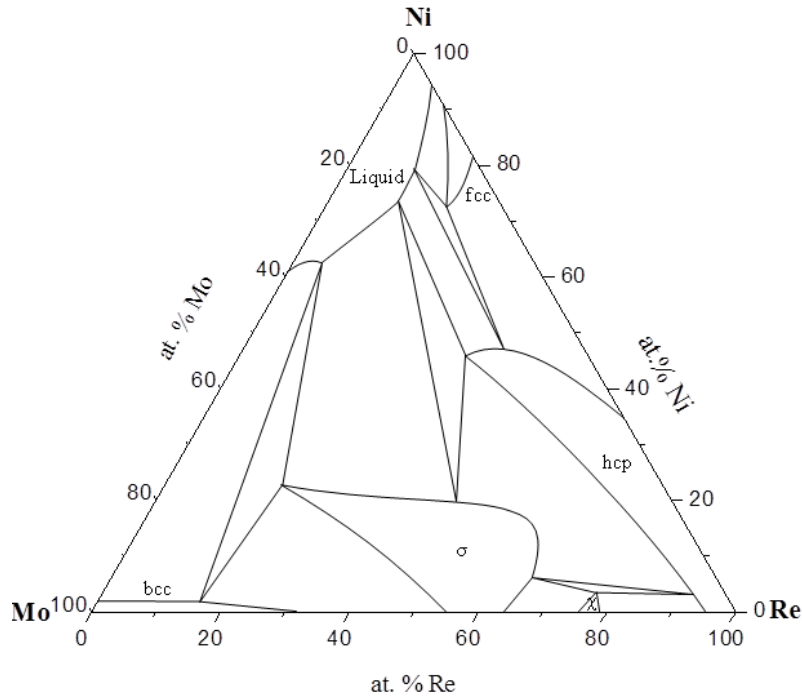


Figure 8-12: Calculated Mo-Ni-Re isothermal section at 1500°C

#### 8.4.4. Conclusion

Thermodynamic assessment of the Mo-Ni-Re system was carried out by combining thermodynamic descriptions of the Mo-Ni and Ni-Re binary systems proposed during the present study and recent assessment of the Mo-Re system performed by Nathalie Dupin [1]. During the present study, minimum number of parameters was optimized to obtain a good

description of the studied system e.g., in case of  $\sigma$  and  $\chi$  phase for which the most complex thermodynamic models were used; only entropy of Ni  $\sigma$  and Ni  $\chi$  was optimized. The parameters corresponding to the enthalpies of formation of the intermetallic phases were fixed to the values obtained from the DFT calculations [21, 22]. The use of DFT values provides a good idea about the starting values of the respective parameters but fixing the parameters to the DFT values (approach used during the present study) also restricts the agreement that can be obtained with the input experimental information. Considering the constraints coming from fixing the enthalpies of formation to the DFT values, and total number of optimized variables, the calculated Mo-Ni-Re phase diagram can be considered as in reasonably good agreement with the input experimental information. As a next step, thermodynamic assessment of the Mo-Ni-Re system can be performed by using simpler models for  $\sigma$  and  $\chi$  phase. Comparison of these thermodynamic descriptions would help in finding out the most suitable model for  $\sigma$  and  $\chi$  phases which exist in number of alloy systems.

## **8.5. Conclusion of the chapter**

The thermodynamic reassessment of the Mo-Ni binary system was carried out to incorporate recent data and to obtain a better description of the system with minimum number of optimized parameter. The calculated experimental phase diagram showed good agreement with selected experimental and calculation data. By combining the thermodynamic descriptions of the Mo-Ni and Ni-Re binary systems (Chapter 4) proposed during the present study with recent description of the Mo-Re system proposed by Nathalie Dupin [1], thermodynamic modeling of the Mo-Ni-Re system was carried out with the help of Calphad method. During thermodynamic assessment of the Mo-Ni-Re system, the phase equilibria information gathered during present study (Chapter 5) and the enthalpies of formation of the constituent phases calculated by J.-C Crivello [21] were used. The calculated isothermal sections of the Mo-Ni-Re system showed fairly good agreement with selected input information. Thermodynamic description of the Mo-Ni-Re system proposed during the present study when combined with description of other subsystems of Ni based superalloys would help in prediction of phase equilibria (by extrapolation) in higher order systems and ultimately in selection of suitable alloy compositions to avoid the precipitation of TCP phases.

**References**

- [1] N. Dupin, UnPublished work.
- [2] J.-C. Crivello, A. Breidi, UnPublished work.
- [3] K. Frisk, A thermodynamic evaluation of the Mo-Ni system, *Calphad* 14 (3) (1990) 311-320.
- [4] Y. Cui, X. Lu, Z. Jin, Experimental study and thermodynamic assessment of the Ni-Mo-Ta ternary system, *Metall. Mater. Trans. A* 30A (1999) 2735-2744.
- [5] M. Morishita, K. Koyama, S. Yagi, G. Zhang, Calculated phase diagram of the Ni-Mo-B ternary system, *Journal of Alloys and Compounds* 314 (2001) 212-218.
- [6] S. H. Zhou, Y. Wang, C. Jiang, J. Z. Zhu, L.-Q. Chen, Z.-K. Liu, First-principles calculations and thermodynamic modeling of the Ni-Mo system, *Materials Science and Engineering A* 397 (2005) 288-296.
- [7] Y. Wang, C. Woodward, S. H. Zhou, Z.-K. Liu, L.-Q. Chen, Structural stability of Ni-Mo compounds from first-principles calculations, *Scr. Mater.* 52 (2005) 17-20.
- [8] J. P. Perdew, J. A. Chevary, S. H. Vosko, K. A. Jackson, M. R. Pederson, D. J. Singh, C. Fiolhais, Atoms, molecules, solids, and surfaces: applications of the generalized gradient approximation for exchange and correlation, *Physical Review B* 46 (1992) 6671-6687.
- [9] C. P. Heijwegen, G. D. Rieck, Determination of the phase diagram of the molybdenum-nickel system using diffusion couples and equilibrated alloys, *Z. Metallkde.* 64 (1973) 450-453.
- [10] C. B. Shoemaker, D. P. Shoemaker, The crystal structure of the  $\delta$  phase, Mo-Ni, *Acta Crystallogr.* 16 (1963) 997-1009.
- [11] B. Sundman, B. Jansson, J. O. Andersson, The Thermo-Calc databank system, *Calphad* 9 (2) (1985) 153-190.
- [12] R. E. W. Casselton, W. Hume-Rothery, The equilibrium diagram of the system molybdenum-nickel, *Journal of the less-common metals* 7 (1964) 212-221.
- [13] S.-J. L. Kang, Y.-D. Song, W. A. Kaysser, H. Hofmann, Determination of Mo solidus in the Mo-Ni system by electrolytic phase separation method, *Z. Metallkde.* 75 (1984) 86-91.
- [14] I. Katayama, H. Shimatani, Z. Kozuka, *J. Japan Inst Metals* 37 (1973) 509-515.
- [15] L. L. Meshkov, L. S. Guzei, E. M. Sokolovskaya, Thermodynamics of nickel-molybdenum alloys, *Russian Journal of Physical Chemistry* 49 (8) (1975) 1128-1129.
- [16] H. L. Tsai, Ph.D. Thesis, University of Tennessee, Knoxville, Tennessee (1983).
- [17] L. Pejryd, Thesis, Department of inorganic chemistry, University of Umeå, Sweden (1985).
- [18] Pingli Mao, Ke Han, Yan Xin, Thermodynamic assessment of the Mo-Re binary system, *J. Alloys Compd.* 464 (2008) 190-196.
- [19] S.-A. Farzadfar, M. Levesque, M. Phejar, J.-M. Joubert, Thermodynamic assessment of the Molybdenum-Rhenium System, *Calphad: Comput. Coupling Phase Diagrams Thermochem.* 33 (2009) 502-510.

- [20] Y. Yang, C. Zhang, S. Chen, D. Morgan, Y. A. Chang, First-principles calculation aided thermodynamic modeling of the Mo-Re system, *Intermetallics* 18 (2010) 574-581.
- [21] J.-C. Crivello, UnPublished work.
- [22] K. Yaqoob, J.-C. Crivello, J.-M. Joubert, Comparison of the site occupancies determined by combined Rietveld refinement and density functional theory calculations: example of the ternary Mo-Ni-Re s phase, *Inorg. Chem.* 51 (2012) 3071-3078.
- [23] E. I. Gladyshevskii, P. I. Kripyakevich, R. V. Skolozdra, Crystal structure of  $\text{Mo}_3\text{CoSi}$ , *Sov. Phys. - Dokl* 12 (8) (1968) 755-758.

# **Conclusion and Perspectives**



## Conclusion and Perspectives

The Mo-Ni-Re is an important subsystem for development of Ni based superalloys because addition of Mo and Re imparts significant resistance to their mechanical degradation provided the precipitation of TCP phases could be avoided. However, it has been the subject of controversial reports. Therefore, phase equilibria determination of the Mo-Ni-Re system was required. In addition, existence of  $\sigma$ ,  $\chi$  and  $\delta$  phases in the constituent binary systems and possible presence of two pure ternary compounds (P and R) makes Mo-Ni-Re an interesting system to study the crystal chemistry of the TCP phases and to test new models for their thermodynamic descriptions. The TCP phases, particularly  $\sigma$  and  $\chi$ , have been the subject of two extensive studies [1, 2] conducted at our lab and are an integral part of the ongoing research activity (Project ARMIDE). During the present study, a complete experimental redetermination of Mo-Ni-Re phase equilibria followed by crystal chemistry study of its constituent TCP phases and thermodynamic modeling of the system with the help of the Calphad method, was carried out.

Prior to the experimental as well as thermodynamic study of the Mo-Ni-Re system, it is important that phase boundaries in the constituent binary systems are well determined. The literature search conducted during present study revealed need of substantial experimentation to determine exact phase relationship in the Ni-Re binary system. The experimental reinvestigation of the Ni-Re binary system was therefore carried out which allowed us to develop better understanding of the system in terms of positions of phase boundaries, freezing ranges of the solid solutions, and the invariant reaction temperature. Most of the results gathered during present study were confirmed by more than one alloy compositions. By combining the results gathered during present study with some of the recent partial investigations, a new experimental Ni-Re phase diagram was proposed which was considerably different from the previously accepted phase diagram. In addition to the Ni-Re system, some experimentation was also carried out for confirmation of phase boundaries in the Mo-Ni and Mo-Re binary systems. The results of experimental investigation of constituent binary systems were used as reference for the experimental investigation of Mo-Ni-Re system.

Once the phase boundaries in the constituent binary systems have been established, complete experimental redetermination of the Mo-Ni-Re system was carried out. Due to refractory nature of constituent elements, high annealing temperatures such as 1200°C and 1600°C were

selected for the present study. At 1200°C, long annealing treatments (1680 hours) were shown to be necessary in order to reach equilibrium whereas 9 hours of annealing were sufficient at 1600°C. The phase equilibria investigation of the Mo-Ni-Re system was achieved by chemical and structural characterization of large number of annealed samples. The isothermal sections proposed during present study revealed very large composition range of  $\sigma$  phase in 1200°C as well as in 1600°C isothermal sections whereas Mo-Ni  $\delta$  phase was found to have considerable extension in the 1200°C isothermal section only as a function of Re content. The ternary extension of Mo-Re  $\chi$  phase in the studied isothermal sections was restricted to only few at. % Ni. In addition to the large extension of  $\sigma$  and  $\delta$  phases, presence of two previously unknown ternary intermetallic compounds was also evidenced in the 1200°C isothermal section. The crystal structure identification of one of the ternary phases was achieved with the help of XRD measurements which showed structural prototype of  $\text{Mo}_3\text{CoSi}$ . However, the crystal structure of the second ternary phase could not be identified with the help of XRD measurements due to poor quality of the quality of diffraction pattern. The single crystal diffraction being a more powerful technique was finally employed for the crystal structure identification of the unknown ternary. A comparison of the XRD and single crystal diffraction measurements revealed that this phase has a modulated structure based on  $\sigma$  structure. This ternary phase because of its similarity with  $\sigma$  was named as  $\sigma'$  phase. The EPMA and XRD measurements of different alloys investigated during present study confirmed that  $\sigma$  and  $\sigma'$  are two distinct phases and are also present in equilibrium in the Mo-Ni-Re system. The  $\sigma$  phase has been previously reported in 43 binary and several ternary systems. However, presence of a modulated  $\sigma$  structure has been evidenced for the first time in any alloy system. In comparison with previous studies of the Mo-Ni-Re system, the 1200°C isothermal section proposed during present study resembles to some extent with the previous study by Borisov et al. [3]. However, crystal structure identification of ternary phases, determination of phase boundaries by chemical and structural characterization of large number of annealed samples, and good agreement with constituent binaries data are the characteristic features of the present experimental investigation of the Mo-Ni-Re system.

In addition to the phase equilibria study, partial investigation of the liquidus projection of the Mo-Ni-Re system was also carried out and primary crystallization fields of different phases have been proposed. The  $\sigma$ , bcc and hcp phases were found to crystallize as primary phases over large composition ranges whereas primary crystallization field  $\delta$  phase will be restricted

to few at. % Re. None of the ternary phase was found to crystallize as primary phase in the studied system.

The site occupancies of a phase play a very important role in selection of suitable thermodynamic model. In case of the binary TCP phases, site occupation trends are well understood. However, atom distribution in ternary extensions of these phases has not been studied in detail. Considering large extension of the Mo-Ni-Re  $\sigma$  phase in the studied isothermal sections, its structural characterization with particular emphasis on determination of site occupancies was carried out. The results gathered during present study clearly showed preference of smaller (Ni) and larger (Mo) atoms for low and high CN sites respectively whereas intermediate size atom (Re) showed dual preference depending on the composition proportions of the other two elements. In addition, determination of site occupancies at different compositions of the Mo-Ni-Re  $\sigma$  phase revealed that crystallographic sites with CN 14 and 15 show similar site occupation behavior whereas sites with CN12 also show similar trends. Therefore, it was concluded that three sites with higher coordination number (CN 14 and CN 15) can be combined on one sublattice whereas two sites with CN 12 can be combined on another sublattice. As a result, ternary  $\sigma$  phase can be described by using two-sublattice model. Furthermore, the comparison of experimental site occupancies with the ones obtained by DFT calculations also showed very good agreement which confirmed the validity of both techniques.

Thermodynamic modeling of a ternary system requires accurate description of the constituent binary systems. Therefore thermodynamic assessment of the Ni-Re binary system was carried out with the help of new experimental information gathered during the present study. The calculated Ni-Re phase diagram reproduced well the selected experimental information. Similarly reassessment of the Mo-Ni binary system was carried out to incorporate DFT data recently calculated by J.-C Crivello [4]. The calculated Mo-Ni phase diagram showed a good agreement with experimental and DFT information with minimum number of optimized variables. The thermodynamic description of the Mo-Re binary system was taken from a recent study [5].

After experimental investigation of Mo-Ni-Re phase equilibria, structural characterization of its constituent phases and thermodynamic modeling of the constituent binary systems, thermodynamic modeling of the Mo-Ni-Re system was carried out. The phase equilibria information gathered during present study were used as input data for thermodynamic modeling of the Mo-Ni-Re system. The DFT calculations of enthalpies of formation of all the

possible ordered configurations of  $\sigma$  and  $\chi$  phases by J.-C Crivello allowed us to study the use of most complex models for these phases. Besides thermodynamic modeling of Mo-Ni-Re system, one of the purposes of present study was to see if DFT values can be directly used in the frame of modeling. Therefore, enthalpies of formation of all end-members of intermetallic phases defined by their respective sublattice model were fixed to the DFT values [6]. Thermodynamic assessment of the Mo-Ni-Re system carried out during present study showed fairly good agreement with experimental data without optimization of excess terms for  $\sigma$  and  $\chi$  phases which showed the possibility of direct use of DFT data in the frame of thermodynamic modeling. The present thermodynamic description of the Mo-Ni-Re system can be combined with thermodynamic description of other important ternary systems to predict phase equilibria in higher order systems.

The work carried out during three years of Ph.D. has allowed us to develop better understanding of the Mo-Ni-Re phase equilibria, primary crystallization fields of the constituent phases, structural characterization of Mo-Ni-Re ternary phases, site occupancy trends in Mo-Ni-Re  $\sigma$  phase and thermodynamic modeling of the Mo-Ni-Re system. In addition, a new experimental and thermodynamic description of the Ni-Re binary system has also been proposed. However, it would be interesting to carry out the following studies in future to further enhance understanding of the Mo-Ni-Re system:

- DTA measurements can be performed on the selected Mo-Ni-Re alloy compositions to study nature of invariant reactions in liquidus projection of the system.
- The crystal structure of the Mo-Ni-Re  $\sigma'$  phase can be studied in more detail after improving the quality of  $\sigma'$  crystals.
- Thermodynamic assessment of the Mo-Ni-Re system can be performed with relatively simpler model for  $\sigma$  and  $\chi$  phase and compared with present thermodynamic assessment of the Mo-Ni-Re system to study the effect of simplification of models on the excess Gibbs energy terms and calculated phase diagrams. The possibility of using two-sublattice model for  $\sigma$  phase has already been shown during the present study

In a much broader scope, the present thermodynamic description of the Ni-Re binary systems as it is based on more consistent results, can be used in thermodynamic assessment/reassessment of several important systems such as Cr-Ni-Re, Fe-Ni-Re, Mn-Ni-Re, Mo-Ni-Re, Nb-Ni-Re, Ni-Re-Ta, Ni-Re-Ti, Ni-Re-V, Ni-Re-Zr. On the other hand, systematic study of ternary TCP phases to determine site preference trends is still an open field of research. The comparison of experimental and calculated site occupancies of Mo-Ni-

Re  $\sigma$  phase determined during present study showed a very good agreement. Although difficult, due to necessary contrast requirements and large number of enthalpies of formation one has to calculate, the approach used during the present study can be extended to other ternary  $\sigma$  and TCP phases to see if the same good agreement between experimental and calculated site occupancies can be obtained.

## References

- [1] J.-M. Joubert, Crystal chemistry and Calphad modelling of the  $\sigma$  phase, *Prog. Mater. Sci.* 53 (2008) 528-583.
- [2] J.-M. Joubert, M. Phejar, The crystal chemistry of the  $\chi$  phase, *Prog. Mater. Sci.* 54 (7) (2009) 945-980.
- [3] V. A. Borisov, A. I. Yaschenko, E. M. Slyusarenko, S. F. Dunaev, An investigation of solid-phase interactions in the Ni-Mo-Re system at 1425 K, *Moscow University Chemistry Bulletin* 47 (5) (1992) 76-79.
- [4] J.-C. Crivello, A. Breidi, UnPublished work.
- [5] N. Dupin, UnPublished work.
- [6] J.-C. Crivello, UnPublished work.



# **Annexes**



# Annex I

Table A-I: Enthalpies of formation of the Mo-Ni-Re  $\sigma$  phase obtained with the help of DFT calculations by J.-C Crivello [1].

End-members	$\Delta H^{\text{for}}$ (J/mole)	End-members	$\Delta H^{\text{for}}$ (J/mole)	End-members	$\Delta H^{\text{for}}$ (J/mole)
Mo:Mo:Mo:Mo:Mo	482948	Re:Ni:Re:Ni:Re	236287	Mo:Mo:Mo:Re:Ni	285703
Ni:Ni:Ni:Ni:Ni	407462	Re:Ni:Re:Re:Ni	365944	Mo:Re:Re:Mo:Ni	410644
Re:Re:Re:Re:Re	279917	Re:Ni:Ni:Re:Re	721124	Mo:Re:Mo:Mo:Ni	449592
Ni:Mo:Mo:Ni:Mo	-23006	Ni:Re:Re:Ni:Re	16196	Re:Re:Re:Mo:Ni	359967
Ni:Mo:Mo:Mo:Ni	457954	Ni:Re:Re:Re:Ni	178921	Re:Re:Mo:Mo:Ni	400377
Mo:Ni:Ni:Mo:Mo	653360	Ni:Re:Ni:Re:Re	349300	Re:Mo:Mo:Re:Ni	227681
Mo:Ni:Mo:Mo:Ni	637869	Re:Re:Re:Ni:Re	55856	Mo:Re:Mo:Re:Ni	254426
Mo:Ni:Mo:Ni:Mo	237678	Re:Re:Re:Re:Ni	205471	Ni:Mo:Ni:Re:Mo	244018
Ni:Ni:Ni:Mo:Mo	522347	Re:Re:Ni:Re:Re	534887	Ni:Mo:Ni:Re:Re	248972
Ni:Ni:Mo:Mo:Ni	520433	Ni:Ni:Re:Re:Re	348598	Ni:Re:Ni:Mo:Mo	340397
Ni:Ni:Mo:Ni:Mo	218956	Re:Ni:Re:Re:Re	415817	Ni:Mo:Ni:Mo:Re	269636
Mo:Mo:Ni:Ni:Mo	221227	Ni:Re:Re:Re:Re	160325	Ni:Re:Ni:Mo:Re	344666
Mo:Mo:Mo:Ni:Ni	203386	Ni:Re:Mo:Mo:Mo	361238	Ni:Re:Ni:Re:Mo	280819
Mo:Mo:Ni:Mo:Ni	325286	Ni:Mo:Mo:Re:Mo	-25655	Ni:Mo:Re:Ni:Mo	-1E+05
Ni:Mo:Ni:Ni:Mo	74007	Ni:Re:Re:Mo:Mo	246762	Ni:Mo:Mo:Ni:Re	-65114
Ni:Mo:Mo:Ni:Ni	178264	Ni:Re:Mo:Re:Mo	5060.9	Ni:Re:Mo:Ni:Mo	-17956
Ni:Mo:Ni:Mo:Ni	122358	Ni:Mo:Mo:Mo:Re	254893	Ni:Mo:Re:Ni:Re	-45809
Mo:Ni:Ni:Ni:Mo	270588	Ni:Re:Mo:Mo:Re	280952	Ni:Re:Mo:Ni:Re	-4155
Mo:Ni:Mo:Ni:Ni	105182	Ni:Mo:Re:Mo:Re	261854	Ni:Re:Re:Ni:Mo	-1E+05
Ni:Ni:Ni:Ni:Mo	198059	Ni:Re:Re:Mo:Re	288612	Ni:Re:Mo:Re:Ni	222892
Mo:Ni:Ni:Mo:Ni	403731	Ni:Mo:Re:Re:Mo	-36044	Ni:Mo:Re:Re:Ni	184990
Ni:Ni:Ni:Mo:Ni	243528	Ni:Mo:Mo:Re:Re	-19147	Ni:Re:Mo:Mo:Ni	381561
Ni:Ni:Mo:Ni:Ni	108559	Ni:Re:Re:Re:Mo	-14978	Ni:Mo:Mo:Re:Ni	235771
Ni:Mo:Mo:Mo:Mo	374649	Ni:Re:Mo:Re:Re	46683	Ni:Mo:Re:Mo:Ni	348439
Ni:Mo:Ni:Ni:Ni	85034	Ni:Mo:Re:Re:Re	84787	Ni:Re:Re:Mo:Ni	307196
Mo:Ni:Ni:Ni:Ni	269155	Ni:Mo:Re:Mo:Mo	261668	Re:Ni:Ni:Mo:Re	634040
Mo:Mo:Ni:Ni:Ni	184113	Mo:Ni:Re:Mo:Re	650958	Mo:Ni:Ni:Re:Re	744186
Ni:Ni:Mo:Mo:Mo	651408	Re:Ni:Re:Mo:Re	628586	Mo:Ni:Ni:Re:Mo	640623
Mo:Mo:Ni:Mo:Mo	456885	Re:Ni:Re:Mo:Mo	629332	Re:Ni:Ni:Mo:Mo	611802
Mo:Ni:Mo:Mo:Mo	812050	Mo:Ni:Re:Mo:Mo	683112	Re:Ni:Ni:Re:Mo	592216
Mo:Mo:Mo:Ni:Mo	44347	Mo:Ni:Re:Re:Mo	381058	Mo:Ni:Ni:Mo:Re	674384
Mo:Mo:Mo:Mo:Ni	539672	Re:Ni:Re:Re:Mo	323048	Re:Ni:Mo:Ni:Re	178167

Ni:Mo:Ni:Mo:Mo	340144	Re:Ni:Mo:Mo:Mo	760003	Re:Ni:Re:Ni:Mo	160233
Re:Mo:Mo:Mo:Mo	405160	Mo:Ni:Mo:Mo:Re	667521	Mo:Ni:Re:Ni:Mo	172487
Mo:Re:Mo:Mo:Mo	481369	Mo:Ni:Mo:Re:Re	392715	Mo:Ni:Re:Ni:Re	213544
Re:Re:Mo:Mo:Mo	421630	Re:Ni:Mo:Re:Re	362508	Re:Ni:Mo:Ni:Mo	238154
Mo:Mo:Mo:Re:Mo	140592	Re:Ni:Mo:Mo:Re	631137	Mo:Ni:Mo:Ni:Re	162706
Mo:Mo:Re:Mo:Mo	385456	Mo:Ni:Mo:Re:Mo	437657	Re:Ni:Mo:Re:Ni	368043
Mo:Mo:Mo:Mo:Re	371133	Mo:Ni:Re:Re:Re	453057	Re:Ni:Re:Mo:Ni	630757
Re:Mo:Mo:Re:Mo	54935	Re:Ni:Mo:Re:Mo	383833	Mo:Ni:Re:Re:Ni	389398
Re:Mo:Re:Mo:Mo	300108	Ni:Ni:Mo:Re:Re	264907	Re:Ni:Mo:Mo:Ni	626933
Re:Mo:Mo:Mo:Re	305993	Ni:Ni:Re:Re:Mo	242750	Mo:Ni:Mo:Re:Ni	387765
Mo:Re:Mo:Re:Mo	171606	Ni:Ni:Re:Mo:Mo	540006	Mo:Ni:Re:Mo:Ni	665732
Mo:Re:Re:Mo:Mo	377065	Ni:Ni:Mo:Mo:Re	537575	Ni:Ni:Ni:Mo:Re	539381
Mo:Re:Mo:Mo:Re	411014	Ni:Ni:Mo:Re:Mo	295671	Ni:Ni:Ni:Re:Mo	484573
Re:Re:Mo:Re:Mo	109576	Ni:Ni:Re:Mo:Re	531589	Ni:Ni:Re:Ni:Mo	142810
Re:Re:Re:Mo:Mo	318049	Re:Mo:Ni:Mo:Re	355867	Ni:Ni:Mo:Ni:Re	176540
Re:Re:Mo:Mo:Re	372490	Mo:Re:Ni:Mo:Re	492190	Ni:Ni:Re:Mo:Ni	543679
Mo:Mo:Re:Mo:Re	364502	Re:Re:Ni:Mo:Re	463203	Ni:Ni:Mo:Re:Ni	331499
Mo:Mo:Mo:Re:Re	107246	Mo:Re:Ni:Re:Mo	494740	Re:Re:Ni:Ni:Mo	180190
Mo:Mo:Re:Re:Mo	113323	Re:Re:Ni:Re:Mo	468276	Re:Mo:Ni:Ni:Mo	138831
Re:Mo:Re:Re:Mo	29635	Mo:Re:Ni:Mo:Mo	472781	Mo:Re:Ni:Ni:Mo	246139
Re:Mo:Re:Mo:Re	309302	Mo:Mo:Ni:Re:Mo	422997	Mo:Mo:Ni:Ni:Re	264596
Re:Mo:Mo:Re:Re	48599	Re:Re:Ni:Mo:Mo	424439	Re:Mo:Ni:Ni:Re	208897
Mo:Re:Re:Re:Mo	157797	Re:Mo:Ni:Mo:Mo	388417	Mo:Re:Ni:Ni:Re	360441
Mo:Re:Re:Mo:Re	424564	Mo:Mo:Ni:Re:Re	469122	Re:Re:Ni:Mo:Ni	238160
Mo:Re:Mo:Re:Re	197915	Re:Mo:Ni:Re:Re	424510	Mo:Re:Ni:Re:Ni	384783
Re:Re:Re:Re:Mo	96754	Mo:Re:Ni:Re:Re	589659	Re:Mo:Ni:Re:Ni	290470
Re:Re:Re:Mo:Re	392450	Re:Mo:Ni:Re:Mo	372921	Mo:Re:Ni:Mo:Ni	310591
Re:Re:Mo:Re:Re	161081	Mo:Mo:Ni:Mo:Re	406789	Mo:Mo:Ni:Re:Ni	360830
Mo:Mo:Re:Re:Re	205631	Mo:Re:Re:Ni:Re	71799	Re:Mo:Ni:Mo:Ni	241865
Re:Mo:Re:Re:Re	160345	Mo:Re:Re:Ni:Mo	-43075	Mo:Re:Mo:Ni:Ni	154349
Mo:Re:Re:Re:Re	313761	Re:Mo:Mo:Ni:Mo	-37637	Re:Mo:Mo:Ni:Ni	173576
Re:Ni:Ni:Ni:Ni	300179	Re:Re:Re:Ni:Mo	-97816	Re:Re:Mo:Ni:Ni	143030
Ni:Re:Ni:Ni:Ni	198703	Mo:Re:Mo:Ni:Re	3501.1	Mo:Re:Re:Ni:Ni	221456
Re:Re:Ni:Ni:Ni	217907	Re:Re:Mo:Ni:Re	-21819	Mo:Mo:Re:Ni:Ni	263254
Ni:Ni:Re:Ni:Ni	243532	Mo:Mo:Mo:Ni:Re	-33036	Re:Mo:Re:Ni:Ni	227942
Ni:Ni:Ni:Re:Ni	353134	Re:Mo:Mo:Ni:Re	-87959	Ni:Re:Ni:Ni:Mo	161279
Ni:Ni:Ni:Ni:Re	361687	Mo:Mo:Re:Ni:Mo	-15976	Ni:Mo:Ni:Ni:Re	188216
Re:Ni:Re:Ni:Ni	255755	Mo:Mo:Re:Ni:Re	19221	Ni:Mo:Ni:Re:Ni	179601

Re:Ni:Ni:Re:Ni	420477	Mo:Re:Mo:Ni:Mo	15814	Ni:Re:Ni:Mo:Ni	148130
Re:Ni:Ni:Ni:Re	436287	Re:Mo:Re:Ni:Re	-25501	Ni:Re:Mo:Ni:Ni	114244
Ni:Re:Re:Ni:Ni	159634	Re:Re:Mo:Ni:Mo	-41416	Ni:Mo:Re:Ni:Ni	171706
Ni:Re:Ni:Re:Ni	214123	Re:Mo:Re:Ni:Mo	-1E+05	Mo:Ni:Ni:Ni:Re	416541
Ni:Re:Ni:Ni:Re	318629	Mo:Mo:Re:Mo:Ni	466454	Re:Ni:Ni:Ni:Mo	272072
Re:Re:Re:Ni:Ni	209158	Re:Re:Mo:Re:Ni	225748	Mo:Ni:Ni:Re:Ni	455472
Re:Re:Ni:Re:Ni	330025	Mo:Re:Re:Re:Ni	246252	Re:Ni:Ni:Mo:Ni	360892
Re:Re:Ni:Ni:Re	331076	Re:Mo:Re:Mo:Ni	392478	Re:Ni:Mo:Ni:Ni	144946
Ni:Ni:Re:Ni:Re	184201	Mo:Mo:Re:Re:Ni	261828	Mo:Ni:Re:Ni:Ni	231147
Ni:Ni:Re:Re:Ni	352366	Re:Mo:Mo:Mo:Ni	467994	Mo:Re:Ni:Ni:Ni	252948
Ni:Ni:Ni:Re:Re	590427	Re:Mo:Re:Re:Ni	195388	Re:Mo:Ni:Ni:Ni	135782

## Annex II

Table A-II: Enthalpies of formation of the Mo-Ni-Re  $\chi$  phase obtained with the help of DFT calculations by J.-C Crivello unpublished work [2].

End-members	$\Delta H^{\text{for}}$ (J/mole)	End-members	$\Delta H^{\text{for}}$ (J/mole)	End-members	$\Delta H^{\text{for}}$ (J/mole)
Mo:Mo:Mo:Mo	1515300	Re:Re:Mo:Re	628540.7	Re:Ni:Re:Mo	1463254
Ni:Ni:Ni:Ni	785886.9	Mo:Mo:Re:Re	-73075.8	Re:Ni:Mo:Mo	2285246
Re:Re:Re:Re	284377.6	Re:Mo:Re:Re	-13923.8	Mo:Ni:Mo:Re	792011.9
Ni:Mo:Mo:Mo	1709858	Mo:Re:Re:Re	200919.3	Ni:Ni:Re:Mo	1512671
Mo:Ni:Mo:Mo	2228822	Re:Ni:Ni:Ni	678899.4	Ni:Ni:Mo:Re	897158.9
Ni:Ni:Mo:Mo	2355029	Ni:Re:Ni:Ni	322911.2	Re:Mo:Ni:Re	630250
Mo:Mo:Ni:Mo	1041246	Re:Re:Ni:Ni	187543.8	Mo:Re:Ni:Re	659201.3
Mo:Mo:Mo:Ni	732230.1	Ni:Ni:Re:Ni	810613.9	Re:Re:Ni:Mo	1086364
Ni:Mo:Ni:Mo	1145223	Ni:Ni:Ni:Re	638283.6	Re:Mo:Ni:Mo	1065866
Ni:Mo:Mo:Ni	835396.2	Re:Ni:Re:Ni	724722.4	Mo:Re:Ni:Mo	1023838
Mo:Ni:Ni:Mo	949494.8	Re:Ni:Ni:Re	520416	Mo:Mo:Ni:Re	558310.8
Mo:Ni:Mo:Ni	580676.8	Ni:Re:Re:Ni	373518.5	Re:Mo:Re:Ni	203444.6
Ni:Ni:Ni:Mo	1102605	Ni:Re:Ni:Re	726923.9	Mo:Mo:Re:Ni	179598.4
Ni:Ni:Mo:Ni	816515.1	Re:Re:Re:Ni	215250.1	Mo:Re:Re:Ni	189896.9
Mo:Mo:Ni:Ni	33929.46	Re:Re:Ni:Re	754395.1	Re:Mo:Mo:Ni	745388.8
Ni:Mo:Ni:Ni	36508.45	Ni:Ni:Re:Re	334484.2	Mo:Re:Mo:Ni	596337.8
Mo:Ni:Ni:Ni	589307.7	Re:Ni:Re:Re	254496.4	Re:Re:Mo:Ni	601202.6
Re:Mo:Mo:Mo	1545752	Ni:Re:Re:Re	380239.9	Ni:Re:Ni:Mo	1162767
Mo:Re:Mo:Mo	1583844	Ni:Mo:Mo:Re	461107.8	Ni:Mo:Ni:Re	589508.5
Re:Re:Mo:Mo	1630154	Ni:Re:Mo:Re	704174.2	Ni:Re:Mo:Ni	784523.1
Mo:Mo:Re:Mo	811122.5	Ni:Mo:Re:Mo	1016226	Ni:Mo:Re:Ni	285241.3
Mo:Mo:Mo:Re	324471	Ni:Re:Mo:Mo	1817105	Re:Ni:Ni:Mo	948295.5
Re:Mo:Re:Mo	836134.9	Ni:Mo:Re:Re	62299.93	Mo:Ni:Ni:Re	408690.5
Re:Mo:Mo:Re	380123.5	Ni:Re:Re:Mo	1177757	Re:Ni:Mo:Ni	680472.6
Mo:Re:Re:Mo	977650.5	Re:Ni:Mo:Re	879271	Mo:Ni:Re:Ni	607442.1
Mo:Re:Mo:Re	535693.2	Mo:Ni:Re:Mo	1438585	Re:Mo:Ni:Ni	6330.553
Re:Re:Re:Mo	1033207	Mo:Ni:Re:Re	184386.5	Mo:Re:Ni:Ni	182701

### Reference

- [1] K. Yaqoob, J.-C. Crivello, J.-M. Joubert, Comparison of the site occupancies determined by combined Rietveld refinement and density functional theory calculations: example of the ternary Mo-Ni-Re  $\chi$  phase, *Inorg. Chem.* 51 (2012) 3071-3078.
- [2] J.-C. Crivello, UnPublished work.

# Annex III

## Mo-Ni-Re TDB file

\$ Database file written 2012-11-19

\$ From database: USER

ELEMENT /- ELECTRON\_GAS 0.0000E+00 0.0000E+00 0.0000E+00!  
ELEMENT VA VACUUM 0.0000E+00 0.0000E+00 0.0000E+00!  
ELEMENT MO BCC\_A2 9.5940E+01 4.5890E+03 2.8560E+01!  
ELEMENT NI FCC\_A1 5.8690E+01 4.7870E+03 2.9796E+01!  
ELEMENT RE HCP\_A3 1.8621E+02 5.3555E+03 3.6526E+01!

FUNCTION GHSERMO 2.98150E+02 -7746.302+131.9197\*T-23.56414\*T\*LN(T)  
-.003443396\*T\*\*2+5.66283E-07\*T\*\*3+65812\*T\*\*(-1)-1.30927E-10\*T\*\*4;  
2.89600E+03 Y  
-30556.41+283.559746\*T-42.63829\*T\*LN(T)-4.849315E+33\*T\*\*(-9); 5.00000E+03 N !

FUNCTION GHSERNI 2.98150E+02 -5179.159+117.854\*T-22.096\*T\*LN(T)  
-.0048407\*T\*\*2; 1.72800E+03 Y  
-27840.655+279.135\*T-43.1\*T\*LN(T)+1.12754E+31\*T\*\*(-9); 3.00000E+03 N !

FUNCTION GHSERRE 2.98150E+02 -7695.279+128.421589\*T-24.348\*T\*LN(T)  
-.00253505\*T\*\*2+1.92818E-07\*T\*\*3+32915\*T\*\*(-1); 1.20000E+03 Y  
-15775.998+194.667426\*T-33.586\*T\*LN(T)+.00224565\*T\*\*2-2.81835E-07\*T\*\*3  
+1376270\*T\*\*(-1); 2.40000E+03 Y  
-70882.739+462.110749\*T-67.956\*T\*LN(T)+.01184945\*T\*\*2-7.88955E-07\*T\*\*3  
+18075200\*T\*\*(-1); 3.45800E+03 Y  
+346325.888-1211.37186\*T+140.831655\*T\*LN(T)-.033764567\*T\*\*2  
+1.053726E-06\*T\*\*3-1.34548866E+08\*T\*\*(-1); 5.00000E+03 Y  
-78564.296+346.997842\*T-49.519\*T\*LN(T); 6.00000E+03 N !

FUNCTION GSERMO 2.98150E+02 -10.949432\*EVTOJ#; 6.00000E+03 N !

FUNCTION GSIGMO 2.98150E+02 +G30SIGMO#\*UNS30#; 6.00000E+03 N !

FUNCTION GSERNI 2.98150E+02 -5.57014\*EVTOJ#; 6.00000E+03 N !

FUNCTION GSIGNI 2.98150E+02 +G30SIGNI#\*UNS30#; 6.00000E+03 N !

FUNCTION GSERRE 2.98150E+02 -12.4224915\*EVTOJ#; 6.00000E+03 N !

FUNCTION GSIGRE 2.98150E+02 +G30SIGRE#\*UNS30#; 6.00000E+03 N !

FUNCTION EVTOJ 2.98150E+02 96485.5547; 6.00000E+03 N !

FUNCTION GCHIMO 2.98150E+02 +G58CHIMO#\*UNS58#; 6.00000E+03 N !

FUNCTION GCHINI 2.98150E+02 +G58CHINI#\*UNS58#; 6.00000E+03 N !

FUNCTION GCHIRE 2.98150E+02 +G58CHIRE#\*UNS58#; 6.00000E+03 N !

FUNCTION UNS30 2.98150E+02 +TRENTE#\*(-1); 6.00000E+03 N!  
 FUNCTION G30SIGMO 2.98150E+02 -323.477558\*EVTOJ#; 6.00000E+03 N!  
 FUNCTION G30SIGNI 2.98150E+02 -162.881156\*EVTOJ#; 6.00000E+03 N!  
 FUNCTION G30SIGRE 2.98150E+02 -369.773611\*EVTOJ#; 6.00000E+03 N!  
 FUNCTION UNS58 2.98150E+02 +CINQ8#\*(-1); 6.00000E+03 N!  
 FUNCTION G58CHIMO 2.98150E+02 -619.36214\*EVTOJ#; 6.00000E+03 N!  
 FUNCTION G58CHINI 2.98150E+02 -314.922996\*EVTOJ#; 6.00000E+03 N!  
 FUNCTION G58CHIRE 2.98150E+02 -717.557146\*EVTOJ#; 6.00000E+03 N!  
 FUNCTION TRENTE 2.98150E+02 30; 6.00000E+03 N!  
 FUNCTION CINQ8 2.98150E+02 58; 6.00000E+03 N!  
 27 V2 48000000 2.0410000E+00  
 29 V4 48000000 -3.1738744E+04  
 31 V6 48000000 -4.8492881E+02  
 33 V8 48000000 3.9859966E+03  
 35 V10 48000000 -4.6223261E+04  
 41 V16 48000000 1.8899344E+00  
 42 V17 48000000 8.1000000E+00  
 60 V35 48000000 -1.6154409E+05  
 65 V40 48000000 -6.0549273E+04  
 75 V50 48000000 8.3286973E+04  
 76 V51 48000000 -7.2933672E+01  
 95 V70 48000000 -2.2580182E+04  
 108 V83 48000000 4.1917705E+01  
 109 V84 48000000 -1.5263670E+05  
 FUNCTION GCH 298.15 0.0; 6000.00 N!  
 FUNCTION GCHI 298.15 0.0; 6000.00 N!  
 FUNCTION H298 298.15 0.0; 6000.00 N!  
 FUNCTION UN\_ASS 298.15 0; 300 N!  
  
 TYPE\_DEFINITION % SEQ \*!  
 DEFINE\_SYSTEM\_DEFAULT ELEMENT 2!  
 DEFAULT\_COMMAND DEF\_SYS\_ELEMENT VA /-!  
  
 TYPE\_DEFINITION & GES A\_P\_D BCC\_A2 MAGNETIC -1.0 4.00000E-01!  
**PHASE BCC\_A2 %& 2 1 3!**  
 CONSTITUENT BCC\_A2 :MO,NI,RE : VA : !  
 PARAMETER G(BCC\_A2,MO:VA;0) 2.98150E+02 +GHSERMO#; 5.00000E+03 N REF1!  
 PARAMETER TC(BCC\_A2,NI:VA;0) 2.98150E+02 575; 3.00000E+03 N REF0!

PARAMETER BMAGN(BCC\_A2,NI:VA;0) 2.98150E+02 .85; 3.00000E+03 N REF0 !  
 PARAMETER G(BCC\_A2,NI:VA;0) 2.98150E+02 +3535.925+114.298\*T  
 -22.096\*T\*LN(T)-.0048407\*T\*\*2; 1.72800E+03 Y  
 -19125.571+275.579\*T-43.1\*T\*LN(T)+1.12754E+31\*T\*\*(-9); 6.00000E+03 N REF0 !  
 PARAMETER G(BCC\_A2,RE:VA;0) 2.98150E+02 +9304.721+124.721589\*T  
 -24.348\*T\*LN(T)-.00253505\*T\*\*2+1.92818E-07\*T\*\*3+32915\*T\*\*(-1); 1.20000E+03 Y  
 +1224.002+190.967426\*T-33.586\*T\*LN(T)+.00224565\*T\*\*2-2.81835E-07\*T\*\*3+1376270\*T\*\*(-1);  
 2.40000E+03 Y  
 -53882.739+458.410749\*T-67.956\*T\*LN(T)+.01184945\*T\*\*2-7.88955E-07\*T\*\*3  
 +18075200\*T\*\*(-1); 3.45800E+03 Y  
 +363325.888-1215.07186\*T+140.831655\*T\*LN(T)-.033764567\*T\*\*2+1.053726E-06\*T\*\*3-  
 1.34548866E+08\*T\*\*(-1); 5.00000E+03 Y  
 -61564.296+343.297842\*T-49.519\*T\*LN(T); 6.00000E+03 N REF1 !  
 PARAMETER G(BCC\_A2,MO,RE:VA;0) 2.98150E+02 -1130-4.138\*T+2796; 6.00000E+03 N REF7 !  
 PARAMETER G(BCC\_A2,MO,RE:VA;1) 2.98150E+02 -53870+16.67\*T-3230; 6.00000E+03 N REF7 !  
 PARAMETER G(BCC\_A2,MO,NI:VA;0) 2.98150E+02 50988.2819; 6.00000E+03 N REF0 !  
 PARAMETER G(BCC\_A2,MO,NI,RE:VA;0) 2.98150E+02 +V30#+V31#\*T; 6.00000E+03 N REF0 !  
 PARAMETER G(BCC\_A2,NI,RE:VA;0) 2.98150E+02 21480.3504; 6.00000E+03 N REF0 !

**PHASE BETA % 2 1 4 !**

CONSTITUENT BETA :MO : NI : !  
 PARAMETER G(BETA,MO:NI;0) 2.98150E+02 -37888+20.823019\*T+GHSERMO# +4\*GHSERNI#;  
 6.00000E+03 N REF0 !

\$ THIS PHASE HAS A DISORDERED CONTRIBUTION FROM DIS\_CHI

**PHASE CHI % 4 2 8 24 24 !**

CONSTITUENT CHI :MO,NI,RE : MO,NI,RE : MO,NI,RE : MO,NI,RE : !  
 PARA G(CHI,MO:MO:MO:MO;0) 298.15 0; 6000 N!  
 PARAMETER G(CHI,NI:MO:MO:MO;0) 2.98150E+02 -606.587106\*EVTOJ#-2\*GCHINI#  
 -8\*GCHIMO#-24\*GCHIMO#-24\*GCHIMO#; 6.00000E+03 N REF5 !  
 PARAMETER G(CHI,RE:MO:MO:MO;0) 2.98150E+02 -621.992644\*EVTOJ#-2\*GCHIRE#  
 -8\*GCHIMO#-24\*GCHIMO#-24\*GCHIMO#; 6.00000E+03 N REF5 !  
 PARAMETER G(CHI,MO:NI:MO:MO;0) 2.98150E+02 -568.93268\*EVTOJ#-2\*GCHIMO#  
 -8\*GCHINI#-24\*GCHIMO#-24\*GCHIMO#; 6.00000E+03 N REF5 !  
 PARAMETER G(CHI,NI:NI:MO:MO;0) 2.98150E+02 -556.86606\*EVTOJ#-2\*GCHINI#  
 -8\*GCHINI#-24\*GCHIMO#-24\*GCHIMO#; 6.00000E+03 N REF5 !  
 PARAMETER G(CHI,RE:NI:MO:MO;0) 2.98150E+02 -571.294008\*EVTOJ#-2\*GCHIRE#  
 -8\*GCHINI#-24\*GCHIMO#-24\*GCHIMO#; 6.00000E+03 N REF5 !

PARAMETER G(CHI,MO:RE:MO:MO;0) 2.98150E+02 -630.436204\*EVTOJ#-2\*GCHIMO#  
-8\*GCHIRE#-24\*GCHIMO#-24\*GCHIMO#; 6.00000E+03 N REF5 !

PARAMETER G(CHI,NI:RE:MO:MO;0) 2.98150E+02 -617.260042\*EVTOJ#-2\*GCHINI#  
-8\*GCHIRE#-24\*GCHIMO#-24\*GCHIMO#; 6.00000E+03 N REF5 !

PARAMETER G(CHI,RE:RE:MO:MO;0) 2.98150E+02 -632.902352\*EVTOJ#-2\*GCHIRE#  
-8\*GCHIRE#-24\*GCHIMO#-24\*GCHIMO#; 6.00000E+03 N REF5 !

PARAMETER G(CHI,MO:MO:NI:MO;0) 2.98150E+02 -495.17233\*EVTOJ#-2\*GCHIMO#  
-8\*GCHIMO#-24\*GCHINI#-24\*GCHIMO#; 6.00000E+03 N REF5 !

PARAMETER G(CHI,NI:MO:NI:MO;0) 2.98150E+02 -483.336104\*EVTOJ#-2\*GCHINI#  
-8\*GCHIMO#-24\*GCHINI#-24\*GCHIMO#; 6.00000E+03 N REF5 !

PARAMETER G(CHI,RE:MO:NI:MO;0) 2.98150E+02 -497.863288\*EVTOJ#-2\*GCHIRE#  
-8\*GCHIMO#-24\*GCHINI#-24\*GCHIMO#; 6.00000E+03 N REF5 !

PARAMETER G(CHI,MO:NI:NI:MO;0) 2.98150E+02 -453.088926\*EVTOJ#-2\*GCHIMO#  
-8\*GCHINI#-24\*GCHINI#-24\*GCHIMO#; 6.00000E+03 N REF5 !

PARAMETER G(CHI,NI:NI:NI:MO;0) 2.98150E+02 -440.74347\*EVTOJ#-2\*GCHINI#  
-8\*GCHINI#-24\*GCHINI#-24\*GCHIMO#; 6.00000E+03 N REF5 !

PARAMETER G(CHI,RE:NI:NI:MO;0) 2.98150E+02 -456.047474\*EVTOJ#-2\*GCHIRE#  
-8\*GCHINI#-24\*GCHINI#-24\*GCHIMO#; 6.00000E+03 N REF5 !

PARAMETER G(CHI,MO:RE:NI:MO;0) 2.98150E+02 -507.137228\*EVTOJ#-2\*GCHIMO#  
-8\*GCHIRE#-24\*GCHINI#-24\*GCHIMO#; 6.00000E+03 N REF5 !

PARAMETER G(CHI,NI:RE:NI:MO;0) 2.98150E+02 -494.93875\*EVTOJ#-2\*GCHINI#  
-8\*GCHIRE#-24\*GCHINI#-24\*GCHIMO#; 6.00000E+03 N REF5 !

PARAMETER G(CHI,RE:RE:NI:MO;0) 2.98150E+02 -509.435306\*EVTOJ#-2\*GCHIRE#  
-8\*GCHIRE#-24\*GCHINI#-24\*GCHIMO#; 6.00000E+03 N REF5 !

PARAMETER G(CHI,MO:MO:RE:MO;0) 2.98150E+02 -662.013824\*EVTOJ#-2\*GCHIMO#  
-8\*GCHIMO#-24\*GCHIRE#-24\*GCHIMO#; 6.00000E+03 N REF5 !

PARAMETER G(CHI,NI:MO:RE:MO;0) 2.98150E+02 -649.129494\*EVTOJ#-2\*GCHINI#  
-8\*GCHIMO#-24\*GCHIRE#-24\*GCHIMO#; 6.00000E+03 N REF5 !

PARAMETER G(CHI,RE:MO:RE:MO;0) 2.98150E+02 -664.700708\*EVTOJ#-2\*GCHIRE#  
-8\*GCHIMO#-24\*GCHIRE#-24\*GCHIMO#; 6.00000E+03 N REF5 !

PARAMETER G(CHI,MO:NI:RE:MO;0) 2.98150E+02 -612.47631\*EVTOJ#-2\*GCHIMO#  
-8\*GCHINI#-24\*GCHIRE#-24\*GCHIMO#; 6.00000E+03 N REF5 !

PARAMETER G(CHI,NI:NI:RE:MO;0) 2.98150E+02 -600.94988\*EVTOJ#-2\*GCHINI#  
-8\*GCHINI#-24\*GCHIRE#-24\*GCHIMO#; 6.00000E+03 N REF5 !

PARAMETER G(CHI,RE:NI:RE:MO;0) 2.98150E+02 -615.166754\*EVTOJ#-2\*GCHIRE#  
-8\*GCHINI#-24\*GCHIRE#-24\*GCHIMO#; 6.00000E+03 N REF5 !

PARAMETER G(CHI,MO:RE:RE:MO;0) 2.98150E+02 -672.07236\*EVTOJ#-2\*GCHIMO#  
-8\*GCHIRE#-24\*GCHIRE#-24\*GCHIMO#; 6.00000E+03 N REF5 !

PARAMETER G(CHI,NI:RE:RE:MO;0) 2.98150E+02 -659.239818\*EVTOJ#-2\*GCHINI#  
 -8\*GCHIRE#-24\*GCHIRE#-24\*GCHIMO#; 6.00000E+03 N REF5 !  
 PARAMETER G(CHI,RE:RE:RE:MO;0) 2.98150E+02 -674.442674\*EVTOJ#-2\*GCHIRE#  
 -8\*GCHIRE#-24\*GCHIRE#-24\*GCHIMO#; 6.00000E+03 N REF5 !  
 PARAMETER G(CHI,MO:MO:MO:NI;0) 2.98150E+02 -498.37505\*EVTOJ#-2\*GCHIMO#  
 -8\*GCHIMO#-24\*GCHIMO#-24\*GCHINI#; 6.00000E+03 N REF5 !  
 PARAMETER G(CHI,NI:MO:MO:NI;0) 2.98150E+02 -486.547226\*EVTOJ#-2\*GCHINI#  
 -8\*GCHIMO#-24\*GCHIMO#-24\*GCHINI#; 6.00000E+03 N REF5 !  
 PARAMETER G(CHI,RE:MO:MO:NI;0) 2.98150E+02 -501.184788\*EVTOJ#-2\*GCHIRE#  
 -8\*GCHIMO#-24\*GCHIMO#-24\*GCHINI#; 6.00000E+03 N REF5 !  
 PARAMETER G(CHI,MO:NI:MO:NI;0) 2.98150E+02 -456.911446\*EVTOJ#-2\*GCHIMO#  
 -8\*GCHINI#-24\*GCHIMO#-24\*GCHINI#; 6.00000E+03 N REF5 !  
 PARAMETER G(CHI,NI:NI:MO:NI;0) 2.98150E+02 -443.708576\*EVTOJ#-2\*GCHINI#  
 -8\*GCHINI#-24\*GCHIMO#-24\*GCHINI#; 6.00000E+03 N REF5 !  
 PARAMETER G(CHI,RE:NI:MO:NI;0) 2.98150E+02 -458.823256\*EVTOJ#-2\*GCHIRE#  
 -8\*GCHINI#-24\*GCHIMO#-24\*GCHINI#; 6.00000E+03 N REF5 !  
 PARAMETER G(CHI,MO:RE:MO:NI;0) 2.98150E+02 -511.567944\*EVTOJ#-2\*GCHIMO#  
 -8\*GCHIRE#-24\*GCHIMO#-24\*GCHINI#; 6.00000E+03 N REF5 !  
 PARAMETER G(CHI,NI:RE:MO:NI;0) 2.98150E+02 -498.85896\*EVTOJ#-2\*GCHINI#  
 -8\*GCHIRE#-24\*GCHIMO#-24\*GCHINI#; 6.00000E+03 N REF5 !  
 PARAMETER G(CHI,RE:RE:MO:NI;0) 2.98150E+02 -514.463642\*EVTOJ#-2\*GCHIRE#  
 -8\*GCHIRE#-24\*GCHIMO#-24\*GCHINI#; 6.00000E+03 N REF5 !  
 PARAMETER G(CHI,MO:MO:NI:NI;0) 2.98150E+02 -376.509392\*EVTOJ#-2\*GCHIMO#  
 -8\*GCHIMO#-24\*GCHINI#-24\*GCHINI#; 6.00000E+03 N REF5 !  
 PARAMETER G(CHI,NI:MO:NI:NI;0) 2.98150E+02 -365.724078\*EVTOJ#-2\*GCHINI#  
 -8\*GCHIMO#-24\*GCHINI#-24\*GCHINI#; 6.00000E+03 N REF5 !  
 PARAMETER G(CHI,RE:MO:NI:NI;0) 2.98150E+02 -379.741552\*EVTOJ#-2\*GCHIRE#  
 -8\*GCHIMO#-24\*GCHINI#-24\*GCHINI#; 6.00000E+03 N REF5 !  
 PARAMETER G(CHI,MO:NI:NI:NI;0) 2.98150E+02 -327.718976\*EVTOJ#-2\*GCHIMO#  
 -8\*GCHINI#-24\*GCHINI#-24\*GCHINI#; 6.00000E+03 N REF5 !  
 PARA G(CHI,NI:NI:NI:NI;0) 298.15 0; 6000 N!  
 PARAMETER G(CHI,RE:NI:NI:NI;0) 2.98150E+02 -329.736544\*EVTOJ#-2\*GCHIRE#  
 -8\*GCHINI#-24\*GCHINI#-24\*GCHINI#; 6.00000E+03 N REF0 !  
 PARAMETER G(CHI,MO:RE:NI:NI;0) 2.98150E+02 -386.75196\*EVTOJ#-2\*GCHIMO#  
 -8\*GCHIRE#-24\*GCHINI#-24\*GCHINI#; 6.00000E+03 N REF5 !  
 PARAMETER G(CHI,NI:RE:NI:NI;0) 2.98150E+02 -374.540202\*EVTOJ#-2\*GCHINI#  
 -8\*GCHIRE#-24\*GCHINI#-24\*GCHINI#; 6.00000E+03 N REF0 !  
 PARAMETER G(CHI,RE:RE:NI:NI;0) 2.98150E+02 -389.647886\*EVTOJ#-2\*GCHIRE#

-8\*GCHIRE#-24\*GCHINI#-24\*GCHINI#; 6.00000E+03 N REF0 !  
PARAMETER G(CHI,MO:MO:RE:NI;0) 2.98150E+02 -539.456078\*EVTOJ#-2\*GCHIMO#  
-8\*GCHIMO#-24\*GCHIRE#-24\*GCHINI#; 6.00000E+03 N REF5 !  
PARAMETER G(CHI,NI:MO:RE:NI;0) 2.98150E+02 -527.602584\*EVTOJ#-2\*GCHINI#  
-8\*GCHIMO#-24\*GCHIRE#-24\*GCHINI#; 6.00000E+03 N REF5 !  
PARAMETER G(CHI,RE:MO:RE:NI;0) 2.98150E+02 -542.155048\*EVTOJ#-2\*GCHIRE#  
-8\*GCHIMO#-24\*GCHIRE#-24\*GCHINI#; 6.00000E+03 N REF5 !  
PARAMETER G(CHI,MO:NI:RE:NI;0) 2.98150E+02 -491.987462\*EVTOJ#-2\*GCHIMO#  
-8\*GCHINI#-24\*GCHIRE#-24\*GCHINI#; 6.00000E+03 N REF5 !  
PARAMETER G(CHI,NI:NI:RE:NI;0) 2.98150E+02 -479.123154\*EVTOJ#-2\*GCHINI#  
-8\*GCHINI#-24\*GCHIRE#-24\*GCHINI#; 6.00000E+03 N REF0 !  
PARAMETER G(CHI,RE:NI:RE:NI;0) 2.98150E+02 -493.718058\*EVTOJ#-2\*GCHIRE#  
-8\*GCHINI#-24\*GCHIRE#-24\*GCHINI#; 6.00000E+03 N REF0 !  
PARAMETER G(CHI,MO:RE:RE:NI;0) 2.98150E+02 -551.133814\*EVTOJ#-2\*GCHIMO#  
-8\*GCHIRE#-24\*GCHIRE#-24\*GCHINI#; 6.00000E+03 N REF5 !  
PARAMETER G(CHI,NI:RE:RE:NI;0) 2.98150E+02 -538.47213\*EVTOJ#-2\*GCHINI#  
-8\*GCHIRE#-24\*GCHIRE#-24\*GCHINI#; 6.00000E+03 N REF0 !  
PARAMETER G(CHI,RE:RE:RE:NI;0) 2.98150E+02 -553.817166\*EVTOJ#-2\*GCHIRE#  
-8\*GCHIRE#-24\*GCHIRE#-24\*GCHINI#; 6.00000E+03 N REF0 !  
PARAMETER G(CHI,MO:MO:MO:RE;0) 2.98150E+02 -667.0576\*EVTOJ#-2\*GCHIMO#  
-8\*GCHIMO#-24\*GCHIMO#-24\*GCHIRE#; 6.00000E+03 N REF5 !  
PARAMETER G(CHI,NI:MO:MO:RE;0) 2.98150E+02 -654.882878\*EVTOJ#-2\*GCHINI#  
-8\*GCHIMO#-24\*GCHIMO#-24\*GCHIRE#; 6.00000E+03 N REF5 !  
PARAMETER G(CHI,RE:MO:MO:RE;0) 2.98150E+02 -669.426922\*EVTOJ#-2\*GCHIRE#  
-8\*GCHIMO#-24\*GCHIMO#-24\*GCHIRE#; 6.00000E+03 N REF5 !  
PARAMETER G(CHI,MO:NI:MO:RE;0) 2.98150E+02 -619.177552\*EVTOJ#-2\*GCHIMO#  
-8\*GCHINI#-24\*GCHIMO#-24\*GCHIRE#; 6.00000E+03 N REF5 !  
PARAMETER G(CHI,NI:NI:MO:RE;0) 2.98150E+02 -607.329198\*EVTOJ#-2\*GCHINI#  
-8\*GCHINI#-24\*GCHIMO#-24\*GCHIRE#; 6.00000E+03 N REF5 !  
PARAMETER G(CHI,RE:NI:MO:RE;0) 2.98150E+02 -621.219296\*EVTOJ#-2\*GCHIRE#  
-8\*GCHINI#-24\*GCHIMO#-24\*GCHIRE#; 6.00000E+03 N REF5 !  
PARAMETER G(CHI,MO:RE:MO:RE;0) 2.98150E+02 -676.652914\*EVTOJ#-2\*GCHIMO#  
-8\*GCHIRE#-24\*GCHIMO#-24\*GCHIRE#; 6.00000E+03 N REF5 !  
PARAMETER G(CHI,NI:RE:MO:RE;0) 2.98150E+02 -664.14815\*EVTOJ#-2\*GCHINI#  
-8\*GCHIRE#-24\*GCHIMO#-24\*GCHIRE#; 6.00000E+03 N REF5 !  
PARAMETER G(CHI,RE:RE:MO:RE;0) 2.98150E+02 -678.636738\*EVTOJ#-2\*GCHIRE#  
-8\*GCHIRE#-24\*GCHIMO#-24\*GCHIRE#; 6.00000E+03 N REF5 !  
PARAMETER G(CHI,MO:MO:NI:RE;0) 2.98150E+02 -535.53101\*EVTOJ#-2\*GCHIMO#

-8\*GCHIMO#-24\*GCHINI#-24\*GCHIRE#; 6.00000E+03 N REF5 !  
PARAMETER G(CHI,NI:MO:NI:RE;0) 2.98150E+02 -524.449084\*EVTOJ#-2\*GCHINI#  
-8\*GCHIMO#-24\*GCHINI#-24\*GCHIRE#; 6.00000E+03 N REF5 !  
PARAMETER G(CHI,RE:MO:NI:RE;0) 2.98150E+02 -537.731532\*EVTOJ#-2\*GCHIRE#  
-8\*GCHIMO#-24\*GCHINI#-24\*GCHIRE#; 6.00000E+03 N REF5 !  
PARAMETER G(CHI,MO:NI:NI:RE;0) 2.98150E+02 -494.047372\*EVTOJ#-2\*GCHIMO#  
-8\*GCHINI#-24\*GCHINI#-24\*GCHIRE#; 6.00000E+03 N REF5 !  
PARAMETER G(CHI,NI:NI:NI:RE;0) 2.98150E+02 -480.909228\*EVTOJ#-2\*GCHINI#  
-8\*GCHINI#-24\*GCHINI#-24\*GCHIRE#; 6.00000E+03 N REF0 !  
PARAMETER G(CHI,RE:NI:NI:RE;0) 2.98150E+02 -495.83554\*EVTOJ#-2\*GCHIRE#  
-8\*GCHINI#-24\*GCHINI#-24\*GCHIRE#; 6.00000E+03 N REF0 !  
PARAMETER G(CHI,MO:RE:NI:RE;0) 2.98150E+02 -546.269828\*EVTOJ#-2\*GCHIMO#  
-8\*GCHIRE#-24\*GCHINI#-24\*GCHIRE#; 6.00000E+03 N REF5 !  
PARAMETER G(CHI,NI:RE:NI:RE;0) 2.98150E+02 -534.80935\*EVTOJ#-2\*GCHINI#  
-8\*GCHIRE#-24\*GCHINI#-24\*GCHIRE#; 6.00000E+03 N REF0 !  
PARAMETER G(CHI,RE:RE:NI:RE;0) 2.98150E+02 -548.229334\*EVTOJ#-2\*GCHIRE#  
-8\*GCHIRE#-24\*GCHINI#-24\*GCHIRE#; 6.00000E+03 N REF0 !  
PARAMETER G(CHI,MO:MO:RE:RE;0) 2.98150E+02 -706.53129\*EVTOJ#-2\*GCHIMO#  
-8\*GCHIMO#-24\*GCHIRE#-24\*GCHIRE#; 6.00000E+03 N REF5 !  
PARAMETER G(CHI,NI:MO:RE:RE;0) 2.98150E+02 -694.369638\*EVTOJ#-2\*GCHINI#  
-8\*GCHIMO#-24\*GCHIRE#-24\*GCHIRE#; 6.00000E+03 N REF5 !  
PARAMETER G(CHI,RE:MO:RE:RE;0) 2.98150E+02 -708.864342\*EVTOJ#-2\*GCHIRE#  
-8\*GCHIMO#-24\*GCHIRE#-24\*GCHIRE#; 6.00000E+03 N REF5 !  
PARAMETER G(CHI,MO:NI:RE:RE;0) 2.98150E+02 -660.828548\*EVTOJ#-2\*GCHIMO#  
-8\*GCHINI#-24\*GCHIRE#-24\*GCHIRE#; 6.00000E+03 N REF5 !  
PARAMETER G(CHI,NI:NI:RE:RE;0) 2.98150E+02 -648.514314\*EVTOJ#-2\*GCHINI#  
-8\*GCHINI#-24\*GCHIRE#-24\*GCHIRE#; 6.00000E+03 N REF0 !  
PARAMETER G(CHI,RE:NI:RE:RE;0) 2.98150E+02 -663.04803\*EVTOJ#-2\*GCHIRE#  
-8\*GCHINI#-24\*GCHIRE#-24\*GCHIRE#; 6.00000E+03 N REF0 !  
PARAMETER G(CHI,MO:RE:RE:RE;0) 2.98150E+02 -715.47601\*EVTOJ#-2\*GCHIMO#  
-8\*GCHIRE#-24\*GCHIRE#-24\*GCHIRE#; 6.00000E+03 N REF5 !  
PARAMETER G(CHI,NI:RE:RE:RE;0) 2.98150E+02 -702.858902\*EVTOJ#-2\*GCHINI#  
-8\*GCHIRE#-24\*GCHIRE#-24\*GCHIRE#; 6.00000E+03 N REF0 !  
PARAMETER G(CHI,RE:RE:RE:RE;0) 298.15 0; 6000 N!

**PHASE DELTA % 3 24 20 12!**

CONSTITUENT DELTA :NI : MO,NI,RE : MO : !  
PARAMETER G(DELTA,NI:MO:MO;0) 2.98150E+02 -164024+39.7185158\*T

+24\*GHSERNI#+32\*GHSERMO#; 6.00000E+03 N REF0 !  
 PARAMETER G(DELTA,NI:NI:MO;0) 2.98150E+02 +26880+85.9201548\*T  
 +44\*GHSERNI#+12\*GHSERMO#; 6.00000E+03 N REF0 !  
 PARAMETER G(DELTA,NI:RE:MO;0) 2.98150E+02 -329112+24\*GHSERNI#  
 +20\*GHSERRE#+12\*GHSERMO#+V83#\*T; 6.00000E+03 N REF0 !  
 PARAMETER G(DELTA,NI:MO,NI:MO;1) 2.98150E+02 -985076.5+892.629624\*T; 6.00000E+03 N REF0 !  
 PARAMETER G(DELTA,NI:MO,NI,RE:MO;0) 2.98150E+02 +V81#+V82#\*T; 6.00000E+03 N REF0 !  
 PARAMETER G(DELTA,NI:MO,RE:MO;0) 2.98150E+02 +V84#+V85#\*T; 6.00000E+03 N REF0 !

TYPE\_DEFINITION ' GES AMEND\_PHASE\_DESCRIPTION CHI DIS\_PART DIS\_CHI,,!

**PHASE DIS\_CHI %' 1 1.0 !**

CONSTITUENT DIS\_CHI :MO,NI,RE : !  
 PARAMETER G(DIS\_CHI,MO;0) 2.98150E+02 +GCHIMO#-GSERMO#+GHSERMO#-5.35\*T;  
 6.00000E+03 N REF7 !  
 PARAMETER G(DIS\_CHI,NI;0) 2.98150E+02 +GCHINI#-GSERNI#+GHSERNI#+V16#\*T;  
 6.00000E+03 N REF0 !  
 PARAMETER G(DIS\_CHI,RE;0) 2.98150E+02 +GCHIRE#-GSERRE#+GHSERRE#+.216\*T;  
 6.00000E+03 N REF7 !

**PHASE DIS\_SIG % 1 1.0 !**

CONSTITUENT DIS\_SIG :MO,NI,RE : !  
 PARAMETER G(DIS\_SIG,MO;0) 2.98150E+02 +GSIGMO#-GSERMO#+GHSERMO#-3.9\*T;  
 6.00000E+03 N REF7 !  
 PARAMETER G(DIS\_SIG,NI;0) 2.98150E+02 +GSIGNI#-GSERNI#+GHSERNI#+V17#\*T;  
 6.00000E+03 N REF0 !  
 PARAMETER G(DIS\_SIG,RE;0) 2.98150E+02 +GSIGRE#-GSERRE#+GHSERRE#-1.024\*T;  
 6.00000E+03 N REF7 !

TYPE\_DEFINITION ( GES A\_P\_D FCC\_A1 MAGNETIC -3.0 2.80000E-01 !

**PHASE FCC\_A1 %( 2 1 1!**

CONSTITUENT FCC\_A1 :MO,NI,RE : VA : !  
 PARAMETER G(FCC\_A1,MO:VA;0) 2.98150E+02 +7453.698+132.5497\*T  
 -23.56414\*T\*LN(T)-.003443396\*T\*\*2+5.66283E-07\*T\*\*3+65812\*T\*\*(-1)  
 -1.30927E-10\*T\*\*4; 2.89600E+03 Y  
 -15356.41+284.189746\*T-42.63829\*T\*LN(T)-4.849315E+33\*T\*\*(-9);  
 5.00000E+03 N REF1 !  
 PARAMETER G(FCC\_A1,NI:VA;0) 2.98150E+02 +GHSERNI#; 3.00000E+03 N REF1 !  
 PARAMETER TC(FCC\_A1,NI:VA;0) 2.98150E+02 633; 3.00000E+03 N REF0 !  
 PARAMETER BMAGN(FCC\_A1,NI:VA;0) 2.98150E+02 .52; 3.00000E+03 N REF0 !

PARAMETER G(FCC\_A1,RE:VA;0) 2.98150E+02 +3304.721+126.921589\*T  
-24.348\*T\*LN(T)-.00253505\*T\*\*2+1.92818E-07\*T\*\*3+32915\*T\*\*(-1);  
1.20000E+03 Y  
-4775.998+193.167426\*T-33.586\*T\*LN(T)+.00224565\*T\*\*2-2.81835E-07\*T\*\*3  
+1376270\*T\*\*(-1); 2.40000E+03 Y  
-59882.739+460.610749\*T-67.956\*T\*LN(T)+.01184945\*T\*\*2-7.88955E-07\*T\*\*3  
+18075200\*T\*\*(-1); 3.45800E+03 Y  
+357325.888-1212.87186\*T+140.831655\*T\*LN(T)-.033764567\*T\*\*2  
+1.053726E-06\*T\*\*3-1.34548866E+08\*T\*\*(-1); 5.00000E+03 Y  
-67564.296+345.497842\*T-49.519\*T\*LN(T); 6.00000E+03 N REF1 !  
PARAMETER G(FCC\_A1,MO,NI:VA;0) 2.98150E+02 -26399.3622+16.5193147\*T;  
6.00000E+03 N REF0 !  
PARAMETER G(FCC\_A1,MO,NI,RE:VA;0) 2.98150E+02 +V40#+V41#\*T;  
6.00000E+03 N REF0 !  
PARAMETER G(FCC\_A1,MO,RE:VA;0) 2.98150E+02 +24197-10.75\*T;  
6.00000E+03 N REF0 !  
PARAMETER G(FCC\_A1,MO,RE:VA;1) 2.98150E+02 -10495; 6.00000E+03 N  
REF0 !  
PARAMETER G(FCC\_A1,NI,RE:VA;0) 2.98150E+02 +5054.48711+8.28748232\*T;  
6.00000E+03 N REF9 !

**PHASE GAMMA % 2 1 3 !**

CONSTITUENT GAMMA :MO : NI : !  
PARAMETER G(GAMMA,MO:NI;0) 2.98150E+02 -34052+19.1361667\*T+GHSERMO#  
+3\*GHSERNI#; 6.00000E+03 N REF0 !

TYPE\_DEFINITION ) GES A\_P\_D HCP\_A3 MAGNETIC -3.0 2.80000E-01 !

**PHASE HCP\_A3 % 2 1 .5 !**

CONSTITUENT HCP\_A3 :MO,NI,RE : VA : !

PARAMETER G(HCP\_A3,MO:VA;0) 2.98150E+02 +3803.698+131.9197\*T  
-23.56414\*T\*LN(T)-.003443396\*T\*\*2+5.66283E-07\*T\*\*3+65812\*T\*\*(-1)  
-1.30927E-10\*T\*\*4; 2.89600E+03 Y  
-19006.41+283.559746\*T-42.63829\*T\*LN(T)-4.849315E+33\*T\*\*(-9);  
5.00000E+03 N REF1 !  
PARAMETER G(HCP\_A3,NI:VA;0) 2.98150E+02 -4133.159+119.109\*T  
-22.096\*T\*LN(T)-.0048407\*T\*\*2; 1.72800E+03 Y  
-26794.655+280.39\*T-43.1\*T\*LN(T)+1.12754E+31\*T\*\*(-9); 3.00000E+03 N

REF1 !

PARAMETER G(HCP\_A3,RE:VA;0) 2.98150E+02 +GHSERRE#; 6.00000E+03 N

REF1 !

PARAMETER G(HCP\_A3,MO,RE:VA;0) 2.98150E+02 +24197-10.75\*T;

6.00000E+03 N REF7 !

PARAMETER G(HCP\_A3,MO,RE:VA;1) 2.98150E+02 -10495; 6.00000E+03 N

REF7 !

PARAMETER G(HCP\_A3,MO,NI:VA;0) 2.98150E+02 -26399.3622+16.5193147\*T;

6.00000E+03 N REF0 !

PARAMETER G(HCP\_A3,MO,NI,RE:VA;0) 2.98150E+02 +V50#+V51#\*T;

6.00000E+03 N !

PARAMETER G(HCP\_A3,NI,RE:VA;0) 2.98150E+02 +9968.56426+7.59954301\*T;

6.00000E+03 N REF9 !

### PHASE LIQUID % 1 1.0 !

CONSTITUENT LIQUID :MO,NI,RE : !

PARAMETER G(LIQUID,MO;0) 2.98150E+02 +34085.045+117.224788\*T

-23.56414\*T\*LN(T)-.003443396\*T\*\*2+5.66283E-07\*T\*\*3+65812\*T\*\*(-1)

-1.30927E-10\*T\*\*4+4.24519E-22\*T\*\*7; 2.89600E+03 Y

+3538.963+271.6697\*T-42.63829\*T\*LN(T); 5.00000E+03 N REF1 !

PARAMETER G(LIQUID,NI;0) 2.98150E+02 +11235.527+108.457\*T -22.096\*T\*LN(T)-.0048407\*T\*\*2-3.82318E-21\*T\*\*7; 1.72800E+03 Y -9549.775+268.598\*T-43.1\*T\*LN(T); 3.00000E+03 N REF1 !

PARAMETER G(LIQUID,RE;0) 2.98150E+02 +16125.604+122.076209\*T-24.348\*T\*LN(T)-.00253505\*T\*\*2+1.92818E-07\*T\*\*3+32915\*T\*\*(-1); 1.20000E+03 Y

+8044.885+188.322047\*T-33.586\*T\*LN(T)+.00224565\*T\*\*2-2.81835E-07\*T\*\*3

+1376270\*T\*\*(-1); 2.00000E+03 Y

+568842.665-2527.83846\*T+314.178898\*T\*LN(T)-.08939817\*T\*\*2

+3.92854E-06\*T\*\*3-1.63100987E+08\*T\*\*(-1); 3.45800E+03 Y

-39044.888+335.723691\*T-49.519\*T\*LN(T); 6.00000E+03 N REF1 !

PARAMETER G(LIQUID,MO,RE;0) 2.98150E+02 -1130-4.138\*T; 6.00000E+03 N REF7 !

PARAMETER G(LIQUID,MO,RE;1) 2.98150E+02 -53870+16.67\*T; 6.00000E+03 N REF7 !

PARAMETER G(LIQUID,MO,NI;0) 2.98150E+02 -20576.3331+8.26842559\*T; 6.00000E+03 N REF0 !

PARAMETER G(LIQUID,MO,NI,RE;0) 2.98150E+02 +V70#+V71#\*T; 6.00000E+03 N REF0 !

PARAMETER G(LIQUID,NI,RE;0) 2.98150E+02 21480.3504; 6.00000E+03 N REF9 !

### PHASE MO3COSI % 3 9 4 1 !

CONSTITUENT MO3COSI :MO,RE : NI,RE : NI : !

PARAMETER G(MO3COSI,MO:NI:NI;0) 2.98150E+02 -28056+9\*GHSERMO# +5\*GHSERNI#+V2#\*T;  
6.00000E+03 N REF0 !

PARAMETER G(MO3COSI,RE:NI:NI;0) 2.98150E+02 -7812+9\*GHSERRE#+5\*GHSERNI# +V2#\*T;  
6.00000E+03 N REF0 !

PARAMETER G(MO3COSI,MO:RE:NI;0) 2.98150E+02 +69748+9\*GHSERMO#+GHSERRE#  
+4\*GHSERNI#+V2#\*T; 6.00000E+03 N REF0 !

PARAMETER G(MO3COSI,RE:RE:NI;0) 2.98150E+02 +153020+10\*GHSERRE#  
+4\*GHSERNI#+V2#\*T; 6.00000E+03 N REF0 !

PARAMETER G(MO3COSI,MO,RE:NI:NI;0) 2.98150E+02 +V4#+V5#\*T; 6.00000E+03 N !

PARAMETER G(MO3COSI,MO,RE:NI:NI;1) 2.98150E+02 +V35#+V36#\*T; 6.00000E+03 N !

\$ THIS PHASE HAS A DISORDERED CONTRIBUTION FROM DIS\_SIG

TYPE\_DEFINITION \* GES AMEND\_PHASE\_DESCRIPTION SIGMA STATUS 02200800 ,,,,, !

TYPE\_DEFINITION + GES AMEND\_PHASE\_DESCRIPTION SIGMA DIS\_PART DIS\_SIG,,,! !

**PHASE SIGMA %\*+ 5 2 4 8 8 8 !**

CONSTITUENT SIGMA :MO,NI,RE : MO,NI,RE : MO,NI,RE : MO,NI,RE : MO,NI,RE : !

PARA G(SIGMA,MO:MO:MO:MO:MO;0) 298.15 0; 6000 N!

PARAMETER G(SIGMA,NI:MO:MO:MO:MO;0) 2.98150E+02 -313.861486\*EVTOJ#  
-2\*GSIGNI#-4\*GSIGMO#-8\*GSIGMO#-8\*GSIGMO#-8\*GSIGMO#; 6.00000E+03 N REF3 !

PARAMETER G(SIGMA,RE:MO:MO:MO:MO;0) 2.98150E+02 -327.229897\*EVTOJ#  
-2\*GSIGRE#-4\*GSIGMO#-8\*GSIGMO#-8\*GSIGMO#-8\*GSIGMO#; 6.00000E+03 N REF3 !

PARAMETER G(SIGMA,MO:NI:MO:MO:MO;0) 2.98150E+02 -298.562044\*EVTOJ#  
-2\*GSIGMO#-4\*GSIGNI#-8\*GSIGMO#-8\*GSIGMO#-8\*GSIGMO#; 6.00000E+03 N REF3 !

PARAMETER G(SIGMA,NI:NI:MO:MO:MO;0) 2.98150E+02 -289.456413\*EVTOJ#  
-2\*GSIGNI#-4\*GSIGNI#-8\*GSIGMO#-8\*GSIGMO#-8\*GSIGMO#; 6.00000E+03 N REF3 !

PARAMETER G(SIGMA,RE:NI:MO:MO:MO;0) 2.98150E+02 -302.035037\*EVTOJ#  
-2\*GSIGRE#-4\*GSIGNI#-8\*GSIGMO#-8\*GSIGMO#-8\*GSIGMO#; 6.00000E+03 N REF3 !

PARAMETER G(SIGMA,MO:RE:MO:MO:MO;0) 2.98150E+02 -329.386161\*EVTOJ#  
-2\*GSIGMO#-4\*GSIGRE#-8\*GSIGMO#-8\*GSIGMO#-8\*GSIGMO#; 6.00000E+03 N REF3 !

PARAMETER G(SIGMA,NI:RE:MO:MO:MO;0) 2.98150E+02 -319.872651\*EVTOJ#  
-2\*GSIGNI#-4\*GSIGRE#-8\*GSIGMO#-8\*GSIGMO#-8\*GSIGMO#; 6.00000E+03 N REF3 !

PARAMETER G(SIGMA,RE:RE:MO:MO:MO;0) 2.98150E+02 -332.95143\*EVTOJ#  
-2\*GSIGRE#-4\*GSIGRE#-8\*GSIGMO#-8\*GSIGMO#-8\*GSIGMO#; 6.00000E+03 N REF3 !

PARAMETER G(SIGMA,MO:MO:NI:MO:MO;0) 2.98150E+02 -280.703448\*EVTOJ#  
-2\*GSIGMO#-4\*GSIGMO#-8\*GSIGNI#-8\*GSIGMO#-8\*GSIGMO#; 6.00000E+03 N REF3 !

PARAMETER G(SIGMA,NI:MO:NI:MO:MO;0) 2.98150E+02 -271.142908\*EVTOJ#  
-2\*GSIGNI#-4\*GSIGMO#-8\*GSIGNI#-8\*GSIGMO#-8\*GSIGMO#; 6.00000E+03 N REF3 !

PARAMETER G(SIGMA,RE:MO:NI:MO:MO;0) 2.98150E+02 -284.369087\*EVTOJ#

-2\*GSIGRE#-4\*GSIGMO#-8\*GSIGNI#-8\*GSIGMO#-8\*GSIGMO#; 6.00000E+03 N REF3 !  
PARAMETER G(SIGMA,MO:NI:NI:MO:MO;0) 2.98150E+02 -257.149887\*EVTOJ#

-2\*GSIGMO#-4\*GSIGNI#-8\*GSIGNI#-8\*GSIGMO#-8\*GSIGMO#; 6.00000E+03 N REF3 !  
PARAMETER G(SIGMA,NI:NI:NI:MO:MO;0) 2.98150E+02 -247.718134\*EVTOJ#

-2\*GSIGNI#-4\*GSIGNI#-8\*GSIGNI#-8\*GSIGMO#-8\*GSIGMO#; 6.00000E+03 N REF3 !  
PARAMETER G(SIGMA,RE:NI:NI:MO:MO;0) 2.98150E+02 -260.5367\*EVTOJ#

-2\*GSIGRE#-4\*GSIGNI#-8\*GSIGNI#-8\*GSIGMO#-8\*GSIGMO#; 6.00000E+03 N REF3 !  
PARAMETER G(SIGMA,MO:RE:NI:MO:MO;0) 2.98150E+02 -286.440837\*EVTOJ#

-2\*GSIGMO#-4\*GSIGRE#-8\*GSIGNI#-8\*GSIGMO#-8\*GSIGMO#; 6.00000E+03 N REF3 !  
PARAMETER G(SIGMA,NI:RE:NI:MO:MO;0) 2.98150E+02 -277.054311\*EVTOJ#

-2\*GSIGNI#-4\*GSIGRE#-8\*GSIGNI#-8\*GSIGMO#-8\*GSIGMO#; 6.00000E+03 N REF3 !  
PARAMETER G(SIGMA,RE:RE:NI:MO:MO;0) 2.98150E+02 -289.887987\*EVTOJ#

-2\*GSIGRE#-4\*GSIGRE#-8\*GSIGNI#-8\*GSIGMO#-8\*GSIGMO#; 6.00000E+03 N REF3 !  
PARAMETER G(SIGMA,MO:MO:RE:MO:MO;0) 2.98150E+02 -336.272469\*EVTOJ#

-2\*GSIGMO#-4\*GSIGMO#-8\*GSIGRE#-8\*GSIGMO#-8\*GSIGMO#; 6.00000E+03 N REF3 !  
PARAMETER G(SIGMA,NI:MO:RE:MO:MO;0) 2.98150E+02 -326.796858\*EVTOJ#

-2\*GSIGNI#-4\*GSIGMO#-8\*GSIGRE#-8\*GSIGMO#-8\*GSIGMO#; 6.00000E+03 N REF3 !  
PARAMETER G(SIGMA,RE:MO:RE:MO:MO;0) 2.98150E+02 -340.103152\*EVTOJ#

-2\*GSIGRE#-4\*GSIGMO#-8\*GSIGRE#-8\*GSIGMO#-8\*GSIGMO#; 6.00000E+03 N REF3 !  
PARAMETER G(SIGMA,MO:NI:RE:MO:MO;0) 2.98150E+02 -311.670319\*EVTOJ#

-2\*GSIGMO#-4\*GSIGNI#-8\*GSIGRE#-8\*GSIGMO#-8\*GSIGMO#; 6.00000E+03 N REF3 !  
PARAMETER G(SIGMA,NI:NI:RE:MO:MO;0) 2.98150E+02 -302.39492\*EVTOJ#

-2\*GSIGNI#-4\*GSIGNI#-8\*GSIGRE#-8\*GSIGMO#-8\*GSIGMO#; 6.00000E+03 N REF3 !  
PARAMETER G(SIGMA,RE:NI:RE:MO:MO;0) 2.98150E+02 -315.173819\*EVTOJ#

-2\*GSIGRE#-4\*GSIGNI#-8\*GSIGRE#-8\*GSIGMO#-8\*GSIGMO#; 6.00000E+03 N REF3 !  
PARAMETER G(SIGMA,MO:RE:RE:MO:MO;0) 2.98150E+02 -342.25167\*EVTOJ#

-2\*GSIGMO#-4\*GSIGRE#-8\*GSIGRE#-8\*GSIGMO#-8\*GSIGMO#; 6.00000E+03 N REF3 !  
PARAMETER G(SIGMA,NI:RE:RE:MO:MO;0) 2.98150E+02 -332.843581\*EVTOJ#

-2\*GSIGNI#-4\*GSIGRE#-8\*GSIGRE#-8\*GSIGMO#-8\*GSIGMO#; 6.00000E+03 N REF3 !  
PARAMETER G(SIGMA,RE:RE:RE:MO:MO;0) 2.98150E+02 -345.809448\*EVTOJ#

-2\*GSIGRE#-4\*GSIGRE#-8\*GSIGRE#-8\*GSIGMO#-8\*GSIGMO#; 6.00000E+03 N REF3 !  
PARAMETER G(SIGMA,MO:MO:MO:NI:MO;0) 2.98150E+02 -284.978817\*EVTOJ#

-2\*GSIGMO#-4\*GSIGMO#-8\*GSIGMO#-8\*GSIGNI#-8\*GSIGMO#; 6.00000E+03 N REF3 !  
PARAMETER G(SIGMA,NI:MO:MO:NI:MO;0) 2.98150E+02 -274.899176\*EVTOJ#

-2\*GSIGNI#-4\*GSIGMO#-8\*GSIGMO#-8\*GSIGNI#-8\*GSIGMO#; 6.00000E+03 N REF3 !  
PARAMETER G(SIGMA,RE:MO:MO:NI:MO;0) 2.98150E+02 -288.784818\*EVTOJ#

-2\*GSIGRE#-4\*GSIGMO#-8\*GSIGMO#-8\*GSIGNI#-8\*GSIGMO#; 6.00000E+03 N REF3 !  
PARAMETER G(SIGMA,MO:NI:MO:NI:MO;0) 2.98150E+02 -261.429115\*EVTOJ#

-2\*GSIGMO#-4\*GSIGNI#-8\*GSIGMO#-8\*GSIGNI#-8\*GSIGMO#; 6.00000E+03 N REF3 !  
PARAMETER G(SIGMA,NI:NI:MO:NI:MO;0) 2.98150E+02 -250.854899\*EVTOJ#

-2\*GSIGNI#-4\*GSIGNI#-8\*GSIGMO#-8\*GSIGNI#-8\*GSIGMO#; 6.00000E+03 N REF3 !  
PARAMETER G(SIGMA,RE:NI:MO:NI:MO;0) 2.98150E+02 -264.409288\*EVTOJ#

-2\*GSIGRE#-4\*GSIGNI#-8\*GSIGMO#-8\*GSIGNI#-8\*GSIGMO#; 6.00000E+03 N REF3 !  
PARAMETER G(SIGMA,MO:RE:MO:NI:MO;0) 2.98150E+02 -291.176964\*EVTOJ#

-2\*GSIGMO#-4\*GSIGRE#-8\*GSIGMO#-8\*GSIGNI#-8\*GSIGMO#; 6.00000E+03 N REF3 !  
PARAMETER G(SIGMA,NI:RE:MO:NI:MO;0) 2.98150E+02 -280.768382\*EVTOJ#

-2\*GSIGNI#-4\*GSIGRE#-8\*GSIGMO#-8\*GSIGNI#-8\*GSIGMO#; 6.00000E+03 N REF3 !  
PARAMETER G(SIGMA,RE:RE:MO:NI:MO;0) 2.98150E+02 -294.716226\*EVTOJ#

-2\*GSIGRE#-4\*GSIGRE#-8\*GSIGMO#-8\*GSIGNI#-8\*GSIGMO#; 6.00000E+03 N REF3 !  
PARAMETER G(SIGMA,MO:MO:NI:NI:MO;0) 2.98150E+02 -240.065279\*EVTOJ#

-2\*GSIGMO#-4\*GSIGMO#-8\*GSIGNI#-8\*GSIGNI#-8\*GSIGMO#; 6.00000E+03 N REF3 !  
PARAMETER G(SIGMA,NI:MO:NI:NI:MO;0) 2.98150E+02 -230.818865\*EVTOJ#

-2\*GSIGNI#-4\*GSIGMO#-8\*GSIGNI#-8\*GSIGNI#-8\*GSIGMO#; 6.00000E+03 N REF3 !  
PARAMETER G(SIGMA,RE:MO:NI:NI:MO;0) 2.98150E+02 -243.921526\*EVTOJ#

-2\*GSIGRE#-4\*GSIGMO#-8\*GSIGNI#-8\*GSIGNI#-8\*GSIGMO#; 6.00000E+03 N REF3 !  
PARAMETER G(SIGMA,MO:NI:NI:NI:MO;0) 2.98150E+02 -218.016614\*EVTOJ#

-2\*GSIGMO#-4\*GSIGNI#-8\*GSIGNI#-8\*GSIGNI#-8\*GSIGMO#; 6.00000E+03 N REF3 !  
PARAMETER G(SIGMA,NI:NI:NI:NI:MO;0) 2.98150E+02 -207.997035\*EVTOJ#

-2\*GSIGNI#-4\*GSIGNI#-8\*GSIGNI#-8\*GSIGNI#-8\*GSIGMO#; 6.00000E+03 N REF3 !  
PARAMETER G(SIGMA,RE:NI:NI:NI:MO;0) 2.98150E+02 -221.023416\*EVTOJ#

-2\*GSIGRE#-4\*GSIGNI#-8\*GSIGNI#-8\*GSIGNI#-8\*GSIGMO#; 6.00000E+03 N REF3 !  
PARAMETER G(SIGMA,MO:RE:NI:NI:MO;0) 2.98150E+02 -245.755471\*EVTOJ#

-2\*GSIGMO#-4\*GSIGRE#-8\*GSIGNI#-8\*GSIGNI#-8\*GSIGMO#; 6.00000E+03 N REF3 !  
PARAMETER G(SIGMA,NI:RE:NI:NI:MO;0) 2.98150E+02 -235.876405\*EVTOJ#

-2\*GSIGNI#-4\*GSIGRE#-8\*GSIGNI#-8\*GSIGNI#-8\*GSIGMO#; 6.00000E+03 N REF3 !  
PARAMETER G(SIGMA,RE:RE:NI:NI:MO;0) 2.98150E+02 -249.385112\*EVTOJ#

-2\*GSIGRE#-4\*GSIGRE#-8\*GSIGNI#-8\*GSIGNI#-8\*GSIGMO#; 6.00000E+03 N REF3 !  
PARAMETER G(SIGMA,MO:MO:RE:NI:MO;0) 2.98150E+02 -297.398681\*EVTOJ#

-2\*GSIGMO#-4\*GSIGMO#-8\*GSIGRE#-8\*GSIGNI#-8\*GSIGMO#; 6.00000E+03 N REF3 !  
PARAMETER G(SIGMA,NI:MO:RE:NI:MO;0) 2.98150E+02 -287.568377\*EVTOJ#

-2\*GSIGNI#-4\*GSIGMO#-8\*GSIGRE#-8\*GSIGNI#-8\*GSIGMO#; 6.00000E+03 N REF3 !  
PARAMETER G(SIGMA,RE:MO:RE:NI:MO;0) 2.98150E+02 -301.267105\*EVTOJ#

-2\*GSIGRE#-4\*GSIGMO#-8\*GSIGRE#-8\*GSIGNI#-8\*GSIGMO#; 6.00000E+03 N REF3 !  
PARAMETER G(SIGMA,MO:NI:RE:NI:MO;0) 2.98150E+02 -273.928228\*EVTOJ#

-2\*GSIGMO#-4\*GSIGNI#-8\*GSIGRE#-8\*GSIGNI#-8\*GSIGMO#; 6.00000E+03 N REF3 !  
PARAMETER G(SIGMA,NI:NI:RE:NI:MO;0) 2.98150E+02 -263.477223\*EVTOJ#

-2\*GSIGNI#-4\*GSIGNI#-8\*GSIGRE#-8\*GSIGNI#-8\*GSIGMO#; 6.00000E+03 N REF3 !  
PARAMETER G(SIGMA,RE:NI:RE:NI:MO;0) 2.98150E+02 -277.001352\*EVTOJ#

-2\*GSIGRE#-4\*GSIGNI#-8\*GSIGRE#-8\*GSIGNI#-8\*GSIGMO#; 6.00000E+03 N REF3 !  
PARAMETER G(SIGMA,MO:RE:RE:NI:MO;0) 2.98150E+02 -303.571781\*EVTOJ#

-2\*GSIGMO#-4\*GSIGRE#-8\*GSIGRE#-8\*GSIGNI#-8\*GSIGMO#; 6.00000E+03 N REF3 !  
PARAMETER G(SIGMA,NI:RE:RE:NI:MO;0) 2.98150E+02 -293.40555\*EVTOJ#

-2\*GSIGNI#-4\*GSIGRE#-8\*GSIGRE#-8\*GSIGNI#-8\*GSIGMO#; 6.00000E+03 N REF3 !  
PARAMETER G(SIGMA,RE:RE:RE:NI:MO;0) 2.98150E+02 -307.085252\*EVTOJ#

-2\*GSIGRE#-4\*GSIGRE#-8\*GSIGRE#-8\*GSIGNI#-8\*GSIGMO#; 6.00000E+03 N REF3 !  
PARAMETER G(SIGMA,MO:MO:MO:RE:MO;0) 2.98150E+02 -338.810302\*EVTOJ#

-2\*GSIGMO#-4\*GSIGMO#-8\*GSIGMO#-8\*GSIGRE#-8\*GSIGMO#; 6.00000E+03 N REF3 !  
PARAMETER G(SIGMA,NI:MO:MO:RE:MO;0) 2.98150E+02 -329.774751\*EVTOJ#

-2\*GSIGNI#-4\*GSIGMO#-8\*GSIGMO#-8\*GSIGRE#-8\*GSIGMO#; 6.00000E+03 N REF3 !  
PARAMETER G(SIGMA,RE:MO:MO:RE:MO;0) 2.98150E+02 -342.644194\*EVTOJ#

-2\*GSIGRE#-4\*GSIGMO#-8\*GSIGMO#-8\*GSIGRE#-8\*GSIGMO#; 6.00000E+03 N REF3 !  
PARAMETER G(SIGMA,MO:NI:MO:RE:MO;0) 2.98150E+02 -314.21427\*EVTOJ#

-2\*GSIGMO#-4\*GSIGNI#-8\*GSIGMO#-8\*GSIGRE#-8\*GSIGMO#; 6.00000E+03 N REF3 !  
PARAMETER G(SIGMA,NI:NI:MO:RE:MO;0) 2.98150E+02 -304.927274\*EVTOJ#

-2\*GSIGNI#-4\*GSIGNI#-8\*GSIGMO#-8\*GSIGRE#-8\*GSIGMO#; 6.00000E+03 N REF3 !  
PARAMETER G(SIGMA,RE:NI:MO:RE:MO;0) 2.98150E+02 -317.718241\*EVTOJ#

-2\*GSIGRE#-4\*GSIGNI#-8\*GSIGMO#-8\*GSIGRE#-8\*GSIGMO#; 6.00000E+03 N REF3 !  
PARAMETER G(SIGMA,MO:RE:MO:RE:MO;0) 2.98150E+02 -344.381107\*EVTOJ#

-2\*GSIGMO#-4\*GSIGRE#-8\*GSIGMO#-8\*GSIGRE#-8\*GSIGMO#; 6.00000E+03 N REF3 !  
PARAMETER G(SIGMA,NI:RE:MO:RE:MO;0) 2.98150E+02 -335.348637\*EVTOJ#

-2\*GSIGNI#-4\*GSIGRE#-8\*GSIGMO#-8\*GSIGRE#-8\*GSIGMO#; 6.00000E+03 N REF3 !  
PARAMETER G(SIGMA,RE:RE:MO:RE:MO;0) 2.98150E+02 -347.970121\*EVTOJ#

-2\*GSIGRE#-4\*GSIGRE#-8\*GSIGMO#-8\*GSIGRE#-8\*GSIGMO#; 6.00000E+03 N REF3 !  
PARAMETER G(SIGMA,MO:MO:NI:RE:MO;0) 2.98150E+02 -292.849049\*EVTOJ#

-2\*GSIGMO#-4\*GSIGMO#-8\*GSIGNI#-8\*GSIGRE#-8\*GSIGMO#; 6.00000E+03 N REF3 !  
PARAMETER G(SIGMA,NI:MO:NI:RE:MO;0) 2.98150E+02 -283.945447\*EVTOJ#

-2\*GSIGNI#-4\*GSIGMO#-8\*GSIGNI#-8\*GSIGRE#-8\*GSIGMO#; 6.00000E+03 N REF3 !  
PARAMETER G(SIGMA,RE:MO:NI:RE:MO;0) 2.98150E+02 -296.31417\*EVTOJ#

-2\*GSIGRE#-4\*GSIGMO#-8\*GSIGNI#-8\*GSIGRE#-8\*GSIGMO#; 6.00000E+03 N REF3 !  
PARAMETER G(SIGMA,MO:NI:NI:RE:MO;0) 2.98150E+02 -269.076346\*EVTOJ#

-2\*GSIGMO#-4\*GSIGNI#-8\*GSIGNI#-8\*GSIGRE#-8\*GSIGMO#; 6.00000E+03 N REF3 !  
PARAMETER G(SIGMA,NI:NI:NI:RE:MO;0) 2.98150E+02 -259.935107\*EVTOJ#

-2\*GSIGNI#-4\*GSIGNI#-8\*GSIGNI#-8\*GSIGRE#-8\*GSIGMO#; 6.00000E+03 N REF3 !  
PARAMETER G(SIGMA,RE:NI:NI:RE:MO;0) 2.98150E+02 -272.524171\*EVTOJ#

-2\*GSIGRE#-4\*GSIGNI#-8\*GSIGNI#-8\*GSIGRE#-8\*GSIGMO#; 6.00000E+03 N REF3 !  
PARAMETER G(SIGMA,MO:RE:NI:RE:MO;0) 2.98150E+02 -297.997717\*EVTOJ#

-2\*GSIGMO#-4\*GSIGRE#-8\*GSIGNI#-8\*GSIGRE#-8\*GSIGMO#; 6.00000E+03 N REF3 !  
PARAMETER G(SIGMA,NI:RE:NI:RE:MO;0) 2.98150E+02 -289.456272\*EVTOJ#

-2\*GSIGNI#-4\*GSIGRE#-8\*GSIGNI#-8\*GSIGRE#-8\*GSIGMO#; 6.00000E+03 N REF3 !  
PARAMETER G(SIGMA,RE:RE:NI:RE:MO;0) 2.98150E+02 -301.218122\*EVTOJ#

-2\*GSIGRE#-4\*GSIGRE#-8\*GSIGNI#-8\*GSIGRE#-8\*GSIGMO#; 6.00000E+03 N REF3 !  
PARAMETER G(SIGMA,MO:MO:RE:RE:MO;0) 2.98150E+02 -350.877403\*EVTOJ#

-2\*GSIGMO#-4\*GSIGMO#-8\*GSIGRE#-8\*GSIGRE#-8\*GSIGMO#; 6.00000E+03 N REF3 !  
PARAMETER G(SIGMA,NI:MO:RE:RE:MO;0) 2.98150E+02 -341.666897\*EVTOJ#

-2\*GSIGNI#-4\*GSIGMO#-8\*GSIGRE#-8\*GSIGRE#-8\*GSIGMO#; 6.00000E+03 N REF3 !  
PARAMETER G(SIGMA,RE:MO:RE:RE:MO;0) 2.98150E+02 -354.690887\*EVTOJ#

-2\*GSIGRE#-4\*GSIGMO#-8\*GSIGRE#-8\*GSIGRE#-8\*GSIGMO#; 6.00000E+03 N REF3 !  
PARAMETER G(SIGMA,MO:NI:RE:RE:MO;0) 2.98150E+02 -326.585362\*EVTOJ#

-2\*GSIGMO#-4\*GSIGNI#-8\*GSIGRE#-8\*GSIGRE#-8\*GSIGMO#; 6.00000E+03 N REF3 !  
PARAMETER G(SIGMA,NI:NI:RE:RE:MO;0) 2.98150E+02 -317.260233\*EVTOJ#

-2\*GSIGNI#-4\*GSIGNI#-8\*GSIGRE#-8\*GSIGRE#-8\*GSIGMO#; 6.00000E+03 N REF3 !  
PARAMETER G(SIGMA,RE:NI:RE:RE:MO;0) 2.98150E+02 -330.132705\*EVTOJ#

-2\*GSIGRE#-4\*GSIGNI#-8\*GSIGRE#-8\*GSIGRE#-8\*GSIGMO#; 6.00000E+03 N REF3 !  
PARAMETER G(SIGMA,MO:RE:RE:RE:MO;0) 2.98150E+02 -356.308695\*EVTOJ#

-2\*GSIGMO#-4\*GSIGRE#-8\*GSIGRE#-8\*GSIGRE#-8\*GSIGMO#; 6.00000E+03 N REF3 !  
PARAMETER G(SIGMA,NI:RE:RE:RE:MO;0) 2.98150E+02 -347.340799\*EVTOJ#

-2\*GSIGNI#-4\*GSIGRE#-8\*GSIGRE#-8\*GSIGRE#-8\*GSIGMO#; 6.00000E+03 N REF3 !  
PARAMETER G(SIGMA,RE:RE:RE:RE:MO;0) 2.98150E+02 -359.887484\*EVTOJ#

-2\*GSIGRE#-4\*GSIGRE#-8\*GSIGRE#-8\*GSIGRE#-8\*GSIGMO#; 6.00000E+03 N REF3 !  
PARAMETER G(SIGMA,MO:MO:MO:MO:NI;0) 2.98150E+02 -279.844268\*EVTOJ#

-2\*GSIGMO#-4\*GSIGMO#-8\*GSIGMO#-8\*GSIGMO#-8\*GSIGNI#; 6.00000E+03 N REF3 !  
PARAMETER G(SIGMA,NI:MO:MO:MO:NI;0) 2.98150E+02 -269.919834\*EVTOJ#

-2\*GSIGNI#-4\*GSIGMO#-8\*GSIGMO#-8\*GSIGMO#-8\*GSIGNI#; 6.00000E+03 N REF3 !  
PARAMETER G(SIGMA,RE:MO:MO:MO:NI;0) 2.98150E+02 -283.544331\*EVTOJ#

-2\*GSIGRE#-4\*GSIGMO#-8\*GSIGMO#-8\*GSIGMO#-8\*GSIGNI#; 6.00000E+03 N REF3 !  
PARAMETER G(SIGMA,MO:NI:MO:MO:NI;0) 2.98150E+02 -257.289102\*EVTOJ#

-2\*GSIGMO#-4\*GSIGNI#-8\*GSIGMO#-8\*GSIGMO#-8\*GSIGNI#; 6.00000E+03 N REF3 !  
PARAMETER G(SIGMA,NI:NI:MO:MO:NI;0) 2.98150E+02 -247.739259\*EVTOJ#

-2\*GSIGNI#-4\*GSIGNI#-8\*GSIGMO#-8\*GSIGMO#-8\*GSIGNI#; 6.00000E+03 N REF3 !  
PARAMETER G(SIGMA,RE:NI:MO:MO:NI;0) 2.98150E+02 -260.379878\*EVTOJ#

-2\*GSIGRE#-4\*GSIGNI#-8\*GSIGMO#-8\*GSIGMO#-8\*GSIGNI#; 6.00000E+03 N REF3 !  
PARAMETER G(SIGMA,MO:RE:MO:MO:NI;0) 2.98150E+02 -286.681171\*EVTOJ#

-2\*GSIGMO#-4\*GSIGRE#-8\*GSIGMO#-8\*GSIGMO#-8\*GSIGNI#; 6.00000E+03 N REF3 !  
PARAMETER G(SIGMA,NI:RE:MO:MO:NI;0) 2.98150E+02 -276.627677\*EVTOJ#

-2\*GSIGNI#-4\*GSIGRE#-8\*GSIGMO#-8\*GSIGMO#-8\*GSIGNI#; 6.00000E+03 N REF3 !  
PARAMETER G(SIGMA,RE:RE:MO:MO:NI;0) 2.98150E+02 -290.137367\*EVTOJ#

-2\*GSIGRE#-4\*GSIGRE#-8\*GSIGMO#-8\*GSIGMO#-8\*GSIGNI#; 6.00000E+03 N REF3 !  
PARAMETER G(SIGMA,MO:MO:NI:MO:NI;0) 2.98150E+02 -238.990083\*EVTOJ#

-2\*GSIGMO#-4\*GSIGMO#-8\*GSIGNI#-8\*GSIGMO#-8\*GSIGNI#; 6.00000E+03 N REF3 !  
PARAMETER G(SIGMA,NI:MO:NI:MO:NI;0) 2.98150E+02 -229.74564\*EVTOJ#

-2\*GSIGNI#-4\*GSIGMO#-8\*GSIGNI#-8\*GSIGMO#-8\*GSIGNI#; 6.00000E+03 N REF3 !  
PARAMETER G(SIGMA,RE:MO:NI:MO:NI;0) 2.98150E+02 -242.85365\*EVTOJ#

-2\*GSIGRE#-4\*GSIGMO#-8\*GSIGNI#-8\*GSIGMO#-8\*GSIGNI#; 6.00000E+03 N REF3 !  
PARAMETER G(SIGMA,MO:NI:NI:MO:NI;0) 2.98150E+02 -216.639706\*EVTOJ#

-2\*GSIGMO#-4\*GSIGNI#-8\*GSIGNI#-8\*GSIGMO#-8\*GSIGNI#; 6.00000E+03 N REF3 !  
PARAMETER G(SIGMA,NI:NI:NI:MO:NI;0) 2.98150E+02 -207.529323\*EVTOJ#

-2\*GSIGNI#-4\*GSIGNI#-8\*GSIGNI#-8\*GSIGMO#-8\*GSIGNI#; 6.00000E+03 N REF3 !  
PARAMETER G(SIGMA,RE:NI:NI:MO:NI;0) 2.98150E+02 -220.102858\*EVTOJ#

-2\*GSIGRE#-4\*GSIGNI#-8\*GSIGNI#-8\*GSIGMO#-8\*GSIGNI#; 6.00000E+03 N REF3 !  
PARAMETER G(SIGMA,MO:RE:NI:MO:NI;0) 2.98150E+02 -245.087476\*EVTOJ#

-2\*GSIGMO#-4\*GSIGRE#-8\*GSIGNI#-8\*GSIGMO#-8\*GSIGNI#; 6.00000E+03 N REF3 !  
PARAMETER G(SIGMA,NI:RE:NI:MO:NI;0) 2.98150E+02 -236.012682\*EVTOJ#

-2\*GSIGNI#-4\*GSIGRE#-8\*GSIGNI#-8\*GSIGMO#-8\*GSIGNI#; 6.00000E+03 N REF3 !  
PARAMETER G(SIGMA,RE:RE:NI:MO:NI;0) 2.98150E+02 -248.784293\*EVTOJ#

-2\*GSIGRE#-4\*GSIGRE#-8\*GSIGNI#-8\*GSIGMO#-8\*GSIGNI#; 6.00000E+03 N REF3 !  
PARAMETER G(SIGMA,MO:MO:RE:MO:NI;0) 2.98150E+02 -292.398643\*EVTOJ#

-2\*GSIGMO#-4\*GSIGMO#-8\*GSIGRE#-8\*GSIGMO#-8\*GSIGNI#; 6.00000E+03 N REF3 !  
PARAMETER G(SIGMA,NI:MO:RE:MO:NI;0) 2.98150E+02 -282.863203\*EVTOJ#

-2\*GSIGNI#-4\*GSIGMO#-8\*GSIGRE#-8\*GSIGMO#-8\*GSIGNI#; 6.00000E+03 N REF3 !  
PARAMETER G(SIGMA,RE:MO:RE:MO:NI;0) 2.98150E+02 -296.111478\*EVTOJ#

-2\*GSIGRE#-4\*GSIGMO#-8\*GSIGRE#-8\*GSIGMO#-8\*GSIGNI#; 6.00000E+03 N REF3 !  
PARAMETER G(SIGMA,MO:NI:RE:MO:NI;0) 2.98150E+02 -268.816105\*EVTOJ#

-2\*GSIGMO#-4\*GSIGNI#-8\*GSIGRE#-8\*GSIGMO#-8\*GSIGNI#; 6.00000E+03 N REF3 !  
PARAMETER G(SIGMA,NI:NI:RE:MO:NI;0) 2.98150E+02 -259.322516\*EVTOJ#

-2\*GSIGNI#-4\*GSIGNI#-8\*GSIGRE#-8\*GSIGMO#-8\*GSIGNI#; 6.00000E+03 N REF3 !  
PARAMETER G(SIGMA,RE:NI:RE:MO:NI;0) 2.98150E+02 -272.12472\*EVTOJ#

-2\*GSIGRE#-4\*GSIGNI#-8\*GSIGRE#-8\*GSIGMO#-8\*GSIGNI#; 6.00000E+03 N REF3 !  
PARAMETER G(SIGMA,MO:RE:RE:MO:NI;0) 2.98150E+02 -298.869313\*EVTOJ#

-2\*GSIGMO#-4\*GSIGRE#-8\*GSIGRE#-8\*GSIGMO#-8\*GSIGNI#; 6.00000E+03 N REF3 !  
PARAMETER G(SIGMA,NI:RE:RE:MO:NI;0) 2.98150E+02 -289.182898\*EVTOJ#

-2\*GSIGNI#-4\*GSIGRE#-8\*GSIGRE#-8\*GSIGMO#-8\*GSIGNI#; 6.00000E+03 N REF3 !  
PARAMETER G(SIGMA,RE:RE:RE:MO:NI;0) 2.98150E+02 -302.340668\*EVTOJ#

-2\*GSIGRE#-4\*GSIGRE#-8\*GSIGRE#-8\*GSIGMO#-8\*GSIGNI#; 6.00000E+03 N REF3 !  
PARAMETER G(SIGMA,MO:MO:MO:NI:NI;0) 2.98150E+02 -240.246658\*EVTOJ#

-2\*GSIGMO#-4\*GSIGMO#-8\*GSIGMO#-8\*GSIGNI#-8\*GSIGNI#; 6.00000E+03 N REF3 !  
PARAMETER G(SIGMA,NI:MO:MO:NI:NI;0) 2.98150E+02 -230.317061\*EVTOJ#

-2\*GSIGNI#-4\*GSIGMO#-8\*GSIGMO#-8\*GSIGNI#-8\*GSIGNI#; 6.00000E+03 N REF3 !  
PARAMETER G(SIGMA,RE:MO:MO:NI:NI;0) 2.98150E+02 -243.561419\*EVTOJ#

-2\*GSIGRE#-4\*GSIGMO#-8\*GSIGMO#-8\*GSIGNI#-8\*GSIGNI#; 6.00000E+03 N REF3 !  
PARAMETER G(SIGMA,MO:NI:MO:NI:NI;0) 2.98150E+02 -219.731417\*EVTOJ#

-2\*GSIGMO#-4\*GSIGNI#-8\*GSIGMO#-8\*GSIGNI#-8\*GSIGNI#; 6.00000E+03 N REF3 !  
PARAMETER G(SIGMA,NI:NI:MO:NI:NI;0) 2.98150E+02 -208.927318\*EVTOJ#

-2\*GSIGNI#-4\*GSIGNI#-8\*GSIGMO#-8\*GSIGNI#-8\*GSIGNI#; 6.00000E+03 N REF3 !  
PARAMETER G(SIGMA,RE:NI:MO:NI:NI;0) 2.98150E+02 -222.340976\*EVTOJ#

-2\*GSIGRE#-4\*GSIGNI#-8\*GSIGMO#-8\*GSIGNI#-8\*GSIGNI#; 6.00000E+03 N REF3 !  
PARAMETER G(SIGMA,MO:RE:MO:NI:NI;0) 2.98150E+02 -246.706817\*EVTOJ#

-2\*GSIGMO#-4\*GSIGRE#-8\*GSIGMO#-8\*GSIGNI#-8\*GSIGNI#; 6.00000E+03 N REF3 !  
PARAMETER G(SIGMA,NI:RE:MO:NI:NI;0) 2.98150E+02 -236.363888\*EVTOJ#

-2\*GSIGNI#-4\*GSIGRE#-8\*GSIGMO#-8\*GSIGNI#-8\*GSIGNI#; 6.00000E+03 N REF3 !  
PARAMETER G(SIGMA,RE:RE:MO:NI:NI;0) 2.98150E+02 -249.770239\*EVTOJ#

-2\*GSIGRE#-4\*GSIGRE#-8\*GSIGMO#-8\*GSIGNI#-8\*GSIGNI#; 6.00000E+03 N REF3 !  
PARAMETER G(SIGMA,MO:MO:NI:NI:NI;0) 2.98150E+02 -197.377056\*EVTOJ#

-2\*GSIGMO#-4\*GSIGMO#-8\*GSIGNI#-8\*GSIGNI#-8\*GSIGNI#; 6.00000E+03 N REF3 !  
PARAMETER G(SIGMA,NI:MO:NI:NI:NI;0) 2.98150E+02 -187.632053\*EVTOJ#

-2\*GSIGNI#-4\*GSIGMO#-8\*GSIGNI#-8\*GSIGNI#-8\*GSIGNI#; 6.00000E+03 N REF3 !  
PARAMETER G(SIGMA,RE:MO:NI:NI:NI;0) 2.98150E+02 -200.918794\*EVTOJ#

-2\*GSIGRE#-4\*GSIGMO#-8\*GSIGNI#-8\*GSIGNI#-8\*GSIGNI#; 6.00000E+03 N REF3 !  
PARAMETER G(SIGMA,MO:NI:NI:NI:NI;0) 2.98150E+02 -174.956301\*EVTOJ#

-2\*GSIGMO#-4\*GSIGNI#-8\*GSIGNI#-8\*GSIGNI#-8\*GSIGNI#; 6.00000E+03 N REF3 !  
PARAMETER G(SIGMA,NI:NI:NI:NI:NI;0) 298.15 0; 6000 N!  
PARAMETER G(SIGMA,RE:NI:NI:NI:NI;0) 2.98150E+02 -177.697766\*EVTOJ#

-2\*GSIGRE#-4\*GSIGNI#-8\*GSIGNI#-8\*GSIGNI#-8\*GSIGNI#; 6.00000E+03 N REF3 !  
PARAMETER G(SIGMA,MO:RE:NI:NI:NI;0) 2.98150E+02 -202.650568\*EVTOJ#

-2\*GSIGMO#-4\*GSIGRE#-8\*GSIGNI#-8\*GSIGNI#-8\*GSIGNI#; 6.00000E+03 N REF3 !  
PARAMETER G(SIGMA,NI:RE:NI:NI:NI;0) 2.98150E+02 -192.454196\*EVTOJ#

-2\*GSIGNI#-4\*GSIGRE#-8\*GSIGNI#-8\*GSIGNI#-8\*GSIGNI#; 6.00000E+03 N REF3 !  
PARAMETER G(SIGMA,RE:RE:NI:NI:NI;0) 2.98150E+02 -205.959867\*EVTOJ#

-2\*GSIGRE#-4\*GSIGRE#-8\*GSIGNI#-8\*GSIGNI#-8\*GSIGNI#; 6.00000E+03 N REF3 !

PARAMETER G(SIGMA,MO:MO:RE:NI:NI;0) 2.98150E+02 -251.470331\*EVTOJ#  
 -2\*GSIGMO#-4\*GSIGMO#-8\*GSIGRE#-8\*GSIGNI#-8\*GSIGNI#; 6.00000E+03 N REF3 !  
 PARAMETER G(SIGMA,NI:MO:RE:NI:NI;0) 2.98150E+02 -241.660577\*EVTOJ#  
 -2\*GSIGNI#-4\*GSIGMO#-8\*GSIGRE#-8\*GSIGNI#-8\*GSIGNI#; 6.00000E+03 N REF3 !  
 PARAMETER G(SIGMA,RE:MO:RE:NI:NI;0) 2.98150E+02 -254.782431\*EVTOJ#  
 -2\*GSIGRE#-4\*GSIGMO#-8\*GSIGRE#-8\*GSIGNI#-8\*GSIGNI#; 6.00000E+03 N REF3 !  
 PARAMETER G(SIGMA,MO:NI:RE:NI:NI;0) 2.98150E+02 -230.285929\*EVTOJ#  
 -2\*GSIGMO#-4\*GSIGNI#-8\*GSIGRE#-8\*GSIGNI#-8\*GSIGNI#; 6.00000E+03 N REF3 !  
 PARAMETER G(SIGMA,NI:NI:RE:NI:NI;0) 2.98150E+02 -219.398982\*EVTOJ#  
 -2\*GSIGNI#-4\*GSIGNI#-8\*GSIGRE#-8\*GSIGNI#-8\*GSIGNI#; 6.00000E+03 N REF3 !  
 PARAMETER G(SIGMA,RE:NI:RE:NI:NI;0) 2.98150E+02 -232.977\*EVTOJ#  
 -2\*GSIGRE#-4\*GSIGNI#-8\*GSIGRE#-8\*GSIGNI#-8\*GSIGNI#; 6.00000E+03 N REF3 !  
 PARAMETER G(SIGMA,MO:RE:RE:NI:NI;0) 2.98150E+02 -257.795775\*EVTOJ#  
 -2\*GSIGMO#-4\*GSIGRE#-8\*GSIGRE#-8\*GSIGNI#-8\*GSIGNI#; 6.00000E+03 N REF3 !  
 PARAMETER G(SIGMA,NI:RE:RE:NI:NI;0) 2.98150E+02 -247.677932\*EVTOJ#  
 -2\*GSIGNI#-4\*GSIGRE#-8\*GSIGRE#-8\*GSIGNI#-8\*GSIGNI#; 6.00000E+03 N REF3 !  
 PARAMETER G(SIGMA,RE:RE:RE:NI:NI;0) 2.98150E+02 -260.869357\*EVTOJ#  
 -2\*GSIGRE#-4\*GSIGRE#-8\*GSIGRE#-8\*GSIGNI#-8\*GSIGNI#; 6.00000E+03 N REF3 !  
 PARAMETER G(SIGMA,MO:MO:MO:RE:NI;0) 2.98150E+02 -294.272002\*EVTOJ#  
 -2\*GSIGMO#-4\*GSIGMO#-8\*GSIGMO#-8\*GSIGRE#-8\*GSIGNI#; 6.00000E+03 N REF3 !  
 PARAMETER G(SIGMA,NI:MO:MO:RE:NI;0) 2.98150E+02 -284.030927\*EVTOJ#  
 -2\*GSIGNI#-4\*GSIGMO#-8\*GSIGMO#-8\*GSIGRE#-8\*GSIGNI#; 6.00000E+03 N REF3 !  
 PARAMETER G(SIGMA,RE:MO:MO:RE:NI;0) 2.98150E+02 -297.819472\*EVTOJ#  
 -2\*GSIGRE#-4\*GSIGMO#-8\*GSIGMO#-8\*GSIGRE#-8\*GSIGNI#; 6.00000E+03 N REF3 !  
 PARAMETER G(SIGMA,MO:NI:MO:RE:NI;0) 2.98150E+02 -271.697031\*EVTOJ#  
 -2\*GSIGMO#-4\*GSIGNI#-8\*GSIGMO#-8\*GSIGRE#-8\*GSIGNI#; 6.00000E+03 N REF3 !  
 PARAMETER G(SIGMA,NI:NI:MO:RE:NI;0) 2.98150E+02 -261.5216\*EVTOJ#  
 -2\*GSIGNI#-4\*GSIGNI#-8\*GSIGMO#-8\*GSIGRE#-8\*GSIGNI#; 6.00000E+03 N REF3 !  
 PARAMETER G(SIGMA,RE:NI:MO:RE:NI;0) 2.98150E+02 -274.847557\*EVTOJ#  
 -2\*GSIGRE#-4\*GSIGNI#-8\*GSIGMO#-8\*GSIGRE#-8\*GSIGNI#; 6.00000E+03 N REF3 !  
 PARAMETER G(SIGMA,MO:RE:MO:RE:NI;0) 2.98150E+02 -300.488396\*EVTOJ#  
 -2\*GSIGMO#-4\*GSIGRE#-8\*GSIGMO#-8\*GSIGRE#-8\*GSIGNI#; 6.00000E+03 N REF3 !  
 PARAMETER G(SIGMA,NI:RE:MO:RE:NI;0) 2.98150E+02 -290.05664\*EVTOJ#  
 -2\*GSIGNI#-4\*GSIGRE#-8\*GSIGMO#-8\*GSIGRE#-8\*GSIGNI#; 6.00000E+03 N REF3 !  
 PARAMETER G(SIGMA,RE:RE:MO:RE:NI;0) 2.98150E+02 -303.731749\*EVTOJ#  
 -2\*GSIGRE#-4\*GSIGRE#-8\*GSIGMO#-8\*GSIGRE#-8\*GSIGNI#; 6.00000E+03 N REF3 !  
 PARAMETER G(SIGMA,MO:MO:NI:RE:NI;0) 2.98150E+02 -250.459029\*EVTOJ#  
 -2\*GSIGMO#-4\*GSIGMO#-8\*GSIGNI#-8\*GSIGRE#-8\*GSIGNI#; 6.00000E+03 N REF3 !

PARAMETER G(SIGMA,NI:MO:NI:RE:NI;0) 2.98150E+02 -241.578744\*EVTOJ#  
 -2\*GSIGNI#-4\*GSIGMO#-8\*GSIGNI#-8\*GSIGRE#-8\*GSIGNI#; 6.00000E+03 N REF3 !  
 PARAMETER G(SIGMA,RE:MO:NI:RE:NI;0) 2.98150E+02 -254.134378\*EVTOJ#  
 -2\*GSIGRE#-4\*GSIGMO#-8\*GSIGNI#-8\*GSIGRE#-8\*GSIGNI#; 6.00000E+03 N REF3 !  
 PARAMETER G(SIGMA,MO:NI:NI:RE:NI;0) 2.98150E+02 -227.960961\*EVTOJ#  
 -2\*GSIGMO#-4\*GSIGNI#-8\*GSIGNI#-8\*GSIGRE#-8\*GSIGNI#; 6.00000E+03 N REF3 !  
 PARAMETER G(SIGMA,NI:NI:NI:RE:NI;0) 2.98150E+02 -218.263036\*EVTOJ#  
 -2\*GSIGNI#-4\*GSIGNI#-8\*GSIGNI#-8\*GSIGRE#-8\*GSIGNI#; 6.00000E+03 N REF3 !  
 PARAMETER G(SIGMA,RE:NI:NI:RE:NI;0) 2.98150E+02 -231.269776\*EVTOJ#  
 -2\*GSIGRE#-4\*GSIGNI#-8\*GSIGNI#-8\*GSIGRE#-8\*GSIGNI#; 6.00000E+03 N REF3 !  
 PARAMETER G(SIGMA,MO:RE:NI:RE:NI;0) 2.98150E+02 -256.103007\*EVTOJ#  
 -2\*GSIGMO#-4\*GSIGRE#-8\*GSIGNI#-8\*GSIGRE#-8\*GSIGNI#; 6.00000E+03 N REF3 !  
 PARAMETER G(SIGMA,NI:RE:NI:RE:NI;0) 2.98150E+02 -247.113195\*EVTOJ#  
 -2\*GSIGNI#-4\*GSIGRE#-8\*GSIGNI#-8\*GSIGRE#-8\*GSIGNI#; 6.00000E+03 N REF3 !  
 PARAMETER G(SIGMA,RE:RE:NI:RE:NI;0) 2.98150E+02 -259.616657\*EVTOJ#  
 -2\*GSIGRE#-4\*GSIGRE#-8\*GSIGNI#-8\*GSIGRE#-8\*GSIGNI#; 6.00000E+03 N REF3 !  
 PARAMETER G(SIGMA,MO:MO:RE:RE:NI;0) 2.98150E+02 -306.303925\*EVTOJ#  
 -2\*GSIGMO#-4\*GSIGMO#-8\*GSIGRE#-8\*GSIGRE#-8\*GSIGNI#; 6.00000E+03 N REF3 !  
 PARAMETER G(SIGMA,NI:MO:RE:RE:NI;0) 2.98150E+02 -296.341703\*EVTOJ#  
 -2\*GSIGNI#-4\*GSIGMO#-8\*GSIGRE#-8\*GSIGRE#-8\*GSIGNI#; 6.00000E+03 N REF3 !  
 PARAMETER G(SIGMA,RE:MO:RE:RE:NI;0) 2.98150E+02 -309.938637\*EVTOJ#  
 -2\*GSIGRE#-4\*GSIGMO#-8\*GSIGRE#-8\*GSIGRE#-8\*GSIGNI#; 6.00000E+03 N REF3 !  
 PARAMETER G(SIGMA,MO:NI:RE:RE:NI;0) 2.98150E+02 -283.464586\*EVTOJ#  
 -2\*GSIGMO#-4\*GSIGNI#-8\*GSIGRE#-8\*GSIGRE#-8\*GSIGNI#; 6.00000E+03 N REF3 !  
 PARAMETER G(SIGMA,NI:NI:RE:RE:NI;0) 2.98150E+02 -273.089814\*EVTOJ#  
 -2\*GSIGNI#-4\*GSIGNI#-8\*GSIGRE#-8\*GSIGRE#-8\*GSIGNI#; 6.00000E+03 N REF3 !  
 PARAMETER G(SIGMA,RE:NI:RE:RE:NI;0) 2.98150E+02 -286.653789\*EVTOJ#  
 -2\*GSIGRE#-4\*GSIGNI#-8\*GSIGRE#-8\*GSIGRE#-8\*GSIGNI#; 6.00000E+03 N REF3 !  
 PARAMETER G(SIGMA,MO:RE:RE:RE:NI;0) 2.98150E+02 -312.357593\*EVTOJ#  
 -2\*GSIGMO#-4\*GSIGRE#-8\*GSIGRE#-8\*GSIGRE#-8\*GSIGNI#; 6.00000E+03 N REF3 !  
 PARAMETER G(SIGMA,NI:RE:RE:RE:NI;0) 2.98150E+02 -302.296848\*EVTOJ#  
 -2\*GSIGNI#-4\*GSIGRE#-8\*GSIGRE#-8\*GSIGRE#-8\*GSIGNI#; 6.00000E+03 N REF3 !  
 PARAMETER G(SIGMA,RE:RE:RE:RE:NI;0) 2.98150E+02 -315.726379\*EVTOJ#  
 -2\*GSIGRE#-4\*GSIGRE#-8\*GSIGRE#-8\*GSIGRE#-8\*GSIGNI#; 6.00000E+03 N REF3 !  
 PARAMETER G(SIGMA,MO:MO:MO:MO:RE;0) 2.98150E+02 -336.420911\*EVTOJ#  
 -2\*GSIGMO#-4\*GSIGMO#-8\*GSIGMO#-8\*GSIGMO#-8\*GSIGRE#; 6.00000E+03 N REF3 !  
 PARAMETER G(SIGMA,NI:MO:MO:MO:RE;0) 2.98150E+02 -326.86707\*EVTOJ#  
 -2\*GSIGNI#-4\*GSIGMO#-8\*GSIGMO#-8\*GSIGMO#-8\*GSIGRE#; 6.00000E+03 N REF3 !

PARAMETER G(SIGMA,RE:MO:MO:MO:RE;0) 2.98150E+02 -340.042158\*EVTOJ#  
 -2\*GSIGRE#-4\*GSIGMO#-8\*GSIGMO#-8\*GSIGMO#-8\*GSIGRE#; 6.00000E+03 N REF3 !  
 PARAMETER G(SIGMA,MO:NI:MO:MO:RE;0) 2.98150E+02 -311.831904\*EVTOJ#  
 -2\*GSIGMO#-4\*GSIGNI#-8\*GSIGMO#-8\*GSIGMO#-8\*GSIGRE#; 6.00000E+03 N REF3 !  
 PARAMETER G(SIGMA,NI:NI:MO:MO:RE;0) 2.98150E+02 -302.420116\*EVTOJ#  
 -2\*GSIGNI#-4\*GSIGNI#-8\*GSIGMO#-8\*GSIGMO#-8\*GSIGRE#; 6.00000E+03 N REF3 !  
 PARAMETER G(SIGMA,RE:NI:MO:MO:RE;0) 2.98150E+02 -315.155119\*EVTOJ#  
 -2\*GSIGRE#-4\*GSIGNI#-8\*GSIGMO#-8\*GSIGMO#-8\*GSIGRE#; 6.00000E+03 N REF3 !  
 PARAMETER G(SIGMA,MO:RE:MO:MO:RE;0) 2.98150E+02 -341.899815\*EVTOJ#  
 -2\*GSIGMO#-4\*GSIGRE#-8\*GSIGMO#-8\*GSIGMO#-8\*GSIGRE#; 6.00000E+03 N REF3 !  
 PARAMETER G(SIGMA,NI:RE:MO:MO:RE;0) 2.98150E+02 -332.489232\*EVTOJ#  
 -2\*GSIGNI#-4\*GSIGRE#-8\*GSIGMO#-8\*GSIGMO#-8\*GSIGRE#; 6.00000E+03 N REF3 !  
 PARAMETER G(SIGMA,RE:RE:MO:MO:RE;0) 2.98150E+02 -345.245205\*EVTOJ#  
 -2\*GSIGRE#-4\*GSIGRE#-8\*GSIGMO#-8\*GSIGMO#-8\*GSIGRE#; 6.00000E+03 N REF3 !  
 PARAMETER G(SIGMA,MO:MO:NI:MO:RE;0) 2.98150E+02 -293.017026\*EVTOJ#  
 -2\*GSIGMO#-4\*GSIGMO#-8\*GSIGNI#-8\*GSIGMO#-8\*GSIGRE#; 6.00000E+03 N REF3 !  
 PARAMETER G(SIGMA,NI:MO:NI:MO:RE;0) 2.98150E+02 -283.679938\*EVTOJ#  
 -2\*GSIGNI#-4\*GSIGMO#-8\*GSIGNI#-8\*GSIGMO#-8\*GSIGRE#; 6.00000E+03 N REF3 !  
 PARAMETER G(SIGMA,RE:MO:NI:MO:RE;0) 2.98150E+02 -296.490917\*EVTOJ#  
 -2\*GSIGRE#-4\*GSIGMO#-8\*GSIGNI#-8\*GSIGMO#-8\*GSIGRE#; 6.00000E+03 N REF3 !  
 PARAMETER G(SIGMA,MO:NI:NI:MO:RE;0) 2.98150E+02 -268.72644\*EVTOJ#  
 -2\*GSIGMO#-4\*GSIGNI#-8\*GSIGNI#-8\*GSIGMO#-8\*GSIGRE#; 6.00000E+03 N REF3 !  
 PARAMETER G(SIGMA,NI:NI:NI:MO:RE;0) 2.98150E+02 -259.367065\*EVTOJ#  
 -2\*GSIGNI#-4\*GSIGNI#-8\*GSIGNI#-8\*GSIGMO#-8\*GSIGRE#; 6.00000E+03 N REF3 !  
 PARAMETER G(SIGMA,RE:NI:NI:MO:RE;0) 2.98150E+02 -272.090694\*EVTOJ#  
 -2\*GSIGRE#-4\*GSIGNI#-8\*GSIGNI#-8\*GSIGMO#-8\*GSIGRE#; 6.00000E+03 N REF3 !  
 PARAMETER G(SIGMA,MO:RE:NI:MO:RE;0) 2.98150E+02 -298.02415\*EVTOJ#  
 -2\*GSIGMO#-4\*GSIGRE#-8\*GSIGNI#-8\*GSIGMO#-8\*GSIGRE#; 6.00000E+03 N REF3 !  
 PARAMETER G(SIGMA,NI:RE:NI:MO:RE;0) 2.98150E+02 -288.794546\*EVTOJ#  
 -2\*GSIGNI#-4\*GSIGRE#-8\*GSIGNI#-8\*GSIGMO#-8\*GSIGRE#; 6.00000E+03 N REF3 !  
 PARAMETER G(SIGMA,RE:RE:NI:MO:RE;0) 2.98150E+02 -301.270702\*EVTOJ#  
 -2\*GSIGRE#-4\*GSIGRE#-8\*GSIGNI#-8\*GSIGMO#-8\*GSIGRE#; 6.00000E+03 N REF3 !  
 PARAMETER G(SIGMA,MO:MO:RE:MO:RE;0) 2.98150E+02 -348.274113\*EVTOJ#  
 -2\*GSIGMO#-4\*GSIGMO#-8\*GSIGRE#-8\*GSIGMO#-8\*GSIGRE#; 6.00000E+03 N REF3 !  
 PARAMETER G(SIGMA,NI:MO:RE:MO:RE;0) 2.98150E+02 -338.579407\*EVTOJ#  
 -2\*GSIGNI#-4\*GSIGMO#-8\*GSIGRE#-8\*GSIGMO#-8\*GSIGRE#; 6.00000E+03 N REF3 !  
 PARAMETER G(SIGMA,RE:MO:RE:MO:RE;0) 2.98150E+02 -351.792339\*EVTOJ#  
 -2\*GSIGRE#-4\*GSIGMO#-8\*GSIGRE#-8\*GSIGMO#-8\*GSIGRE#; 6.00000E+03 N REF3 !

PARAMETER G(SIGMA,MO:NI:RE:MO:RE;0) 2.98150E+02 -323.788038\*EVTOJ#  
 -2\*GSIGMO#-4\*GSIGNI#-8\*GSIGRE#-8\*GSIGMO#-8\*GSIGRE#; 6.00000E+03 N REF3 !  
 PARAMETER G(SIGMA,NI:NI:RE:MO:RE;0) 2.98150E+02 -314.266628\*EVTOJ#  
 -2\*GSIGNI#-4\*GSIGNI#-8\*GSIGRE#-8\*GSIGMO#-8\*GSIGRE#; 6.00000E+03 N REF3 !  
 PARAMETER G(SIGMA,RE:NI:RE:MO:RE;0) 2.98150E+02 -326.966036\*EVTOJ#  
 -2\*GSIGRE#-4\*GSIGNI#-8\*GSIGRE#-8\*GSIGMO#-8\*GSIGRE#; 6.00000E+03 N REF3 !  
 PARAMETER G(SIGMA,MO:RE:RE:MO:RE;0) 2.98150E+02 -353.543856\*EVTOJ#  
 -2\*GSIGMO#-4\*GSIGRE#-8\*GSIGRE#-8\*GSIGMO#-8\*GSIGRE#; 6.00000E+03 N REF3 !  
 PARAMETER G(SIGMA,NI:RE:RE:MO:RE;0) 2.98150E+02 -344.194316\*EVTOJ#  
 -2\*GSIGNI#-4\*GSIGRE#-8\*GSIGRE#-8\*GSIGMO#-8\*GSIGRE#; 6.00000E+03 N REF3 !  
 PARAMETER G(SIGMA,RE:RE:RE:MO:RE;0) 2.98150E+02 -356.822818\*EVTOJ#  
 -2\*GSIGRE#-4\*GSIGRE#-8\*GSIGRE#-8\*GSIGMO#-8\*GSIGRE#; 6.00000E+03 N REF3 !  
 PARAMETER G(SIGMA,MO:MO:MO:NI:RE;0) 2.98150E+02 -297.575496\*EVTOJ#  
 -2\*GSIGMO#-4\*GSIGMO#-8\*GSIGMO#-8\*GSIGNI#-8\*GSIGRE#; 6.00000E+03 N REF3 !  
 PARAMETER G(SIGMA,NI:MO:MO:NI:RE;0) 2.98150E+02 -287.149373\*EVTOJ#  
 -2\*GSIGNI#-4\*GSIGMO#-8\*GSIGMO#-8\*GSIGNI#-8\*GSIGRE#; 6.00000E+03 N REF3 !  
 PARAMETER G(SIGMA,RE:MO:MO:NI:RE;0) 2.98150E+02 -301.090847\*EVTOJ#  
 -2\*GSIGRE#-4\*GSIGMO#-8\*GSIGMO#-8\*GSIGNI#-8\*GSIGRE#; 6.00000E+03 N REF3 !  
 PARAMETER G(SIGMA,MO:NI:MO:NI:RE;0) 2.98150E+02 -274.029599\*EVTOJ#  
 -2\*GSIGMO#-4\*GSIGNI#-8\*GSIGMO#-8\*GSIGNI#-8\*GSIGRE#; 6.00000E+03 N REF3 !  
 PARAMETER G(SIGMA,NI:NI:MO:NI:RE;0) 2.98150E+02 -263.127641\*EVTOJ#  
 -2\*GSIGNI#-4\*GSIGNI#-8\*GSIGMO#-8\*GSIGNI#-8\*GSIGRE#; 6.00000E+03 N REF3 !  
 PARAMETER G(SIGMA,RE:NI:MO:NI:RE;0) 2.98150E+02 -276.815486\*EVTOJ#  
 -2\*GSIGRE#-4\*GSIGNI#-8\*GSIGMO#-8\*GSIGNI#-8\*GSIGRE#; 6.00000E+03 N REF3 !  
 PARAMETER G(SIGMA,MO:RE:MO:NI:RE;0) 2.98150E+02 -303.089052\*EVTOJ#  
 -2\*GSIGMO#-4\*GSIGRE#-8\*GSIGMO#-8\*GSIGNI#-8\*GSIGRE#; 6.00000E+03 N REF3 !  
 PARAMETER G(SIGMA,NI:RE:MO:NI:RE;0) 2.98150E+02 -292.409821\*EVTOJ#  
 -2\*GSIGNI#-4\*GSIGRE#-8\*GSIGMO#-8\*GSIGNI#-8\*GSIGRE#; 6.00000E+03 N REF3 !  
 PARAMETER G(SIGMA,RE:RE:MO:NI:RE;0) 2.98150E+02 -306.297599\*EVTOJ#  
 -2\*GSIGRE#-4\*GSIGRE#-8\*GSIGMO#-8\*GSIGNI#-8\*GSIGRE#; 6.00000E+03 N REF3 !  
 PARAMETER G(SIGMA,MO:MO:NI:NI:RE;0) 2.98150E+02 -251.456422\*EVTOJ#  
 -2\*GSIGMO#-4\*GSIGMO#-8\*GSIGNI#-8\*GSIGNI#-8\*GSIGRE#; 6.00000E+03 N REF3 !  
 PARAMETER G(SIGMA,NI:MO:NI:NI:RE;0) 2.98150E+02 -241.489464\*EVTOJ#  
 -2\*GSIGNI#-4\*GSIGMO#-8\*GSIGNI#-8\*GSIGNI#-8\*GSIGRE#; 6.00000E+03 N REF3 !  
 PARAMETER G(SIGMA,RE:MO:NI:NI:RE;0) 2.98150E+02 -254.979821\*EVTOJ#  
 -2\*GSIGRE#-4\*GSIGMO#-8\*GSIGNI#-8\*GSIGNI#-8\*GSIGRE#; 6.00000E+03 N REF3 !  
 PARAMETER G(SIGMA,MO:NI:NI:NI:RE;0) 2.98150E+02 -228.364456\*EVTOJ#  
 -2\*GSIGMO#-4\*GSIGNI#-8\*GSIGNI#-8\*GSIGNI#-8\*GSIGRE#; 6.00000E+03 N REF3 !

PARAMETER G(SIGMA,NI:NI:NI:NI:RE;0) 2.98150E+02 -218.174387\*EVTOJ#  
 -2\*GSIGNI#-4\*GSIGNI#-8\*GSIGNI#-8\*GSIGNI#-8\*GSIGRE#; 6.00000E+03 N REF3 !  
 PARAMETER G(SIGMA,RE:NI:NI:NI:RE;0) 2.98150E+02 -231.10592\*EVTOJ#  
 -2\*GSIGRE#-4\*GSIGNI#-8\*GSIGNI#-8\*GSIGNI#-8\*GSIGRE#; 6.00000E+03 N REF3 !  
 PARAMETER G(SIGMA,MO:RE:NI:NI:RE;0) 2.98150E+02 -256.355297\*EVTOJ#  
 -2\*GSIGMO#-4\*GSIGRE#-8\*GSIGNI#-8\*GSIGNI#-8\*GSIGRE#; 6.00000E+03 N REF3 !  
 PARAMETER G(SIGMA,NI:RE:NI:NI:RE;0) 2.98150E+02 -246.030063\*EVTOJ#  
 -2\*GSIGNI#-4\*GSIGRE#-8\*GSIGNI#-8\*GSIGNI#-8\*GSIGRE#; 6.00000E+03 N REF3 !  
 PARAMETER G(SIGMA,RE:RE:NI:NI:RE;0) 2.98150E+02 -259.605763\*EVTOJ#  
 -2\*GSIGRE#-4\*GSIGRE#-8\*GSIGNI#-8\*GSIGNI#-8\*GSIGRE#; 6.00000E+03 N REF3 !  
 PARAMETER G(SIGMA,MO:MO:RE:NI:RE;0) 2.98150E+02 -308.81836\*EVTOJ#  
 -2\*GSIGMO#-4\*GSIGMO#-8\*GSIGRE#-8\*GSIGNI#-8\*GSIGRE#; 6.00000E+03 N REF3 !  
 PARAMETER G(SIGMA,NI:MO:RE:NI:RE;0) 2.98150E+02 -298.733766\*EVTOJ#  
 -2\*GSIGNI#-4\*GSIGMO#-8\*GSIGRE#-8\*GSIGNI#-8\*GSIGRE#; 6.00000E+03 N REF3 !  
 PARAMETER G(SIGMA,RE:MO:RE:NI:RE;0) 2.98150E+02 -312.227999\*EVTOJ#  
 -2\*GSIGRE#-4\*GSIGMO#-8\*GSIGRE#-8\*GSIGNI#-8\*GSIGRE#; 6.00000E+03 N REF3 !  
 PARAMETER G(SIGMA,MO:NI:RE:NI:RE;0) 2.98150E+02 -285.287181\*EVTOJ#  
 -2\*GSIGMO#-4\*GSIGNI#-8\*GSIGRE#-8\*GSIGNI#-8\*GSIGRE#; 6.00000E+03 N REF3 !  
 PARAMETER G(SIGMA,NI:NI:RE:NI:RE;0) 2.98150E+02 -274.832718\*EVTOJ#  
 -2\*GSIGNI#-4\*GSIGNI#-8\*GSIGRE#-8\*GSIGNI#-8\*GSIGRE#; 6.00000E+03 N REF3 !  
 PARAMETER G(SIGMA,RE:NI:RE:NI:RE;0) 2.98150E+02 -287.997586\*EVTOJ#  
 -2\*GSIGRE#-4\*GSIGNI#-8\*GSIGRE#-8\*GSIGNI#-8\*GSIGRE#; 6.00000E+03 N REF3 !  
 PARAMETER G(SIGMA,MO:RE:RE:NI:RE;0) 2.98150E+02 -314.165674\*EVTOJ#  
 -2\*GSIGMO#-4\*GSIGRE#-8\*GSIGRE#-8\*GSIGNI#-8\*GSIGRE#; 6.00000E+03 N REF3 !  
 PARAMETER G(SIGMA,NI:RE:RE:NI:RE;0) 2.98150E+02 -303.983367\*EVTOJ#  
 -2\*GSIGNI#-4\*GSIGRE#-8\*GSIGRE#-8\*GSIGNI#-8\*GSIGRE#; 6.00000E+03 N REF3 !  
 PARAMETER G(SIGMA,RE:RE:RE:NI:RE;0) 2.98150E+02 -317.277027\*EVTOJ#  
 -2\*GSIGRE#-4\*GSIGRE#-8\*GSIGRE#-8\*GSIGNI#-8\*GSIGRE#; 6.00000E+03 N REF3 !  
 PARAMETER G(SIGMA,MO:MO:MO:RE:RE;0) 2.98150E+02 -350.940389\*EVTOJ#  
 -2\*GSIGMO#-4\*GSIGMO#-8\*GSIGMO#-8\*GSIGRE#-8\*GSIGRE#; 6.00000E+03 N REF3 !  
 PARAMETER G(SIGMA,NI:MO:MO:RE:RE;0) 2.98150E+02 -341.491771\*EVTOJ#  
 -2\*GSIGNI#-4\*GSIGMO#-8\*GSIGMO#-8\*GSIGRE#-8\*GSIGRE#; 6.00000E+03 N REF3 !  
 PARAMETER G(SIGMA,RE:MO:MO:RE:RE;0) 2.98150E+02 -354.494334\*EVTOJ#  
 -2\*GSIGRE#-4\*GSIGMO#-8\*GSIGMO#-8\*GSIGRE#-8\*GSIGRE#; 6.00000E+03 N REF3 !  
 PARAMETER G(SIGMA,MO:NI:MO:RE:RE;0) 2.98150E+02 -326.464541\*EVTOJ#  
 -2\*GSIGMO#-4\*GSIGNI#-8\*GSIGMO#-8\*GSIGRE#-8\*GSIGRE#; 6.00000E+03 N REF3 !  
 PARAMETER G(SIGMA,NI:NI:MO:RE:RE;0) 2.98150E+02 -317.030592\*EVTOJ#  
 -2\*GSIGNI#-4\*GSIGNI#-8\*GSIGMO#-8\*GSIGRE#-8\*GSIGRE#; 6.00000E+03 N REF3 !

PARAMETER G(SIGMA,RE:NI:MO:RE:RE;0) 2.98150E+02 -329.723731\*EVTOJ#  
 -2\*GSIGRE#-4\*GSIGNI#-8\*GSIGMO#-8\*GSIGRE#-8\*GSIGRE#; 6.00000E+03 N REF3 !  
 PARAMETER G(SIGMA,MO:RE:MO:RE:RE;0) 2.98150E+02 -355.892909\*EVTOJ#  
 -2\*GSIGMO#-4\*GSIGRE#-8\*GSIGMO#-8\*GSIGRE#-8\*GSIGRE#; 6.00000E+03 N REF3 !  
 PARAMETER G(SIGMA,NI:RE:MO:RE:RE;0) 2.98150E+02 -346.701734\*EVTOJ#  
 -2\*GSIGNI#-4\*GSIGRE#-8\*GSIGMO#-8\*GSIGRE#-8\*GSIGRE#; 6.00000E+03 N REF3 !  
 PARAMETER G(SIGMA,RE:RE:MO:RE:RE;0) 2.98150E+02 -359.220781\*EVTOJ#  
 -2\*GSIGRE#-4\*GSIGRE#-8\*GSIGMO#-8\*GSIGRE#-8\*GSIGRE#; 6.00000E+03 N REF3 !  
 PARAMETER G(SIGMA,MO:MO:NI:RE:RE;0) 2.98150E+02 -304.155473\*EVTOJ#  
 -2\*GSIGMO#-4\*GSIGMO#-8\*GSIGNI#-8\*GSIGRE#-8\*GSIGRE#; 6.00000E+03 N REF3 !  
 PARAMETER G(SIGMA,NI:MO:NI:RE:RE;0) 2.98150E+02 -295.678579\*EVTOJ#  
 -2\*GSIGNI#-4\*GSIGMO#-8\*GSIGNI#-8\*GSIGRE#-8\*GSIGRE#; 6.00000E+03 N REF3 !  
 PARAMETER G(SIGMA,RE:MO:NI:RE:RE;0) 2.98150E+02 -307.563963\*EVTOJ#  
 -2\*GSIGRE#-4\*GSIGMO#-8\*GSIGNI#-8\*GSIGRE#-8\*GSIGRE#; 6.00000E+03 N REF3 !  
 PARAMETER G(SIGMA,MO:NI:NI:RE:RE;0) 2.98150E+02 -279.787469\*EVTOJ#  
 -2\*GSIGMO#-4\*GSIGNI#-8\*GSIGNI#-8\*GSIGRE#-8\*GSIGRE#; 6.00000E+03 N REF3 !  
 PARAMETER G(SIGMA,NI:NI:NI:RE:RE;0) 2.98150E+02 -270.622482\*EVTOJ#  
 -2\*GSIGNI#-4\*GSIGNI#-8\*GSIGNI#-8\*GSIGRE#-8\*GSIGRE#; 6.00000E+03 N REF3 !  
 PARAMETER G(SIGMA,RE:NI:NI:RE:RE;0) 2.98150E+02 -282.972607\*EVTOJ#  
 -2\*GSIGRE#-4\*GSIGNI#-8\*GSIGNI#-8\*GSIGRE#-8\*GSIGRE#; 6.00000E+03 N REF3 !  
 PARAMETER G(SIGMA,MO:RE:NI:RE:RE;0) 2.98150E+02 -308.798429\*EVTOJ#  
 -2\*GSIGMO#-4\*GSIGRE#-8\*GSIGNI#-8\*GSIGRE#-8\*GSIGRE#; 6.00000E+03 N REF3 !  
 PARAMETER G(SIGMA,NI:RE:NI:RE:RE;0) 2.98150E+02 -300.530993\*EVTOJ#  
 -2\*GSIGNI#-4\*GSIGRE#-8\*GSIGNI#-8\*GSIGRE#-8\*GSIGRE#; 6.00000E+03 N REF3 !  
 PARAMETER G(SIGMA,RE:RE:NI:RE:RE;0) 2.98150E+02 -312.312225\*EVTOJ#  
 -2\*GSIGRE#-4\*GSIGRE#-8\*GSIGNI#-8\*GSIGRE#-8\*GSIGRE#; 6.00000E+03 N REF3 !  
 PARAMETER G(SIGMA,MO:MO:RE:RE:RE;0) 2.98150E+02 -361.705173\*EVTOJ#  
 -2\*GSIGMO#-4\*GSIGMO#-8\*GSIGRE#-8\*GSIGRE#-8\*GSIGRE#; 6.00000E+03 N REF3 !  
 PARAMETER G(SIGMA,NI:MO:RE:RE:RE;0) 2.98150E+02 -352.199048\*EVTOJ#  
 -2\*GSIGNI#-4\*GSIGMO#-8\*GSIGRE#-8\*GSIGRE#-8\*GSIGRE#; 6.00000E+03 N REF3 !  
 PARAMETER G(SIGMA,RE:MO:RE:RE:RE;0) 2.98150E+02 -365.120645\*EVTOJ#  
 -2\*GSIGRE#-4\*GSIGMO#-8\*GSIGRE#-8\*GSIGRE#-8\*GSIGRE#; 6.00000E+03 N REF3 !  
 PARAMETER G(SIGMA,MO:NI:RE:RE:RE;0) 2.98150E+02 -337.623615\*EVTOJ#  
 -2\*GSIGMO#-4\*GSIGNI#-8\*GSIGRE#-8\*GSIGRE#-8\*GSIGRE#; 6.00000E+03 N REF3 !  
 PARAMETER G(SIGMA,NI:NI:RE:RE:RE;0) 2.98150E+02 -327.947676\*EVTOJ#  
 -2\*GSIGNI#-4\*GSIGNI#-8\*GSIGRE#-8\*GSIGRE#-8\*GSIGRE#; 6.00000E+03 N REF3 !  
 PARAMETER G(SIGMA,RE:NI:RE:RE:RE;0) 2.98150E+02 -340.955701\*EVTOJ#  
 -2\*GSIGRE#-4\*GSIGNI#-8\*GSIGRE#-8\*GSIGRE#-8\*GSIGRE#; 6.00000E+03 N REF3 !

PARAMETER G(SIGMA,MO:RE:RE:RE:RE;0) 2.98150E+02 -366.47672\*EVTOJ#  
-2\*GSIGMO#-4\*GSIGRE#-8\*GSIGRE#-8\*GSIGRE#-8\*GSIGRE#; 6.00000E+03 N REF3 !  
PARAMETER G(SIGMA,NI:RE:RE:RE:RE;0) 2.98150E+02 -357.308387\*EVTOJ#  
-2\*GSIGNI#-4\*GSIGRE#-8\*GSIGRE#-8\*GSIGRE#-8\*GSIGRE#; 6.00000E+03 N REF3 !  
PARA G(SIGMA,RE:RE:RE:RE:RE;0) 298.15 0; 6000 N!

#### PHASE SigmaPrime % 2 2 1 !

CONSTITUENT SIGMAPRIME\_PHASE :MO,RE : NI : !  
PARAMETER G(SigmaPrime,MO:NI;0) 2.98150E+02 +2\*GHSERMO#+GHSERNI#+V6#+V7#\*T;  
6.00000E+03 N !  
PARAMETER G(SigmaPrime,RE:NI;0) 2.98150E+02 +2\*GHSERRE#+GHSERNI#+V8#+V9#\*T;  
6.00000E+03 N !  
PARAMETER G(SigmaPrime,MO,RE:NI;0) 2.98150E+02 +V10#+V11#\*T; 6.00000E+03 N !  
PARAMETER G(SigmaPrime,MO,RE:NI;1) 2.98150E+02 +V12#+V13#\*T; 6.00000E+03 N !

#### LIST\_OF\_REFERENCES

##### NUMBER SOURCE

- REF1 'PURE4 - SGTE Pure Elements (Unary) Database (Version 4.6),  
developed by SGTE (Scientific Group Thermodata Europe), 1991-2008,  
and provided by TCSAB (Jan. 2008).'  
REF3 'JC Crivello 2011, Armide project v1.5 sigma phase'  
REF5 'JC Crivello 2011, Armide project v1.5 chi phase'  
REF7 'N. Dupin, december 2011; Nb-Re and Mo-Re'  
REF9 'Khuram, May 2012; Ni-Re'

!